A Thesis Submitted for the Degree of PhD at the University of Warwick

Permanent WRAP URL:

http://wrap.warwick.ac.uk/133932

Copyright and reuse:

This thesis is made available online and is protected by original copyright.

Please scroll down to view the document itself.

Please refer to the repository record for this item for information to help you to cite it.

Our policy information is available from the repository home page.

For more information, please contact the WRAP Team at: wrap@warwick.ac.uk

warwick.ac.uk/lib-publications

The Interaction of the Prion Protein

with Lipid Membranes

and

Implications for Prion Conversion

Thesis submitted for the degree of Doctor of
Philosophy

Narinder Sanghera B. Sc. (Hons.)

Department of Biological Sciences, University of Warwick

September 2001

Contents

Chapter 2: Biophysical Techniques

Chapter 3: Expression and Purification of Syrian Hamster Prion Protein (SHaPrP) Residues 90–231

Chapter 4: Binding of Syrian Hamster Prion Protein (SHaPrP) Residues 90–231 to Model Lipid Membranes

Chapter 6: Membrane Binding/Insertion Kinetics of Syrian Hamster Prion Protein (SHaPrP) Residues 90–231 and PrP-Induced Membrane Destabilisation

Chapter 7: General Discussion and conclusions

Figures and Tables

Chapter 5: Secondary Structural Changes in Syrian Hamster Prion Protein (SHaPrP) Residues 90–231 Upon binding to Lipid Membranes

Chapter 6: Membrane Binding/Insertion Kinetics of Syrian Hamster Prion Protein (SHaPrP) Residues 90–231 and PrP-Induced Membrane Destabilisation

Acknowledgements

Declaration

I hereby declare that the research submitted in this thesis was conducted by myself under the supervision of Dr T. J. T. Pinheiro at the Department of Biological Sciences, University of Warwick.

No part of this work has previously been submitted to be considered for a degree. All sources of information have been specifically acknowledged in the form of references.

Some of the work presented herein has been accepted for publication:

Sanghera, N. and Pinheiro, T. J. T. (2001). Binding of prion protein to lipid membranes and implications for prion conversion. *J. Mol. Biol.* in print

ABSTRACT

The Interaction of the Prion Protein with Lipid Membranes and Implications for Prion Conversion

Prion diseases are characterised by the conversion of the normal α-helical prion protein (PrP^C), to the abnormal β-sheet isoform (PrP^{Sc}). Biophysical studies using recombinant prion proteins have helped our understanding of the structural events associated with the transition of PrP^C to PrP^{Sc}. These studies were performed in an aqueous environment, however PrP in living cells is anchored to cholesterol/sphingomyelin rich raft-domains. Evidence suggests that the lipid environment plays' a role in the conversion of PrP^C to PrP^{Sc}. Therefore in this thesis the biophysical properties of PrP in lipid membranes were evaluated.

The binding of Syrian hamster prion protein, SHaPrP (90–231) to model lipid membranes was investigated by tryptophan fluorescence spectroscopy. Membranes composed of negatively charged lipids, zwitterionic lipids and raft-like membranes containing DPPC, cholesterol and sphingomyelin, were investigated. The results show that PrP has an affinity for negatively charged and gel-phase zwitterionic membranes. Binding of PrP to raft-like membranes was also observed. The interaction of PrP to negatively charged membranes involved both electrostatic and hydrophobic lipid-protein interactions, whereas the binding of PrP to raft-like membranes was predominantly driven by hydrophobic lipid-protein interactions.

CD and ATR FTIR were used to investigate the secondary structure of PrP in lipid membranes. The interaction of PrP to negatively charged membranes was accompanied by an increase in β-sheet structure and EM showed extensive aggregation of the protein. In contrast, the binding of PrP to gel-phase zwitterionic membranes and raft-like membranes induced the formation of stable α-helical structure. No evidence of aggregation was detected in the EM images.

The ability of PrP to perturb lipid membranes was examined. Evidence for the partial insertion of PrP into negatively charged membranes was obtained and the resulting β-sheet state was capable of disrupting lipid membranes, leading to total release of vesicle contents. The α-helical membrane bound state of PrP did not affect the integrity of the raft-like membranes. These finding support the view that the interaction of PrP with lipid membranes may play a role in PrP conversion.

Abbreviations

ATR FTIR	attenuated total reflection Fourier transform infrared
BSE	bovine spongiform encephalopathy
CD	circular dichroism
chol	cholesterol
CJD	Creutzfeldt-Jakob disease
DOPC	dioleoylphosphatidylcholine (1,2-dioleoyl-*sn*-glycero-3-phosphocholine)
DPPC	dipalmitoylphosphatidylcholine (1,2-dipalmitoyl-*sn*-glycero-3-phosphocholine)
DTT	dithiothreitol
EDTA	ethylenediamine tetra-acetic acid
EM	electron microscopy
FFI	fatal familial insomnia
FPE	fluorescein-phosphatidyl-ethanolamine (N-(5-fluoresceinthiocarbamoyl)-1,2-dihexadecanoyl-*sn*-glycero-3-phosphoethanolamine)
GdnHCl	Guanidine hydrochloride
GPI	glycosylphosphatidylinositol
GSS	Gerstmann-Stäussler-Scheinker
MES	2-(N-morpholino) ethanesulphonic acid
NMR	nuclear magnetic resonance
PIPLC	phosphatidylinositol-specific phospholipase C
POPC	palmitoyloleoylphosphatidylcholine (1-palmitoyl-2-oleoyl-*sn*-glycero-3-phospho-*rac*-1-choline)
POPG	palmitoyloleoylphosphatidylglycerol (1-palmitoyl-2-oleoyl-*sn*-glycero-3-phospho-*rac*-1-glycerol)
PrP	prion protein
PrP$^{0/0}$	mice lacking PrP gene
PrP^{C}	normal cellular PrP isoform
PrP^{Sc}	infectious scrapie PrP isoform
SDS-PAGE	sodium dodecyl sulphate polyacrylamide gel electrophoresis
SEC	Size-exclusion chromatography
SHa	Syrian hamster

SM   sphingomyelin

RP HPLC   reverse phase high performance liquid chromatography

rPrP   recombinant PrP

TFA   trifluoroacetic acid

TSE   transmissible spongiform encephalopathy

vCJD   new variant Creutzfeldt-Jakob disease

Chapter 1:   Introduction

1.1   Prions

Transmissible   spongiform   encephalopathies   (TSEs)   are   fatal

neurodegenerative diseases that occur in humans and in a variety of other animals.

In humans, TSE diseases include Kuru, Creutzfeldt-Jakob disease (CJD), fatal

familial insomnia (FFI) and Gerstmann-Stäussler-Scheinker (GSS); in animals

include scrapie of sheep and bovine spongiform encephalopathy (BSE or mad cow

disease).   Examination of the brains of individuals with TSE diseases shows

spongiform degeneration and astrocytic gliosis (review Prusiner, 1998). So far, the

occurrence of TSE diseases in humans is rare, however the recent cases of new

variant (v) CJD in the UK has been related to the recent epidemic of BSE. This has

lead to a new urgency in the study of TSE diseases especially since there is

substantial evidence to suggest that vCJD may have been caused by the consumption

of BSE contaminated products (Bruce *et al.*, 1997; Hill *et al.*, 1997).

1.1.1   Discovery of the prion protein

There has been a great deal of speculation regarding the nature of the

infectious agent in TSE diseases: suggestions included small DNA viruses,

replicating polysaccharides, membrane fragments and proteins (for review, see

Prusiner, 1982).   Scrapie infectivity was retained after the infectious material was

subjected to procedures that altered or destroyed nucleic acids.   However, methods

that modify or hydrolyse proteins were found to diminish infectivity (Prusiner, 1982;

Prusiner *et al.*, 1982). These observations led to the proposal of the *'protein-only'*

hypothesis, which states that TSE causing agent is devoid of nucleic acid and the

essential pathogenic component is a protein. According to the protein-only hypothesis TSEs are a result of a conformational transition, in which a normal energetically favoured conformation is converted to a disease causing isoform, either spontaneously or by exogenous introduction of the altered conformation. The term 'prion' was introduced to distinguish the infectious agent that causes TSEs from viruses.

Scrapie infectivity was purified from Syrian hamster (SHa) brain, through a series of steps, which included multiple detergent extractions, limited proteinase K digestion and a sucrose density gradient (Prusiner, 1982; Prusiner et al., 1982). Analysis of the fractions enriched for scrapie infectivity revealed a protease-resistant protein of 27–30 kDa; the protein was named prion protein (PrP) 27–30. The protein was absent from similar fractions purified from normal brain. The determination of the amino acid sequence of the amino-terminus of PrP 27–30 made it possible to subsequently carry out molecular cloning studies of the PrP gene. It was found that PrP was encoded by a chromosomal gene and not by a nucleic acid within the infectious material (Chesebro et al., 1985; Oesch et al., 1985). The normal cellular PrP gene product was determined, as a protein of 33–35 kDa, termed cellular prion protein (PrP^C). A protein of identical size was also detected in scrapie infected brain extracts, in which proteinase K was absent from the purification protocol and was named scrapie or infectious prion protein (PrP^{Sc}).

Proteinase K digestion studies revealed that PrP^C was completely degraded, whereas PrP^{Sc} was partially cleaved to produce PrP 27–30. Furthermore, no significant difference in the specific infectivity of preparations purified with or without proteinase K digestion has been found (Mckinley et al., 1991). The findings

suggested that PrP could be present in at least two distinct conformational states: a protease-sensitive one found ubiquitously and a protease-resistant one identified in the setting of infection.

Over the last two decades, substantial amount of evidence both *in vivo* and *in vitro* has accumulated supporting the protein-only hypothesis (reviewed in Prusiner, 1998). The strongest evidence for this hypothesis has been provided by genetic studies carried out with mice lacking the PrP gene ($Prnp^{0/0}$). These mice were both resistant to prions and unable to generate new infectious particles. Re-introduction of PrP-encoding gene restored their susceptibility to infection (Büeler *et al.*, 1993; Manson *et al.*, 1994).

1.1.2 *Search for a scrapie-specific nucleic acid*

The lack of pure preparations of infectious prions and the fact that the minimum dose of purified hamster scrapie necessary to establish infection contains ~100,000 PrP^{Sc} molecules (Prusiner *et al.*, 1982) has led some researchers to suggest that these preparations may harbour a unique virus. Despite intensive efforts to identify a nucleic acid within the infectious material, none has been found to date (Oesch *et al.*, 1985; Meyer *et al.*, 1991; Kellings *et al.*, 1992). These studies argue that if such a molecule exists, then its size is 80 nucleotides or less. Despite the large accumulation of evidence supporting the importance of PrP in TSE diseases, one cannot eliminate the possibility of a small nucleic acid molecule bound to PrP^{Sc} as an essential component of the infectious prion particle or a yet unidentified covalent modification of the protein.

1.1.3 Human TSE diseases

Human TSE or prion diseases maybe presented as genetic, infectious, or sporadic disorders (Prusiner, 1997). Typically the diseases are diagnosed in adults between 40 and 80 years of age, however new vCJD appears in younger people (Prusiner & Scott, 1997).

• *Inherited diseases:* Familial CJD, GSS and FFI are all dominantly inherited diseases, which have been linked to specific mutations in the PrP gene. The Pro^{102} → Leu (P102L) was the first mutation to be genetically linked to GSS. Transgenic studies confirmed that mutations of the PrP gene could cause neurodegeneration. Mice overexpressing a mutant PrP transgene with a mutation corresponding to P102L spontaneously developed a scrapie-like disease (Hsiao *et al.*, 1994). Polymorphisms in the PrP gene have also been identified and are thought to influence the clinical and neuropathologic phenotype of the disease (Prusiner & Scott, 1997).

• *Sporadic diseases:* Sporadic forms of TSE diseases constitute most cases of CJD and a few of GSS. Mutations of the PrP gene are not found in patients. It is not known how prions are able to cause disease in these cases; hypotheses include somatic mutation of the PrP gene and rare spontaneous conversion of PrP^C to PrP^{Sc} (Prusiner, 1998).

• *Infectious diseases:* The infectious diseases include Kuru of the Fore people in New Guinea, where prions were transmitted by ritualistic cannibalism (reviewed in Prusiner, 1998). Sources of prions causing infectious CJD include improperly sterilized depth electrodes, which were used during neurosurgical procedures, transplanted corneas and the human growth hormone. There is compelling evidence supporting the proposal that vCJD is caused by the

consumption of BSE contaminated food products (Bruce *et al.*, 1997; Hill *et al.*, 1997).

1.1.4 PrP gene structure, organisation and expression

The human PrP gene is present on chromosome 20 and contains three exons, the open reading frame is encoded by the third exon (Sparkes *et al.*, 1986). Since the entire protein-coding region of all known mammalian genes, resides within a single exon the possibility that the two PrP isoforms are products of alternatively spliced mRNAs is eliminated (Basler *et al.*, 1986). Furthermore, no evidence for rearrangement of the PrP gene in scrapie infected animals has been found (Oesch *et al.*, 1985; Basler *et al.*, 1986). Amino acid sequencing of PrP^{Sc} and PrP 27–30 correspond precisely to the translated genomic DNA sequence (Basler *et al.*, 1986; Hope *et al.*, 1986; Stahl *et al.*, 1993). The difference in the properties of the two isoforms of PrP is therefore most likely to be due to a post-translational event.

PrP is expressed as a protein of ~ 250 amino acids; human PrP consists of 253 amino acids (Kretzschmar *et al.*, 1986); Syrian hamster PrP is expressed as a 254 amino acid protein (Oesch *et al.*, 1985; Basler *et al.*, 1986). PrP^{C} is expressed in normal and scrapie-infected animals whereas PrP^{Sc} is observed only in scrapie-infected brain (Oesch *et al.*, 1985). The appearance and abundance of PrP mRNA in the brains of adult animals is constant throughout the course of infection (Chesebro *et al.*, 1985; Oesch *et al.*, 1985).

Immunohistochemistry was used to detect PrP^{C} expression in the brain and the highest levels of PrP^{C} were found in the hippocampus. In contrast, PrP^{Sc} was

found to be minimal in this region and was present in the white matter and bundles of myelinated axons (DeArmond *et al.*, 1987; Taraboulos *et al.*, 1992).

An amino-terminal 22-residue signal peptide is cleaved during the biosynthesis of PrP in the endoplasmic reticulum (Hope *et al.*, 1986; Turk *et al.*, 1988). A 23-residue carboxyl-terminal peptide is lost upon addition of a glycosylphosphatidylinositol (GPI) anchor to the carboxyl-terminus of PrP^C at Ser231, which anchors the protein to the cell membrane. The GPI anchor has also been detected for PrP^{Sc} (Stahl *et al.*, 1987; Stahl *et al.*, 1990). Both isoforms of PrP contain a disulphide bond between Cys179 and Cys214 (Turk *et al.*, 1988) and two glycosylation sites at Asn181 and Asn197 (Endo *et al.*, 1989). A schematic representation of the biosynthesis of PrP isoforms is shown in Figure 1.1.

Analysis of the primary structure of PrP revealed several unusual features. The amino-terminal region of mammalian PrP, residues 51–91 contains five glycine-rich repeats; this sequence is termed the octarepeat region and is among the most conserved parts of PrP in mammals thus implying a functional role (Harris *et al.*, 1991). The octarepeat region of human PrP contains the sequence Pro-(Gln/His)-Gly$_3$-(G/-)Trp-Gly-Gln (Prusiner, 1992). The other region of notable conservation among mammals is a Gly- and Ala-rich hydrophobic domain from residues 113 to 128 (Wopfner *et al.*, 1999).

1.1.5 Properties of PrP isoforms

The isoforms of PrP have very different biochemical properties:

- PrP^{Sc} is insoluble in detergents, whereas PrP^C is readily solubilised under non-denaturing conditions (Meyer *et al.*, 1986).
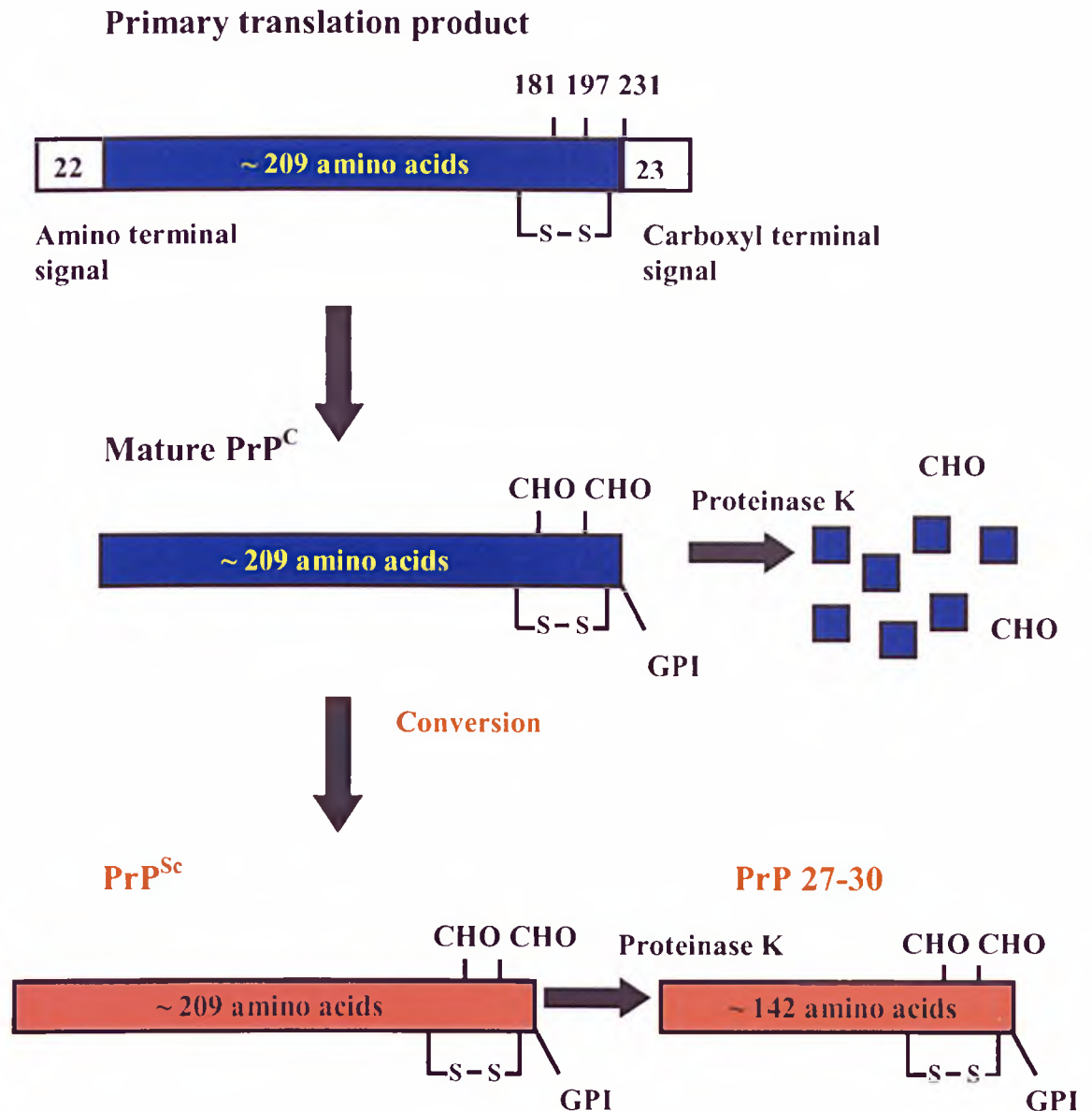
Figure 1.1: **Schematic representation of the biosynthesis of PrP.** Mammalian PrP gene encodes a protein of ~ 250 amino acids. The amino-terminal signal peptide of 22 amino acids is cleaved during maturation of PrP^C. 23 amino acids are removed from the carboxyl-terminus upon attachment of the GPI anchor at Ser231. PrP is glycosylated (CHO) at positions Asn181 and Asn197. Mature PrP^C is anchored to the outer surface of the plasma membrane and is sensitive to proteinase K. The partial protease resistance of PrP^{Sc} is acquired as a result of a post-translational event. Proteinase K digestion of PrP^{Sc} removes ~ 67 amino acids to produce PrP 27–30, which corresponds to the amino acid region from 90 to 231. The protease resistant core retains the ability to re-infect laboratory rodents (Mckinley *et al.*, 1983).

- PrP^{Sc} is partially hydrolysed by proteinase K to form a fragment designated PrP 27–30 (amino acids 90–231) while PrP^{C} is completely degraded under the same conditions (Oesch *et al.*, 1985).

- PrP^{C} is removed from the cell surface with phosphatidylinositol-specific phospholipase C (PIPLC), in contrast cleavage of the GPI anchor attached to PrP^{Sc} by PIPLC does not result in the release of the protein from the cell surface. No evidence for the resistance of the GPI anchor to cleavage was detected, thereby suggesting that the polypeptide chain of PrP^{Sc} may itself interact with lipid membranes (Stahl *et al.*, 1990; Safar *et al.*, 1991).

- PrP^{Sc} accumulates within cells whereas PrP^{C} has a rapid turn over (Borchelt *et al.*, 1990).

Extensive biochemical characterisation failed to identify any covalent chemical differences between PrP^{C} and PrP^{Sc} this led investigators to suggest that the two isoforms of PrP were likely to differ in their conformation. Analysis of the secondary structure of PrP^{C} and PrP^{Sc} by Fourier transform infrared (FTIR) spectroscopy revealed that the structures of PrP^{C} and PrP^{Sc} were indeed different (Pan *et al.*, 1993).

Table 1.1: Content of secondary structure of purified SHaPrP[a]

Structure	PrP^{C}	PrP^{Sc}	PrP 27–30
α-Helix	42	30	21
β-Sheet	3	43	54
Turn	32	11	9
Coil/Random	23	16	16

[a]Pan *et al.*, 1993

8

The results from the above study as well as others (Caughey *et al.*, 1991; Gasset *et al.*, 1993; Nguyen *et al.*, 1995) suggest that PrP^C is converted into PrP^Sc through a process whereby a portion of its structure is refolded into β-sheet structure. This conformational transition is accompanied by profound changes in the biochemical properties of PrP and is most probably the key molecular event that underlies prion propagation.

1.1.6 Structure of prion proteins

1.1.6.1 NMR structure of recombinant PrP

The three-dimensional structure of recombinant PrP proteins derived from *E. coli* have been determined by nuclear magnetic resonance (NMR) spectroscopy. The structure of the refolded recombinant protein into an α-helical conformation is thought to resemble that of PrP^C. This is supported by studies with recombinant antibody fragments showing that GPI-anchored PrP^C on the surface of cells exhibits an immunoreactivity similar to that of recombinant PrP prepared with an α-helical conformation (Peretz *et al.*, 1997). The recombinant proteins also share many spectral properties with PrP^C (Hornemann & Glockshuber, 1996; Zhang *et al.*, 1997; Zahn *et al.*, 1997). Difficulties in the purification and low yields of PrP^C mean that so far recombinant PrP is the only viable model of the cellular protein.

The first structure to be reported was that of the amino-terminally truncated segment of mouse PrP comprising residues 121 to 231 (*m*PrP 121–231). The NMR structure revealed three α-helices (A, B & C) with a disulphide bond connecting helix B with C and a two stranded anti-parallel β-sheet (S1 & S2) (Riek *et al.*, 1996). This was followed by the analysis of recombinant SHaPrP, residues 90–231 (Figure

1.2A) which also exhibited three α-helices and two β-sheets (James *et al.*, 1997). The NMR structure of SHaPrP (90–231) revealed that the amino-terminus region from residues 90 to 128 is unstructured and this portion of the protein has been proposed to provide the plasticity required for the conformational transition of PrP^C to PrP^{Sc}. The NMR results agree well with the FTIR study (Pan *et al.*, 1993); out of 142 resolvable residues in SHaPrP (90–231) 63 are present in the α-helical component of the protein (44 %) while only 6 residues lie in the short anti-parallel β strands (4 %).

Eventually the full-length structures of recombinant prion proteins from SHaPrP (29–231), *m*PrP (23–231), human (*h*)PrP (23–231) and bovine (*b*) (23–230) were solved (Donne *et al.*, 1997; Riek *et al.*, 1997; García *et al.*, 2000; Zahn *et al.*, 2000). The presence of the additional residues in the full-length proteins did not have a significant effect on the secondary structure elements. The prion proteins from the different species were shown to contain a structured domain that extended approximately from residues 128–228 and a flexible random coil-like amino-terminus. Differences in the lengths of helices B and C especially between SHaPrP and *m*PrP however were evident (Table 1.2); helix B is seven residues longer and helix C is ten residues longer in SHaPrP compared to *m*PrP.

Superposition of the NMR structures of SHaPrP, *m*PrP, *h*PrP and *b*PrP is displayed in Figure 1.2B. This shows that the three-dimensional structures of the domains are similar, as would be expected for amino acid sequences that exhibit ~ 90 % homology (Schätzl *et al.*, 1995; Wopfner *et al.*, 1999). There is however, some
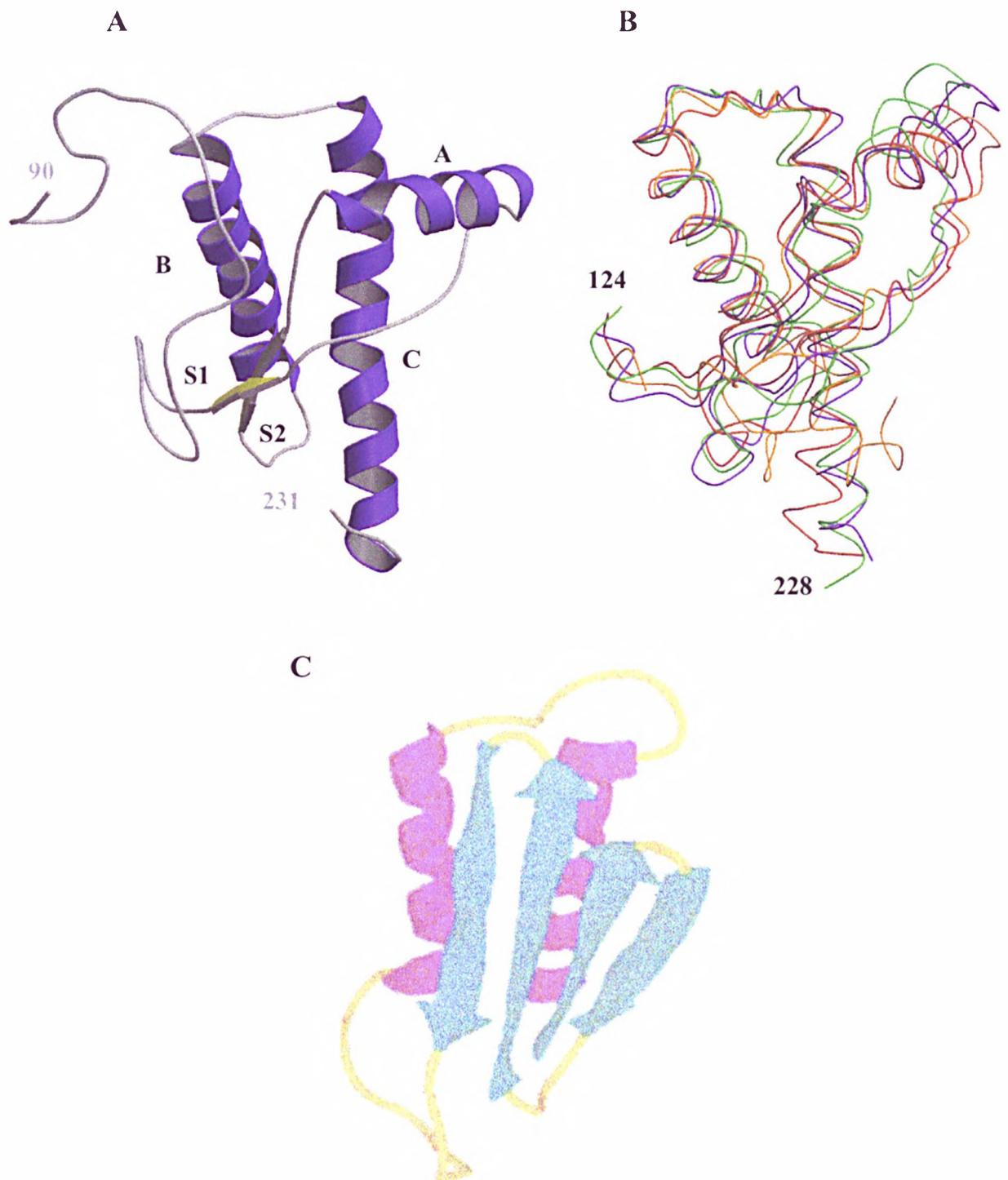
Figure 1.2: **Representations of the three-dimensional structures of prion proteins.** (A) Ribbon diagram of the NMR structure of recombinant SHaPrP (90–231) in aqueous solution (James *et al.*, 1997) indicating the positions of the three α-helices (A, B & C) and the two anti-parallel β-strands (S1 & S2). The structure was drawn using the program Molscript (Kraulis, 1991) and rendered with RASTER3D (Merritt & Bacon, 1997). (B) Superposition of the NMR structures of the polypeptide segment 124–228 of SHaPrP (red), *m*PrP (orange), *h*PrP (green) and *h*PrP (purple). Structures have been superimposed to obtain the best fit of the polypeptide backbone residues 124–228. (C) Plausible model for the tertiary structure of *h*PrP^Sc (108–217) (Huang *et al.*, 1995).

structural variability in the amino- and carboxyl-termini between the different species. The difference may be due to (*i*) the differences in the aqueous environment in which the structures were recorded, and (*ii*) although the sequence homology between the different protein domains is ~ 90 %, species-specific difference in the sequences may nevertheless account for the observed variability.

Table 1.2: The lengths of the helices (A, B & C) and the β-strands (S1 & S2) in the NMR structures of different domains of recombinant PrP

PrP Construct	Helix A	Helix B	Helix C	S1	S2	pH
SHa(29–231)[a]	144–156	172–193	200–227	137–140[g]	160–163	5.2
SHa(90–231)[b]	144–156	172–193	200–227	129–131	161–163	5.2
h(23–230)[c]	144–154	173–194	200–228	128–131	161–164	4.5
h(90–230)[c]	144–154	173–194	200–228	128–131	161–164	4.5
m(23–231)[d]	144–154	179–193	200–217	128–131	161–164	4.5
m(121–231)[e]	144–154	179–193	200–217	128–131	161–164	4.5
b(23–230)[f]	144–154	173–194	200–226	128–131	161–164	4.5

[a]Donne *et al.*, 1997; [b]James *et al.*, 1997; [c]Zahn *et al.*, 2000; [d]Riek *et al.*, 1997; [e]Riek *et al.*, 1996; [f]García *et al.*, 2000. [g]The NMR data did not suggest a β-sheet between residues 129–131 instead it indicated the possibility of a β-strand located between residues 137–140. This discrepancy may reflect the poor prediction power of the method especially as the β-strands are short and some assignments are missing, or it may show the presence of alternative native conformation for the protein in the presence of the 29–89 region.

1.1.6.2   Model structure of PrP[Sc]

Difficulties in the purification of PrP[Sc], such as instability and its ability to aggregate, have prevented the use of high-resolution techniques for structural

studies. Studies with PrP-specific recombinant antibody fragments suggest that the structural transition underlying PrP^{Sc} formation from PrP^C occurs within the region 90–145 (Peretz *et al.*, 1997). A model structure for PrP^{Sc} residues 108–217 has been proposed (Figure 1.2C) in which the unstructured amino-terminal region and helix A are in a β-sheet conformation (Huang *et al.*, 1995). The single disulphide bond joining helices B and C would remain intact (Turk *et al.*, 1988; Muramoto *et al.*, 1996).

1.1.7 PrP biosynthesis and metabolism

Three alternative topological forms of PrP with respect to the ER membrane were identified with cell-free translation studies (Figure 1.3) (Lopez *et al.*, 1990).

- *Secretory PrP:* this form is translocated across the ER membrane and is the precursor of the GPI-anchored molecule.

- *Transmembrane PrP:* two different orientations with respect to the ER membrane have been identified; ^{Ctm}PrP is glycosylated with the carboxyl-terminus in the ER lumen, and the other, ^{Ntm}PrP is unglycosylated and has the amino-terminus in this location.

1.1.7.1   GPI-anchored PrP

The first step in the biogenesis of secretory proteins is the targeting and translocation of these proteins across the impermeable ER membrane. A complex macromolecular machine, termed translocon, is responsible for the proper transport and biogenesis of proteins at the ER membrane (reviewed in Rapoport *et al.*, 1996; Hegde & Lingappa, 1997). In addition to the known components in the translocation

A

STE TM   CHO CHO

1   22   104 112 135   231 254

GPI

B

Protein **Ethanolamine Glycan**

Phosphatidylinositol

PIPLC

Plasma membrane

^{Sec}PrP ^{Ntm}PrP ^{Ctm}PrP

C

Lumen of ER

N   N

N

ER membrane

C   C

N

Cytosol
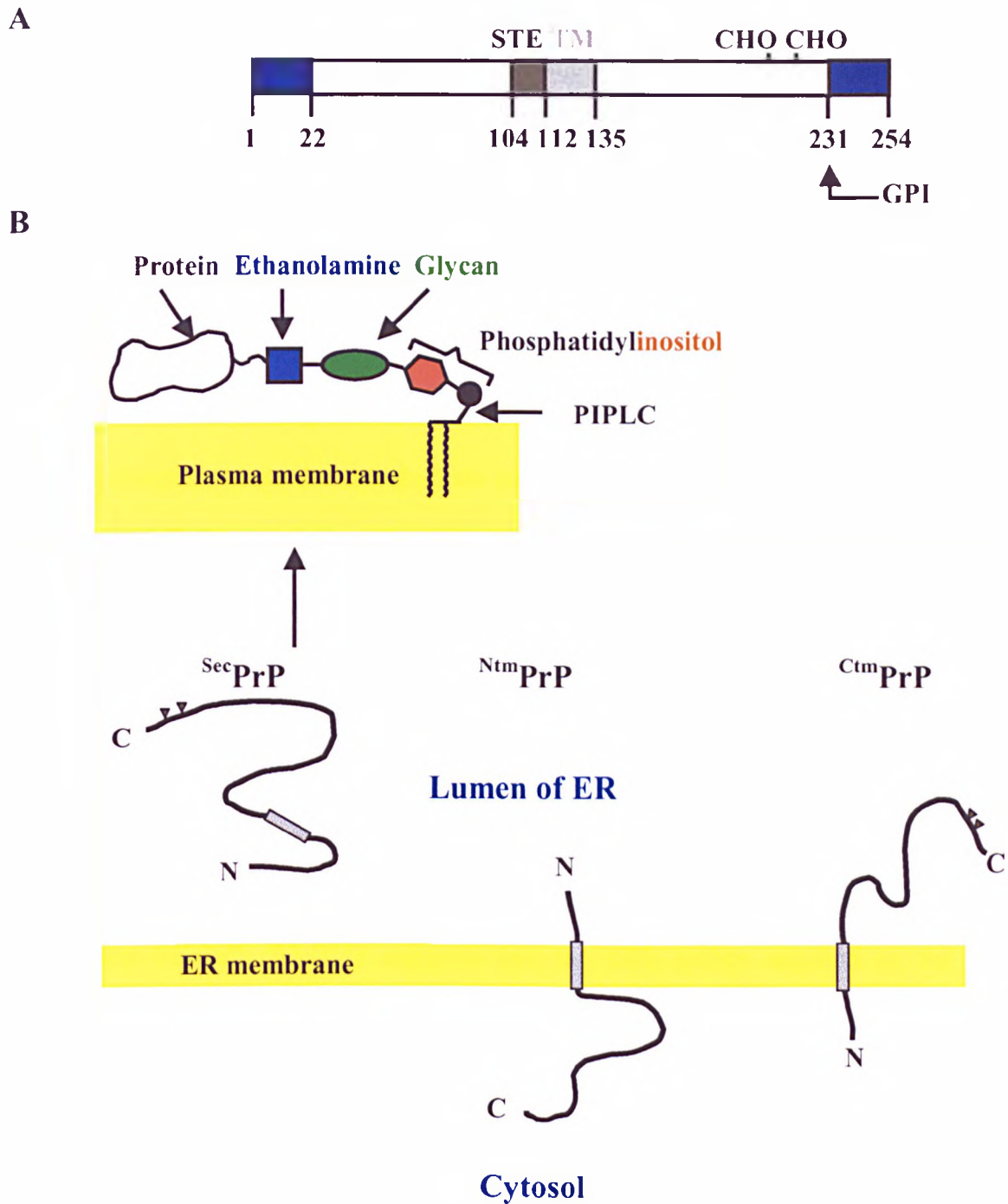
Figure 1.3: **Schematic representation of the topologic forms of PrP.** (A) Regions of PrP implicated in decisions about its topology with respect to the membrane: 1–22 amino-terminal signal peptide; 231–254 carboxyl-terminal signal peptide; 104–112 stop transfer effector (STE); 113–135 transmembrane domain (TM). (B) The three topologic forms of PrP are shown, ^{sec}PrP is the precursor for the GPI anchored form of PrP. The illustration highlights the components of the GPI anchor, the polypeptide domain position and the PIPLC cleavage site. The transmembrane forms of PrP, ^{Ntm}PrP and ^{Ctm}PrP have the amino-terminus and carboxyl-terminus in lumen of the ER, respectively. Both span the membrane at the region comprising residues 112–135. The glycosylation sites (CHO) at amino acids Asn181 and Asn197 are also highlighted (▲).

14

machinery (Sec61 complex, SRP receptor and translocating chain-associated membrane protein, TRAM), the transport of PrP into the lumen of the ER appears to involve translocation accessory factors at the translocon, the identity of which remains to be determined (Hegde *et al.*, 1998*b*).

In the lumen of the ER the amino-terminal signal sequence is cleaved by signal peptidase and disulphide isomerase catalyses the disulphide bond formation. The GPI anchor and carbohydrate moieties are also attached. PrP^C proceeds through the Golgi complex where the carbohydrate units are further processed. Ultimately, most of the PrP^C is anchored to the cell surface by the GPI anchor (Borchelt *et al.*, 1990; Caughey & Raymond, 1991). Analysis of the GPI anchor of PrP revealed the presence of ethanolamine, mannose, inositol, phosphate and saturated fatty acids. The lipid component of the GPI anchor is responsible for the insertion of the anchor into membranes (Figure 1.3B) (Stahl *et al.*, 1987).

Recent molecular modelling of PrP^C based on the solution NMR structure of recombinant SHaPrP (90–231) suggests that the GPI anchor attached to the carboxyl-terminus of PrP is flexible and as a result PrP most likely makes contact with the lipids/or other membrane proteins (Rudd *et al.*, 2001).

Like other GPI anchored proteins, PrP^C is targeted to detergent insoluble domains of the plasma membrane that are rich in cholesterol and sphingolipids (Taraboulos *et al.*, 1995; Vey *et al.*, 1996; Naslavsky *et al.*, 1997). These lipid domains are commonly referred to as lipid rafts (Brown & Rose, 1992; Harder & Simons, 1997; Simon & Ikonen, 1997). Once PrP^C has been transported to the plasma membrane it has a half-life of 3–6 h (Borchelt *et al.*, 1990; Caughey *et al.*, 1989). The degradation of PrP^C appears to involve two distinct steps. The first

occurs in a non-acidic compartment bound by a cholesterol rich membrane most probably at the plasma membrane in which approximately 90 amino acids are removed from the amino-terminus of PrP^C to produce a 17-kDa polypeptide (unglycosylated molecular weight). The acidic endosomal pathway is involved in the second degradation step. Depletion of cholesterol from cells slowed the degradation of PrP^C suggesting that the lipid environment features in the metabolism of PrP^C (Taraboulos et al., 1995).

1.1.7.2   Transmembrane PrP

^{Ctm}PrP and ^{Ntm}PrP span the membrane at the same stretch of amino acids (113–135), interestingly this includes the conserved hydrophobic region. ^{Ctm}PrP in addition can also acquire a carboxyl-terminus GPI anchor in the lumen of the ER, which inserts into the inner membrane of the ER (Stewart & Harris, 2001). A relatively hydrophilic region between amino acids 104 and 112, termed the stop transfer effector (STE) precedes the transmembrane segment. The STE plays a critical role in the determination of topology by promoting the integration of the hydrophobic sequence into the lipid bilayer (Lopez et al., 1990; Yost et al., 1990). Studies with the currently known translocation machinery (Sec61 complex, SRP receptor and translocating chain-associated membrane protein, TRAM) generates ^{Ctm}PrP, suggesting that this is the default pathway of PrP biogenesis (Hegde et al., 1998b). This coincides with the proposal that PrP was originally an integral membrane protein and that mutations in the amino acid sequence during its evolution resulted in a change in the topology of PrP to an anchored protein (Tompa et al., 2001). The generation of ^{Ntm}PrP like ^{sec}PrP requires translocation accessory factor(s) (Hegde et al., 1998b).

The roles of the transmembrane forms of PrP in TSE diseases have only recently been uncovered (Hegde *et al.*, 1998*a*, 1999). Mutations within or near the transmembrane domain of PrP result in an increased amount of ^{Ctm}PrP at the ER membrane, this has shown to cause neurodegeneration in mice with features that are typical of TSEs. Analysis of brain tissue failed to detect protease-resistant PrP^{Sc} (Hegde *et al.*, 1998*a*; Stewart & Harris, 2001) leading to the suggestion that ^{Ctm}PrP is involved in disease.

The substitution of the amino acid alanine at position 117 in PrP for valine causes the human disorder GSS. This mutation is of particular interest because it occurs in the transmembrane domain of PrP. *In vitro* and *in vivo* studies strongly suggest that this disease-causing mutation increases the production of ^{Ctm}PrP at the ER membrane compared to normal brains and that this is the cause of neurodegeneration. Although TSE diseases are normally characterised by the accumulation of PrP^{Sc} in brains of humans and animals, in certain cases of inherited TSE diseases, neurodegeneration occurs in the absence of PrP^{Sc} plaques. It has been proposed that in these circumstances ^{Ctm}PrP is synthesised instead of PrP^{Sc}. Furthermore, brain homogenate from clinically ill mice with a mutation favouring the formation of ^{Ctm}PrP when inoculated into healthy mice failed to induce disease. This finding was particularly interesting since GSS caused by the A117V mutation has not been transmitted to laboratory animals (Hegde *et al.*, 1999). Figure 1.4 shows a model for the relationship between the accumulation of PrP^{Sc} and the formation of ^{Ctm}PrP.
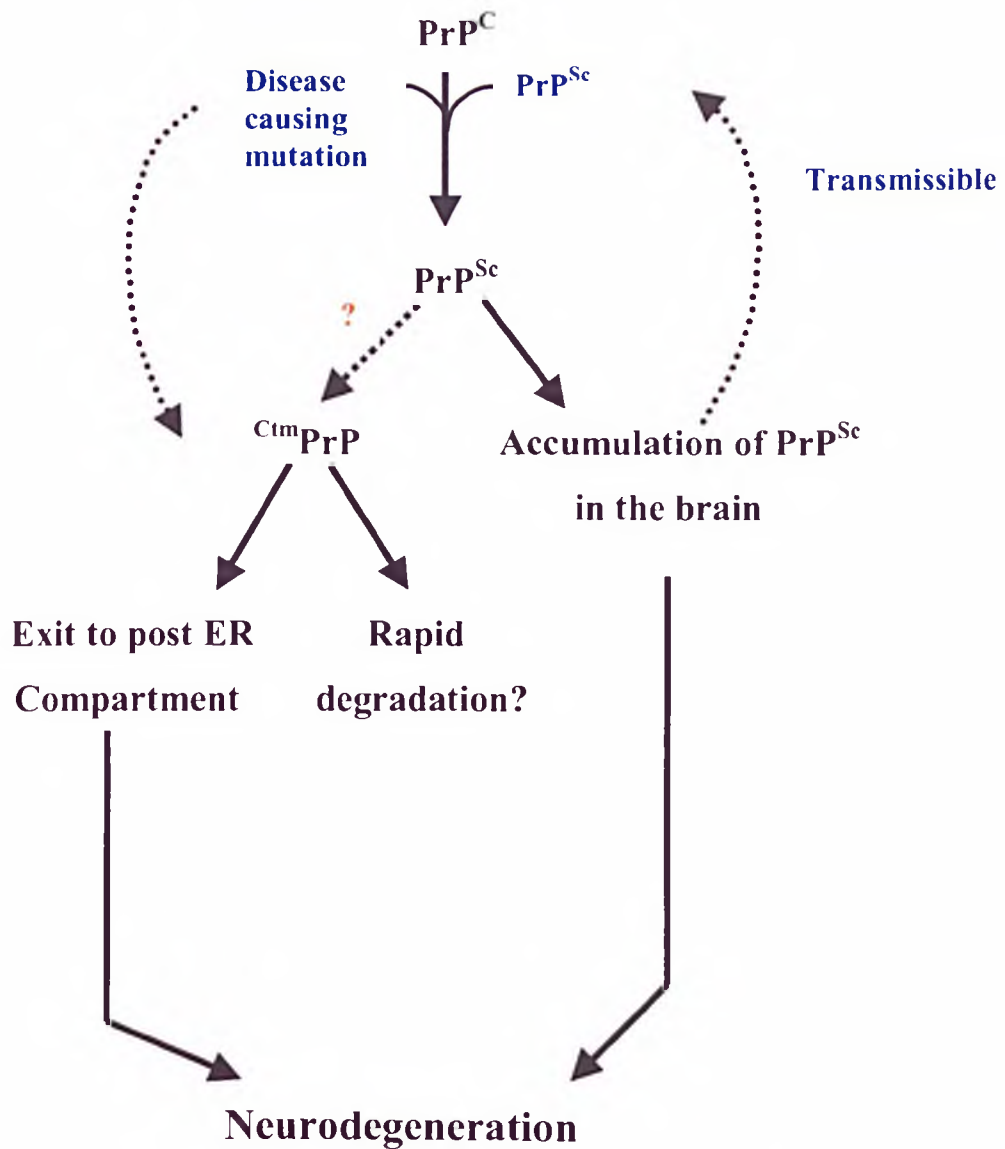
Figure 1.4: **Model demonstrating the relationship of PrP^{Sc} and ^{Ctm}PrP in TSE diseases.** Transmissible TSE diseases arise by converting PrP^C to PrP^{Sc}. This could be initiated either by inoculation of infectious material, spontaneous conversion or mutations in the PrP gene. Accumulation of PrP^{Sc} may increase the generation of ^{Ctm}PrP by an unknown step (dashed line with question mark). Alternatively, other mutation such as those in the TM domain could bypass the first step and directly cause an increase in ^{Ctm}PrP. Detection of PrP^{Sc} in brains may suggest that disease is caused by the first pathway and in the case of no detectable levels of PrP^{Sc}, the synthesis of ^{Ctm}PrP may be responsible for neurodegeneration (adapted from Hegde et al., 1999).

1.1.8 Conversion of PrP^C to PrP^{Sc}

Conversion of $PrP^C \rightarrow PrP^{Sc}$ is a post-translational process that occurs after PrP^C reaches the plasma membrane (Caughey & Raymond, 1991; Taraboulos *et al.*, 1995). Studies with transgenic mice demonstrated that PrP^{Sc} molecules must interact with endogenous PrP^C to induce the conversion of the latter to generate more PrP^{Sc} (Prusiner *et al.*, 1990; Scott *et al.*, 1993).

Glycosylation of PrP^C is not essential for the formation of PrP^{Sc}. The presence of bulky oligosaccarides is thought to interfere with PrP^C-PrP^{Sc} interactions. In circumstances where glycosylation was prevented the rate of PrP^{Sc} synthesis actually increased (Taraboulos *et al.*, 1990*a*; Lehmann & Harris, 1997).

Many studies of the PrP have concentrated on determining the minimum sequence requirements for developing or transmitting disease. Rogers *et al.* (1993) showed that the deletion of amino acids 23–88, which included the five octarepeat units did not prevent the synthesis of PrP^{Sc} in scrapie-infected cultured cells. A peptide of 55 amino acids that corresponded to MoPrP region 89–143 carrying the GSS causing mutation P101L (102 in human protein) in a β-sheet rich conformation when inoculated into Tg (MoPrP, P101L) Prnp$^{0/0}$ mice, expressing low levels of the 55-residue peptide produced clinical signs of neurologic dysfunction and neuropathology similar to changes observed in patients with GSS. These changes were not observed when the peptide was inoculated in a α-helical state (Kaneko *et al.*, 2000).

Once formed, PrP^{Sc} accumulates in a number of cellular locations: late endosomes and lysosomes (Borchelt *et al.*, 1992; Arnold *et al.*, 1995), in the cytoplasm (Taraboulos *et al.*, 1990*b*), on the cell surface (Vey *et al.*, 1996; Naslavsky *et al.*, 1997) and in extracellular spaces in the form of amorphous deposits, diffuse fibrils or dense amyloid plaques (DeArmond & Prusiner, 1995). Evidence implicates the plasma membrane and endocytic organelles as relevant sites for PrP^{Sc} formation, but it is unclear which of these is most important. Also, it is not known whether the secretory pathway is involved in the conversion process. Figure 1.5 shows a model of the probable subcellular sites for PrP^{Sc} formation. Depletion of cholesterol from scrapie infected cells not only slowed PrP^{C} degradation but also inhibited PrP^{Sc} formation (Taraboulos *et al.*, 1995; Vey *et al.*, 1996; Naslavsky *et al.*, 1997). This observation suggests that various aspects of PrP metabolism occurs within lipid rafts rich in cholesterol and sphingolipids. The rafts may promote the formation of PrP^{Sc} by concentrating PrP^{C} on the membrane surface.

Biophysical studies with recombinant PrP indicates the presence of equilibrium intermediates that are populated at acidic pH's and show spectral characteristics of β-sheet proteins. In contrast, no such intermediates were populated at pH 7, suggesting that PrP folds via an alternative pathway at lower pH's (Swietnicki *et al.*, 1997; Zhang *et al.*, 1997; Hornemann & Glockshuber, 1998; Jackson *et al.*, 1999*a,b*). This is of potential significance, since the endocytic pathway is implicated as one of the subcellular sites for the conversion of PrP^{C} to PrP^{Sc}.
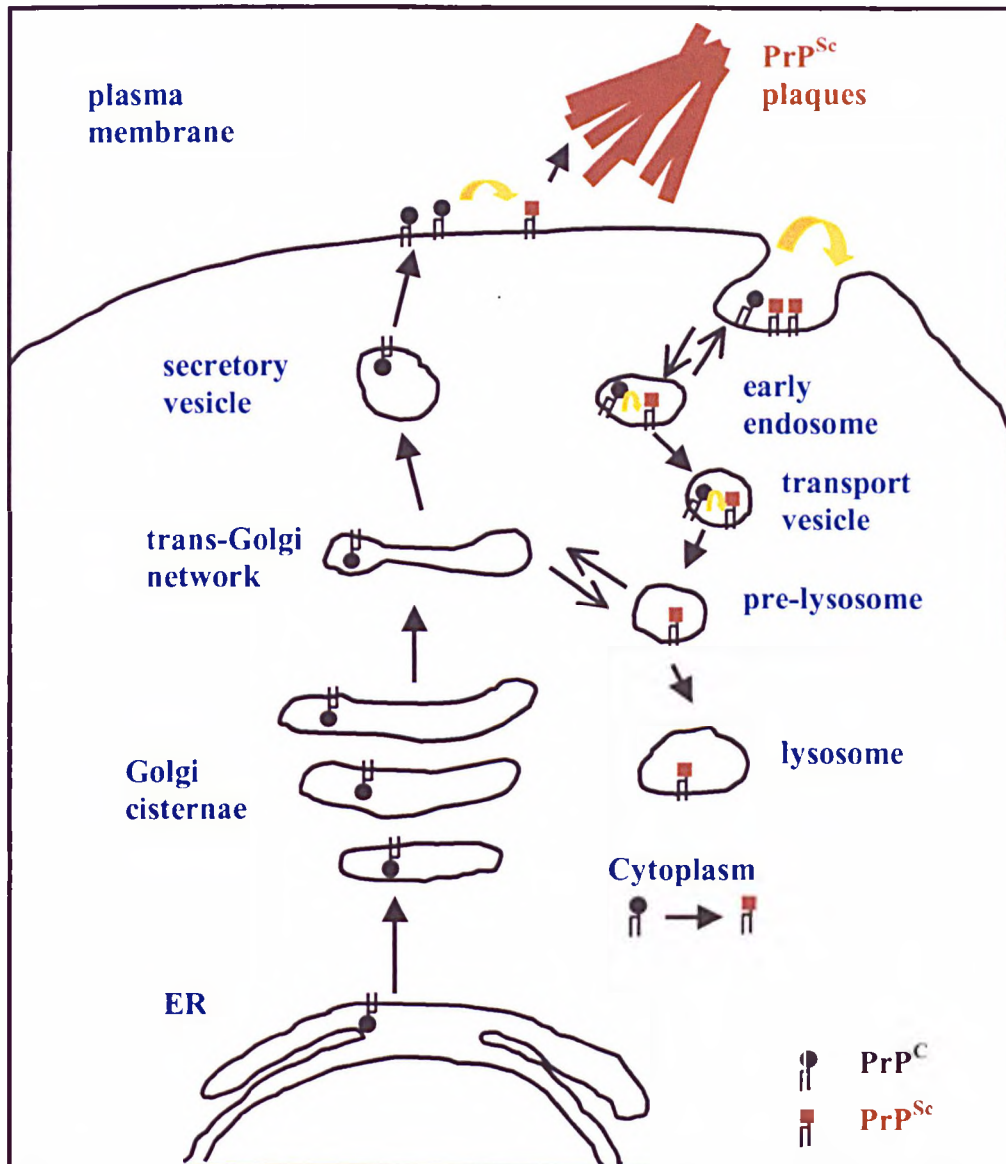
Figure 1.5: **Schematic representation showing the probable sites of PrP^{Sc} formation**. The major routes for cellular membrane trafficking in the biosynthetic pathway of PrP are shown. Both PrP isoforms are GPI-anchored to the cell surface. The plasma membrane and endocytic organelles have been implicated as the sites for PrP^{Sc} formation (reproduced from Caughey, 1991). Recent evidence suggest that the reducing environment of the cytoplasm may favour spontaneous conversion of PrP^{C} to PrP^{Sc} (Ma & Lindquist, 1999).

Recent evidence suggests that the reducing environment of the cytoplasm may favour the spontaneous conversion of PrP^C to PrP^{Sc} (Jackson *et al.*, 1999*b*; Ma & Lindquist, 1999). Ma & Lindquist (1999) showed that high level expression of mouse PrP in the cytoplasm of yeast cells led to the formation of a detergent insoluble protein with a distinct pattern of protease resistance that was identical to PrP^{Sc} isolated from the brains of diseased hamsters. These observations suggest that the expression of PrP in yeast cytoplasm, produced PrP in a PrP^{Sc}-like conformation. The above study also noted an increase in the formation of the PrP^{Sc}-like conformation under conditions, which prevented the glycosylation of PrP. These results suggest that blocking glycosylation and providing a reducing environment promotes conversion of PrP^C to a PrP^{Sc}-like form in mammalian cells. The above results led the authors to propose a mechanism whereby the mistargeting of PrP and/or retrograde transport of misfolded PrP from ER to the cytoplasm for deglycosylation and degradation could facilitate the initial production of PrP^{Sc}.

PrP during its cell cycle is therefore likely to encounter different cellular compartments with specific lipid compositions. A particular lipid environment may be more favouring towards the formation of PrP^{Sc}. In addition, the different cellular compartments may contain auxiliary factors such as proteins, which may participate in the conversion of PrP^C to PrP^{Sc}.

1.1.8.2   In vitro conversion

Despite considerable effort, it has not been possible to demonstrate the production of infectious particles *in vitro* (Kocisko *et al.*, 1994; Hill *et al.*, 1999; Horiuchi *et al.*, 2000). However, PrP^{Sc}, isolated from hamster infected brain tissue can convert PrP^C *in vitro* to a form that has proteolytic resistance, resembling that of

PrP^{Sc} (Kocisko *et al.*, 1994). In this experiment ^{35}S-labelled hamster PrP^C derived from uninfected tissue culture cells was treated with 3 M guanidine HCl and then diluted into a 50-fold excess of purified non-labelled PrP^{Sc}, a labelled proteinase K resistant form was produced, which was comparable to proteinase K digested PrP^{Sc} from scrapie-infected sources. The large molar excess of PrP^{Sc} used in the experiments made it difficult to demonstrate whether the *in vitro* conversion of PrP^C gave rise to infectivity and not only to a protease-resistant form.

1.1.9   Species barrier

The transmission of TSE disease from one species to another occurs much less efficiently, if at all, than within the same species and is characterised by prolonged incubation times. Factors that contribute to the species barrier are:

● *Differences in the amino acid sequence of PrP:* The introduction of SHaPrP gene into wild-type mice abrogated the species barrier (Prusiner *et al.*, 1990). The properties of the prions produced in the transgenic mice corresponded to SHaPrP^{Sc}. This provided evidence for the direct interaction of PrP^{Sc} with endogenous PrP^C during the conversion process. Differences in the amino acid sequences reduce the efficiency of such interactions. In general, PrP^{Sc} replication is most efficient with the shortest incubation times when PrP^{Sc} in the inoculum and PrP^C of the host are identical in their amino acid sequence.

● *Prion strains:* Different strains of PrP can be classified according to their specific phenotypic profiles such as incubation times, distribution of lesions in the brain, relative abundance of mono-, di-, and un-glycosylated PrP^{Sc} and electrophoretic mobility of the protease-resistant domains of PrP^{Sc}. Each strain has been suggested to be associated with different conformations of PrP^{Sc}, which can

convert its host's PrP^C into a likeness of itself (Bessen & Marsh, 1994; Bessen *et al.*, 1995; Telling *et al.*, 1996). Variations in the Asn-linked oligosaccharides may modify the conformation of PrP and this difference may also account for the selective targeting of PrP^{Sc} to particular areas of the brain (Prusiner & Scott, 1997).

• *Protein X*: The involvement of another host factor other than PrP^C in the conversion of PrP^C → PrP^{Sc} was proposed following studies with transgenic mice that expressed both mouse (*m*) and human (*h*) PrP^C. These mice were resistant to *h*PrP^{Sc}, whereas those expressing only *h*PrP^C were susceptible to infection (Telling *et al.*, 1995). Mice expressing both *m*PrP and chimeric human/mouse PrP genes (mouse PrP sequence containing human residues at positions 90–167) were also susceptible to *h*PrP^{Sc}. The results from the study led to the postulation of the involvement of another host protein. This protein is temporarily referred to as protein X. It was proposed that *m*PrP^C prevented the conversion of *h*PrP^C into PrP^{Sc} because mouse protein X had a greater affinity for *m*PrP^C than for *h*PrP^C. In contrast, *m*PrP^C had little effect on the conversion of chimeric *h/m* PrP^C because both share the same amino acid sequence at the carboxyl-terminus. Further studies revealed that substitution of human residues at the carboxyl-terminus of chimeric *h/m* PrP genes prevented the formation of PrP^{Sc} by possibly inhibiting the binding of protein X to PrP^C (Kaneko *et al.*, 1997).

1.1.10 Models for the conversion of PrP^C to PrP^{Sc}

Two models have been proposed to explain the conversion of PrP^C → PrP^{Sc}. Both predict that the infectious protein interacts directly with endogenous PrP^C to induce the conversion of the latter to generate more PrP^{Sc}. Passage of PrP^{Sc} from

one host to another might then constitute infection by initiating PrP^{Sc} formation in the new host.

- *Template-assisted model:* In this model PrP^C is partially unfolded to an intermediate (PrP^*) which is refolded under the influence of a PrP^{Sc} molecule, a process that would have to overcome a high activation barrier and requires the presence of the additional host factor protein X (Figure 1.6A). Infectivity would therefore rely on the ability of PrP^{Sc} to bind and catalyse the conversion of existing intermediate molecules (Prusiner *et al.*, 1998). Genetically inherited diseases resulting from mutations would increase the population of unstable intermedaite and/or enhance the rate at which this form spontaneously converts to PrP^{Sc}. The transition from PrP^C to monomeric PrP^{Sc} is the rate-limiting step and the reaction is a first-order process. This model is supported by studies in which the length of scrapie incubation time has been demonstrated to be inversely proportional to the level of PrP^C expression in the brain, which is consistent with a first-order process (Prusiner *et al.*, 1990; Carlson *et al.*, 1994).

- *Nucleation-dependent polymerisation:* This model proposes that PrP^C is in equilibrium with PrP^{Sc} (or a precursor) and that PrP^{Sc} is only stabilized when it adds onto a crystal-like seed or aggregate of PrP^{Sc}, which acts as a stable nucleus. In the absence of a pre-existing aggregate, the conversion between PrP^C and PrP^{Sc} is reversible. Aggregates of PrP^{Sc} would promote the conversion of PrP^C by binding to and stabilizing the otherwise unfavoured PrP^{Sc} conformation (Figure 1.6B). The rate-limiting step would be the formation of a stable nucleus and consequently the nucleation step has to proceed as a higher-order reaction (Jarrett & Lansbury, 1993).

25
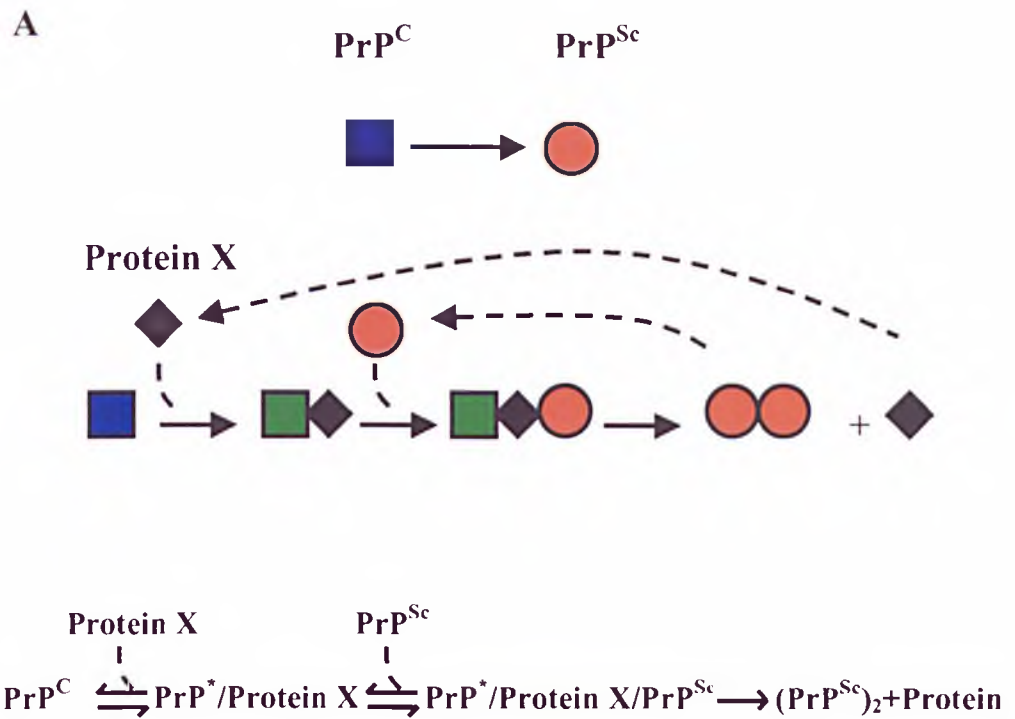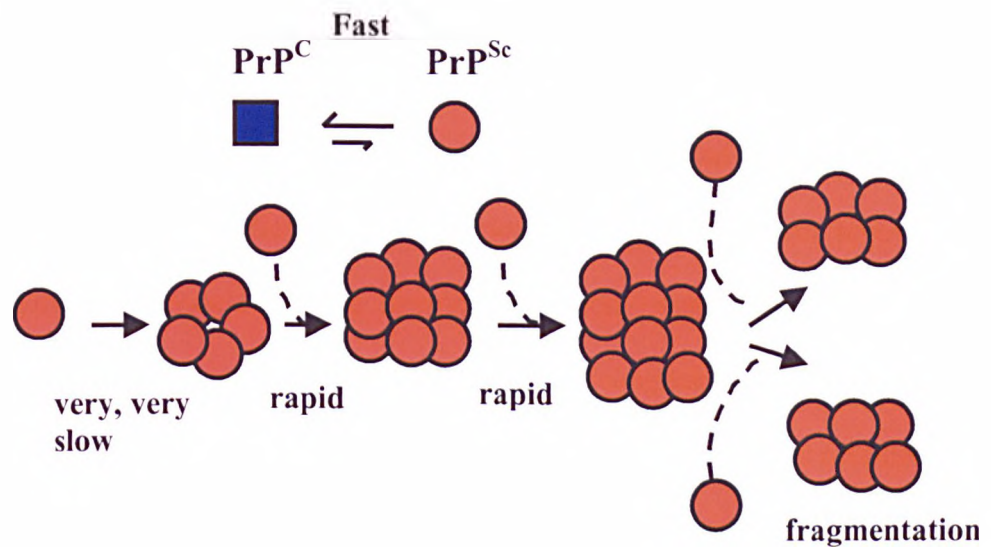
Figure 1.6: **Models for the conversion of PrP^C to PrP^{Sc}.** (A) Template-assisted model. In the initial step PrP^C binds to protein X to form a complex. Next PrP^{Sc} interacts with PrP*/protein X complex. PrP* is transformed to PrP^{Sc}, protein X is released and a dimer of PrP^{Sc} remains. (B) Nucleation-dependent polymerisation. PrP^C and PrP^{Sc} are in equilibrium strongly favouring PrP^C. PrP^{Sc} is only stabilised when it adds on to a crystal-like seed or aggregate. Seed formation is slow, but once present monomers can add on rapidly (adapted from Weissmann, 1999).

In vitro conversion studies exhibit many of the features of the nucleation-dependent model, such as dependence on exceeding a critical protein concentration for the initial formation of the aggregates and the kinetics displaying a lag phase (Jarrett & Lansbury, 1993). While studies with transgenic mice expressing both the SHaPrP transgene and endogenous *m*PrP gene show that PrP^{Sc} provides a template for directing prion replication (Prusiner *et al.*, 1990).

The propagation of PrP^{Sc} may actually involve a hybrid mechanism whereby a nucleation seed is initially formed, which then catalyses the conformational change of the normal cellular isoform (Horwich & Weissman, 1997).

1.1.11 Function of PrP^C

The function of PrP^C remains unresolved, mice lacking the PrP gene ($Prnp^{0/0}$) develop into adults without gross abnormalities (Büeler *et al.*, 1992; Manson *et al.*, 1994) but several differences between the PrP-null mice and controls have been noted, such as altered sleep-wake cycles (Tobler *et al.*, 1996) and synaptic behaviour (Collinge *et al.*, 1994). Mice of certain prion-deficient strain were reported to develop symptoms associated with neurodegeneration (ataxia and Purkinje cell degeneration) that led to their premature death (Sakaguchi *et al.*, 1996). A comparison of the knockout strategies used by the different groups later revealed that in the case where the mice became ill, additional deletions of the PrP genes as well as the open reading frame were made. Moore *et al.* (1999) discovered a second PrP-like gene located downstream of mouse PrP gene, the newly discovered gene was found to encode a protein of 179 amino acids termed doppel. In contrast to PrP, doppel is expressed at low-levels in adult central nervous system (CNS). However, the protein was found to be up regulated in the CNS of the ill $Prnp^{0/0}$ mice, leading

27

investigators to suggest that the additional deletions resulted in the over-expression of doppel in the CNS and as a consequence provoked neurodegeneration in the PrP-deficient mice.

Current work on understanding the physiological role of PrP^C at the cell surface has involved investigating its interaction with copper ions (Cu^{2+}). PrP^c has been shown to have a specific affinity for Cu^{2+} ions (Brown *et al.*, 1997*a*; Stöckel *et al.*, 1998; Miura *et al.*, 1999; Viles *et al.*, 1999). These studies suggest that copper ions bind to the octarepeat region of PrP^C. Mice brains had a much higher level of membrane-associated copper than PrP-deficient mice, which had a higher concentration of serum copper (Brown *et al.*, 1997*a*). PrP^C may be involved in the regulation of copper levels and therefore in the internalization of copper into the cytoplasm. Copper is an important catalytic constituent of oxidative enzymes, including superoxide dismutase, which protects cells from oxidative damage; the activity of these enzymes may be affected in prion diseases. In fact, it has been shown that in $Prnp^{0/0}$ mice, the activity of the anti-oxidant enzyme Cu/Zn superoxide dismutase is reduced (Brown *et al.*, 1997*b*) which indicates that PrP^C may play a role in cell resistance to oxidative stress (Milhavet *et al.*, 2000).

1.1.12 What causes cell death?

It remains unclear whether the accumulation of PrP^{Sc} or the loss of function of PrP^C is the cause of cell death. Hypotheses that have been proposed to explain neuronal cell death include: direct neurotoxic effect of PrP^{Sc} (Forloni *et al.*, 1993) which may also involve the destabilisation of the plasma membrane (Pillot *et al.*, 1997) and increased oxidative stress in neurons as a result of the depletion of PrP^C (Brown *et al.*, 1997*b*).

1.1.13 Yeast prions

A great deal of evidence supporting the protein-only or prion hypothesis comes from the non-Mendelian inheritance phenomenon in yeast. Two prion-like traits in yeast *Saccharomyces cerevisiae,* [PSI$^+$] and the [URE3] have been identified. The [PSI$^+$] phenotype propagates through a conformational change of an otherwise soluble protein, Sup35, to a β-sheet rich insoluble complex, as a consequent there is a loss of normal function (protein ensures that ribosomes terminate correctly at the end of the coding region). The inactive complexes have been shown to capture newly made Sup35 and convert it to the same form. Similarly [URE3] phenotype is caused by a conformational prion-like change of the Ure2 protein (nitrogen regulatory protein). The altered conformation encourages new Ure2 proteins to adopt the same prion-like structural state. No mutations in the genes encoding the two proteins have been identified (Glover *et al.*, 1997; Lindquist, 1997; Sparrer *et al.*, 2000).

1.2   Membranes

Membranes are asymmetric bilayer structures with a thickness between 60 (6 nm) to 100 Å (10 nm) and consist mainly of proteins and lipids. The functions that are performed by membranes are indispensable for life, they not only provide a barrier between different cellular compartments but also allow communication between them. Membranes are held together by non-covalent interactions, which enables lipid molecules and proteins to diffuse in the plane of the membrane.

1.2.1 Membrane proteins

Membrane proteins are responsible for most of the processes performed by membranes. Membrane proteins are classified into two groups according to their interactions with the lipid bilayer.

1.2.1.1 Integral membrane proteins

Integral membrane proteins are embedded in the lipid bilayer. The simplest integral membrane proteins will have a region of hydrophobic amino acid residues that span the membrane only once and hydrophilic residues will be in contact with the aqueous solvent on both sides. Other membrane proteins have several regions of hydrophobic amino acid residues, which span the membrane more than once.

1.2.1.2 Peripheral proteins

Peripheral proteins are bound to membranes primarily by electrostatic interactions. The electrostatic interactions may be disrupted by the addition of salt or by altering the pH. Peripheral membrane proteins bind to the surface of integral membrane proteins or with other components of the membrane surface. Other proteins may be anchored to membranes by lipids, which are covalently attached to them.

Fatty acids such as myristate and palmitate are attached to the amino-terminus of a number of proteins, which participate in their binding to the surface of cell membranes.

A diverse group of proteins are anchored to the external surface of plasma membranes *via* the attachment of a complex glycosylphosphatidylinositol (GPI)

anchor to their carboxyl-terminal. Examples of GPI anchored proteins are PrP (Stahl *et al.*, 1987), placental alkaline phosphatase and acetylcholinesterase (Ferguson & Williams, 1988). An advantage of the GPI anchor over that provided by transmembrane domains is that it allows the protein to diffuse much more rapidly within the plane of the membrane. Specific enzymes can be used to release the protein from the cell surface, which suggests that anchoring may be regulated. GPI-anchored proteins are found in detergent-insoluble raft domains within the plasma membrane that are rich in cholesterol and sphingolipids. These lipid domains are insoluble in non-ionic detergents such as Triton X-100 at 4 °C and solubilised if warmed to 37 °C (Brown & Rose, 1992; Friedrichson & Kurzchalia, 1998).

1.2.2 Lipid composition of the plasma membrane

The major components of biological membranes, lipids, are amphiphilic molecules with a hydrophilic head group and hydrophobic hydrocarbon chains (fatty acid chains). All organelles possess more or less the same lipid groups; however, the amounts of the different lipids vary among the organelles and are found to change with age.

• *Glycerophospholipids constitutes the main lipid mass of eukaryotic cell membranes.* This group of lipids is derived from glycerol, a three-carbon alcohol. The fatty acid chains in glycerophospholipids usually contain between 14- and 24-carbon atoms. The 16- and 18-carbon fatty acids are commonly found in membranes. The fatty acids can be saturated or contain one or more double bonds, all in *cis* configuration. Structures of fatty acids that are found in mammalian membranes are presented in Figure 1.7. The majority of glycerophospholipids found in biological membranes are *1, 2*-diacyl-*sn*-glycerophospholipids consisting of a

31

glycerol backbone, two fatty acid chains and an additional group is attached to the phosphate, and this is usually one of several alcohols (Figure 1.8). In addition to the fatty acid chains the alcohol headgroups are responsible for the properties of glycerophospholipids. For example, negatively charged glycerophospholipids have glycerol (PG), inositol (PI) or serine (PS) as the headgroup. Zwitterionic glycerophospholipids carry both a positive and negative charge *i.e.* have no net charge and contain choline (PC) or ethanolamine (PE) headgroup (Figure 1.8). The acyl chain in the *sn-2* position is typically unsaturated in most glycerophospholipids, whereas the chain in the *sn-*1 position is normally saturated.

The other lipid constituents of biological membranes are:

• *Sphingolipids:* The backbone of this group of lipids is derived from sphingosine, an amino alcohol that contains a long, unsaturated hydrocarbon chain. Unlike with unsaturated fatty acids, the double bond in sphingosine is in the *trans* configuration. A commonly occurring sphingolipid is sphingomyelin, the structure of which is shown in Figure 1.9. The amide-linked fatty acid in brain is predominately stearic acid (18:0) (Agranoff & Hajra, 1994).

• *Glycolipids are sugar containing lipids:* In mammalian cells glycolipids are also derived from sphingosine. Instead of a phosphoryl choline group attached to the hydroxyl group of sphingosine, as in sphingolipids, one or more sugars are attached (Figure 1.9).

• *Cholesterol:* This sterol is abundant in the plasma membrane of mammalian cells (Figure 1.9).
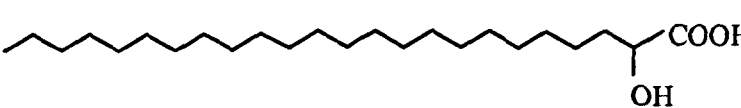
Structure	Name	Abbreviation
	Lauric acid	12:0
	Myristic acid	14:0
	Palmitic acid	16:0
	Stearic acid	18:0
COOH	Oleic acid	18:1 (Δ^9)
COOH	Linoleic acid	18:2 ($\Delta^{9,12}$)
COOH	Linolenic acid	18:3 ($\Delta^{9,12,15}$)
COOH	Arachidonic acid	20:4 ($\Delta^{5,8,11,14}$)
COOH	Lignoceric acid	24:0
COOH	Nervonic acid	24:1 (Δ^{15})
COOH / OH	Cerebronic acid	24:0

Figure 1.7: **Structures of commonly occurring fatty acids.** The "Δ^x" gives the position of the double bond(s) (Agranoff & Hajra, 1994). Ionised forms of the lipid are referred to as myristate, palmitate, *etc.*

33

Typical structure of a glycerophospholipid (1-palmitoyl-2-oleoyl-sn-glycero-3-phosphoR)
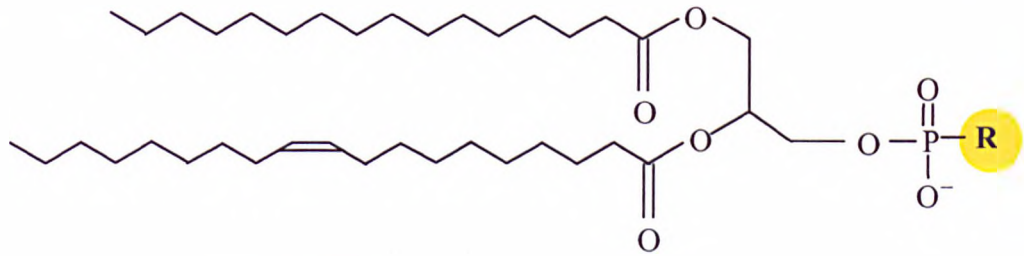
Negatively charged lipids, R=
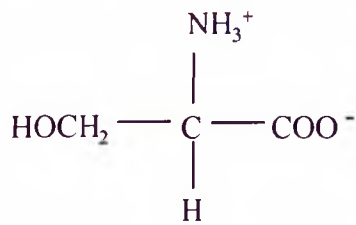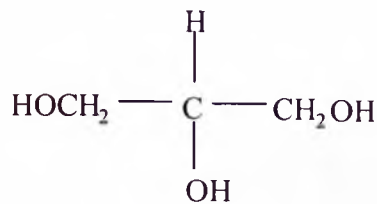
Serine (PS)   Glycerol (PG)   Inositol (PI)
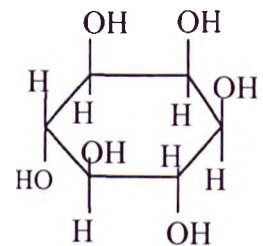
Zwitterionic lipids, R=
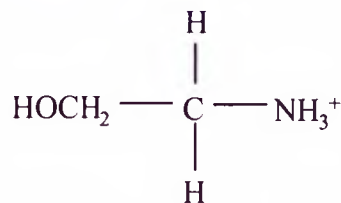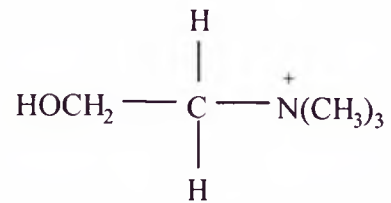
Ethanolamine (PE)   Choline (PC)

Figure 1.8: **Structures of the commonly occurring glycerophospholipids in mammalian cells.**

Sphingomyelin

Glycolipid: cerebroside

Cholesterol
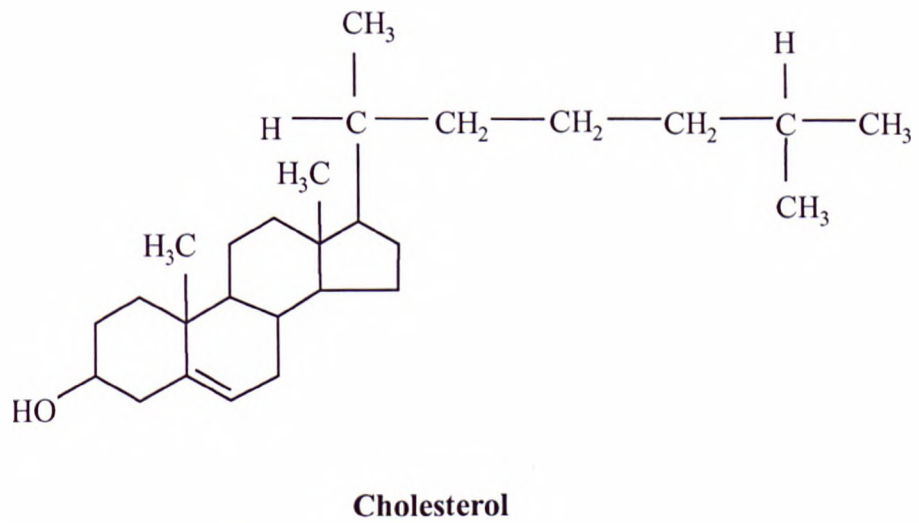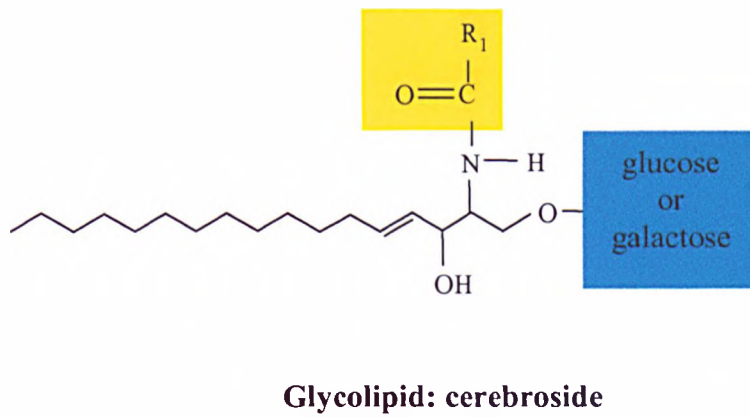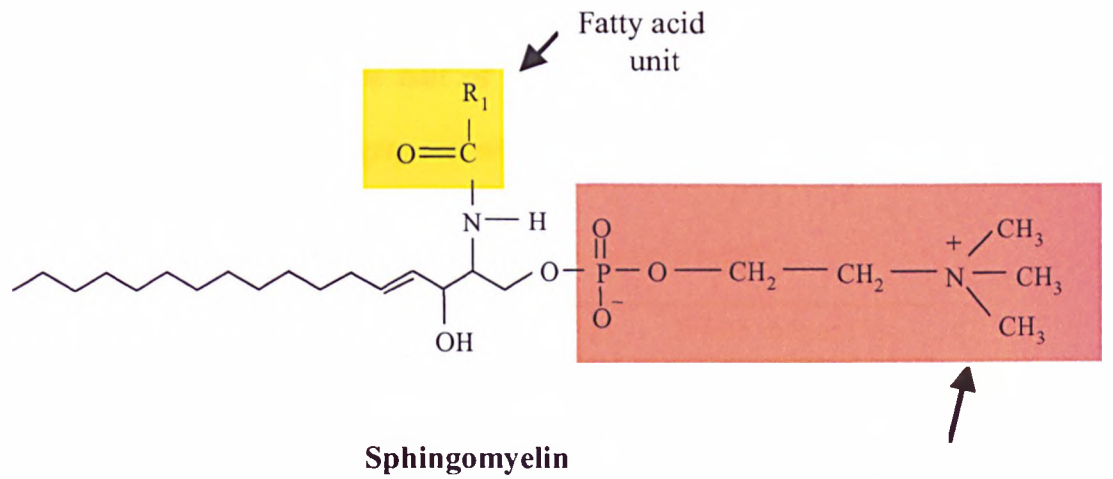
Figure 1.9: **Structures of other lipid constituents of membranes.**

Lipids make up about one half of the brain tissue dry weight. Table 1.3 presents the lipid composition of gray and white matter of adult human brain.

Table 1.3: Lipid composition of normal adult human brain[a]

Constituent	Gray matter (%)	White matter (%)
Cholesterol	22	28
Total Phospholipid[b]	69	48
PE	27	24
PS	9	8
PC	30	15
PI	3	1
Sphingomyelin	7	8
Galactocerebroside sulphate	2	5
Galactocerebroside	5	20

[a]Agranoff & Hajra, 1994. [b]Phospholipid fractions include plasmalogen present as PE and PC with a ratio of 4:1 in white matter and 1:1 in gray matter.

1.2.3 Lipid-lipid interactions

The formation of a lamellar bilayer is the common structure of lipids in an aqueous environment, however amphipathic molecules can aggregate in the aqueous phase to form a variety of other phases including, micelles, inverted hexagonal phases and cubic phases (Epand, 1998). The driving force behind the self-assembly of lipid molecules into bilayer structures are hydrophobic interactions, which occur among non-polar groups when present in aqueous solution. Hydrophobic interactions arise because interactions between polar water molecules and non-polar groups, such as the hydrocarbon tail of glycerophospholipids are unfavourable. Van der Waals attractive forces between the hydrocarbon tails and electrostatic and

hydrogen-bonding attractions between the polar headgroups and water molecules stabilise the bilayer structure.

1.2.4 Physical properties of lipids and their effects on bilayer structure

The fatty acid chains of glycerophospholipids and sphingolipids can exist in an ordered, rigid gel-state or in a relatively disordered, liquid-crystalline state. For pure lipids these states can inter-convert at a well-defined transition temperature. The transition temperature is dependent on the degree of unsaturation. A *cis* double bond, such as that present in oleic acid, introduces a bend in the fatty acid chain, which interferes with the packing of lipids within the bilayer and results in lowered transition temperatures. Whereas in saturated lipids, the straight fatty acid chains interact favourably with one another, as a result the lipids are densely packed within membranes. The length of the fatty acid chain also influences the transition temperature; long hydrocarbon chains interact more strongly with each other than shorter chains, resulting in higher transition temperatures.

Cholesterol is intercalated between the lipid hydrocarbon chains with its long axis perpendicular to the plane of the membrane. The —OH group of cholesterol hydrogen bonds to oxygen atom of the C=O group of a glycerophospholipid head group, the hydrocarbon tail is positioned in the non-polar core of the bilayer. Cholesterol has a profound effect on the physical properties of glycerophospholipid bilayers. It moderates the fluidity of membranes. The presence of cholesterol can prevent the crystallisation of the hydrocarbon chains by increasing fluidity of the hydrocarbon fatty acid chains when the system is below the phase transition. However, an opposite effect of cholesterol is found when the system is above the phase transition. High enough concentrations of cholesterol can sterically reduce

motions of the hydrocarbon chains, thus decreasing fluidity. The heterogeneity of cell membranes with regard to both the polar headgroups of glycerophospholipids and non-polar fatty acids, as well as the presence of cholesterol, maintains cell membranes in a fluid state over a broad range of temperatures. In this state the membrane components are very mobile within the plane of the bilayer (Jacobson *et al.*, 1995).

1.2.5 Membrane structure

The inner and outer surfaces of membranes have different lipid compositions making them structurally and functionally asymmetric. The exoplasmic side of the plasma membrane contains mostly PC and sphingolipids, whereas PS and PE are on the cytoplasmic side, which means that the outerleaf of the plasma membrane is mainly neutral while the inner is negatively charged. Cholesterol is present in large amounts in both sides of the membrane (van Meer, 1989). There appears to be two pools of cholesterol in cell membranes, one which found in the fluid PC regions and another that is associated with sphingolipid to form phase-separated domains. A model for the organisation of cholesterol-sphingolipid rafts is presented in Figure 1.10. The principle that governs the formation of raft lies in the high phase temperatures of sphingolipids and the preference of cholesterol to interact with this lipid (Harder & Simons, 1997). Rafts have been isolated from a wide variety of cell types, which include muscle cells, neurons and endothelial cells (Brown & London, 1998), they also appear to exist in endocytic compartments (Kobayashi *et al.*, 1998).
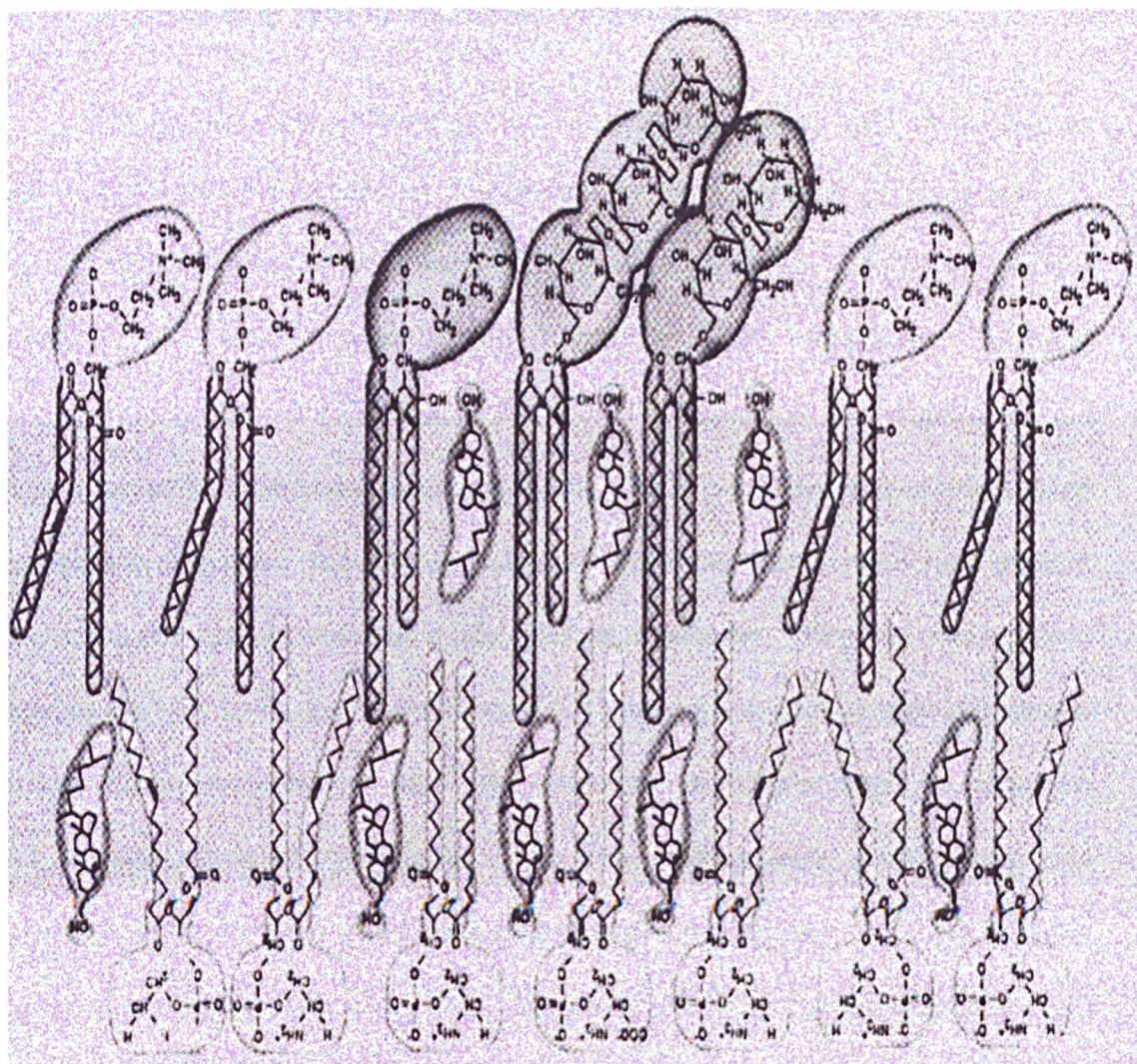
Figure 1.10: **Model of the lipid organisation of raft domains.** The outer leaflet of membranes contains sphingomyelin, glycosphinolipids, which are shown in dark grey and PC lipids (medium grey). Cholesterol intercalates between the lipid fatty acid chains of sphingomyelin and glycosphingolipids. The tight acyl chain packing is probably responsible for the detergent insolubility of lipid rafts and the proteins contained within them. PC-rich regions are less densely packed and more fluid than the cholesterol and sphingomyelin domains. The inner leaflet contains PE, PC and cholesterol (repoduced from Harder & Simons, 1997).

1.2.6 Interaction of lipid-anchored proteins with lipid membranes

Studies with lipid-anchored proteins suggest that protein-lipid interactions as well as lipid-lipid interactions are responsible for the attachment of the proteins to the cell surface. Electrostatic interactions between positively charged amino acid residues in some myristoylated proteins and negatively charged glycerophospholipids are necessary for the attachment of the proteins to the membrane surface (McLaughlin & Aderem, 1995). For example myristoylated alanine-rich C-Kinase substrate (MARCKS) is a peripheral membrane protein located on the cytoplasmic side of the plasma membrane. Membrane association requires both the hydrophobic insertion of the lipid anchor into the lipid bilayer and electrostatic interactions between a region containing positively charged amino acids and negative glycerophospholipids. The lipid anchor alone does not provide sufficient energy to anchor the protein to the membrane (Peitzsch et al., 1993). GPI-anchored neuronal glycoprotein, Thy-1 has also been shown to make direct contact with the plasma membrane (Homans et al., 1988).

1.3 Aims

The availability of recombinant mammalian prion proteins has enabled structural and biophysical studies to be performed. The three-dimensional structure of recombinant mammalian prion proteins have been solved by nuclear magnetic resonance (NMR) spectroscopy (Riek et al., 1996; Donne et al., 1997; James et al., 1997; García et al., 2000; Zahn et al., 2000). Biophysical studies have been directed to decipher the mechanism of PrP conversion (Swietnicki et al., 1997; Zhang et al., 1997; Hornemann & Glockshuber, 1998; Jackson et al., 1999a,b; Wildegger et al., 1999). The above solution studies have provided valuable information, which has

helped our understanding of the conformational transition associated with the conversion of $PrP^C \rightarrow PrP^{Sc}$. However, PrP in cells is localised to cholesterol-sphingolipid rafts. The lipid environment of PrP appears to play a crucial role in its cell cycle. It is probable that the transformation of PrP^C to PrP^{Sc} occurs within these raft domains and therefore lipid interactions are likely to feature in the formation and propagation of PrP^{Sc}.

The aim of this thesis was to provide a detailed insight into the biophysical properties of membrane-bound PrP. The interaction of recombinant Syrian hamster (SHa) PrP residues 90–231 in a conformation resembling PrP^C, with a range of lipid membrane systems was investigated at both pH 7, to represent the pH surrounding the plasma membrane, and pH 5, which models the acidic environment in endosomes. The plasma membranes and endocytic organelles have been proposed as cellular sites for PrP^{Sc} formation. This PrP segment corresponds to the protease-resistant core of PrP^{Sc} and contains the structured domain of PrP.

The specific points addressed in this thesis were:

• binding properties of SHaPrP (90–231) to various model lipid membranes, at pH 5 and 7.

• structural changes in SHaPrP (90–231) upon binding to lipid membranes, at pH 5 and 7.

• binding/insertion kinetics of SHaPrP (90–231) to lipid membranes.

• changes in membrane integrity and/or permeability upon binding of SHaPrP (90–231).

1.4 Layout of this thesis

Chapter 2 will give a background to the spectroscopic techniques used. Chapters 3 through to 6 describe the experimental work for this thesis and each starts with a brief introduction relevant to the work contained within it. Each chapter has separate Material & Methods, Results and Discussion sections. The expression purification and subsequent characterisation of recombinant PrP is discussed in Chapter 3. The binding of recombinant PrP to lipid membranes monitored by fluorescence spectroscopy is presented and discussed in Chapter 4. In Chapter 5 changes in the structure of PrP upon interaction with lipid membranes are discussed. Binding/insertion kinetics of PrP and membrane integrity upon PrP binding are examined in Chapter 6. The final chapter (Chapter 7) discusses the general conclusions that can be drawn from the work described and discussed in this thesis.

Chapter 2:   Biophysical Techniques

This chapter will introduce the main biophysical techniques that were used to investigate the interaction of SHaPrP (90–231) with lipid membranes. The techniques are based upon the absorption or emission of electromagnetic radiation. The output is generated in the form of a spectrum, which displays some function of radiant intensity versus wavelength or wavenumber.

2.1   Electromagnetic Radiation

2.1.1   General properties of electromagnetic radiation

Electromagnetic radiation emanating from a source consists of electric and magnetic fields that oscillate at right angles to each other and to the direction of propagation. Figure 2.1A shows a single ray of electromagnetic radiation in which the oscillations of either the electric or magnetic fields lie within a single plane. Since the electric and the magnetic components are always perpendicular to each other, it is sufficient, to consider only the electric component when describing the electromagnetic wave, however the wave parameters will also apply to the magnetic component (Figure 2.1B).

Wave parameters of the electric component:

• *Amplitude, A*: length of the electric vector at a maximum in the wave.

• *Period, p*: time in seconds required for the passage of successive maxima or minima through a fixed point in space.

• *Frequency, ν*: number of oscillations of the field that occur per second and is equal to $1/p$. Unit of frequency is Hertz (Hz); $1\ Hz = 1\ s^{-1}$.

A
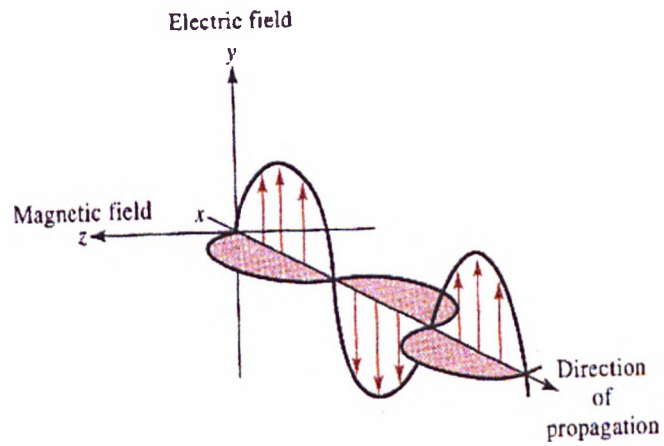
B
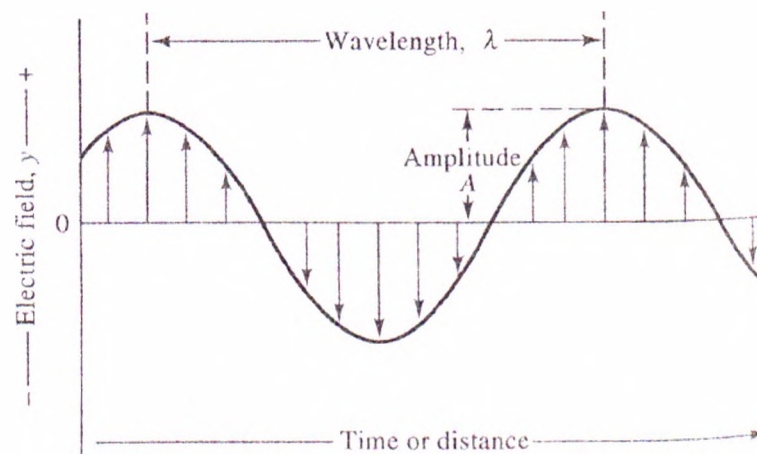
Figure 2.1: **Wave representation of electromagnetic radiation.** (A) Electric and magnetic fields at right angles to one another and to the direction of propagation. (B) Two-dimensional representation of the electric vector (reproduced from Skoog *et al.*, 1996).

- *Wavelength, λ:* linear distance between any two equivalent points on successive waves.

- Wavenumber, $\bar{v}$: reciprocal of the wavelength in centimetres. The wavenumber is a useful unit because, in contrast to wavelength, it is directly proportional to the frequency (and thus the energy) of radiation.

$$\bar{v} = \frac{1}{\lambda} \qquad \text{(Eq. 2.1)}$$

The amplitude and frequency of the wave are determined by the intensity of the radiation and the energy associated with it respectively. Thus,

$$I \propto A^2$$

and

$$E \propto v$$

where I is the intensity and E the energy. Frequency and wavelength are related by the expression

$$v = \frac{c}{\lambda} \qquad \text{(Eq. 2.2)}$$

where c is the velocity of propagation of the wave in a vacuum and is independent of frequency. The energy of radiation and frequency are *directly* proportional but energy and wavelength are *inversely* related.

To understand many of the interactions between radiation and matter, it is necessary to view electromagnetic radiation in terms of packets of energy called *photons*. The energy of a photon depends upon the frequency of radiation and is given by

$$E = hv \qquad \text{(Eq. 2.3)}$$

where h is Planck's constant (6.63×10^{-34} J.s). Equation 2.3 can be re-written in terms of wavelength and wavenumber as

$$E = \frac{hc}{\lambda} = hc\bar{v}$$ (Eq. 2.4)

Wavenumber and frequency are directly proportional to energy.

2.1.2 Polarisation of electromagnetic radiation

Electromagnetic light can be described as unpolarised if the electric component oscillates in any direction perpendicular to the direction of propagation. By placing a polariser between the radiation source and sample the electric component oscillates in the same plane and the beam of radiation is now polarised. The three spectroscopic techniques described here are fluorescence, Fourier transform infrared (FTIR) and circular dichroism (CD). In the first two unpolarised light is absorbed by the sample however, in CD the electromagnetic radiation is circularly polarised.

• *Circularly polarised light:* Plane linearly polarised light consists of right- and left-circularly polarised beams of equal intensity. For the formation of circularly polarised light the plane linearly polarised beam is split into two plane polarised beams that are at right angles to each other and 90° out of phase. The addition of the two beams, which are now 90° out of phase results in the electric vector moving in a circular manner as it travels in the z direction. A right-handed-circularly polarised beam is shown in Figure 2.2. By alternating the applied voltage of an electric field, the emergent beam can be made to alternate between left- and right-circularly polarised light (Woody, 1996).
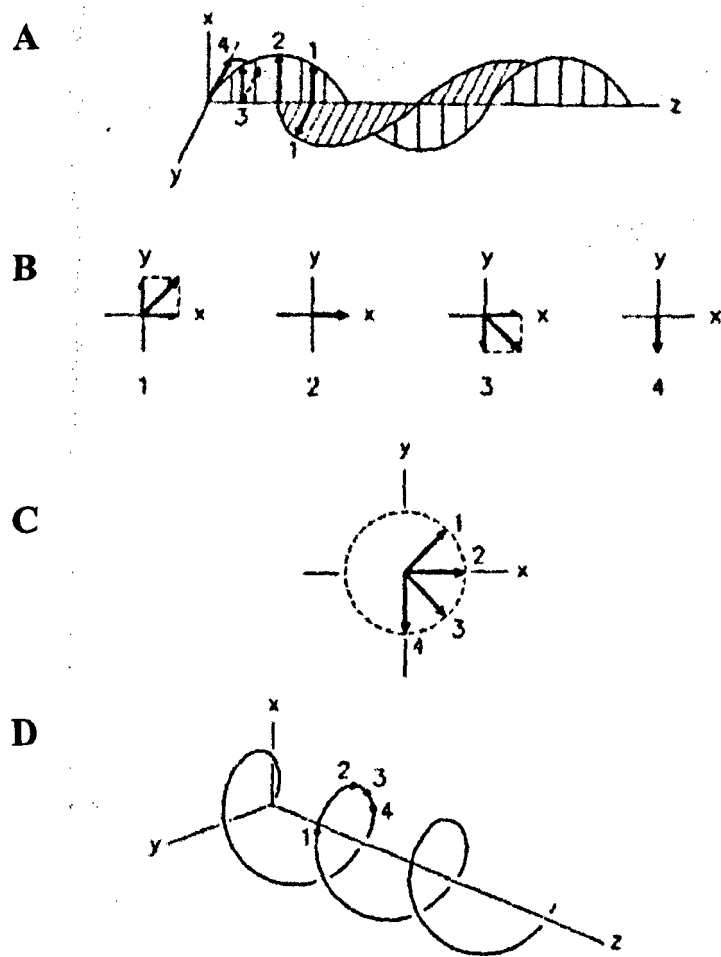
Figure 2.2: **A right-handed-circularly polarised beam.** (A) The electric component of perpendicular polarised beams 90° out of phase. (B) The x and y components together with their resultants are shown at points along the z-axis which are labelled 1–4 in (A). (C) The vector sums when positioned onto a plane normal to the z direction show that the tip of the electric component follows a circular path when viewed along the direction of propagation, looking toward the light source. (D) Right-circularly polarised light, which shows electric component forming right-handed helix along the direction of propagation and appears to rotate in a clockwise direction. In left-circularly polarised light, the tip of the electric vector forms a left-handed helix (reproduced from Woody, 1996).

2.1.3 The electromagnetic spectrum

The electromagnetic spectrum is made up of a wide range of wavelengths and frequencies (and thus energies). The different regions of the spectrum are shown in Figure 2.3 and Table 2.1 lists the wavelength and wavenumber ranges for different regions of the spectrum that are commonly used in the analysis of proteins and peptides.

Table 2.1: Common spectroscopic methods based on electromagnetic radiation

Type of Spectroscopy	Wavelength Range	Wavenumber Range (cm^{-1})	Type of Quantum Transition
X-Ray absorption, emission, and diffraction	0.1–100 Å	—	Inner shell electrons
Ultraviolet (UV) and visible absorption, emission and fluorescence	180–780 nm	5×10^4– 1.3×10^4	Valence electrons and bonding electrons
Infrared (IR) absorption and Raman scattering	0.78–300 μm	1.3×10^4– 3.3×10^1	Rotation/vibration of molecules
Electron spin resonance	3 cm	0.33	Spin of electrons in a magnetic field
Nuclear magnetic resonance	0.6–10 cm	1.7×10^{-2}– 1×10^3	Spin of nuclei in a magnetic field
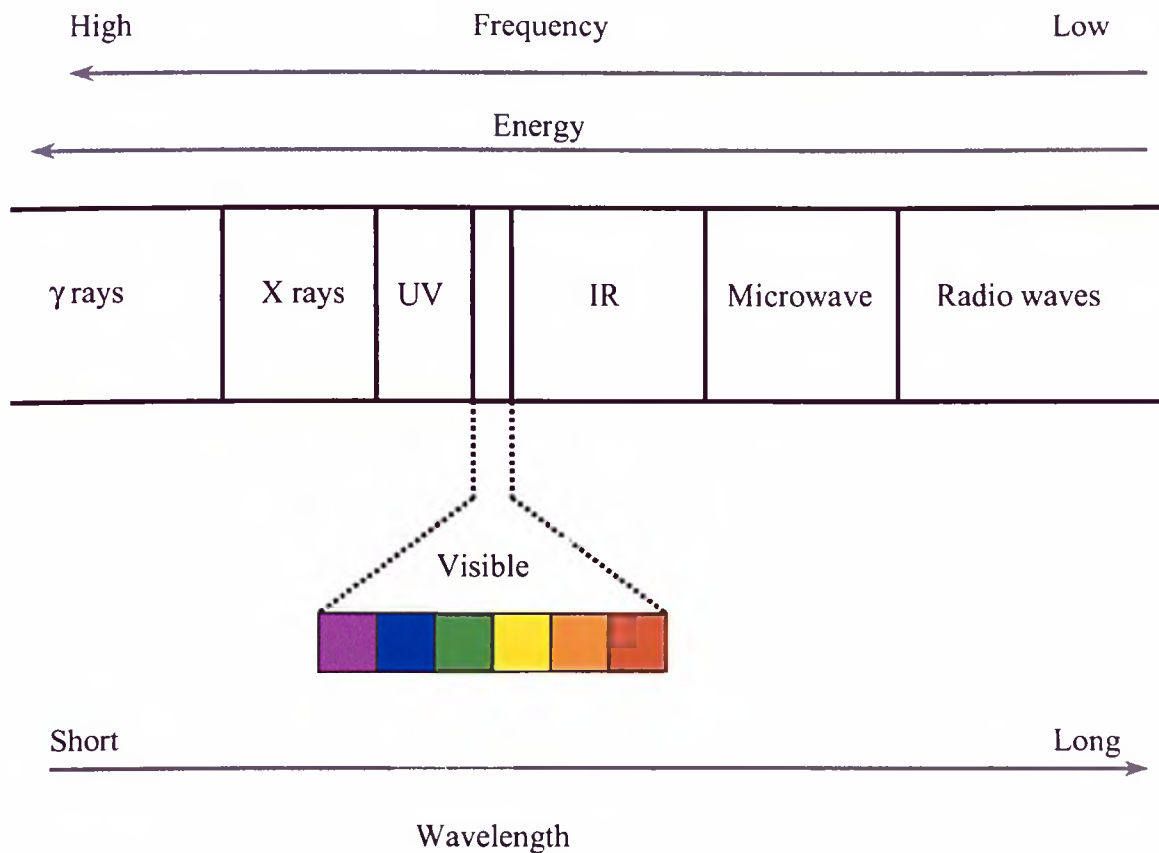
Figure 2.3: **The electromagnetic spectrum.** The radiation energy increases from the radio wave end of the spectrum (10^{-17} J) to the γ-ray (10^{-13} J) end. Frequency ranges from 10^{0} Hz at the radio wave end of the spectrum to 10^{24} Hz at the γ-ray end of the spectrum and wavelength ranges from 10^{3} to 10^{-11} cm, respectively.

2.1.4 Absorption of electromagnetic radiation

Absorption is a process in which a substance in a transparent medium selectively attenuates (decreases the intensity) certain frequencies of electromagnetic radiation. Quantum theory states that every elementary particle (atom, ion, or molecule) has a unique set of energy states, the lowest being the ground state. Absorption of a photon of radiation by the elementary particle only occurs if the energy of the photon matches exactly the energy difference between the ground state and one of the higher energy states of the particle. When this occurs the energy of the photon is transferred to the atom, ion, or molecule, converting it to the higher energy state, which is now known as the excited state (M^*).

$$M + h\nu \rightarrow M^*$$
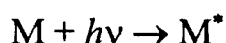
After a brief period (10^{-9} to 10^{-6} s) the excited species relaxes to the ground state, as it does it transfers its excess energy to other atoms or molecules in the medium. The process causes a small rise in the temperature of the surrounding. Relaxation may also occur by the fluorescent or phosphorescent emission of radiation.

2.2 The Theory of Fluorescence

2.2.1 Fluorescence, quantum yields and lifetimes

A ground state species is raised to a higher electronic state following the absorption of energy from electromagnetic radiation in the UV-visible region of the spectrum (180–780 nm). If the electron in the higher energy orbital has the opposite spin orientation to the electron in the ground state the electrons are paired and the electron is not required to change its electron spin orientation to return to the ground

state, this is a singlet state (S). Fluorescence is the emission, which results from the return of a paired electron to the ground state from a higher energy orbital. In a triplet state (T) the electrons are unpaired, *i.e.* their spins have the same orientation and the return of an electron in the triplet state from a higher energy orbital requires a change in the spin orientation. Phosphorescence is the emission from the transition of unpaired electron as it returns to the ground state. The absorption and emission properties of a fluorophore (fluorescent substance) can be illustrated in energy level diagrams (see below). This diagram shows the different processes that usually occur following light absorption. The transitions that occur as a result of light absorption are represented as vertical lines. Absorption of light is too fast for significant displacement of nuclei but adequate for the redistribution of electrons (10^{-15} sec).
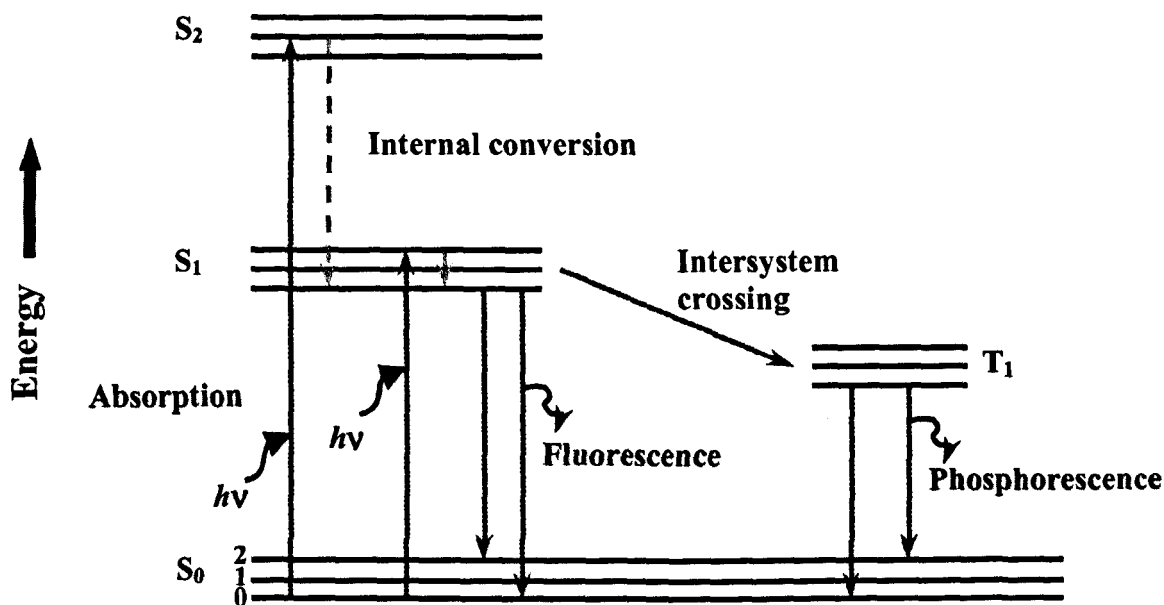
S_0, S_1 and S_2 are the ground, first and second electronic states, respectively. Within each electronic state there exists a number of vibrational energy levels denoted 0, 1, and 2 in S_0. At room temperature, the fluorophore is in the lowest

electronic, *i.e* ground state and vibrational energy level (0). The Boltzmann distribution describes the number of molecules in 0 and 1 vibrational states and the ratio R of molecules in each state is given by the expression

$$R = e^{-\Delta E/kT}$$

<div align="right">(Eq. 2.5)</div>

where ΔE is the energy difference, k is the Boltzmann constant, and T is the temperature in K. The energy difference between the states S_0 and S_1 is too large for any fluorophore to populate the higher electronic state as a result of thermal energy.

Fluorescence occurs via the following process: When a solution of a fluorophore is illuminated with a beam of light of wavelength λ, the molecules absorb energy from the beam if the photon energy matches the energy difference between the ground level and one of the upper levels (ΔE). Each molecule absorbs one photon at a time and during the absorption process a molecule undergoes a transition from the ground state to one of the upper states. Light absorption excites the fluorophore into a higher vibrational level of either S_1 or S_2. With most molecules this is followed by relaxation via internal conversion to the lowest vibrational level of S_1. This occurs at a rate of 10^{-12} sec and is complete before fluorescent emission begins. This means that fluorescence emission occurs from a thermally equilibrated state. Fluorescence displays a number of general characteristics. There is a shift to longer wavelengths (*i.e.* lower energy) of the emission relative to the absorption wavelength (Stokes' shift). This loss is caused by the rapid decay to the lowest S_1 vibrational level. The rapid relaxation from higher electronic and vibrational levels to the lowest vibrational level of S_1 is also responsible for the observed emission spectrum of a fluorophore remaining the same irrespective of the excitation wavelength. Further energy losses are due to the return

of electron to the lowest vibrational level of S_0. In addition to these effects, fluorophores can display further Stokes' shifts due to the solvent environment.

The quantum yield (Q) of a fluorophore is the ratio of the number of photons emitted to the number absorbed and can be defined as

$$Q = \frac{\Gamma}{\Gamma + k} \qquad \text{(Eq. 2.6)}$$

where Γ is the emissive rate of the fluorophore and k is the rate of radiationless decay to S_0, both Γ and k depopulate the excited state.

The lifetime (τ) of an excited state is the average time the fluorophore spends in the excited state before emission and return to the ground state. Lifetime can be defined

$$\tau = \frac{1}{\Gamma + k} \qquad \text{(Eq. 2.7)}$$

Generally, fluorescence lifetimes are near 10 nsec. The value given for the lifetime of fluorescence is an average of the time spent in the excited state.

The intrinsic lifetime of a fluorophore is the lifetime in the absence of nonradiative process and is defined as

$$\tau_0 = \frac{1}{\Gamma} \qquad \text{(Eq. 2.8)}$$

From these equations the relationship between quantum yield and lifetime can be calculated

$$Q = \frac{\tau}{\tau_0} \qquad \text{(Eq. 2.9)}$$

The quantum yield and lifetime of the fluorophore can be modified by any factors, which affect either of the rate constants.

2.2.2 Solvent effects on the fluorescence spectra

The fluorescence emission spectra of fluorophores are sensitive to the polarity of their surrounding environment. In general, a decrease in solvent polarity of the fluorophore results in a shift of the emission spectrum to shorter wavelengths (blue shift). Conversely, an increase in solvent polarity causes a shift of the emission maximum to longer wavelengths (red shift) and a possible reduction in the quantum yield of the fluorophore. The loss of energy that occurs between absorption and emission of fluorescence or Stokes' shifts can be a result of general and specific solvent effects. General solvent effects on the fluorescence spectra result from the redistribution of electrons in the surrounding solvent molecules induced by altered (generally increased) dipole moment of the excited fluorophore. Generally the excited states of fluorophores possess dipole moments (μ^*) which are larger than in the ground state (μ). This is because light absorption occurs in a time scale that is too short for the displacement of nuclei, but long enough for the redistribution of electrons. The absorption of a photon of electromagnetic radiation by a fluorophore therefore results in the instantaneous formation of a dipole, which would perturb the environment surrounding the fluorophore. The solvent responds by reorganisation around the fluorophore subsequent to excitation. This process is called solvent relaxation and results in a shift of the emission spectrum to longer wavelengths (i.e less energy).

The Lippert equation describes the general solvent effects on the emission spectra of fluorophores:

$$\bar{\nu}_a - \bar{\nu}_f \approx \frac{2}{hc} \left(\frac{\varepsilon - 1}{2\varepsilon + 1} - \frac{n^2 - 1}{2n^2 + 1} \right) \frac{(\mu^* - \mu)^2}{a^3} + A \quad \text{(Eq. 2.10)}$$

54

where h is Planck's constant, c is the speed of light, and a is the radius of the cavity in which the fluorophore resides, n and ε are the refractive index and dielectric constant of the solvent, respectively and A, a constant. Absorption and emission wavenumbers are $\bar{v}_a$ and $\bar{v}_f$, respectively. Briefly, an increase in n will decrease the energy loss by allowing the ground and excited states to be instantaneously stabilised by movement of electrons within the solvent molecules. This decreases the energy difference between the ground and excited states. Whereas an increase in ε results in an increase in $\bar{v}_a - \bar{v}_f$ because the reorientation of the solvent dipoles requires the movement of the entire solvent molecule and not just electrons. Non-polar solvents, such as hexane, do not possess a dipole moment. Hence there are no dipoles to reorient around the excited state of the fluorophore. However, even in these cases the absorption and emission maxima do not coincide closely because small amount of energy is always rapidly dissipated to solvents. This sensitivity of the Stokes' shift to solvent polarity is the reason why fluorescence emission spectra are frequently used to estimate the polarity of the environment surrounding the fluorophore.

Specific solvent effects are results of chemical interactions between the fluorophore and the solvent molecules, such as hydrogen bonding. Both general and specific solvent interactions result in spectral shifts. General solvent effects are expected to always be present. In contrast, specific solvent effects will depend upon the precise chemical structures of the solvent and the fluorophore.

2.2.3 Fluorophores

Fluorescent substances generally have delocalised electrons present in conjugated double bonds. A variety of biological molecules contain naturally

occurring intrinsic fluorophores. In proteins the indole ring of tryptophan is the most highly fluorescent amino acid as it accounts for ~90 % of the total fluorescence from proteins. Tyrosine and phenylalanine also make minor contributions to the overall intrinsic protein fluorescence. Tryptophan is highly sensitive to the polarity of its surrounding environment, therefore emission maxima of proteins are considered to reflect the average degree of exposure of the Trp residues to the aqueous phase. Spectral shifts are normally observed as a result of binding of ligands, membranes and protein denaturation. Extrinsic fluorophores are substances, which are foreign to the system under investigation. These include fluorescein-based compounds, which can be used to label non-fluorescent compounds such as lipids.

2.3 Circular Dichroism Spectroscopy

2.3.1 Theory of circular dichroism

Circular dichroism (CD) is a form of absorption spectroscopy that measures the difference between absorption of left circularly polarised (lcp) and right circularly polarised (rcp) light. The absorbance of lcp light is defined as

$$A_l = \log_{10}(I^0_l/I_l) = \varepsilon_l C l \qquad \textbf{(Eq. 2.11)}$$

where I^0_l and I_l are the intensities of lcp light entering the sample and after travelling a distance l through a medium containing the molar concentration of the sample and ε_l is the molar extinction coefficient of the sample for lcp light. Circular dichroism can therefore be defined as

$$\Delta A = A_l - A_r = \varepsilon_l C l - \varepsilon_r C l = \Delta\varepsilon C l \qquad \textbf{(Eq. 2.12)}$$

$$\Delta\varepsilon = \varepsilon_l - \varepsilon_r \qquad \textbf{(Eq. 2.13)}$$

Units for $\Delta\varepsilon$ are the same as ε, namely M^{-1} cm^{-1}.

Chiral or asymmetric molecules produce a CD spectrum because they absorb left- and right-circularly polarised light to different extents and are therefore considered to be optically active.

Most CD instruments measure differential absorbance, however the output is often given in ellipticity (θ) instead of ΔA versus λ. This measurement relies on the two circular components of plane-polarised light having different amplitudes after passing through an optically active sample. The sum of the two components no longer produces a plane-polarised beam and the direction of electric vector no longer traces a circle but instead gives an ellipse. The ellipticity is defined as an angle, θ whose tangent is the ratio of the minor and major amplitudes of the ellipse (see Figure 2.4).

Ellipticity can be related to ΔA by

$$\theta \text{ (degrees)} = 180 \times \ln 10 \times \Delta A / 4\pi = 32.98 \ \Delta A \quad \textbf{(Eq. 2.14)}$$

To eliminate the effects of pathlength and concentration, θ is often converted to molar ellipticity by

$$[\theta] = \frac{100 \ \theta}{Cl} \quad \textbf{(Eq. 2.15)}$$

so that $[\theta]$ has the dimensions of deg cm^2 $dmol^{-1}$.

Therefore from equations 2.12 to 2.14 $[\theta]$ can be defined as

$$[\theta] = 3298\Delta\varepsilon \quad \textbf{(Eq. 2.16)}$$
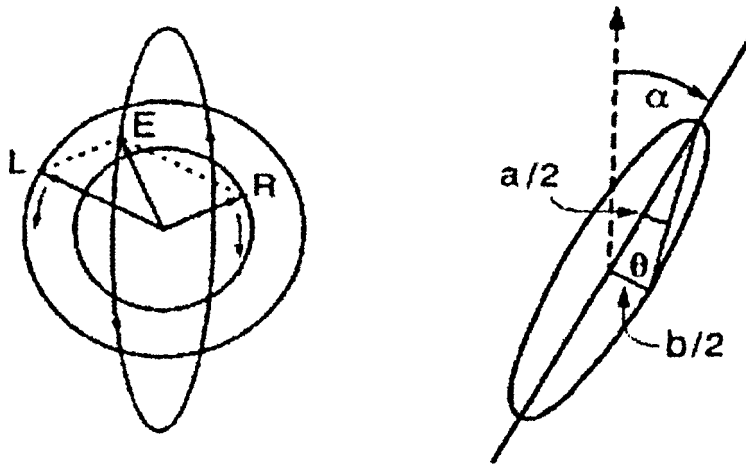
Figure 2.4: **Elliptically polarised light is formed by right- and left-circularly polarised light of unequal intensities.** Ellipticity is the angle θ, the tangent of which is the ratio of the minor to the major axis of the ellipse. The angle α is known as the optical rotation and is the angle between the major axis of the ellipse and the plane of polarisation of the initially plane-polarised light (reproduced from Woody, 1996).

To be able to compare the ellipticity values, they are usually converted into a normalised value. The mostly commonly used unit in protein and peptide work is the mean molar ellipticity per residue or mean residue weight (MRW).

$$[\theta]_{MRW} = \frac{[\theta]}{N}$$ (Eq. 2.17)

where N is the number of residues in the protein. The CD spectra presented in this thesis are all shown as mean molar ellipticity per residue, $[\theta]$ (deg cm^2 dmol^{-1}).

2.3.2 The physical basis of optical activity

As already discussed the absorption of electromagnetic radiation results in the transition of the molecule from the ground state to the excited state. There are two types of charge displacement during the transition.

- *Linear displacement*: This constitutes an electric dipole because of the separation of charge and is called an electric transition dipole (μ_e).

- *Rotation of charge*: This would generate a magnetic moment perpendicular to the rotation and is called a magnetic transition dipole (μ_m).

The applied electromagnetic radiation interacts with these dipoles to cause the changes in the energy states; the electric component interacts with electric transition dipole, μ_e and the magnetic component interacts with the magnetic transition dipole, μ_m. In general magnetic transition dipoles are much smaller than electric ones since separating charges creates a larger effect than rotating them. Optical activity requires an electric dipole transition moment and a magnetic transition dipole moment. The combination of the two corresponds to a helical

displacement of charge. The result is that left- or right-circularly polarised beams then interact differently with molecules in solution.

Electric   Magnetic   Optically active
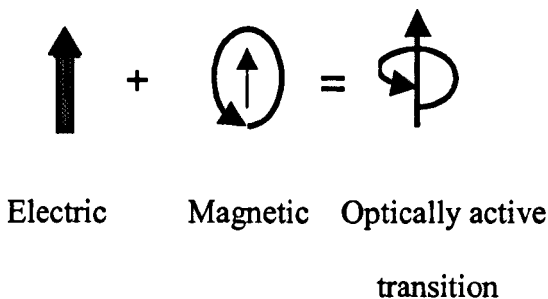
transition

2.3.3 Optically active chromophores

Optical activity is observed only when the environment in which a transition occurs is asymmetric. The absorption bands may be such that $\varepsilon_l - \varepsilon_r$ is positive or negative. The electronic transitions that occur involve a number of different molecular orbitals. The interaction of atomic orbitals leads to the formation of bonding and anti-bonding orbitals (*). Depending on the nature of the overlapping atomic orbitals, molecular orbitals may be of the σ type, the electron density being concentrated along the internuclear axis or of the π type, where the electron density is concentrated on either side of the internuclear axis. The relative energies of these orbitals and that of a non-bonding orbital n, which may be occupied by electrons not participating in bonding, are shown.
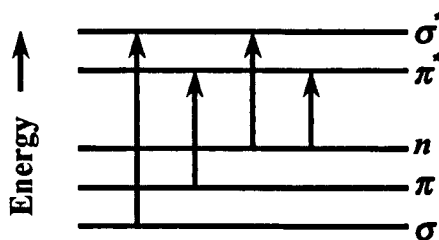
From the diagram it can be seen that the lowest energy and therefore the longest wavelength transitions are from the non-bonding orbitals to anti-bonding π orbitals, which give rise to bands in the UV region. Other allowed transitions in order of increasing energy (shorter wavelengths) are $n \rightarrow \sigma^*$ and $\pi \rightarrow \pi^*$.

Proteins and peptides are optically active and possess two kinds of asymmetry: configurational and conformational. Amino acids residues, except for glycine, have intrinsic optical activity because of the L configuration about their α-carbon atom and as a result they are chiral molecules. The secondary structures of proteins also contribute to optical activity. UV spectra of proteins are divided into two regions

- *Near-UV CD region (250–300 nm):* the aromatic side chains of phenylalanine, tyrosine and tryptophan have $\pi \rightarrow \pi^*$ transitions in this region (Figure 2.5A). This region is sensitive to the environment and as a result reflects the tertiary structural features in a protein.

- *Far-UV CD region (<250 nm):* peptide amide group gives rise to the transitions observed in the far-UV region. Non-bonding electrons are present on the oxygen and also on the nitrogen. π-electrons are delocalised over the carbon, oxygen and nitrogen atoms. The lowest energy transition of the peptide group is $n \rightarrow \pi^*$ which gives rise to a magnetic transition dipole. The $\pi \rightarrow \pi^*$ causes an electric transition dipole. The contributions of the aromatic amino acids in the far-UV CD are small compared with those of the peptide group. The far-UV CD spectra of proteins gives information about the asymmetric features of the backbone and

61
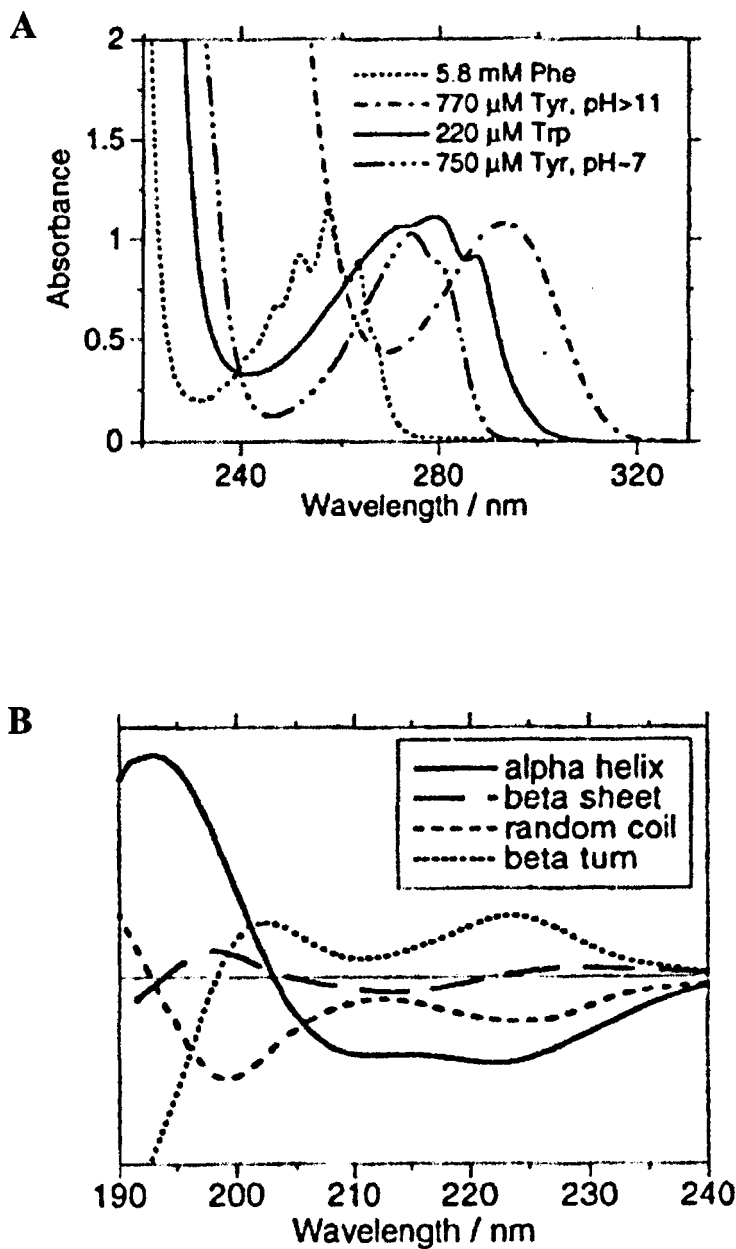
Figure 2.5: **CD spectra of protein in the (A) near-UV region and (B) far-UV region.** (A) Aromatic absorption spectra of tryptophan, tyrosine and phenylalanine. (B) CD spectra of α-helix, β-sheet, β-turn and unordered structures (reproduced from Rodger & Norden, 1997).

therefore the common types of secondary structure adopted by peptides and proteins have distinctive CD spectra (Figure 2.5 B).

- α-*helix:* the CD spectra of this structural motif is characterised with a negative peak at 222 nm ($n \rightarrow \pi^*$). The $\pi \rightarrow \pi^*$ transitions produces a negative band near 208 nm and a positive band at about 190 nm. The splitting of the $\pi \rightarrow \pi^*$ absorption bands occurs because the transition dipole moments interact with one another.

- β-*sheet:* proteins and peptides adopting this conformation have a negative band at about 217 nm ($n \rightarrow \pi^*$) and a positive band near 195 nm ($\pi \rightarrow \pi^*$).

- β-*turn:* CD spectrum has a positive band near 225 nm ($n \rightarrow \pi^*$) and between 200 and 205 nm ($\pi \rightarrow \pi^*$). However, the CD spectrum of this structural motif is not as well characterised as the other structural motifs and may vary considerably.

- *Unordered/random coil structure:* the CD spectra of unordered polypeptides are characterised by a strong negative band near 200 nm.

2.4   Infrared Spectroscopy

2.4.1   Physical basis of infrared spectroscopy

The absorption of electromagnetic radiation in the infrared region (IR) of the spectrum does not result in electronic transitions, instead changes in the vibrational energy levels of the ground (lowest) electronic state of molecules occurs. Molecules, which have a charge separation either across the whole molecule or across a specific bond, are said to possess a permanent dipole moment. When a molecule vibrates, this permanent dipole also vibrates and can interact with the

oscillating electric field of incident infrared radiation. Molecules, which do not have a permanent dipole moment, do not absorb IR radiation.

2.4.1.1   Diatomic molecules

At room temperature the molecules are in the lowest vibrational level of the ground electronic state. The absorption of IR radiation of the correct frequency by a bond between two atoms causes transition from the lowest vibrational state to the next highest. In a simple diatomic molecule A–B, the only vibration, which can occur is a periodic stretching along the A–B bond which is accompanied by a change in the dipole moment. Stretching vibrations resemble the oscillations of two bodies connected by a spring. For stretching of the bond A–B, the vibrational frequency ν (cm^{-1}) is given by Hooke's law

$$\nu = \frac{1}{2\pi c}\left(\frac{f}{\mu}\right)$$ (Eq. 2.18)

where c is the velocity of light, f the force constant of the bond and μ the reduced mass of the system, as defined by

$$\mu = \frac{m_A\, m_B}{m_A + m_B}$$ (Eq. 2.19)

where m_A and m_B are the individual masses of A and B.

Predictions based on Hooke's law:

• The greater the strength of the bond (*i.e.* the larger the value for f) the higher the frequency (and hence wavenumber) of the vibration. For example a double bond is stronger than a single bond and would therefore appear at a higher wavenumber than a single bond.

- The heavier the masses of the atoms attached to the bond, the lower the absorption frequency of the vibration. For example a C–H bond would occur at a higher wavenumber than a C–C bond.

2.4.1.2   Polyatomic molecules

In diatomic molecules there is only one mode of vibration, which is the stretching of the bond hence only one IR absorption band. If there are more atoms, there will be more bonds, and therefore more modes of vibrations. In polyatomic molecules the bonds can stretch and bend upon absorption. For a molecule that consist of N atoms, there are $(3N - 6)$ ways in which the molecule can vibrate, or $(3N - 5)$ if the molecule is linear. The different types of molecular vibrations are shown in Figure 2.6 and Table 2.2 shows the wavenumber ranges of characteristic vibrations.

Table 2.2: Wavenumbers of characteristic IR vibrations

Bond Type	Stretch (cm^{-1})	Bend (cm^{-1})
C–H	2700–3300	1300–1500
		600–900
O–H	3000–3700	1200–1500
N–H	3000–3700	1500–1700
S–H	2550–2600	700–900
C–C, C–N, C–O	400–1300	——
C=C, C=N, C=O	1550–1900	——
C≡C, C≡N	2100–2400	——
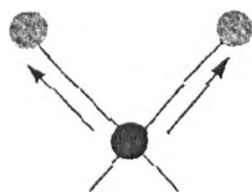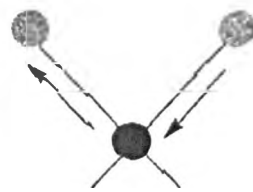
Symmetric   **Asymmetric**

Stretching vibrations
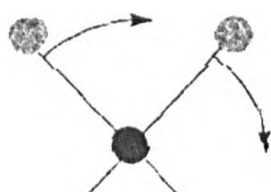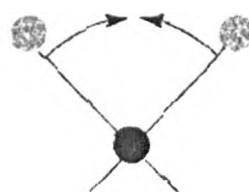
Rocking   **Scissoring**

In-plane bending vibrations
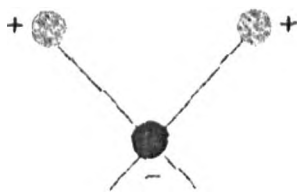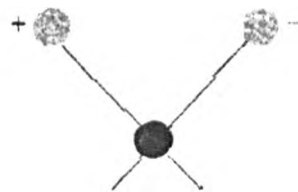
Wagging   **Twisting**

Out-of-plane bending vibrations

Figure 2.6: **The different types of molecular vibrations that occur upon absorption of IR radiation.** + indicates motion from the page toward reader; − indicates motion away from reader (reproduced from Skoog *et al.*, 1996).

Although equation 2.18 shows that the force constant, f and the relative masses of the bonded atoms constitute the two most important factors determining frequency, there are also other factors, which influence the absorption frequency and these include:

- *Hydrogen bonding:* Compounds that contain proton donor groups such as O–H and N–H can be involved in intra- or inter-molecular hydrogen bonding in the presence of proton acceptors, e.g. O, N. The stiffness of the X–H bond is thereby lessened resulting in a lowering of the stretching frequency and the band is shifted to lower wavenumbers.

- *Adjacent groups:* Shifts occur on altering the atoms or structures adjacent to a group that gives rise to a particular absorption band.

- *Coupled vibrations:* Groups in which two or more atoms of an element when bonded to a common atom are mechanically coupled, result in a band, which is resolved into two components. These correspond to symmetric and asymmetric modes of vibration (Figure 2.6).

Molecules absorb IR radiation at characteristic wavelengths determined by their atomic composition and bond structure as a result each molecule will produce a unique IR absorption spectra.

2.4.2 Protein secondary structure

Infrared spectroscopy has been widely used to determine the secondary structure of peptides and proteins. The infrared spectra of peptides and proteins exhibit a number of amide bands, which represent different vibrations of the peptide group (Goormaghtigh *et al.*, 1994). Nine characteristic amide bands are observed in

the IR spectra of proteins with the amide I (1600–1700 cm^{-1}) and amide II (1500–1580 cm^{-1}) being the two predominant bands. The amide I band is the most widely used in secondary structural studies of proteins. Amide I is composed mainly (80 %) of C=O stretching (v) vibration of the peptide group coupled to the in-plane bending of the N–H bond and the stretching of the C–N bond (Goormaghtigh *et al.*, 1994).

Using synthetic polypeptides it was shown that this band was conformation sensitive, the α-helical structure having a maximum near 1655 cm^{-1} and the β-sheet structure having a maximum around 1630 cm^{-1} (Goormaghtigh *et al.*, 1994). The major factors responsible for the conformational sensitivity of the amide I band includes hydrogen bonding and coupling between transition dipoles. The latter leads to the splitting of the amide I band. The magnitude of this splitting depends on the orientation and distance of the interacting dipoles, and therefore provides information on the geometrical arrangements of the peptide groups in a polypeptide chain. The nature of the hydrogen bonding is determined by the particular secondary structure adopted by polypeptide chains. An increase in hydrogen bonding induces a shift to lower frequencies for the stretching modes (Krimm & Bandekar, 1986; Bandekar, 1992).

Proteins usually fold into complex three-dimensional structures, which consist of different types of secondary structural elements. The observed amide I band is therefore a complex composite that consist of a number of overlapping component-bands representing the secondary structural elements such as α-helices, β-sheets, turns, and non-ordered structures. The bands cannot be resolved by altering experimental conditions and therefore other methods are employed to

separate and identify the different structural components. The use of resolution enhancement methods such as Fourier self-deconvolution, which narrows the bands, allows the identification of these otherwise hidden component bands. Band fitting procedures can then be used to obtain a quantitative assessment of the various components of the proteins such as α-helix, β-sheet and unordered structures (Goormaghtigh *et al.*, 1990).

Chapter 3: Expression and Purification of Syrian Hamster Prion Protein (SHaPrP) Residues 90–231

3.1 Introduction

Purification of cellular PrP^C from brain extracts is difficult and yields are low, for example 230 μg of PrP^C is obtained from 40 g of hamster brain (Pergani *et al.*, 1996). The lack of enough pure protein has hindered detailed biophysical studies. However, this has changed in the last few years with the development of high-level expression systems in bacterial cells. Recombinant (r) prion proteins have been successfully expressed and purified from a number of different species; hamster (Mehlhorn *et al.*, 1996), mouse (Hornemann & Glockshuber, 1996; Hornemann *et al.*, 1997), cow (Negro *et al.*, 1997), chicken (Marcotte & Eisenberg, 1999) and human (Swientnicki *et al.*, 1997; Zahn *et al.*, 1997; Jackson *et al.*, 1999*a*). This chapter will describe the expression and purification of the domain of Syrian hamster (SHa) PrP comprising residues 90–231. The amino acid sequence of this segment corresponds to the protease-resistant core of PrP^{Sc}. SHaPrP sequence was chosen for the present study for two reasons, the first being that SHaPrP^C and SHaPrP^{Sc} are the most extensively studied prion proteins. Secondly, the Syrian hamster prion protein has 93 % amino acid sequence identity with human prion protein (Schätzl *et al.*, 1995).

3.1.1 Expression plasmid

Recombinant Syrian hamster prion protein was expressed using an alkaline phosphatase (*pho*A) promoter in a protease-deficient strain of *Escherichia coli* (27C7). The expression plasmid plngPrP, encoding SHaPrP residues 90–231, was

obtained from Professor Stanley Prusiner's laborotory. Construction of PlngPrP is described in detail in Mehlhorn *et al.* (1996). A simplified map of the PlngPrP plasmid is shown in Figure 3.1. This plasmid is a derivative of phGH1 (Chang *et al.*, 1987) and contains a signal sequence, coding for the *E. coli* heat-stable enterotoxin II (STII). This signal peptide promotes the transport of SHaPrP (90–231) from the site of its synthesis in the cytoplasm to the periplasmic space of *E. coli* cells. The signal sequence is cleaved by a signal peptidase and the mature protein is released into the periplasmic space. The periplasm offers several advantages for protein targeting. It contains approximately 4 % of the total cell protein; thus the target protein can be effectively concentrated. The oxidising environment of the periplasm facilitates the proper cleaving of the signal peptide during translocation to yield the authentic sequence of the target protein. Protein degradation in the periplasm is also less extensive (Makrides, 1996). SHaPrP genes of varying lengths including full-length mature protein, residues 23 to 231, were also inserted into expression plasmids. These were found to give unsatisfactory expression yields compared to SHaPrP residues 90–231 (Mehlhorn *et al.*, 1996).

The protease deficient strain of *E. coli* 27C7 was transformed with the plngPrP plasmid containing the truncated SHaPrP sequence 90–231. An overnight culture was used to inoculate the low-phosphate medium. The recombinant protein accumulated as insoluble aggregates in the periplasmic space. Purification of rPrP (90–231) followed an adaptation of the method originally described in Mehlhorn *et al.* (1996).

Processing site

5′AACGCGTATGCA ┊ GGTCCAGGA 3′
      Ala   Tyr Ala ┊   Gly Gln Gly
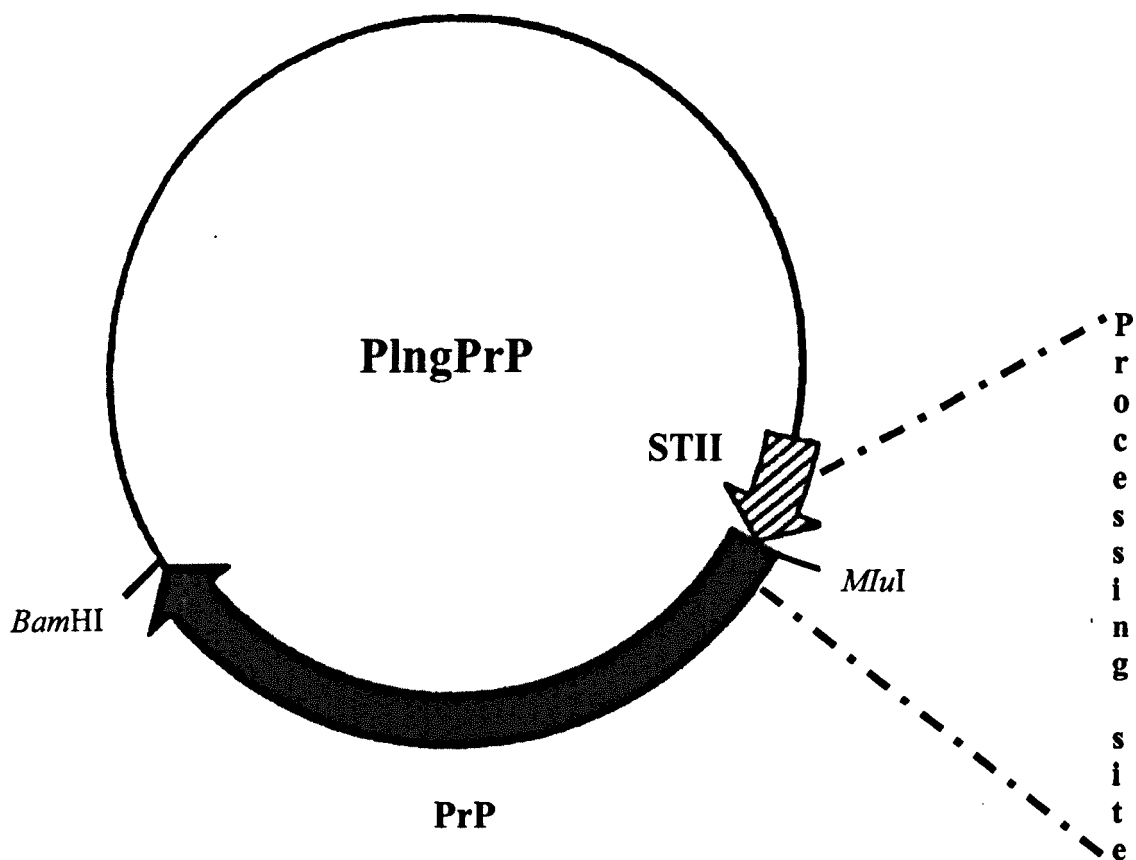
  STII signal peptide ┊   PrP sequence
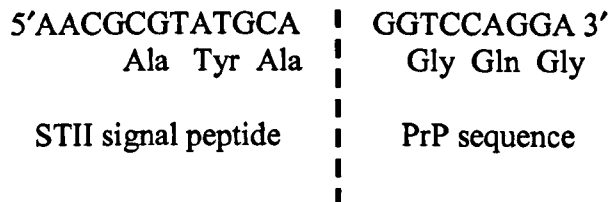
Figure 3.1: **PlngPrP plasmid.** PrP sequence coding residues 90–231 was inserted between the *MluI* and *BamHI* sites. Processing site for the removal of the STII signal peptide is illustrated. The plasmid also contains the ampicillin resistance gene (not shown) (adapted from Mehlhorn *et al.*, 1996).

This chapter describes the expression and purification of recombinant SHaPrP (90–231). The results of the characterisation of the refolded protein are also presented. Recombinant PrP was analysed by gel electrophoresis, immunoblots, mass spectroscopy and circular dichroism (CD) to determine the purity, molecular mass, and the secondary and tertiary structure of the protein.

3.2 Materials and Methods

3.2.1 Materials

The following reagents were purchased from BDH (Poole, UK): dithiothreitol (DTT), trifluoroacetic acid Hipersolv for HPLC use (TFA), Acrylogel 2.6 acrylamide solution (40 % T total monomer concentration) and HPLC grade acetonitrile. Yeast extract was obtained from Difco laboratories (Detroit, USA). Triethanolamine was purchased from Lancaster (Morecombe, UK). Protease deficient expression strain of *E. coli* 27C7 was purchased from American Type Culture Collection (ATCC 55244). The mouse anti-PrP monoclonal antibody (MAB1562 IgG) was purchased from Chemicon International Ltd (Harrow, UK). Pre-stained markers were purchased from Novex (San Diego, USA). Dialysis tubing with a 7000 molecular weight cut-off was obtained from Medicell International Ltd (London, UK). Coomassie protein assay reagent and bovine serum albumin (BSA) standards were obtained from Pierce (Illinois, USA). All other chemicals were purchased from Sigma-Aldrich (Poole, UK) unless otherwise stated.

Glass beads for the cell homogeniser (0.5-mm diameter) were purchased from Glen Creston (Stanmore, UK). The beads were washed with 50 % HCl followed by de-ionised water until the pH was neutral and dried in an oven at 40 °C.

Hiload Superdex 200 was purchased from Pharmacia and Poros R1 resin (20 μm particle size) for reverse phase chromatography was obtained from PerSeptive Biosystems (Hertfordshire, UK).

AP5 expression medium per litre contained; 1.5 g glucose, 11 g casein acid hydrolysate, 0.6 g yeast extract, 0.19 g $MgSO_4$, 1.07 g NH_4Cl, 3.73 g KCl, 1.2 g NaCl, 120 mL 1 M triethanolamine, pH 7.4 and 100 μg/mL ampicillin. The medium was filter sterilised through a 0.22-μm membrane.

The following buffers were used during the purification of rPrP:

Buffer A: 25 mM TrisHCl, pH 8.0 containing 5 mM EDTA.

Buffer B: 25 mM TrisHCl, pH 8.0 containing 8 M GdnHCl and 100 mM DTT.

Buffer C: 50 mM TrisHCl, pH 8.0 containing 6 M GdnHCl and 1 mM EDTA.

Buffers for reverse phase HPLC: Buffer 1, H_2O/0.1 % TFA

Buffer 2, acetonitrile/0.09 % TFA

Buffers C, 1 and 2 were filtered using a 0.22-μm membrane and degassed.

3.2.2 Safety issues

SHaPrP domain 90–231 was expressed in *E. Coli* within a level 3* containment laboratory and all material was handled inside a class III hood within the containment laboratory. The cells were harvested and disrupted within the containment laboratory. The recombinant prion protein was solubilised in 8 M GdnHCl and filtered through a 0.22-μm membrane before removing from the containment laboratory. Further purification of rPrP was carried out within a class II

hood. Pipetting of rPrP solutions or any other operation with the potential of creating an aerosol was performed within the class II hood.

Decontamination and disposal of waste was carried out according to the guidelines established by the Health and Safety Executive in 'Precautions for work with human and animal Transmissible Spongiform Encephalopathies.'

3.2.3 Expression of SHaPrP (90–231)

Competent *E. coli* 27C7 cells were prepared using calcium chloride, the method is a variation of that described in Sambrook *et al.* (1996) volume 1, p1.82. Briefly, 100 mL of TY broth was inoculated with *E. coli* strain 27C7 and incubated at 37 °C with vigorous shaking, until the optical density at 600 nm reached a value between 0.6 to 0.8. The culture was cooled to 0 °C by storing the tubes on ice for 15 minutes after which the cells were recovered by centrifugation at 3000 rpm for 5 minutes at 4 °C. The supernatant was decanted and the cells were resuspended in 50 mL of freshly made ice cold 100 mM $MgCl_2$. Again the cells were recovered by centrifugation at 3000 rpm for 5 minutes at 4 °C. The supernatant was decanted and the cells were resuspended in 10 mL freshly made ice cold 100 mM $CaCl_2$. The cells were left on ice for 1 hour before transformation with the plngPrP plasmid.

Competent 27C7 cells (50 μL) were transformed with 4 μL of plngPrP plasmid (100 ng). The sample and control, *i.e.* no plasmid, were incubated on ice for 30 minutes after which they were transferred to a water bath that had been pre-heated to 42 °C for 2 minutes. This was followed by a further 30-minute incubation on ice. LB medium (200 μL) was added to the samples and the cultures were incubated for 1 hour at 37 °C. The transformed bacteria were spread on a LB agar

plate containing 100 µg/mL ampicillin and incubated overnight at 37 °C. Frozen

stocks of transformed *E. coli* 27C7 cells were prepared according to Sambrook *et al.*

(1989) appendix A5. LB medium (5 mL) was inoculated with a single colony from

freshly transformed cells and incubated at 37 °C for 3 hours. For storage 1 mL

aliquots in 20 % (v/v) glycerol were prepared in 2 mL biofreeze sterile

polypropylene vials and stored at –20 °C until required.

Frozen transformed *E. coli* 27C7 cells containing the plngPrP plasmid were

plated onto a LB agar plate containing 100 µg/mL ampicillin and incubated

overnight at 37 °C. LB medium (5 mL) supplemented with 50 µg/mL ampicillin

was inoculated with transformed *E. coli* 27C7 cells and incubated for 3 hours at 37

°C with vigorous shaking (200 rpm in a rotary shaker). This was followed by a 100-

fold dilution into AP5 medium. Typically 2–3 litres were cultured at any one time.

The cultures were incubated at 37 °C with vigorous shaking for 21 h or until the

optical density at 600 nm reached a value between 1.0 to 1.4. The cells were

harvested by centrifugation at 10,000 *g* for 20 minutes. The resulting cell paste was

stored at –20 °C.

3.2.4 Purification of recombinant SHaPrP (90–231)

The purification of rPrP (90–231) followed an adaptation of the method

originally described in Mehlhorn *et al.* (1996). A schematic diagram of the

purification of rPrP is outlined in Figure 3.2. The cell paste was resuspended in

buffer A and centrifuged at 10,000 *g* for 20 minutes at 4 °C. The supernatant

containing the soluble periplasmic proteins was discarded. The recombinant protein

E. coli paste

Resuspend in 25 mM TrisHCl, pH 8.0/5 mM EDTA, 10,000 ×g 20 min

S1   **P1**

Resuspend in 25 mM TrisHCl, pH 8.0/5 mM EDTA

Cell Homogeniser: 5 × 2-min

periods spaced by 1-min intervals

30,000 ×g 60 min

S2   **P2**

Resuspend in 25 mM TrisHCl, pH 8.0/5 mM EDTA
30,000 ×g 60 min

S3   **P3**

Resuspend in 8 M GdnHCl/25 mM TrisHCl, pH 8.0/100 mM DTT
32,000 ×g 20 min

S4   **P4**

Superdex 200 size exclusion column

Poros R1 RP HPLC column

Figure 3.2: **Purification protocol for recombinant SHaPrP (90–231).** Cell paste was resuspended in Tris buffer and centrifuged to remove soluble periplasmic proteins. A cell homogeniser was used to disrupt the cells. The pellet (P2) was washed once to remove contaminating cytoplasmic E. coli proteins. The pellet (P3) was finally solubilised in 8 M GdnHCl. The resulting supernatant (S4) was applied to a size exclusion column and the final step in the purification involved reverse-phase high performance liquid chromatography.

remained in the pellet, which was again resuspended in buffer A and disrupted in a homogeniser (Bead Beater with a ice jacket, Stratech Scientific Limited) half-full with pre-chilled 0.5-mm diameter glass beads, for 5×2-min periods spaced by 1-min intervals. The suspension was centrifuged at 30,000 g for 1 hr at 4 °C, after which the supernatant was discarded. The pellet was washed once in buffer A and centrifuged again at 30,000 g for 1 hr. The pellet containing rPrP was subsequently solublised in 15 to 20 mL of buffer B and centrifuged at 32,000 g for 20 minutes at 4 °C. The supernatant was passed through a 0.22-μm membrane. At this stage it was possible to take the protein out of the level 3* containment laboratory.

Aliquots of the supernatant (4 mL) containing approximately 30 mg of total protein, as determined by Coomassie protein assay (Biorad) using BSA as standards, were applied to a Hiload Superdex 200 column (26 mm × 60 cm). The column had been pre-equilibrated with buffer C at a flow rate of 2 mL/min. Fractions (4 mL) were collected and absorbance at 280 nm was measured. Initially fractions enriched for rPrP were identified by SDS polyacrylamide gel electrophoresis. However, later the elution profiles were used and those fractions containing the recombinant protein were pooled (Figure 3.3A). The combined fractions were incubated at 4 °C for 2–3 days, during this period oxygen in the air oxidised the two cysteines to form the disulphide bond.

Further purification involved reverse-phase high performance liquid chromatography (RP HPLC), employing a 4.6 × 100 mm poros R1 perfusion chromatography column on a BioCAD SPRINT system (PerSeptive Biosystems, Hertfordshire, UK). The column was equilibrated with 8 column volumes of buffer
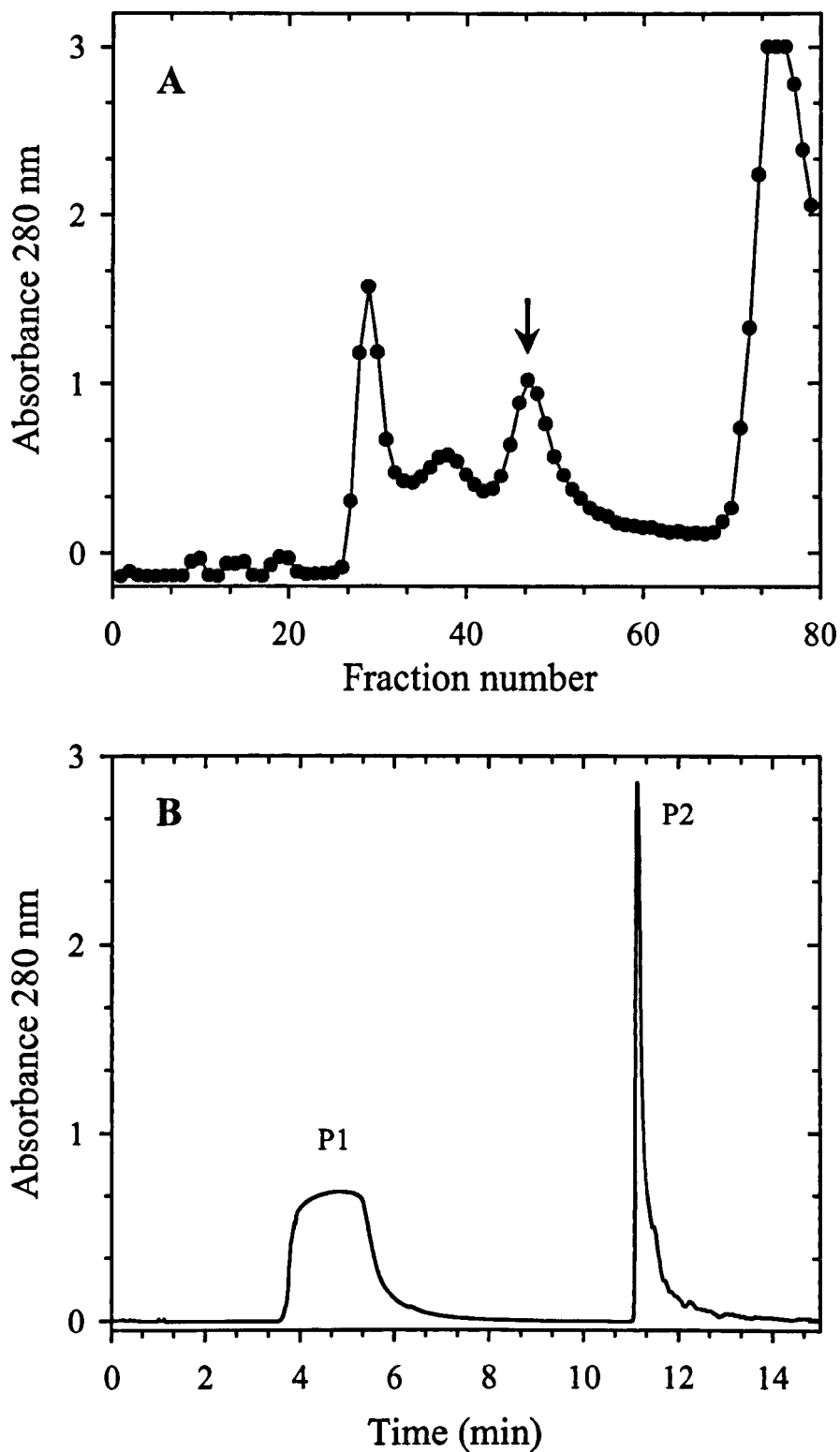
Figure 3.3: **Purification of recombinant SHaPrP (90–231).** (A) Elution profile of the solubilised pellet containing rPrP from the SEC column. The arrow indicates the peak that was collected. (B) Elution of rPrP from the Poros R1 RP HPLC column with a linear gradient of 0–10 % acetonitrile/0.09 % TFA. GdnHCl was washed from the column (P1) with buffer 1. P2 was eluted with 1 % acetonitrile and contained oxidised rPrP.

1 at a flow rate of 5 mL/min. The sample (10 mL) was loaded onto the column, followed by a wash step with buffer 1 (5 minutes) this removed the GdnHCl. The recombinant protein was eluted with a 90-minute linear acetonitrile gradient from 0 to 10 % (buffer 2). Fractions (0.2 mL) were collected and those containing purified rPrP were identified from the chromatogram and pooled (Figure 3.3B). The column was regenerated with buffer 2.

3.2.5   Refolding of recombinant SHaPrP (90–231)

Purified recombinant protein was dialysed overnight at 4 °C, against 20 mM sodium acetate, pH 5.5 (5 L) using dialysis tubing with a 7000 molecular weight cut-off. The dialysis tubing had been boiled in a solution of sodium bicarbonate and EDTA in 50 % ethanol to remove impurities before use. The buffer was changed the following morning (5 L) and the protein was further dialysed for 6 hours. Aliquots (0.5 mL) of the purified protein were prepared and snap frozen in liquid nitrogen for long term storage at –20 °C. Sample vials were thawed individually when required, any insoluble material was separated by centrifugation.

3.2.6   Characterisation of purified recombinant SHaPrP (90–231)

3.2.6.1   Determination of protein concentration

Protein concentration was determined spectrophotometrically using a molar extinction coefficient ε_{280} of 24,420 M^{-1} cm^{-1} (Gill & von Hippel, 1989).

3.2.6.2   SDS-polyacrylamide gel electrophoresis and Western blotting

Protein samples were analysed by discontinuous SDS-PAGE according to Laemmli (1970). Samples were analysed on 15 % mini polyacrylamide gels. Each

sample was denatured in sample buffer by boiling at 100 °C for 5 minutes. The gel was visualised using Coomassie brilliant blue (Sambrook *et al.*, 1989 volume 1, p18.55). SDS-PAGE requires relatively salt-free protein samples, therefore GdnHCl was removed when present from protein samples before analysis by using acetone as a precipitating agent. Cold acetone (–20 °C) was added to the protein solution to a final concentration of 50 % (v/v) and left on dry ice for 15 minutes. Centrifugation resulted in a protein pellet, which was resuspended in de-ionised water and precipitated again with cold acetone (Pohl, 1990). The protein pellet was resuspended in sample buffer and prepared as above.

For Western blotting the proteins were transferred from an unstained SDS-PAGE gel to nitrocellulose membrane, using a mini TransBlot Electrophoretic Transfer Cell-System (BioRad) at 100 V for 1 hour. After blocking with 2 % (w/v) skimmed milk powder in 10 mM TrisHCl, pH 7.4 containing 0.15 M NaCl and 0.05 % Tween 20, the membrane was incubated with the mouse anti-PrP monoclonal antibody (MAB1562 IgG) at room temperature for 1 hour (1:4000 dilution in the above Tris buffer containing 2 % (w/v) skimmed milk powder). Unbound antibody was removed from the membrane by intensive washing in the Tris buffer, pH 7.4 (no skimmed milk powder) and incubated with the secondary horseradish peroxidase conjugated goat anti-mouse antibody (Sigma-Aldrich, Poole, UK). After repeated washes the labelled protein was detected by the formation of a coloured product. A tablet of chloronaphthol (30 mg) was dissolved in 10 mL of methanol and made up to 50 mL with de-ionised water. This solution was added to 50 mL of 20 mM TrisHCl, pH 7.5, 1.5 g of NaCl and 50 μL H_2O_2 (20 volumes). The chloronaphthol mix was poured over the drained blot, and the reaction was terminated once the bands were visible by washing the membrane in water.

3.2.6.3   *Mass spectrometry*

An aliquot (10 μL) of purified rPrP was analysed by electrospray ionization (ESI) mass spectrometry using a Quattro II tandem quadrupole instrument (Micromass UK Ltd) equipped with a commercial Z-spray ionisation source operating in continuous flow nanospray mode. Calibration of the ESI mass spectrometer with myoglobin allowed the molecular mass of rPrP to be determined.

Mass spectrometry was kindly performed by Dr Andrew C Gill at the Institute for Animal Health, Compton.

3.2.6.4   *CD spectroscopy*

CD spectra of the far-UV (185–260 nm) and near-UV (250–350) regions were recorded on a JASCO J-715 spectropolarimeter. Spectra were obtained for samples in 20 mM sodium acetate, pH 5.5 containing 7.5 μM rPrP (0.12 mg/mL) for far-UV and 46 μM rPrP (0.74 mg/mL) for near-UV. CD spectra were recorded at 20 °C using quartz cells of 0.1 mm pathlength for far-UV and 5 mm for near-UV. The measurements were recorded with a bandwidth of 1 nm, a scanning rate of 100 nm/min and a time constant of 1 s. Spectral resolution was 0.5 nm and 16 scans were averaged per spectrum. The corresponding spectra for buffer background were subtracted from protein spectra.

3.3   *Results and Discussion*

3.3.1   *Expression and purification of SHaPrP (90–231)*

SHaPrP (90–231) was successfully expressed in a protease deficient strain of

E. coli. During expression rPrP aggregated into insoluble particles in the periplasmic space. After cell disruption in a homogeniser the recombinant protein remained in the pellet and was solubised in 8 M GdnHCl containing 100 mM DTT, thus reducing the single disulphide bond in PrP. Approximately 50–80 % of the recombinant protein was solublised from the pellet. The recombinant protein was separated from the high molecular weight *E. coli* proteins by size exclusion chromatography under denaturing conditions. The absence of a reducing reagent from the SEC buffer meant that the pooled fractions from the SEC column when stored at 4 °C for 2–3 days resulted in formation of the disulphide bond.

RP HPLC was used in the last purification step of recombinant PrP. PerSeptive Biosystems POROS R1 column was used instead of a conventional C-4 column. POROS media allows for higher flow rates to be used during separation, thereby reducing the time required to purify large volume samples. The elution time of rPrP in reverse-phase chromatography is dependent on the oxidation state of Cys179, and Cys214 (Mehlhorn *et al.*, 1996; Zhang *et al.*, 1997; Jackson *et al.*, 1999*a*). Mehlhorn *et al.* (1996) reported that oxidised rPrP eluted in earlier fractions containing 35 % acetonitrile, while the reduced protein eluted later and was usually contaminated with co-eluting proteins. Purification of recombinant PrP under oxidising conditions was demonstrated to yield a protein with a high α-helical content (Mehlhorn *et al.*, 1996; Zhang *et al.*, 1997). However under reducing conditions the protein was shown to contain a greater amount of β-sheet structure.

The recombinant protein eluted as a single peak from the POROS R1 column with 1 % acetonitrile. The elution point is very different from the reported value of 35 % acetontrile from a Vydac C-4 column (Mehlhorn *et al.*, 1996). Although R1

resin [poly(styrene-divinylbenzene)] is suggested to be similar to C-4, the chromatographic matrix is qualitatively different from C-4 chains bonded to silica. This difference may result in different elution points in the acetonitrile gradient. Recombinant PrP was refolded by dialysis against 20 mM sodium acetate, pH 5.5. The final yield of rPrP was 10–12 mg per litre of bacterial culture.

3.3.2 Characterisation of purified recombinant SHaPrP (90–231)

3.3.2.1 Analysis by SDS-PAGE and Western blotting

Electrophoresis and immunoblots confirmed the presence and purity of rPrP (Figure 3.4). Mouse anti-PrP monoclonal antibody (MAB1562 IgG) binds to an epitope at the unstructured amino-terminus (amino acids 109–112) in hamster PrP. The protein appeared as a single band, within the correct molecular weight range (16–17 kDa) on SDS-PAGE gels and nitrocellulose membranes. The calculated molecular weight for the oxidised protein is 16,241.13 Da.

3.3.2.2 Mass spectrometry

The molecular mass of recombinant SHaPrP (90–231) was verified by ESI mass spectrometry as 16,241.70 ± 0.16 Da (Figure 3.5). The calculated mass for the oxidised protein is 16,241.13 Da the result is therefore in excellent agreement with the expected mass for the oxidised protein containing a disulphide bond.

3.3.2.3 Spectroscopic characterisation of recombinant SHaPrP (90–231)

The far-UV region of the CD spectrum provides a qualitative measure of the
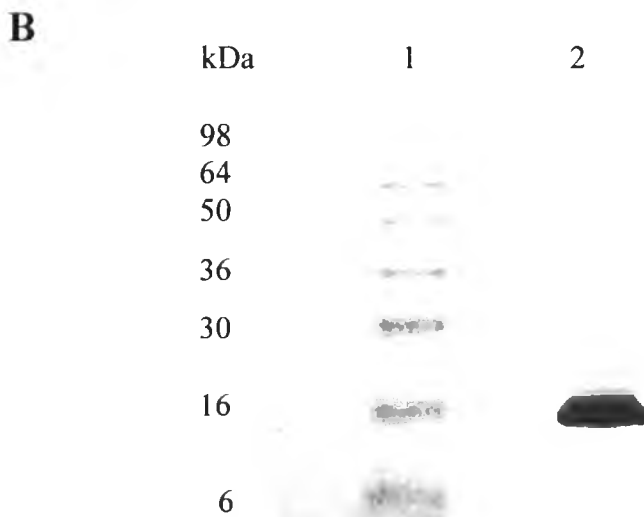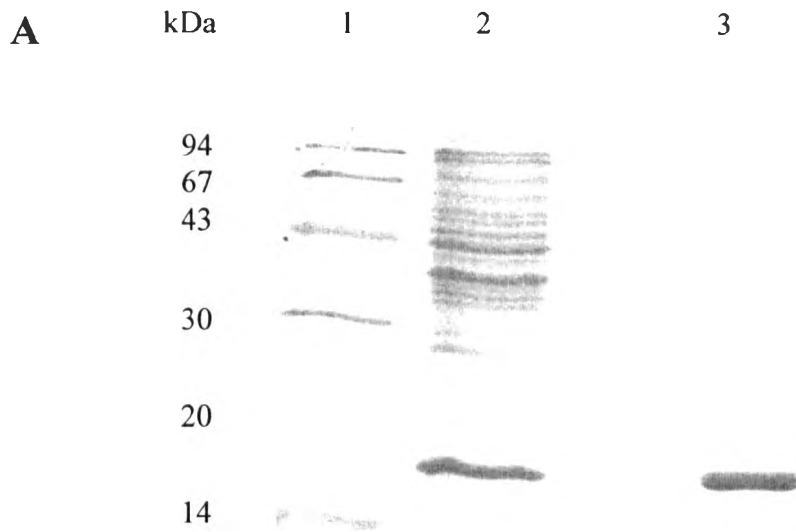
Figure 3.4: **Analysis of recombinant SHaPrP (90–231) by SDS-PAGE and Western blotting.** (A) Coomassie stained 15 % polyacrylamide gel. Lane: (1) molecular mass standards, (2) total cell extract and (3) purified rPrP following RP HPLC. (B) Western blot analysis using monoclonal antibody MAB1562 IgG following the purification of rPrP. 300 ng of total protein was loaded. Lane: (1) molecular mass standards and (2) purified rPrP.
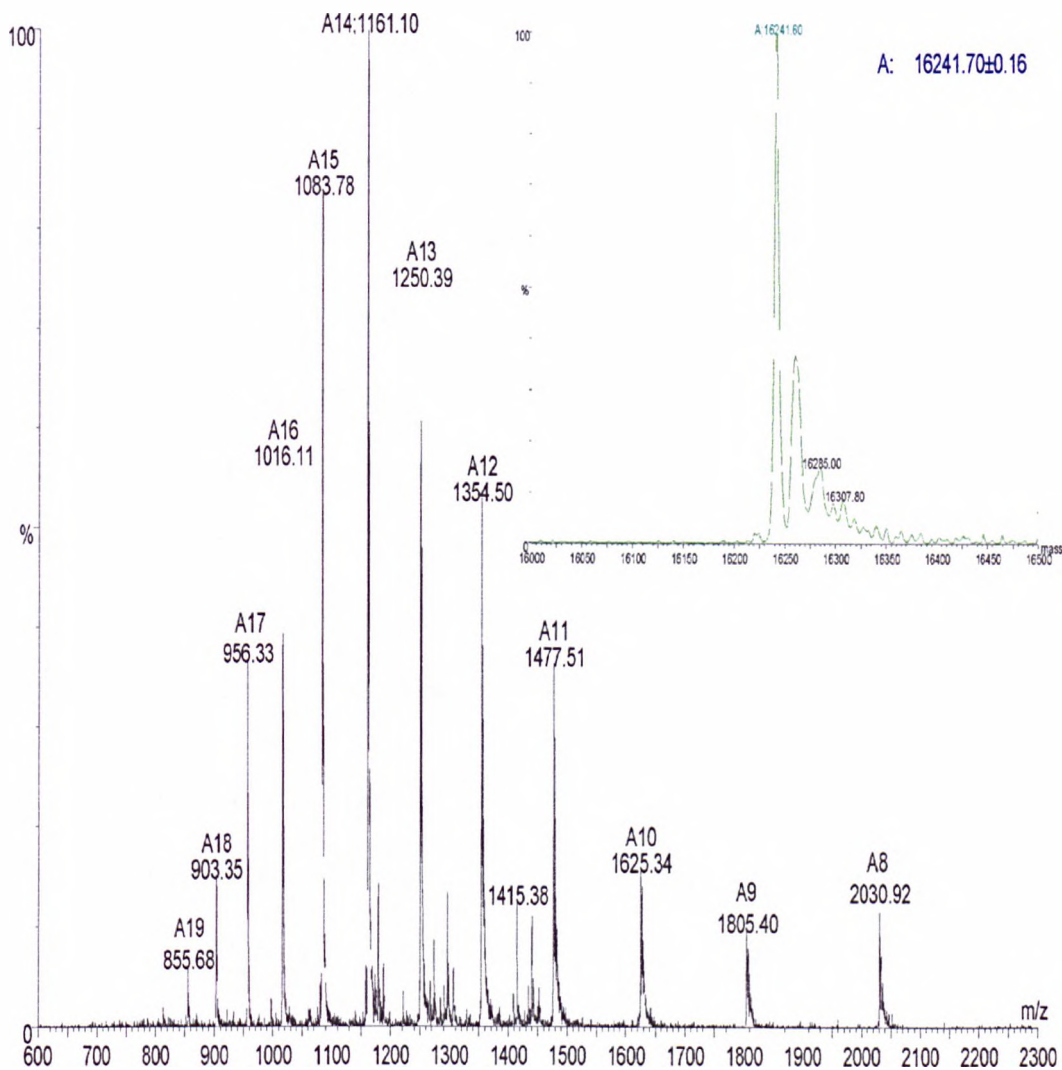
Figure 3.5: **ESI mass spectrometry of purified recombinant SHaPrP (90–231).** Mass spectrum of purified SHaPrP. The inset shows the maximum entropy deconvoluted mass spectrum of SHaPrP (90–231). Calculated mass for SHaPrP (90–231) assuming formation of the single disulphide bond is 16,241.13 Da and the measured mass is 16,241.70 ± 0.16 Da.

average secondary structure content of a protein. The far-UV CD spectrum of refolded recombinant SHaPrP (90–231) exhibits a double minimum at 208 and 222 nm with a mean molar ellipticity per residue at 222 nm of $-8,000$ deg cm^2 $dmol^{-1}$ and a strong positive band near 195 nm (Figure 3.6A). The spectrum is characteristic of proteins with high α-helical content (Woody, 1996). This is in good agreement with the NMR structure of recombinant SHaPrP (90–231), which shows a mainly helical protein with small amount of β-sheet structure (James *et al.*, 1997). In contrast, rPrP in 6 M GdnHCl shows a spectrum, which is characteristic of a unordered protein, however because of the light scattering defects associated with high concentrations of GdnHCl the strong negative band near 200 nm, which is a feature of an unordered polypeptide is not resolved.

The far-UV CD spectrum of recombinant human PrP residues 90–231 displays two minimum at 208 and 222 nm with a mean molar ellipticity per residue at 222 nm of $-10,000$ deg cm^2 $dmol^{-1}$. Comparison of the CD spectrum of human PrP with SHaPrP domains 90–231 indicates that the percentage of α-helical structure is remarkably similar in the two proteins (Swietnicki *et al.*, 1997). Furthermore, the far-UV CD spectrum of PrP purified directly from hamster brain is also indicative of a protein containing mainly α-helical structure (Pan *et al.*, 1993; Baldwin *et al.*, 1995). Comparison of the spectroscopic measurements suggests that recombinant PrP was refolded into a conformer that resembled native PrP[C].

The near-UV CD region (250–330 nm) provides information on the packing of aromatic side chains in the protein and generally give rise to a CD band if they are tightly packed within the core of a stable folded protein. The overall features of the
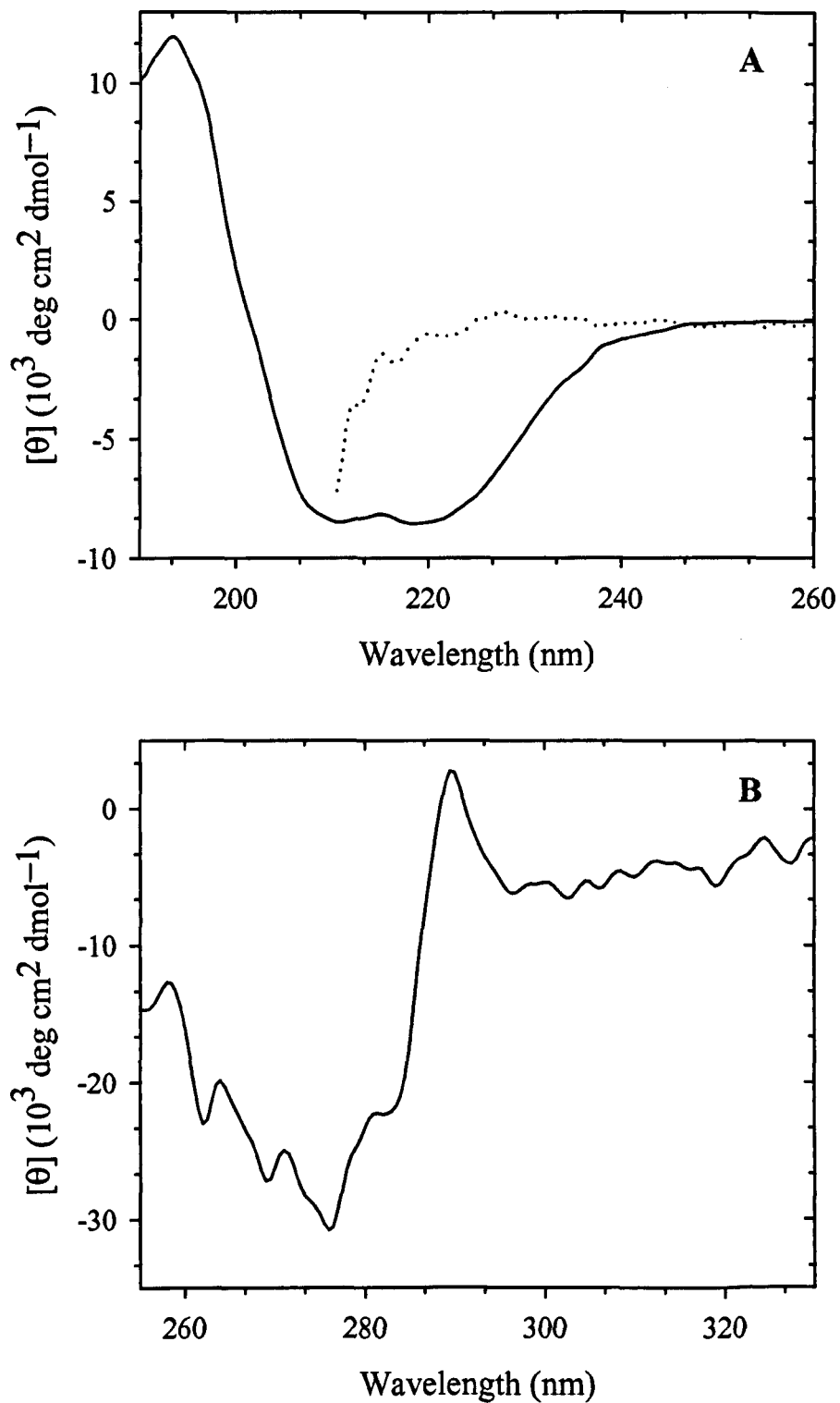
Figure 3.6: **CD spectra of recombinant SHaPrP (90–231).** (A) Far-UV CD spectra of refolded rPrP (solid line) under oxidising conditions at pH 5.5 and unfolded rPrP (dotted line) in 6 M GdnHCl. (B) Near-UV CD spectrum of refolded rPrP under oxidising conditions at pH 5.5. CD spectrum was recorded at protein concentrations of 7.5 μM for far-UV and 46 μM for near-UV at 20 °C. [θ] represents mean molar ellipticity per residue.

near-UV CD spectrum of recombinant SHaPrP (90–231) indicate the presence of tertiary structure (Figure 3.6B). In the 275–285 nm region the spectrum is dominated by tyrosine absorption and in the 260–270 nm region by phenylalanine absorption. The distinct positive peak near 292 nm suggests that one or both of the tryptophan residues are located in an asymmetric environment (Woody, 1996).

3.3.3 Summary

Recombinant SHaPrP (90–231) was expressed in a protease deficient strain of *E. coli* and purified by two sequential chromatographic procedures: SEC and RP HPLC. The protein was refolded under oxidising conditions by dialysis against acetate buffer, pH 5.5.

SDS-PAGE and Western blotting confirmed the purity and presence of rPrP. Mass spectrometry revealed that purified protein had a molecular weight of 16,241.70 ± 0.16 Da, which is in excellent agreement with oxidised PrP containing a disulphide bond between Cys179 and Cys214.

The far-UV CD spectrum was indicative of a protein with a high α-helical content. In addition near-UV CD indicated the presence of a folded state with stable tertiary structure. These data taken together provided strong evidence for the conformation of oxidised recombinant SHaPrP (90–231) to resemble that of PrP^{C}.

Chapter 4:   Binding of Syrian Hamster Prion Protein (SHaPrP) Residues 90–231 to Model Lipid Membranes

4.1   Introduction

The three-dimensional structure of several recombinant mammalian prion proteins have been solved by nuclear magnetic resonance (NMR) spectroscopy (Riek *et al.*, 1996; Donne *et al.*, 1997; James *et al.*, 1997; García *et al.*, 2000; Zahn *et al.*, 2000). Biophysical studies have been directed to decipher the mechanism of PrP^C conversion to PrP^{Sc}. (Swietnicki *et al.*, 1997; Zhang *et al.*, 1997; Hornemann & Glockshuber, 1998; Jackson *et al.*, 1999*a,b*; Wildegger *et al.*, 1999). Although the above solution studies have all provided valuable information on the complex mechanism of PrP conversion they however failed to take into consideration that the carboxyl-terminus of PrP is attached to a flexible GPI anchor, which targets the protein to cholesterol-sphingolipid rich raft domains within the plasma membrane (Vey *et al.*, 1996; Naslavsky *et al.*, 1997).

The precise subcellular site for the formation of PrP^{Sc} is unknown. Evidence implicates the plasma membrane and endocytic organelles as relevant sites (Taraboulos *et al.*, 1995; Vey *et al.*, 1996). Lipid interactions are thus likely to feature in the formation and propagation of PrP^{Sc}. Furthermore, studies with lipid-anchored proteins have shown that in addition to the anchor direct interactions between the polypeptide chain and lipid membranes may be involved in membrane association (Sigal *et al.*, 1994; Zhou *et al.*, 1994; Arbuzova *et al.*, 1998). It is therefore likely that the polypeptide chain of PrP can also participate in direct membrane-protein interactions. The flexible character of the GPI anchor of PrP provides the protein with dynamic freedom relative to the membrane, thus increasing

the probability of direct interactions of PrP with lipid membranes (Rudd *et al.*, 2001). Given that the lipid environment appears to play a crucial role in the cell cycle of PrP the biophysical properties of PrP in lipid membranes were investigated.

Few studies have investigated the structural characteristics of PrP when associated with model lipid membranes. Morillas *et al.* (1999) recently described conformation changes in human prion protein upon interaction with lipid membranes. Binding of various recombinant human PrP variants including full-length protein (minus the GPI anchor) to glycerophospholipid vesicles was investigated as a function of pH. Human PrP was reported only to bind to mixed membranes containing negatively charged lipid PS and zwitterionic lipid PC, with the interaction becoming much stronger under acidic conditions. The study concluded that even in the absence of the GPI anchor recombinant human PrP had a propensity to interact with lipid bilayers. The requirement of negatively charged lipids led the authors to suggest that binding of human PrP to membranes is driven by electrostatic lipid-protein interactions. However, the involvement of hydrophobic lipid-protein interactions was not completely excluded.

De Gioia *et al.* (1994) examined the lipid binding properties of a synthetic peptide spanning residues 106 to 126 of human PrP. This peptide had in a previous study been shown to be neurotoxic toward primary cultures of rat hippocampal neurons (Forloni *et al.*, 1993). The peptide interacted with neutral lipid vesicles (PC/cholesterol) and negatively charged membranes (PG/cholesterol) and the association was accompanied by a secondary structural transition from a random coil conformation to a predominant β-sheet structure.

In this chapter, the lipid binding properties of recombinant SHaPrP comprising of residues 90–231 have been characterised by monitoring changes in the fluorescence properties of PrP. SHaPrP (90–231) contains two tryptophan residues at positions 99 and 145 (Figure 4.1) that serve as intrinsic fluorophores. Fluorescence quenching experiments further provided information on the solvent accessibility of the tryptophan residues for the lipid-free and lipid-bound states of PrP.

Specifically, the interactions of SHaPrP (90–231) with a range of lipid membrane systems both at pH 7, to represent the pH surrounding the plasma membrane and pH 5, which models the acidic environment in endosomes, were investigated. In this comparative study, three types of model lipid systems were investigated: negatively charged glycerophospholipids (POPG and DOPG), zwitterionic glycerophospholipids (POPC, DOPC and DPPC) and mixed membranes composed of zwitterionic glycerophospholipids, cholesterol and sphingomyelin. The interaction of PrP with mixed membranes composed of DPPC, cholesterol and sphingomyelin is of particular interest. This composition of lipids has been shown to possess the same properties, such as detergent insolubility as raft domains isolated from the plasma membrane and therefore serve as good models of lipid rafts (Schroeder *et al.*, 1994, 1998). This systematic study provided a comprehensive insight into the nature of lipid-PrP interactions.

4.2   *Materials and Methods*

4.2.1   *Materials*

Glycerophospholipids (POPG, DOPG, POPC and DOPC), cholesterol and

Trp 99

Trp 145
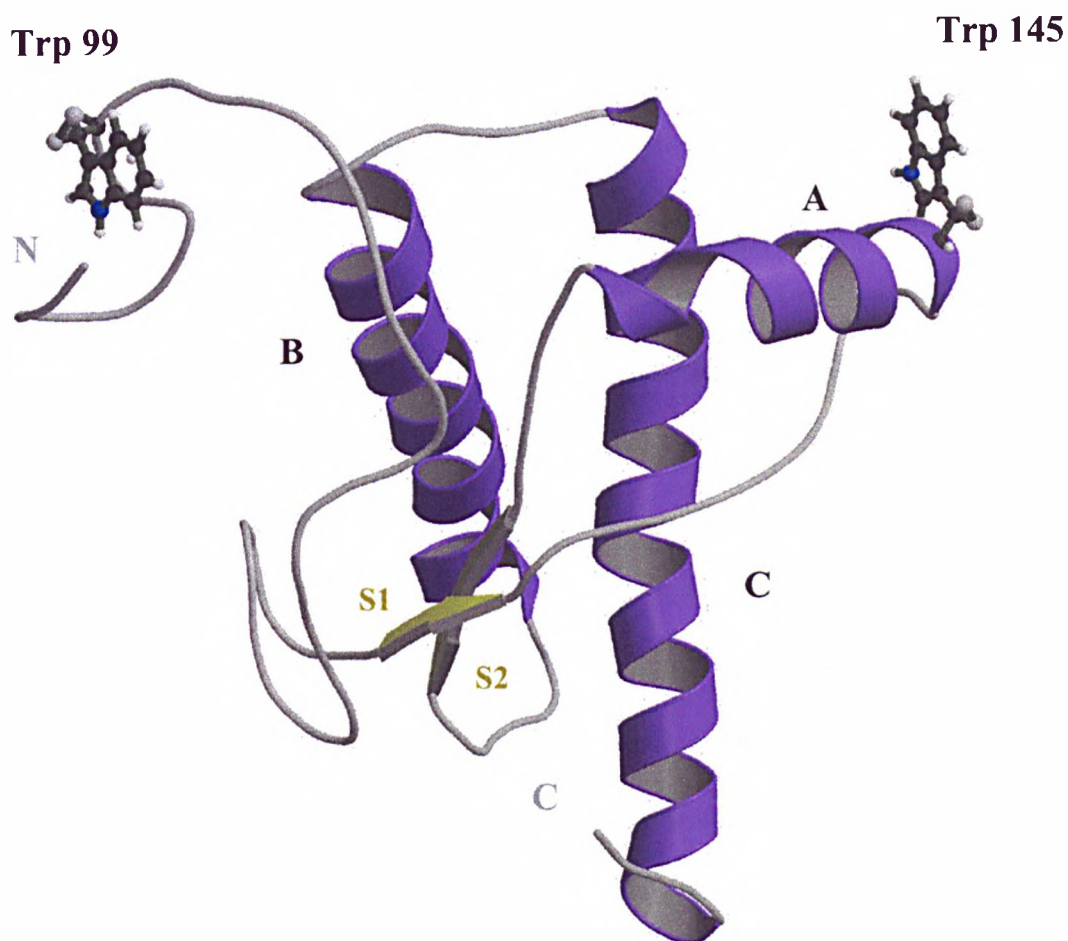
Figure 4.1: **Ribbon diagram of the three-dimensional structure of recombinant SHaPrP (90–231)**. The NMR structure of recombinant SHaPrP (90–231) in aqueous solution (James *et al.*, 1997) indicating the positions of the three α-helices (A, B and C) and the two antiparallel β-strands (S1 and S2). The tryptophan residues (Trp99 and Trp145) are highlighted in ball-and-stick representation. The structure was drawn using the program Molscript (Kraulis, 1991) and rendered with RASTER3D (Merritt & Bacon, 1997).

sphingomyelin were purchased from Avanti Polar lipids (Birmingham, AL). DPPC was obtained from Sigma-Aldrich (Poole, UK). All other chemicals were obtained from Sigma-Aldrich (Poole, UK), unless otherwise stated.

4.2.2 Lipid vesicles

Lipids in chloroform solutions were dried under a rotary evaporator and the resulting lipid film left under vacuum overnight to remove all traces of the organic solvent. For the preparation of mixed lipid membranes, lipids were co-dissolved in chloroform and a lipid film was formed as described above. Small unilamellar lipid vesicles were prepared by hydrating the required amount of dried lipid or the lipid films with the desired buffer: 20 mM sodium phosphate, pH 7.2 or 20 mM sodium acetate, pH 5.0. To avoid oxidative degradation of the lipids, buffers were deoxygenated with nitrogen gas and the hydrated lipids were maintained under a nitrogen atmosphere. After lipid hydration the resulting multilamellar liposome suspension was sonicated in a bath sonicator until a clear suspension of small unilamellar vesicles was obtained (typically $6 \times \frac{1}{2}$ h periods). These preparations typically yield vesicles with diameters ranging from 300 to 600 Å (Rankin *et al.*, 1998).

4.2.3 Binding of recombinant SHaPrP (90–231) to lipid membranes

Binding of recombinant PrP to various lipid vesicles was studied at 20 °C by monitoring the shift in the wavelength of the fluorescence emission maxima (λ_{max}). Binding of PrP to lipid vesicles was investigated at pH 7 and 5. For measurements at pH 7, vesicles were prepared in 20 mM sodium phosphate buffer, pH 7.2, whereas for measurements at pH 5 vesicles were in 20 mM sodium acetate buffer, pH 5.0.

The protein concentration was kept constant at 7.5 μM and the lipid concentration varied from 10 μM up to 10 mM. Lipid-protein complexes were prepared by adding 1 part of a 15 μM stock protein solution in 20 mM sodium acetate buffer, pH 5.5, to an equal volume of lipid vesicles at pH 7.2 or pH 5.0. The final pH of the lipid-protein samples were ~ 6.9 and ~ 5.2, respectively. Lipid-protein samples were mixed thoroughly and equilibrated for 2–3 minutes before fluorescence emission spectra were recorded on a Photon Technology International spectrofluorimeter. Emission spectra were recorded using 4 mm pathlength quartz cells. The excitation wavelength was 295 nm (2 nm bandwidth) and emission spectra were recorded from 300 to 450 nm (2 nm bandwidth). For samples containing raft-like membranes of DPPC/chol/SM at pH 7 the concentration of PrP and lipid were changed to 1 μM PrP and lipid concentration varied from 1.3 μM to 1.3 mM and a longer pathlength of 1 cm was used. This was necessary because scattering of light by mixed membranes containing saturated lipids, cholesterol and sphingomyelin tends to be higher, which distorts the emission spectra of PrP preventing the accurate determination of the λ_{max}. The concentration of both protein and lipid was reduced so that the lipid-protein ratio remained the same as for the binding studies with single lipid membranes i.e. lipid/protein ratio varying from 1.3:1 to 1300:1. Combining the lower protein concentration with a longer pathlength allowed for a comparable signal-to-noise ratio to be achieved as for spectra recorded with higher protein concentrations. Typically, 4 scans were averaged per spectrum in all experiments. The corresponding spectra for buffer background or lipid alone were subtracted from protein spectra.

Samples with increasing ionic strengths were prepared by adding aliquots of NaCl from a 5 M stock solution prepared in 20 mM sodium phosphate, pH 7.2 to either pre-existing lipid-protein complexes or to lipid vesicles alone prior to the addition of protein. The lipid-protein samples were prepared as above; protein concentration was 7.5 µM and lipid was 1 or 3 mM. The fluorescence spectra were recorded as described above and the corresponding backgrounds (buffer for protein solutions, or lipid with the equivalent salt concentration) were subtracted from protein spectra.

4.2.4 Quenching of tryptophan fluorescence

Fluorescence quenching experiments were performed in the absence and presence of lipid vesicles. One part of a 10 µM stock protein solution in 20 mM sodium acetate buffer, pH 5.5, was added to an equal volume of freshly prepared acrylamide solution from a 1 M acrylamide stock in 20 mM sodium phosphate, pH 7.2, or in 20 mM sodium acetate, pH 5.0. For samples containing lipid vesicles one part of the stock protein solution was added to an equal volume of lipid vesicles and quencher solution at pH 7.2 or pH 5.0. The final protein and lipid concentrations were 5 µM and 3 mM, respectively except for mixed membranes composed of DPPC/chol/SM where a lower lipid concentration of 1 mM was used to avoid light scattering problems. Acrylamide concentration varied from 0–0.3 M.

Tryptophan fluorescence emission spectra were recorded at each quencher concentration. The excitation wavelength was 295 nm and emission spectra were recorded from 300 to 450 nm. The excitation and emission bandwidths were 2 nm. The fluorescence quenching data were analysed according to the Stern-Volmer

equation (Eq. 4.1) for collisional quenching between the fluorophore and quencher (Lakowicz, 1983).

$$F_0/F = 1 + K_{SV}[Q] = \tau_0 / \tau = 1 + k_q \tau_0 [Q] \qquad \text{(Eq. 4.1)}$$

where, F_0 and F are the fluorescence intensities at λ_{max} in the absence and presence of quencher, respectively. K_{SV} is the Stern-Volmer constant for the collisional quenching process, [Q] is quencher concentration, τ_0 and τ are fluorescence lifetimes of the fluorephore in the absence and presence of the quencher, respectively and k_q is the rate constant for the bimolecular quenching process. The above equation predicts a linear plot of F_0/F *versus* [Q] for a homogeneously emitting solution. The slope of this plot yields the Stern-Volmer constant (K_{SV}).

4.3   Results

4.3.1   Changes in the tryptophan fluorescence upon binding of PrP to model lipid membranes

The fluorescence emission of most proteins originates from the indole ring of the tryptophan residues. Unlike, the emission of tyrosine fluorescence, tryptophan fluorescence is highly sensitive to the polarity of its surrounding environment (Lakowicz, 1983). As a result, the wavelength of the emission maxima (λ_{max}) of proteins can provide information on the average exposure of their tryptophan residues to the aqueous phase.

Binding studies of peptides to lipid membranes have confirmed the preference of aromatic residues for the lipid-water interface (Deber & Goto, 1996; Wimley & White, 1996). A shift in the λ_{max} to shorter wavelengths and increase in the fluorescence intensity are normally associated with the transfer of the tryptophan

residues from the hydrophilic environment in aqueous solution to the hydrophobic lipid phase. Although increases in fluorescence intensity concomitantly occurs with binding of peptides and proteins to lipid membranes this measurement does not reliably reflect lipid-protein interactions. Deviations from Beer-Lambert law are often encountered due to scattering of light by lipid-protein complexes. Shifts in the fluorescence wavelength maxima (λ_{max}) of proteins are a more reliable indicator of lipid-protein interactions.

SHaPrP (90–231) has two tryptophan residues at positions 99 and 145 (Figure 4.1), which dominate the fluorescence spectrum, ten tyrosine and three phenyalanine residues that make minor contributions to the overall intrinsic protein fluorescence. It is often necessary to eliminate this additional source of heterogeneity in the fluorescence of proteins. This is generally accomplished by using an excitation wavelength of 295 nm, where the absorption of tyrosine and phenylalanine is minimal. The fluorescence emission spectrum of SHaPrP (90–231) in solution has a maximum intensity (λ_{max}) at 348 nm. This value is typical of tryptophan residues in an aqueous environment (Lakowicz, 1983) and is in good agreement with the NMR structure, which shows the iodole rings partially exposed on the protein surface.

4.3.1.1   Interaction of recombinant SHaPrP (90–231) with negatively charged membranes

The fluorescence properties of PrP were considerably altered upon addition of negatively charged membranes. Representative emission spectra of PrP in the

presence of POPG membranes at pH 5 and 7 are shown in Figure 4.2. The wavelength of the emission maxima (λ_{max}) of PrP at both pH 7 and 5 is shifted to shorter wavelengths (blue shift) in the presence of POPG membranes. The observed blue shifts reflect the partitioning of the tryptophan residues into a more hydrophobic environment and are indicative of PrP binding to POPG membranes. A blue shift of λ_{max} of approximately 16 nm was observed with the binding of PrP to POPG membranes at pH 5 for a lipid-protein ratio of 1333:1 (7.5 μM PrP and 10 mM POPG), whereas a blue shift of about 10 nm was detected upon binding to POPG membranes at pH 7 for the equivalent lipid-protein ratio. This implies that the tryptophan residues of PrP when bound to negatively charged membranes of POPG at pH 5 were less exposed to the hydrophilic aqueous environment presumably due to a deeper penetration into the hydrophobic lipid phase.

Binding of PrP to DOPG membranes at pH 7 resulted in a blue shift of 12 nm, suggesting that the composition of the fatty acid chains have no major influence on the binding of PrP to negatively charged membranes.

4.3.1.2   *Interaction of recombinant SHaPrP (90–231) with zwitterionic membranes*

The incubation of PrP with liquid-crystalline zwitterionic membranes of DOPC at pH 7 and POPC at both pH 7 and pH 5 (Figure 4.3) showed a negligible blue shift in the λ_{max} (1 nm) of PrP, the results indicated a lack of lipid-protein interactions. In contrast, a blue shift in the λ_{max} of PrP with gel-phase zwitterionic membranes of DPPC at pH 7 (Figure 4.4) and raft-like membranes composed of DPPC, cholesterol and spingomyelin at pH 7 (DPPC/chol/SM, 50:30:20 molar ratio)
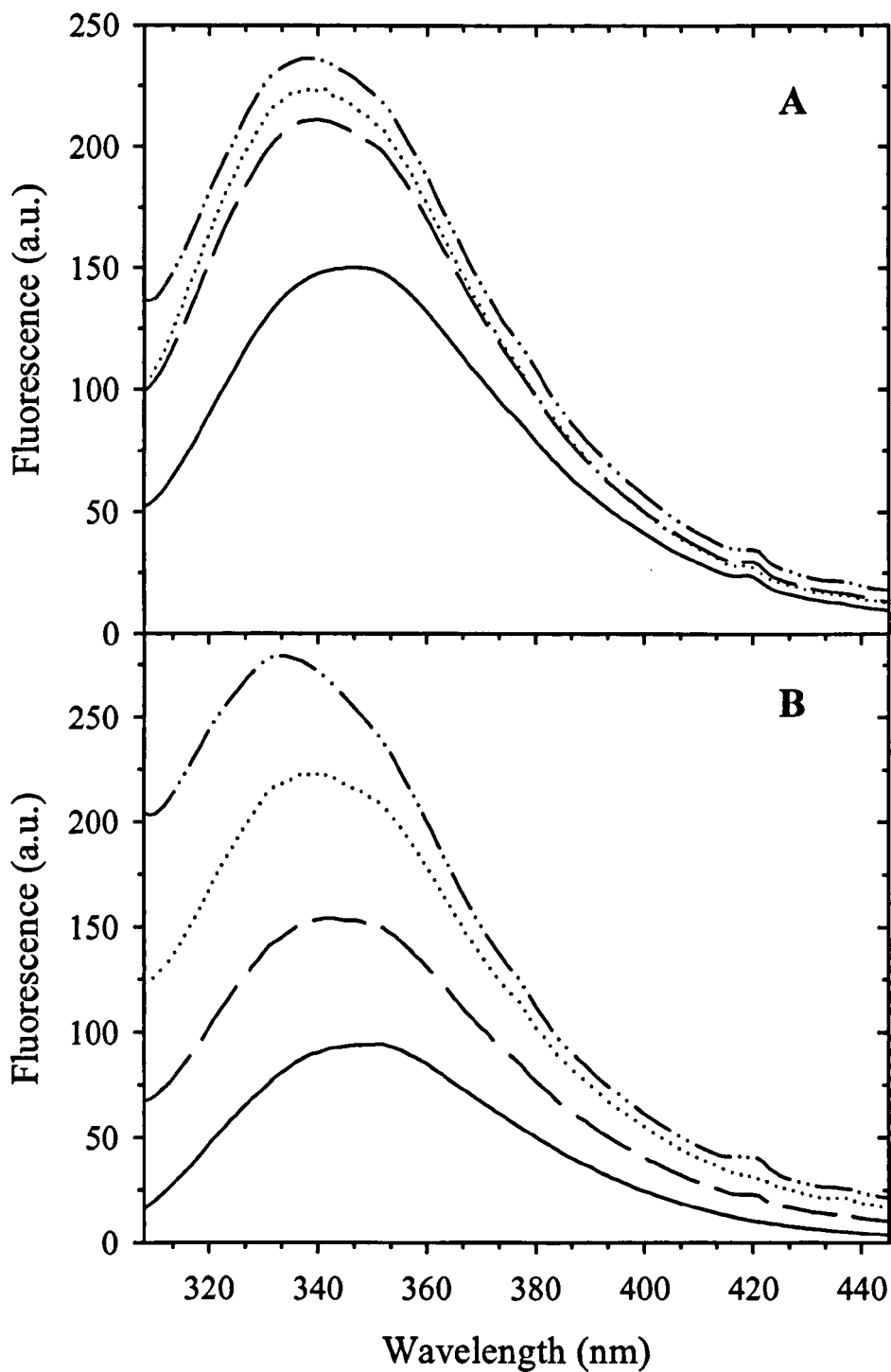
Figure 4.2: **Equilibrium fluorescence spectra of SHaPrP (90–231) in solution and in the presence of POPG membranes.** (A) Emission spectra of PrP in solution, pH 7 (solid line) and in the presence of increasing concentrations of POPG, pH 7: 0.05 (dashed line), 0.25 (dotted line) and 0.5 mM (dash-dot-dot line). (B) Emission spectra of PrP in solution, pH 5 (solid line) and in the presence of increasing concentrations of POPG, pH 5: 0.03 (dashed line), 0.05 (dotted line) and 0.5 mM (dash-dot-dot line). The final protein concentration was 7.5 μM. The excitation wavelength was 295 nm and spectra were recorded at 20 °C.
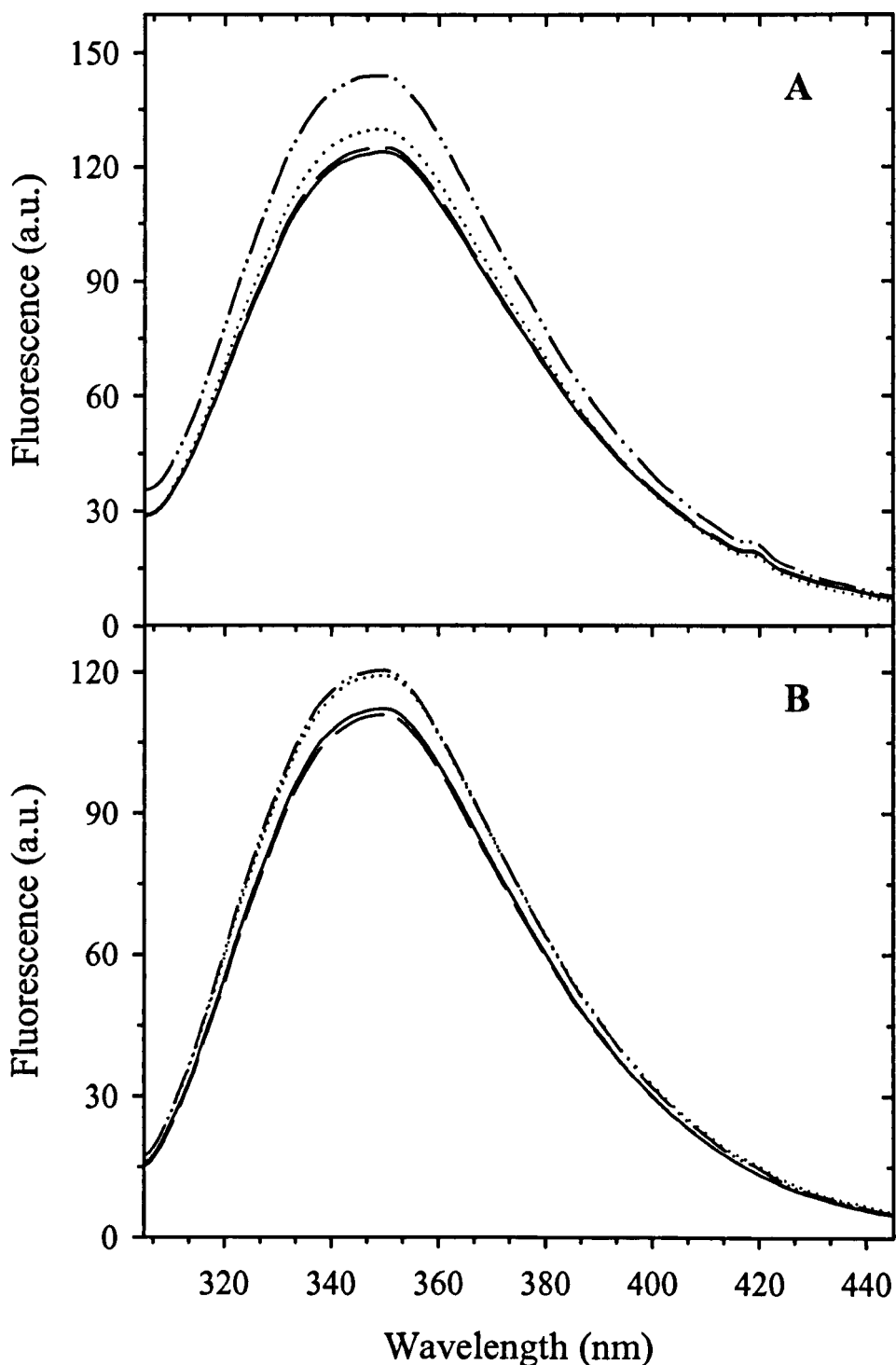
Figure 4.3: **Equilibrium fluorescence spectra of SHaPrP (90–231) in solution and in the presence of POPC membranes.** (A) Emission spectra of PrP in solution, pH 7 (solid line) and in the presence of increasing concentrations of POPC, pH 7: 0.01 (dashed line), 2 (dotted line) and 5 mM (dash-dot-dot line). (B) Emission spectra of PrP in solution, pH 5 (solid line) and in the presence of increasing concentrations of POPC vesicles, pH 5: 0.01 (dashed line), 2 (dotted line) and 5 mM (dash-dot-dot line). The final protein concentration was 7.5 μM. The excitation wavelength was 295 nm and spectra were recorded at 20 °C.
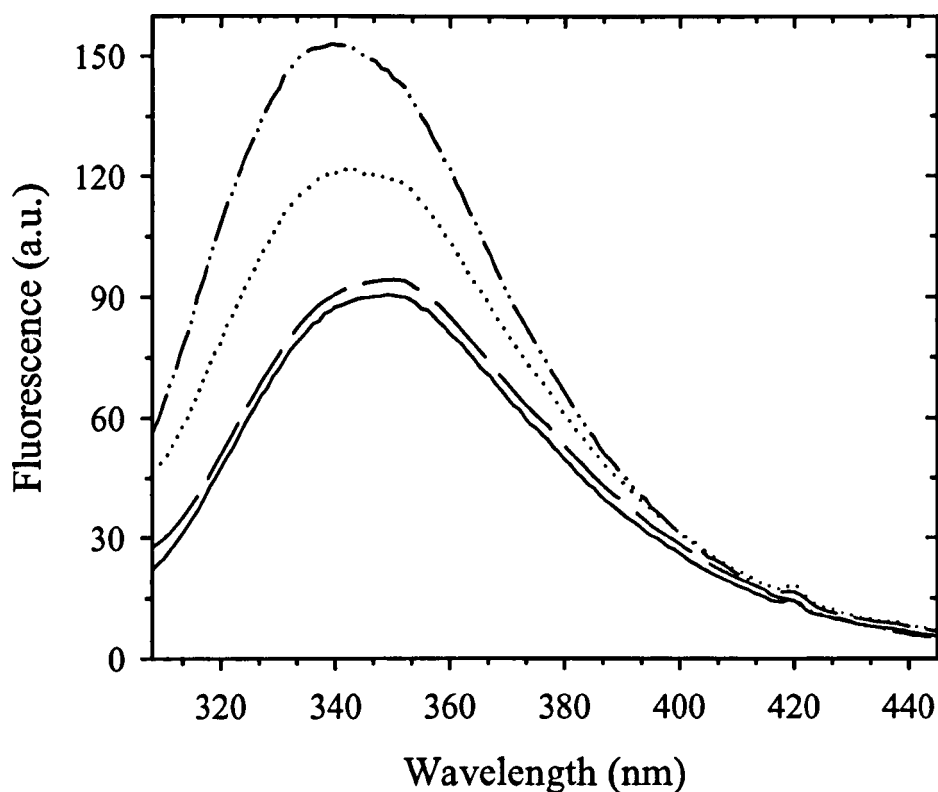
Figure 4.4: **Equilibrium fluorescence spectra of SHaPrP (90–231) in solution and in the presence of DPPC membranes, pH 7.** Emission spectra of PrP in solution (solid line) and in the presence of increasing concentrations of DPPC: 0.2 (dashed line), 1.5 (dotted line) and 3 mM (dash-dot-dot line). The final protein concentration was 7.5 μM. The excitation wavelength was 295 nm and spectra were recorded at 20 °C.

(Figure 4.5A) was detected. A shift of ~ 11 nm and ~ 9 nm, respectively, was observed at a lipid-protein ratio of 1333:1. Interestingly, no significant binding was observed with DPPC/chol/SM membranes (50:30:20 molar ratio) at pH 5 (Figure 4.5B).

No change in the fluorescence properties of PrP were detected with mixed membranes composed of DOPC with cholesterol (DOPC/chol, 70:30 molar ratio) and cholesterol plus sphingomyelin (DOPC/chol/SM, 50:25:25 molar ratio), suggesting a lack of lipid-protein interactions. The results demonstrate that PrP exhibits a preference for zwitterionic lipids in the gel-crystalline phase and for raft-like membranes composed of DPPC/chol/SM at pH 7.

A summary of the different lipid systems studied is given in Table 4.1, in which the emission λ_{max} values of PrP upon addition of the different membranes are shown. Figure 4.6 shows the dependence of the blue shift in the emission maxima of PrP as a function of lipid concentration. The blue shift was determined by subtracting the λ_{max} for PrP in the presence of lipid from the λ_{max} for PrP in solution $(\lambda_{max}^{sol} - \lambda_{max}^{lip})$.

4.3.1.3   Influence of ionic strength on PrP-lipid interactions

Binding of PrP to lipid membranes was also examined in the presence of high salt concentrations. These experiments were performed in order to examine the nature of PrP association with lipid membranes. Binding of human PrP with negatively charged membranes was suggested to be predominantly driven by electrostatic interactions between the positively charged amino acid
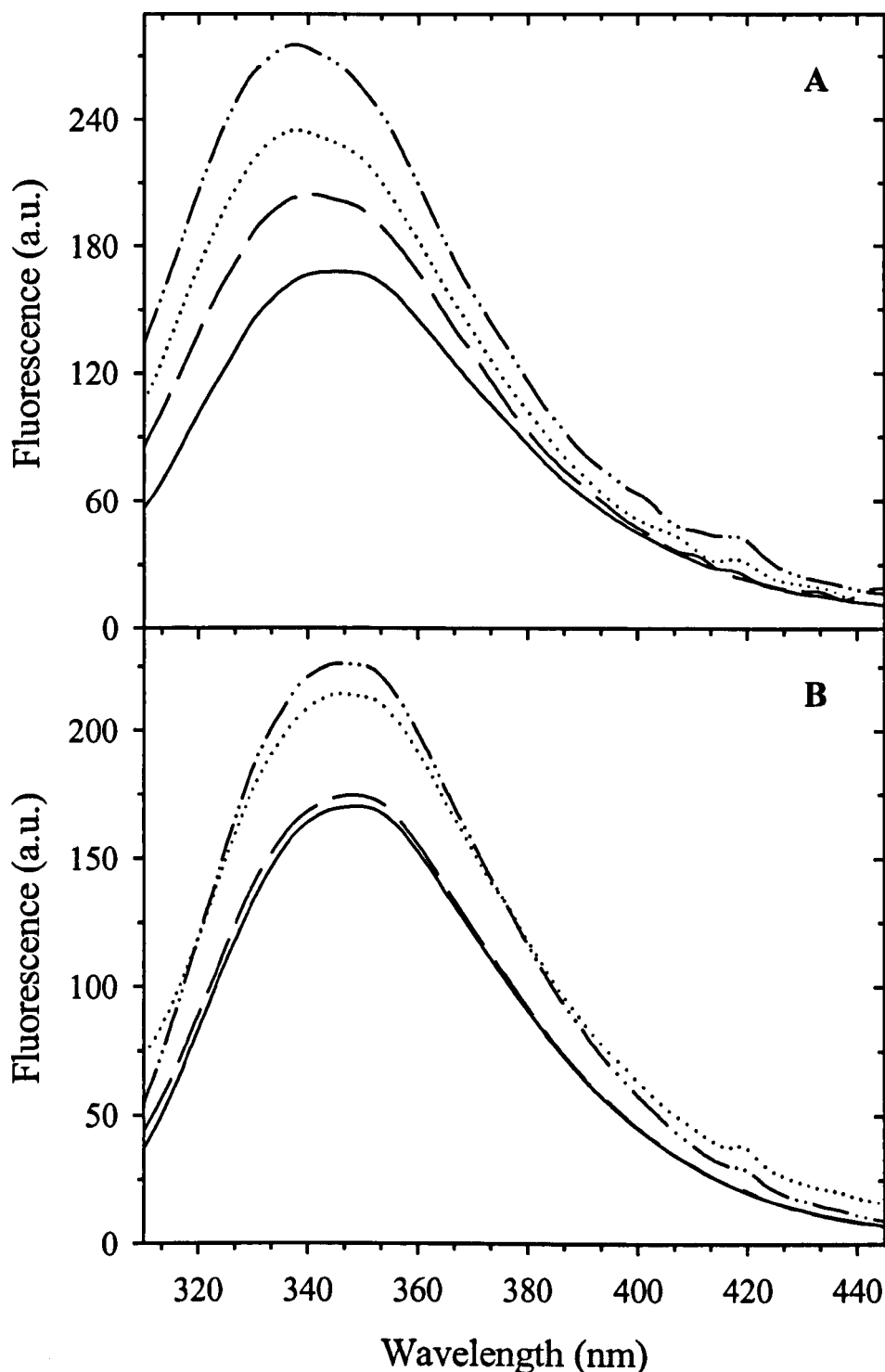
Figure 4.5: **Equilibrium fluorescence spectra of SHaPrP (90–231) in solution and in the presence of raft-like membranes of DPPC/chol/SM (50:30:20 molar ratio).** (A) Emission spectra of PrP in solution, pH 7 (solid line) and in the presence of increasing concentrations of DPPC/chol/SM, pH 7: 0.1 (dashed line), 0.5 (dotted line) and 0.6 mM (dash-dot-dot line). (B) Emission spectra of PrP in solution, pH 5 (solid line) and in the presence of increasing concentrations of DPPC/chol/SM, pH 5: 1 (dashed line), 2 (dotted line) and 5 mM (dash-dot-dot line). The final protein concentration was 1 μM for PrP at pH 7 and 7.5 μM for protein at pH 5. The excitation wavelength was 295 nm and spectra were recorded at 20 °C.

Table 4.1: Lipid-induced changes in the wavelength of the fluorescence maximum of SHaPrP (90–231)[a]

System	pH	Lipid-Protein Molar Ratio	λ_{max} (nm)
PrP in solution	7	——	348
	5	——	348
PrP + POPG	7	1333:1	338
	5	1333:1	332
PrP +DOPG	7	1333:1	336
PrP + POPC	7	1333:1	347
	5	1333:1	347
PrP + DOPC	7	1333:1	347
PrP + DOPC/chol[b]	7	1333:1	348
PrP + DOPC/chol/SM[c]	7	1333:1	348
PrP + DPPC	7	1333:1	337
PrP + DPPC/chol/SM[d]	7[e]	1333:1	339
	5	1333:1	347

[a]Protein concentration was 7.5 µM and pathlength was 4 mm. [b]DOPC/chol, 70:30 molar ratio. [c]DOPC/chol/SM, 50:25:25 molar ratio. [d]DPPC/chol/SM 50:30:20 molar ratio. [e]Protein concentration was 1 µM and pathlength was 1 cm.
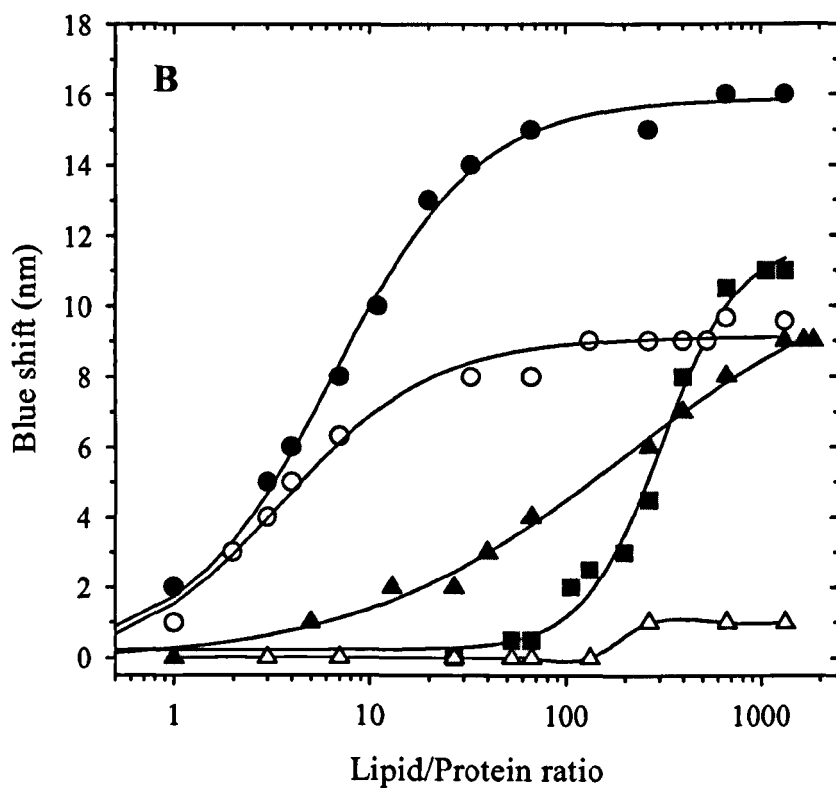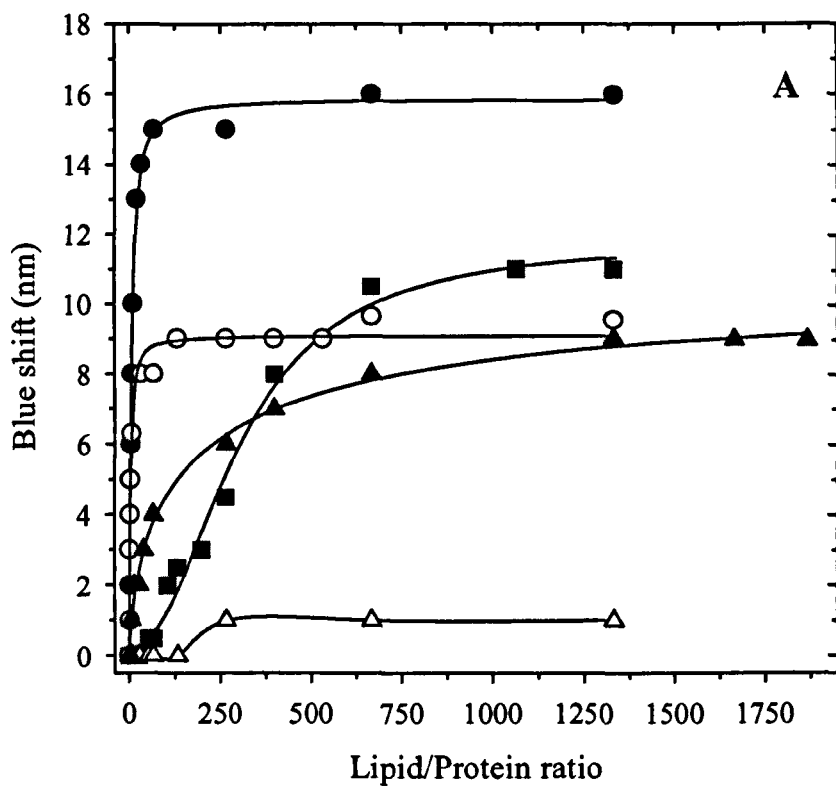
Figure 4.6: **Blue shift of λ_max of SHaPrP (90–231) with increasing lipid.** PrP fluorescence was measured in the presence of increasing concentrations of POPG vesicles at pH 7 (open circles) and pH 5 (closed circles), DPPC vesicles, pH 7 (closed squares), DPPC/chol/SM vesicles at pH 7 (closed triangles) and pH 5 (open triangles). The protein concentration was kept constant at 7.5 μM except for binding to DPPC/chol/SM where the concentration of PrP was kept at 1 μM. The data is displayed in both linear (A) and logarithmic (B) scale for the x-axis. The logarithmic scale representation highlights the changes at lower lipid concentrations, whereas the linear representation highlights the saturation levels at higher lipid concentrations.

residues of the protein and negatively charged lipid headgroups (Morillas *et al.*, 1999).

Two different experiments were performed; in the first NaCl was also added to the lipid vesicles prior to the addition of PrP and in the second the ionic strength of the lipid-PrP complexes was increased. A high lipid-protein ratio of either 133:1 or 400:1 was used in these experiments to ensure saturation of the lipid binding sites with protein.

The addition of NaCl to negatively charged POPG lipid vesicles at pH 7 prior to the addition of PrP resulted in the shielding of charges at the membrane and protein surfaces. In the presence of salt (0.3 M NaCl) a shift in the λ_{max} of only 4 nm was observed compared to a shift of 11 nm in the absence of salt at pH 7(Figure 4.7). This observation suggests that shielding of charges on both the protein and membrane surfaces strongly diminished binding of PrP to negatively charged membranes.

In another experiment increasing concentrations of NaCl (0–0.3 M) were added to PrP-POPG complexes at pH 7. If binding of PrP to negatively charged membranes was primarily due to electrostatic interactions between charged groups on the surface of PrP and lipid membranes then such interactions would be disrupted with increasing amounts of salt. This would eventually result in the emission spectra of PrP in the presence of lipid membranes to reach the characteristic spectral parameters of protein in solution. However, only a small fraction of the protein appeared to be released, as judged by a small red shift in the λ_{max} of 2 nm with 0.2 M NaCl relative to the lipid-bound state. Increasing concentrations of NaCl did not induce a further shift in the λ_{max} of PrP (Figure 4.8).
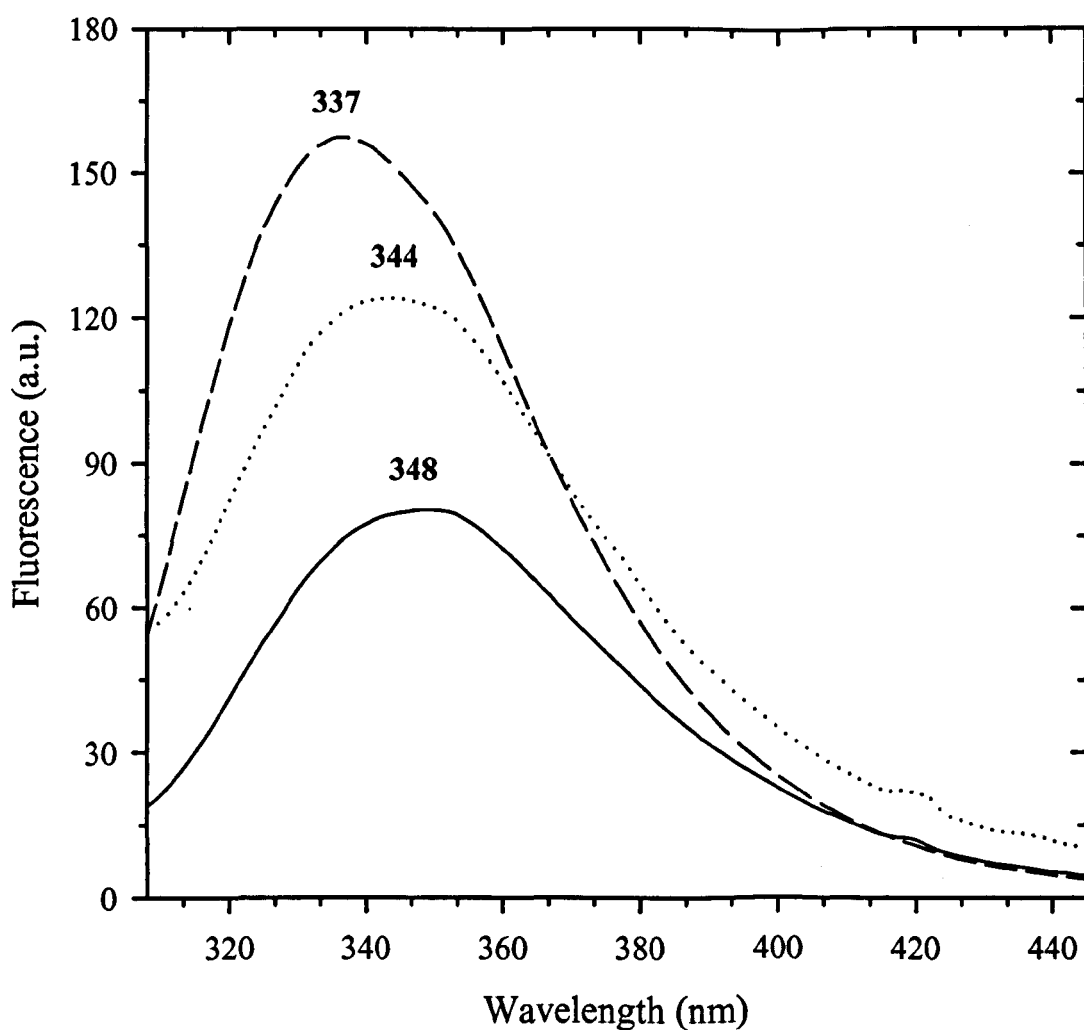
Figure 4.7: **Changes in the tryptophan fluorescence of SHaPrP (90–231) upon binding to POPG membranes in the presence of salt.** Emission spectra of PrP in solution at pH 7 with 0.3 M NaCl (solid line), bound to POPG vesicles (dashed line) with no salt and in the presence of POPG vesicles with 0.3 M NaCl (dotted line). Concentration of PrP was 7.5 µM and lipid 3 mM. Final pH of lipid-protein complex was 7.0. The excitation wavelength was 295 nm and spectra were recorded at 20 °C. The numbers above each spectrum show the value of λ_{max} in nm.
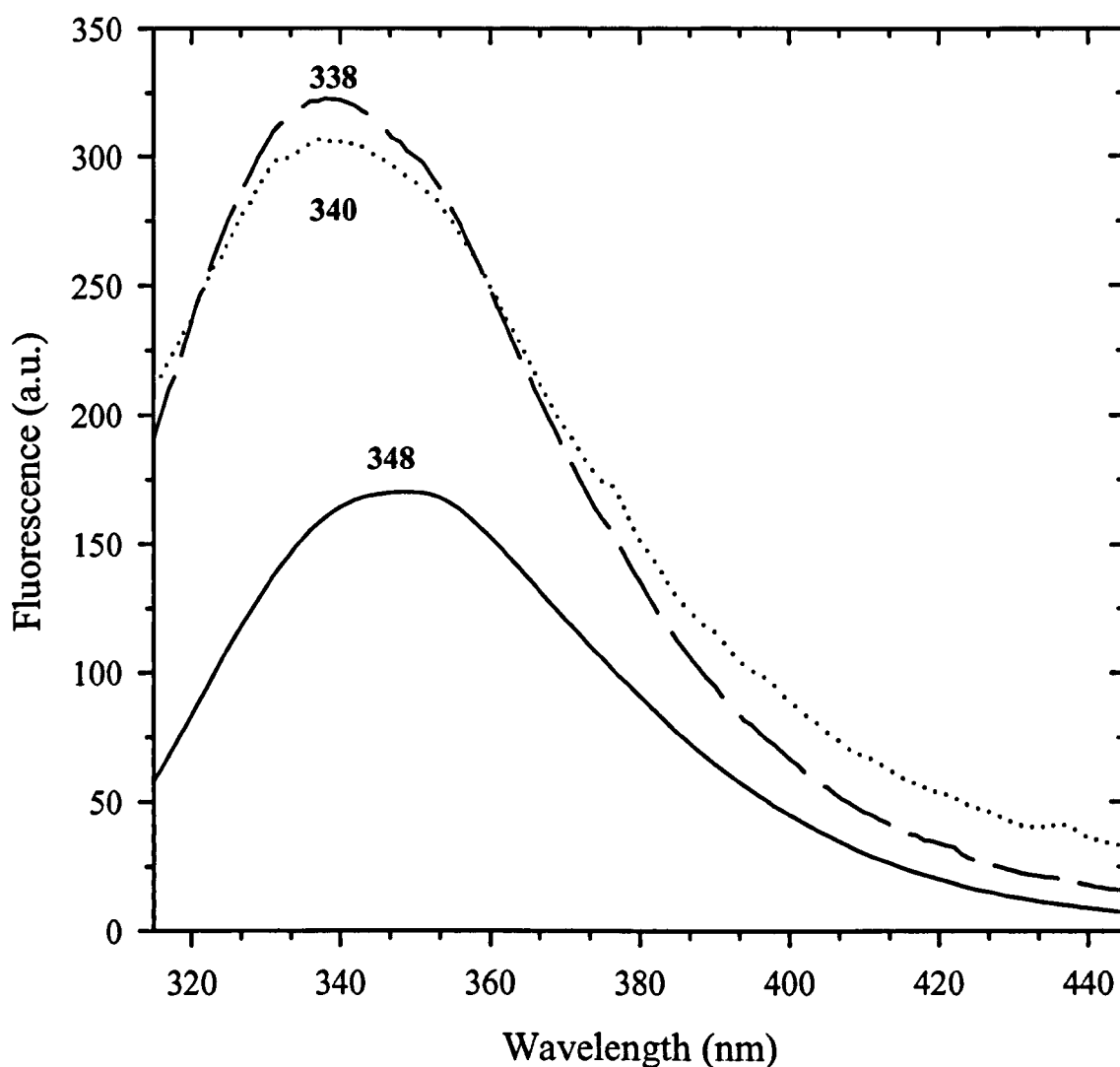
Figure 4.8: **Changes in tryptophan fluorescence of PrP-POPG complexes upon addition of salt.** Emission spectrum of PrP in solution at pH 7 with 0.25 M NaCl (solid line) and bound to POPG vesicles in the absence of salt (dashed line) and in the presence of 0.25 M NaCl (dotted line). Concentration of PrP was 7.5 μM and lipid 1 mM. Final pH of lipid-protein complex was 7.0. The excitation wavelength was 295 nm and spectra were recorded at 20 °C. The numbers above and below each spectrum show the value of λ_{max} in nm.

Trp fluorescence measurements in the presence of salt (Figure 4.7) support the interpretation that binding of PrP to lipid bilayers composed of negatively charged lipids is driven by electrostatic interactions between positively charged residues on the protein surface and negative charges on the lipid headgroups. However, the salt experiments described in Figure 4.8 showed that PrP is not released from the membrane by the addition of salt. This result suggests that once the protein is bound to the membrane surface probable structural rearrangements occur in the protein that expose hydrophobic surfaces, which then interact with hydrophobic regions of the lipid membrane. Based on these results the interaction of PrP with negatively charged membranes appears to be a complex process that involves a combination of electrostatic and hydrophobic lipid-protein interactions.

Binding of PrP to the raft-like membranes composed of DPPC, cholesterol and sphingomyelin at pH 7 was also investigated in the presence of increasing concentrations of salt (0–0.3 M). In contrast, to POPG membranes, where binding was significantly diminished in the presence of salt, binding of PrP to the raft-like membranes of DPPC/chol/SM at pH 7 was not affected by the addition of salt. Furthermore, increase in ionic strength led to an additional increase in fluorescence intensity (Figure 4.9) and a further shift in the λ_{max} of 1 nm. In this situation high ionic strength did not interfere with the binding process and shielding of the charges at the surface of PrP and lipid bilayers slightly increased the lipid affinity of PrP for zwitterionic membranes. The addition of salt to pre-formed DPPC/chol/SM-PrP complexes at pH 7 failed to dissociate the protein-lipid complexes (Figure 4.10) as judged by a lack of change in the emission spectra.
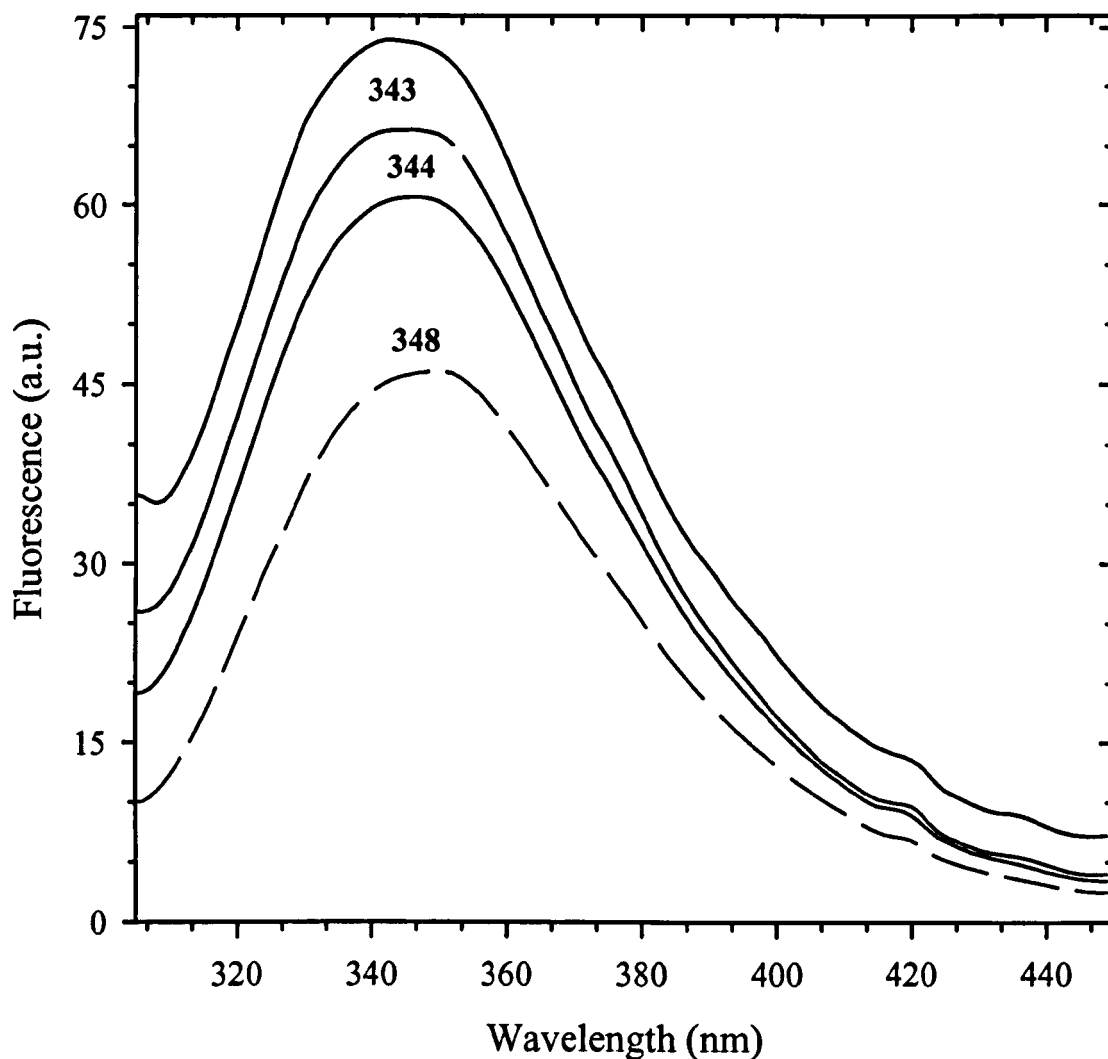
Figure 4.9: **Changes in the tryptophan fluorescence of SHaPrP (90–231) upon binding to raft-like membranes of DPPC/chol/SM (50:30:20 molar ratio) in the presence of salt.** Emission spectra of PrP in solution at pH 7 with 0.3 M NaCl (dashed line), PrP bound to DPPC/chol/SM vesicles (solid lines) with increasing concentrations of NaCl: 0, 0.2, 0.3 M (lower to upper spectrum). Concentration of PrP was 7.5 μM and lipid 1 mM. Final pH of lipid-protein complex was 7. The excitation wavelength was 295 nm and spectra were recorded at 20 °C. The numbers above and below each spectrum show the value of the λ_{max} in nm.
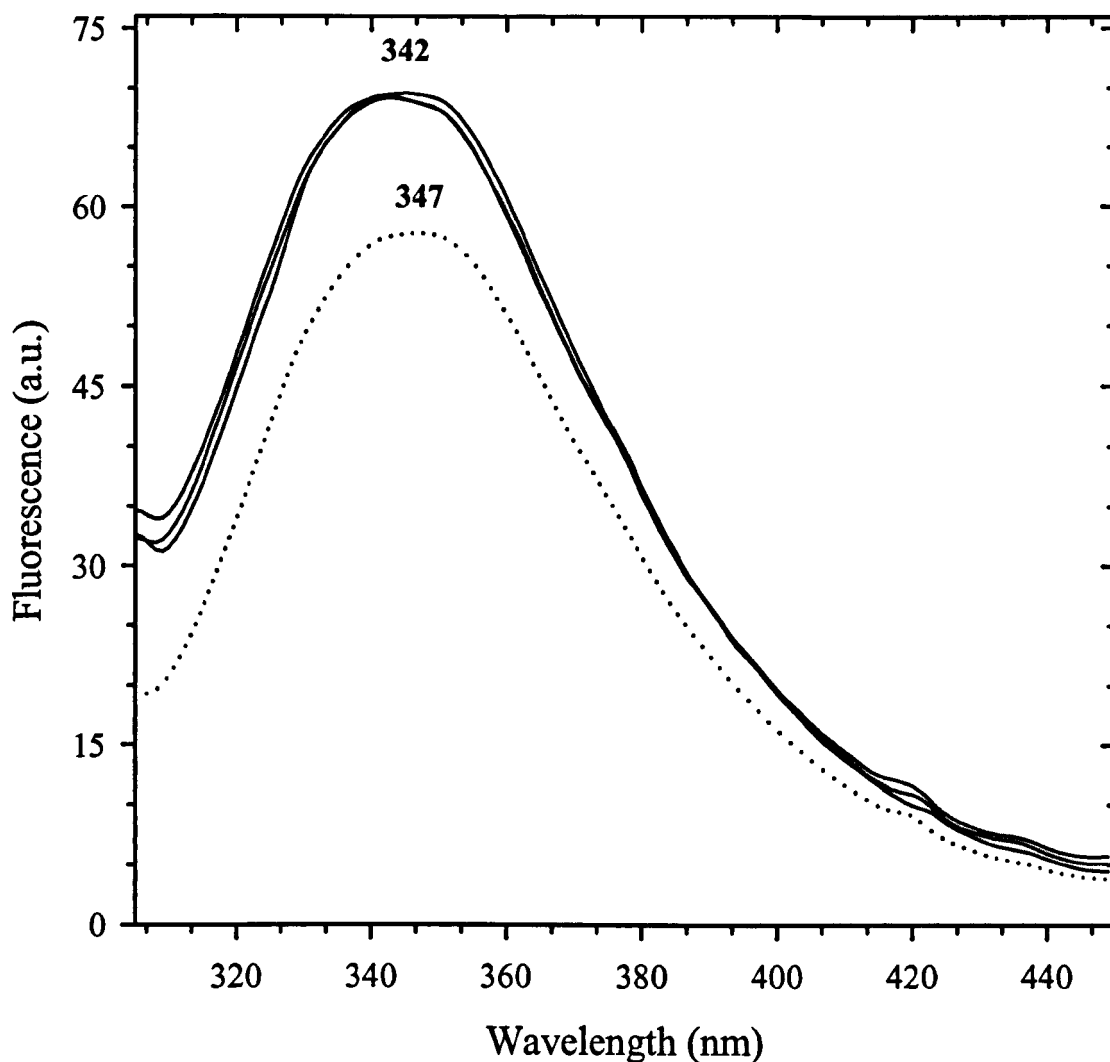
Figure 4.10: **Changes in the tryptophan fluorescence of DPPC/chol/SM-PrP complexes upon addition of salt.** Emission spectra of PrP in solution at pH 7 with 0.3 M NaCl (dotted line), PrP bound to DPPC/chol/SM vesicles (solid lines) with increasing concentrations of NaCl: 0, 0.2, 0.3 M. Concentration of PrP was 7.5 μM and lipid 1 mM. Final pH of lipid-protein complex was 7. The excitation wavelength was 295 nm and spectra were recorded at 20 °C. The numbers above each spectrum show the value of the λ_{max} in nm.

The results imply that the interaction of PrP to raft-like membranes involves hydrophobic interactions. The electrostatic contribution to binding of PrP to the raft-like membranes appears to be less important.

4.3.2 Acrylamide quenching of PrP fluorescence

To further examine the location of the tryptophan residues of PrP when bound to lipid membranes, fluorescence quenching experiments with acrylamide were performed. Acrylamide is a neutral but polar quencher and is considered to have access to all but the most highly buried tryptophan residues of proteins and peptides (Kurzban *et al.*, 1989) and it is also unable to penetrate into the hydrophobic core of the lipid bilayer. Therefore, efficient quenching of tryptophan fluorescence by acrylamide would indicate the exposure of the residues to the aqueous solvent, while protection from the quenching solutions would occur when protein tryptophan residues are sequestered away from the aqueous solvent (Lakowicz, 1983).

Negatively charged POPG vesicles, zwitterionic vesicles composed of POPC and mixed raft-like membranes consisting of DPPC, cholesterol and sphingomyelin (50:30:20 molar ratio) were investigated in the fluorescence quenching experiments.

Increasing concentrations of acrylamide gradually quenched the tryptophan fluorescence of PrP in aqueous buffer at pH 5 (Figure 4.11A). In contrast, to PrP in solution, the presence of POPG membranes at pH 5 appeared to lead to a smaller reduction in the fluorescence intensity (Figure 4.11B). Figure 4.12 illustrates the emission spectra of PrP at pH 7 in aqueous solution and in the presence of POPG, POPC vesicles and raft-like membranes of DPPC/chol/SM at pH 7 in the absence
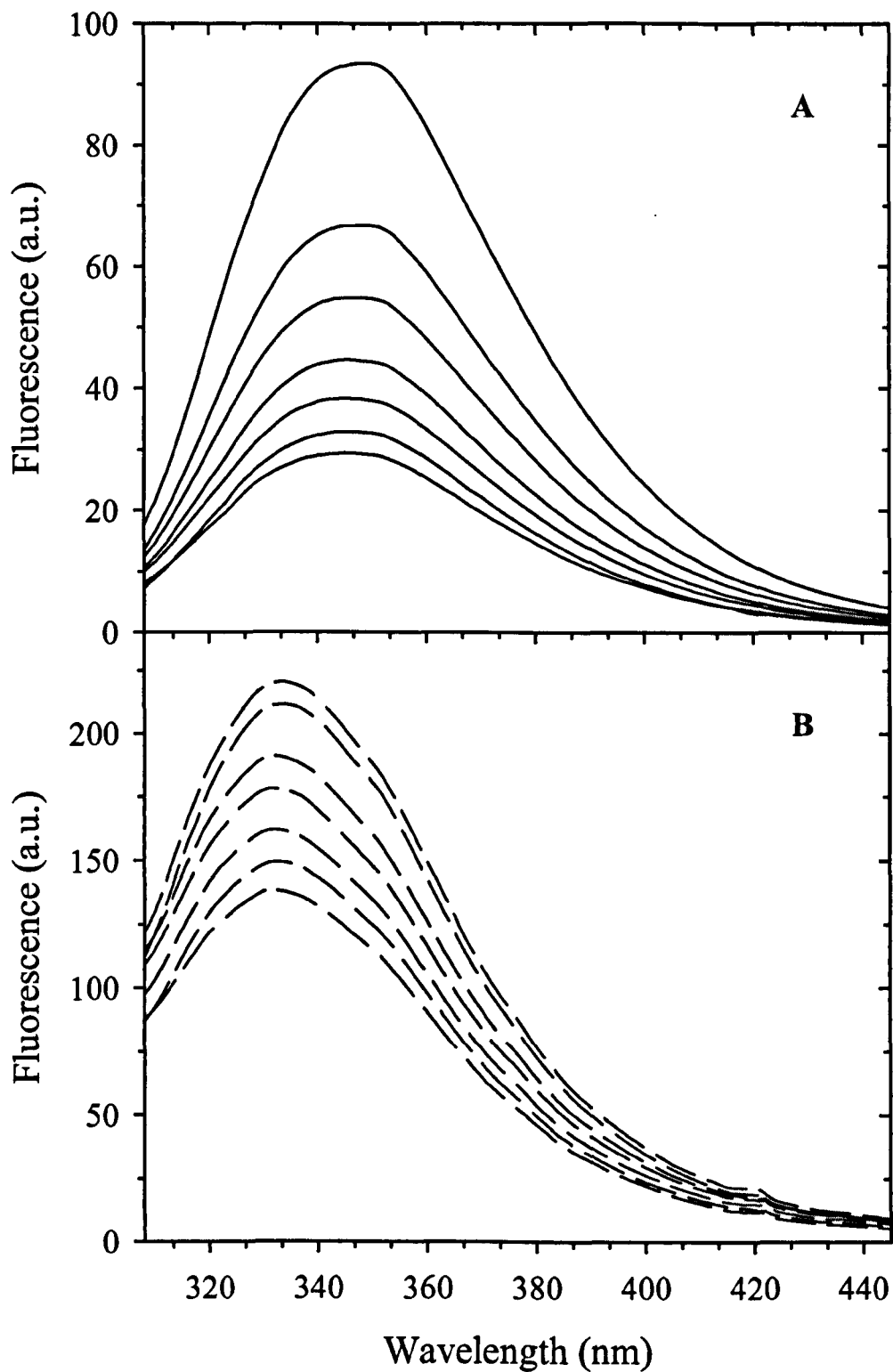
Figure 4.11: **Quenching of tryptophan fluorescence by acrylamide at pH 5.** (A) Emission spectra of PrP in solution at pH 5 and (B) with POPG membranes with increasing concentrations of acrylamide: 0, 0.05, 0.10, 0.15, 0.20, 0.25, 0.30 M (upper to lower spectrum). The final protein and lipid concentrations were 5 μM and 3 mM, respectively.
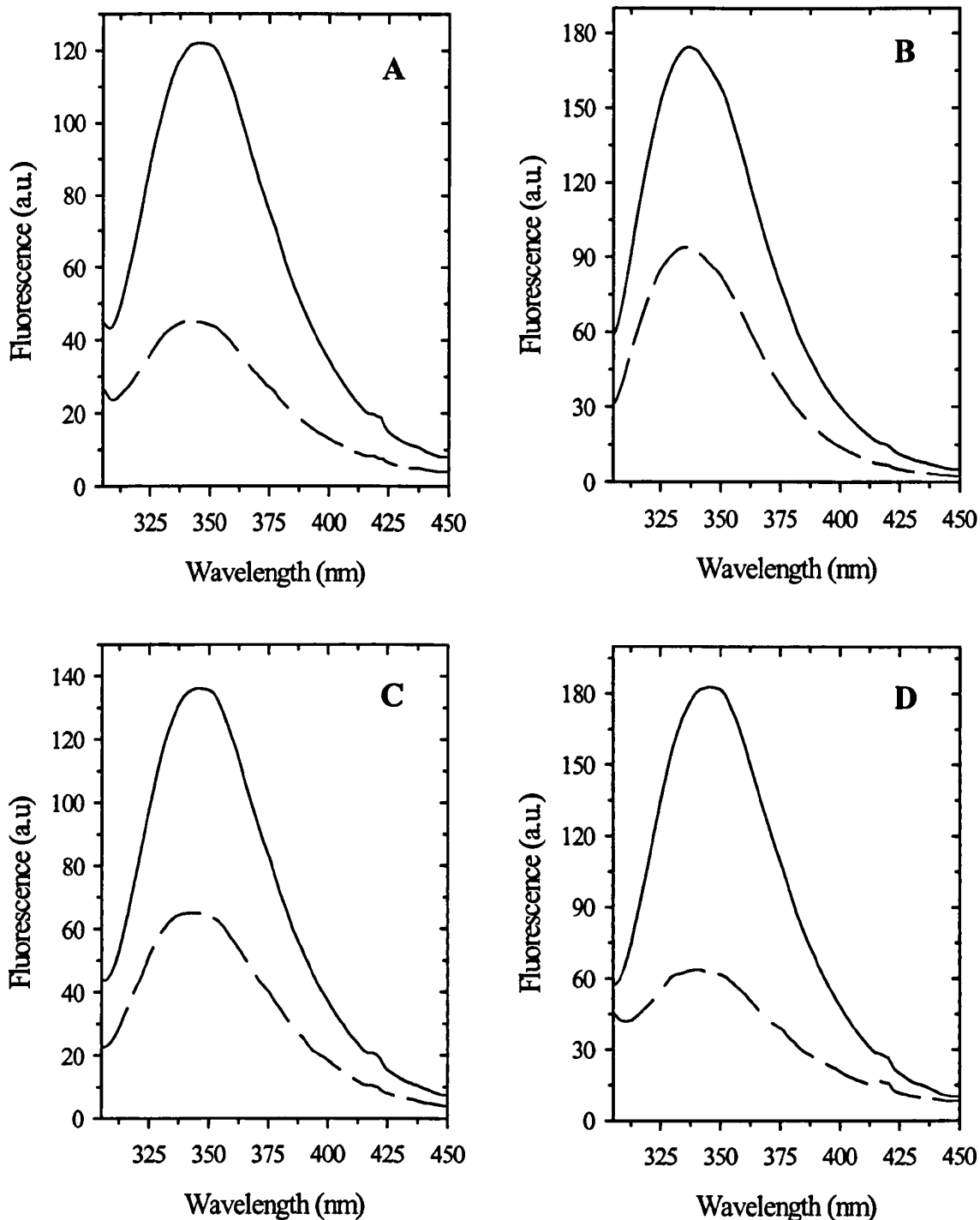
Figure 4.12: **Quenching of tryptophan fluorescence by acrylamide at pH 7.** A–D emission spectra of PrP in the absence (solid line) and presence of 0.3 M acrylamide (dashed line). (A) PrP in solution and with (B) POPG vesicles, (C) DPPC/chol/SM vesicles, (D) POPC vesicles. The final protein and lipid concentrations were 5 μM and 3 mM, respectively except for DPPC/chol/SM membranes where lipid concentration was 1 mM.

115

and presence of 0.3 M acrylamide. For the quenching experiments the protein concentration was kept constant at 5 μM. At first inspection the results suggested that negatively charged membranes of POPG at both pH 5 and 7 and raft-like membranes of DPPC/chol/SM at pH 7, shielded the tryptophan residues of PrP from the aqueous quencher solution. Little or no protection appeared to occur with POPC membranes, in good agreement with the tryptophan results, which showed no significant binding of PrP to POPC membranes.

The fluorescence quenching data were quantitatively analysed according to the Stern-Volmer equation for collisional quenching (Equation 4.1). Figure 4.13 shows the Stern-Volmer plots for acrylamide quenching of tryptophan fluorescence of PrP in the absence and presence of the different membrane systems at pH 7 and 5. Both protein in solution and in the presence of membranes exhibited linear Stern-Volmer plots, suggesting that both tryptophan residues (Trp99 and Trp145) are equally accessible to the quencher (Lakowicz, 1983). The Stern-Volmer quenching constants (K_{SV}) were determined from the slopes of the Stern-Volmer plots and are presented in Table 4.2.

Table 4.2   ***Stern-Volmer quenching constants (K_{SV}) for SHaPrP (90–231) in solution and in the presence of lipid membranes[a]***

System	pH	K_{SV} (M^{-1})	λ_{max} (nm)[c]
PrP	7	5.78	347
	5	7.31	347
PrP + POPG	7	2.58	336
	5	1.87	333
PrP + DPPC/chol/SM[b]	7	3.46	343
PrP + POPC	7	5.79	346
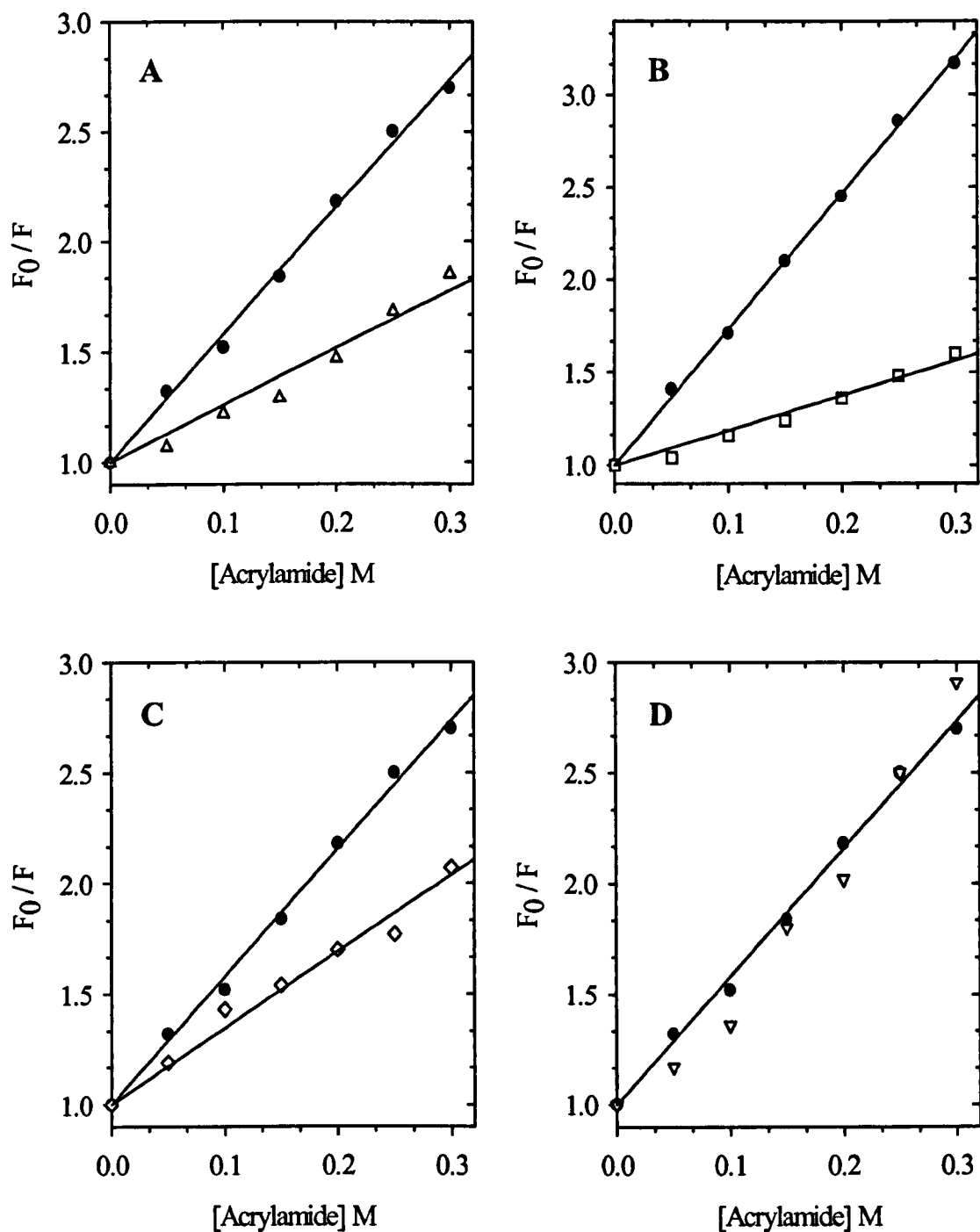
Figure 4.13: **Stern-Volmer plots for the fluorescence quenching of SHaPrP (90–231) by acrylamide.** Fluorescence quenching of PrP in solution at pH 7 (A, C & D) and pH 5 (B) (closed circles). (A) Fluorescence quenching in the presence of POPG vesicles, pH 7 (open triangles); (B) POPG vesicles, pH 5 (open squares); (C) DPPC/chol/SM mixed lipid vesicles, pH 7 (open diamonds) and (D) POPC vesicles, pH 7 (downward open triangles). Fluorescence emission spectra of PrP were recorded at 20 °C, using an excitation wavelength of 295 nm and the fluorescence intensities in the absence (F_0) and presence of acrylamide (F) were determined at the λ_{max}.

The extent of protection of the Trp residues from acrylamide quencher solution is reflected by the Stern-Volmer constants, which decrease when tryptophan residues are shielded from the aqueous environment. The Stern-Volmer constant indicated that tryptophan residues of PrP in solution at pH 5 are slightly more exposed to the aqueous environment compared to the protein at pH 7 (Table 4.2). Lower Stern-Volmer constants were derived from the plots of PrP with POPG membranes at pH 5 and 7 (Figure 4.13A,B & Table 4.2). This indicates that the tryptophan residues of PrP become less accessible to quenching by acrylamide upon binding and possibly partially inserting into the POPG lipid bilayer. Binding of PrP to raft-like membranes of DPPC/chol/SM, pH 7 produced an intermediate value for the Stern-Volmer constant, which still indicated an appreciable protection of the tryptophan residues from the quencher relative to protein in solution (Figure 4.13C & Table 4.2). Finally in the presence of POPC vesicles at pH 7 an equivalent degree of quenching is observed to that of PrP in solution, suggesting that the protein remained in the aqueous environment. The extent of protection from acrylamide paralleled the magnitude of the lipid-induced blue shifts.

4.4 Discussion

Intrinsic protein fluorescence is a very sensitive tool for monitoring binding of proteins and peptides to lipid membranes. In general, tryptophan residues buried

118

within a hydrophobic milieu, such as that of lipid membranes exhibit, an increased fluorescence intensity and the positions of their emission maxima (λ_{max}) are blue shifted when compared with surface exposed tryptophan residues (Lakowicz, 1983). SHaPrP (90–231) has two tryptophan residues, Trp99 and Trp145 (Figure 4.1), which are partially exposed on the protein surface. In this chapter the fluorescence emission of these two Trp residues is used to describe the binding of SHaPrP (90–231) to model lipid membrane systems containing a single type of lipid or mixtures of different lipids. The binding of PrP to lipid membranes was investigated at pH 7, to represent the pH surrounding the plasma membrane and pH 5, to model the acidic environment of endosomes. The plasma membrane and endocytic organelles have been proposed as relevant sites for PrP^{Sc} formation.

The Trp fluorescence results with SHaPrP (90–231), without the GPI anchor, shows that PrP binds to negatively charged membranes at both pH 5 and 7 and to gel-phase zwitterionic membranes at pH 7. Binding was also observed for raft-like membranes composed of DPPC, cholesterol and sphingomyelin (DPPC/chol/SM, 50:30:20 molar ratio) at pH 7, but not at pH 5. No significant binding was observed for liquid-crystalline zwitterionic membranes of DOPC or POPC, nor their mixtures with cholesterol and sphingomyelin at pH 7 (Table 4.1 & Figure 4.6).

Like most GPI-anchored membrane proteins, PrP in living cells segregates into lipid rafts, which are rich in saturated fatty acid lipids, containing mainly phosphatidylcholine lipids, cholesterol and sphingomyelin (Vey *et al.*, 1996; Naslavsky *et al.*, 1997). Mixed membranes composed of DPPC, cholesterol and sphingomyelin have been shown to serve as good models of lipid rafts (Schroeder *et al.*, 1994). Thus in the present study the interaction of PrP with DPPC/chol/SM was

investigated. Trp fluorescence measurements show that PrP binds to raft-like membranes at pH 7 and indicates that a direct interaction of PrP with lipid membranes can not be excluded as an additional mode of attachment of PrP to the cell surface.

Trp fluorescence measurements in the presence of salt revealed that the binding of PrP to liquid-crystalline lipid bilayers composed of negatively charged lipids is a complex process that involves both electrostatic and hydrophobic lipid-protein interactions. The salt experiments demonstrated that shielding of charges on both the protein and membrane surface reduced the affinity of PrP for negatively charged membranes (Figure 4.7). These results suggest that electrostatic interactions between positively charged residues on the protein surface and negatively charged lipid headgroups on the membrane are likely to drive the initial binding of PrP to negatively charged membranes. Figure 4.14 shows the primary structure of SHaPrP (90–231). The charged amino acids are highlighted: blue for the positively charged amino acids lysine, arginine and histidine; red for the negatively charged amino acids aspartic acid and glutamic acid. The protein at both pH 5 and 7 is positively charged with a net charge at pH 5 of + 9 and at pH 7 of + 4. The difference in the charge at the two pHs is attributable to the protonation of the histidine residues (pKa is 6.5). Inspection of the distribution of charges on the protein surface revealed a cluster of positive charges at the amino-terminus of the protein (Figure 4.15). Therefore, one could speculate that the binding of PrP to negatively charged membranes is mediated by the binding of the positive face of PrP containing the amino-terminus and is driven primarily by electrostatic interactions between protein and membrane. This is in good agreement with studies that model PrP interactions with negatively charged membranes (Warwicker, 1997 & 1999). In this model the

positively charged face of PrP that includes helix A has been proposed as the membrane binding face. In addition this model suggest that this particular orientation of PrP at the membrane surface might favour PrP-PrP interactions across the membrane surface and would involve the conserved non-polar domain of PrP. The membrane may therefore play a role in the polymerisation of PrP *in vivo* through biasing the orientation and conformation of the protein. The above model was based on the solution structure of mouse PrP residues 124–226. A more recent model of PrP-membrane interactions also shows the positively charged face of the protein oriented toward the membrane (Rudd *et al.*, 2001). However, unlike the above study, this model was based on the solution structure of SHaPrP residues 90–231 and also took in to consideration the GPI anchor and the N-linked sugars. This study proposed that the polar carboxyl terminus, which links the protein to the GPI anchor, makes very few non-covalent interactions with anchor. This provides the protein with considerable dynamic freedom relative to the membrane. This model also suggests that the N-linked sugars at Asn181 and Asn197 are flexible and as a result shield large surface areas of the protein. In general glycosylation increases the stability of proteins. The sugar residues may therefore protect PrP^C by sterically hindering protein-protein interactions that occur during the conversion to PrP^{Sc}.

The inability of salt to displace PrP from negatively charged membranes suggest the involvement of additional hydrophobic lipid-protein interactions following the initial charge driven binding (Figure 4.8).

Gly-Gln[91]-Gly-Gly-Gly-Thr-His-Asn-Gln-Trp-Asn-Lys[101]-Pro-Ser-Lys-

Pro-Lys-Thr-Asn-Met-Lys-His[111]-Met-Ala-Gly-Ala-Ala-Ala-Ala-Gly-Ala-

Val[121]-Val-Gly-Gly-Leu-Gly-Gly-Tyr-Met-Leu-Gly[131]-Ser-Ala-Met-Ser-Arg-

Pro-Met-Met-His-   S1

Phe[141]-Gly-Asn-Asp-Trp-Glu-Asp-Arg-Tyr-Tyr-Arg[151]-Glu-Asn-Met-Asn-Arg-

Helix A

Tyr-Pro-Asn-Gln-Val[161]-Tyr-Tyr-Arg-Pro-Val-Asp-Gln-Tyr-Asn-Asn[171]-Gln-

S2

Asn-Asn-Phe-Val-His-Asp-Cys-Val-Asn[181]-Ile-Thr-Ile-Lys-Gln-His-Thr-Val-

Helix B

Thr-Thr[191]-Thr-Thr-Lys-Gly-Glu-Asn-Phe-Thr-Glu-Thr[201]-Asp-Ile-Lys-Ile-

Met-Glu-Arg-Val-Val-Glu[211]-Gln-Met-Cys-Thr-Thr-Gln-Tyr-Gln-Lys-Glu[221]-

Helix C

Ser-Gln-Ala-Tyr-Tyr-Asp-Gly-Arg-Arg-Ser[231]

Figure 4.14: **Amino acid sequence of SHaPrP (90–231).** The secondary structural components are underlined (═══); helix A consists of residues 144–156, B 172–193 and C 200–227. Beta strands (▬▬); S1 consists of residues 128–131 and S2 161–164. The positively charged amino acids are shown in blue, negatively charged are in red, polar residues are in green and the remaining are the hydrophobic amino acids. The histidine residues are shown in blue and underlined, as they are only positively charged at pH 6.5 or below. Sequence was obtained from the protein database (PDB) reference 1BI0.
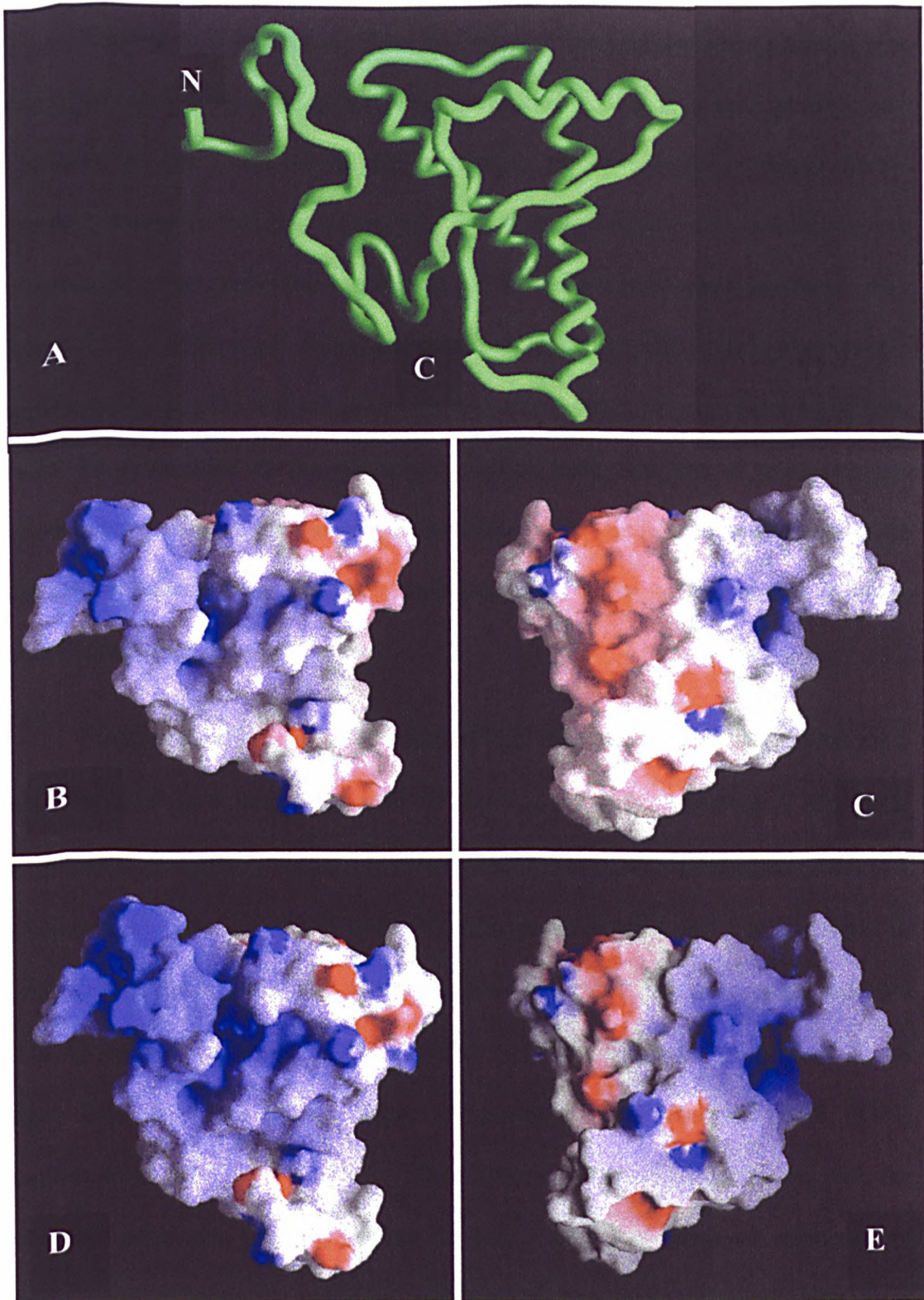
Figure 4.15: **Different representations of the three-dimensional structure of SHaPrP (90–231).** (A) Worm representation of the NMR structure of SHaPrP (90–231) indicating the amino- and carboxyl-termini. (B-E) Surface views of SHaPrP (90–231) coloured according to the electrostatic potential (Nicholls *et al.*, 1991), with blue for positive charges and red for negative charges. B shows the surface potential at pH 7, with the same orientation as A. View C shows the same orientation as B after 180° rotation about a vertical axis. D and E are equivalent orientations as B and C, respectively but for PrP at pH 5.

The degree of protection of the Trp residues from acrylamide quenching was investigated and these experiments were performed with PrP in the lipid-free and lipid-bound states. The acrylamide quenching results revealed a higher Stern-Volmer constant for PrP in solution at pH 5 than at pH 7 (Table 4.2), which suggests a greater exposure of the Trp residues at pH 5 due to a more open structure. The higher charged state at pH 5 can lead to a more open structure due to electrostatic repulsions between the ionized groups on the surface of the protein. Such repulsions would be minimized in the partially unfolded state and this in turn exposes hydrophobic patches onto the protein surface. ANS binding measurements have demonstrated the exposure of hydrophobic patches on the surface of PrP at acidic pHs (Swietnicki *et al.*, 1997).

Binding of PrP to negatively charged lipid membranes of POPG at both pH 5 and 7 resulted in a large blue shift of the λ_{max} of PrP, indicating a less polar environment of the Trp residues of PrP when bound to POPG membranes (Table 4.1 & Figure 4.6). Binding of PrP to POPG membranes at pH 5 and 7 also resulted in lower Stern-Volmer constants, which suggests that the Trp residues were shielded from acrylamide quenching in the presence of POPG membranes (Table 4.2). A larger blue shift and higher degree of protection was observed with POPG membranes at pH 5 than at pH 7. These observations can be correlated with the enhanced positively charged surface at pH 5 and the increased exposure of hydrophobic patches at the acidic pH, which in turn may lead to a deeper insertion of the hydrophobic amino acids of PrP in POPG membranes.

Binding of PrP to zwitterionic membranes in the gel-phase and raft-like membranes of DPPC, cholesterol and sphingomyelin at pH 7 resulted in a blue shift

of the λ_{max} of PrP (Table 4.1 & Figure 4.6). An intermediate protection to acrylamide quenching was observed for the raft-like membranes at pH 7, which suggests a different orientation of PrP in the mixed membranes relative to the orientation in POPG membranes. At pH 5 PrP displays little or no binding to the raft-like membranes of DPPC/chol/SM. At this pH PrP has a greater net positive charge than the protein at pH 7. The binding of peptides and proteins to lipid membranes depends on the balance between hydrophobic and electrostatic interactions, and other bilayer effects such as curvature, fluidity of the membrane and on the conformational states available to the peptide or protein. Thermodynamic studies with peptides have shown that the transfer of positively charged peptides from the aqueous phase to the interface of zwitterionic membranes is energetically unfavourable (White & Wimley, 1998). This observation may explain the lack of binding of PrP to raft-like membranes at pH 5. At neutral pH the net charge of PrP is smaller implying that charge interactions were unlikely to drive the binding of PrP to gel-phase zwitterionic membranes and raft-like membranes. To further investigate the nature of PrP-DPPC/chol/SM interactions, binding was carried out in the presence of salt. In contrast, to POPG membranes, where the binding of PrP was significantly diminished in the presence of salt, binding of PrP to raft-like membranes of DPPC/chol/SM was not affected by addition of salt (Figure 4.9). Furthermore, addition of salt to pre-existing lipid-protein complexes failed to displace the protein from the lipid membranes (Figure 4.10). These findings suggest that the partitioning of PrP into gel-phase zwitterionic membranes of DPPC and raft-like membranes at pH 7 involve primarily hydrophobic lipid-protein interactions. Therefore, the binding of PrP to raft-like membranes probably involves hydrophobic surfaces of PrP.

125

No binding was detected between PrP and liquid-crystalline zwitterionic membranes of POPC, DOPC and DOPC/chol (70:30 molar ratio) and DOPC/chol/SM (50:25:25 molar ratio) membranes at pH 5 and 7 (Table 4.1). Binding of PrP to zwitterionic lipids in the gel-crystalline phase and not in the liquid crystalline phase suggests that factors other than specific molecular recognition of the lipid headgroup structure by PrP regulates binding. Thus implying that other physical properties of zwitterionic membranes such as vesicle curvature, lateral pressure and fluidity may determine binding.

In summary, the binding studies of SHaPrP (90–231) to model lipid membranes show that: (a) PrP binds to negatively charged lipids at both pH 7 and pH 5. A larger blue shift in the λ_{max} was observed at pH 5; (b) addition of liquid-crystalline zwitterionic membranes of POPC, DOPC and its mixtures with cholesterol and cholesterol plus sphingomyelin did not result in any measurable spectral changes, which suggests that PrP does not interact with these lipid membranes; (c) PrP was found to bind to gel-phase membranes of DPPC and raft-like membranes composed of DPPC, cholesterol and sphingomyelin at pH 7 and (d) no interaction between PrP and the raft-like membranes of DPPC/chol/SM was detected at pH 5.

Combining the Trp fluorescence with the acrylamide quenching results a model for the binding of PrP to lipid membranes is proposed in Figure 4.16. In this model, PrP in solution at pH 5 and pH 7 is represented as two different starting states with PrP at pH 5 having a more open structure that exposes hydrophobic surfaces. The binding of PrP to negatively charged membranes is driven by electrostatic lipid-protein interactions. Once bound at the lipid-water interface PrP undergoes a

(A) Negatively Charged Membranes

PrP

PrP

Lipid binding, pH 5

Lipid binding, pH 7

pH 5

pH 7

Hydrocarbon Core

Interface

(B) Zwitterionic and Raft-like Membranes

PrP

PrP

Lipid binding, pH 5

Lipid binding, pH 7

PrP

pH 7

Hydrocarbon Core
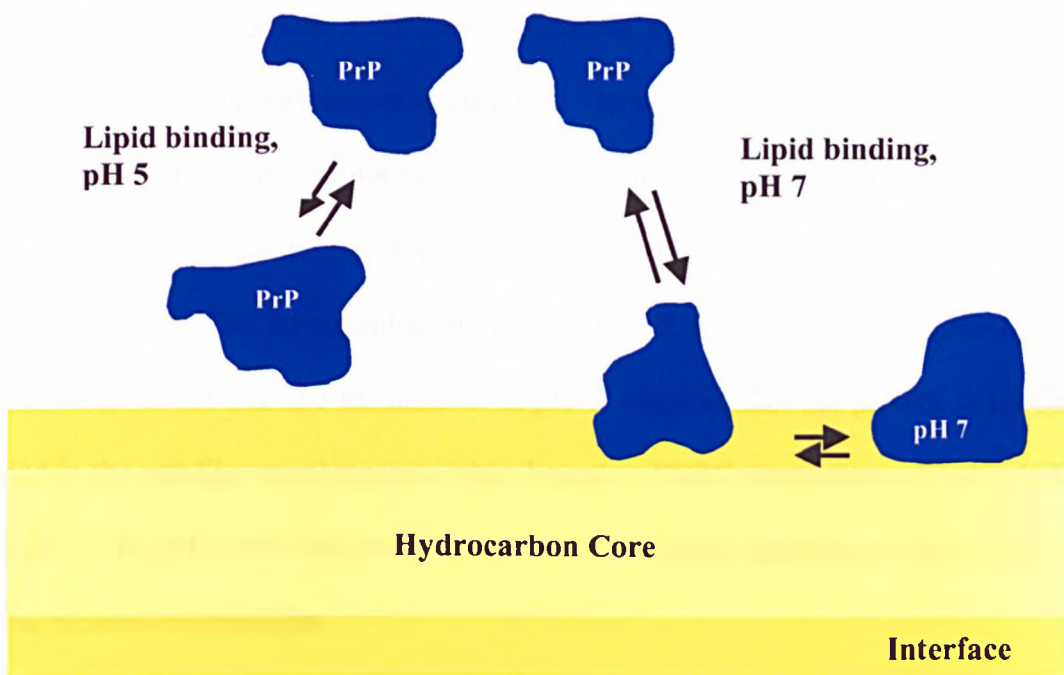
Interface

Figure 4.16: **Schematic model for PrP-lipid interactions.** PrP at pH 5 has a more open structure than at pH 7. (A) Binding to negatively charged membranes. Electrostatic lipid-protein interactions drive PrP to the lipid-water interface. Once bound to the surface of negatively charged membranes, PrP undergoes a conformational change, which would permit the exposure of hydrophobic residues and these would preferably insert into the lipid bilayer. PrP at pH 5 is more buried within the lipid bilayer than at pH 7. (B) Binding to zwitterionic lipids in the gel-phase and raft-like membranes composed of DPPC/chol/SM. At pH 7 hydrophobic lipid-protein interactions drive the protein to the lipid-water interface where PrP undergoes a conformational transition. No membrane interaction was detected with raft-like membranes at pH 5.

conformational change, whereby hydrophobic amino acids, normally buried within the protein become exposed. The exposed hydrophobic residues can partially insert into the lipid bilayer. The greater blue shift of the λ_{max} for PrP and the higher protection to acrylamide quenching for PrP with POPG membranes at pH 5 point to a deeper insertion of the protein in these membranes at pH 5 relative to the inserted state at pH 7. Figure 4.16A highlights differences for the binding of PrP to negatively charged membranes at pH 5 and 7.

A tentative model for binding of PrP to gel-phase zwitterionic and raft-like membranes composed of DPPC/chol/SM at pH 7 is shown in Figure 4.16B. The binding of PrP to these membranes is driven by hydrophobic lipid-protein interactions. In this model a different orientation of PrP to that illustrated in the binding to negatively membranes is proposed. In this orientation, PrP binds to the gel-phase zwitterionic membranes and the raft-like membranes though a hydrophobic face of the protein resulting in a conformational transition at the lipid-water interface. The intermediate protection of PrP from acrylamide quenching, when bound to the raft-like membranes at pH 7, suggests that the protein is not as buried in the raft-like membranes as when bound to POPG membranes at both pH 5 and pH 7. At pH 5 PrP does not interact with the raft-like membranes and remains in the aqueous environment.

4.5 Conclusions

The Trp fluorescence results shows that PrP binds to negatively charged lipid membranes at both pH 5 and 7, gel-phase zwitterionic lipids and to raft-like membranes composed of DPPC/chol/SM at pH 7. This finding is of particular importance since PrP in cells is localised within cholesterol and sphingomyelin rich

raft domains. Electrostatic lipid-protein interactions are involved in the initial binding of PrP to the surface of negatively charged membranes and hydrophobic lipid-protein interactions occur after the initial charge driven binding. Binding of PrP to gel-phase zwitterionic membranes and raft-like membranes is driven by hydrophobic lipid-protein interactions. Acrylamide quenching of the Trp fluorescence revealed a high degree of protection of PrP when bound to negatively charged membranes at pH 5 and 7, indicating partial insertion into the lipid bilayer. In addition the Trp fluorescence blue shift and protection from acrylamide quenching indicate that PrP when bound to negatively membranes is more buried within the lipid bilayer at pH 5 than at pH 7. The intermediate protection of PrP from acrylamide quenching when bound to raft-like membranes indicates that the protein is not as buried in these membranes as with negatively charged membranes.

Chapter 5:   Secondary Structural Changes in Syrian Hamster Prion Protein (SHaPrP) Residues 90–231 Upon Binding to Lipid Membranes

5.1   Introduction\

In Chapter 4 the interaction of PrP with various lipid membranes was investigated. The fluorescence binding data suggests that PrP undergoes a conformational change upon association with negatively charged membranes at pH 5 and 7, zwitterionic membranes in the gel-crystalline phase and raft-like membranes composed of DPPC, cholesterol and sphingomyelin at pH 7. In this chapter changes in PrP secondary structure upon interaction with lipid membranes was investigated by circular dichroism (CD) and attenuated total reflection Fourier transform infrared (ATR FTIR) spectroscopy. Negative-stain electron microscopy was employed to examine the morphology of the lipid-PrP complexes.

Although CD and FTIR fail to establish the precise three-dimensional location of individual elements they do provide a global insight into the overall secondary structure of proteins and are particularly useful in probing structural changes induced by events such as membrane and ligand binding. Both techniques are extremely useful in providing an alternative or as a complement to X-ray crystallography or nuclear magnetic resonance (NMR) spectroscopy and are widely used in the study of membrane proteins where high-resolution studies are not always feasible.

Far-UV CD provides information on the backbone of proteins. The common types of secondary structures adopted by proteins and peptides have distinctive CD spectra. The CD spectra of proteins which have more than one type of structure can

be defined as a linear combination of CD spectra of each contributing secondary structural element (*e.g.* pure α-helix, pure β-strand) weighed by its abundance in the polypeptide chain. Optical artifacts of light scattering and absorption flattening due to lipid-protein complexes can sometimes cause distortions in the CD spectra of membrane proteins.

The light scattering problems often experienced in CD spectroscopy are virtually non-existent with IR techniques because of the long IR wavelengths (Goormaghtigh *et al.*, 1999). Furthermore, most lipids do not interfere with the protein IR signal, making this an attractive technique for the study of membrane proteins. The development of Fourier transform spectrophotometers offers the advantage of high sensitivity, resolution and speed of data acquisition. All wavelengths are detected and measured simultaneously and subsequently decoded by Fourier transformation. Fourier transform infrared spectroscopy represents a powerful tool to investigate proteins and lipids together, and thus, it is a very useful technique for studying protein structure in a membrane environment. Secondary structural information can be obtained by applying a mathematical approach to the analysis of the FTIR spectra of proteins and peptides.

Sampling techniques other than transmission are commonly used in FTIR studies. Here attenuated total reflection (ATR) was employed to characterise the secondary structure of PrP in lipid membranes at pH 5 and 7. In this technique, the secondary structure of proteins in a membrane environment is determined from thin hydrated films of lipid-protein complexes. A major advantage of ATR FTIR over conventional transmission technique is that absorption by water molecules is

131

strongly reduced, as a consequence small amounts of material are required (typically 10 μg of protein). Other advantages include the analysis of highly turbid samples and possibility of determining the orientation of the secondary structures for membrane proteins with respect to the bilayer plane (Goormaghtigh *et al.*, 1990, 1999).

5.2 Materials and Methods

5.2.1 Materials

POPG, POPC, sphingomyelin and cholesterol were purchased from Avanti Polar lipids (Birmingham, AL). DPPC was obtained from Sigma-Aldrich (Poole, UK). All other chemicals were obtained from Sigma-Aldrich (Poole, UK) unless otherwise stated.

5.2.2 Lipid vesicles

Small unilamellar vesicles were prepared as described in Chapter 4; section 4.2.2.

5.2.3 Circular dichroism

Lipid-protein samples were prepared by mixing one part of a 15 μM stock PrP protein solution in 20 mM sodium acetate buffer, pH 5.5 to an equal volume of lipid vesicles prepared in 20 mM sodium phosphate buffer, pH 7.2 or 20 mM sodium acetate, pH 5.0. This resulted in a final pH of the lipid-protein samples ~ 6.9 and ~ 5.2, respectively. The samples were mixed thoroughly and equilibrated for 2–3 minutes before recording the far-UV (185–260 nm) CD spectra on a JASCO J-715 spectropolarimeter using 1 mm pathlength quartz cells. Typically, a scanning rate of

100 nm/min, a time constant of 1 s, and a bandwidth of 1.0 nm were used. Spectra were measured at 20 ± 0.2 °C, with a resolution of 0.5 and 16 scans were averaged per spectrum. The corresponding backgrounds (buffer for protein solutions or lipid alone) were subtracted from the protein spectra.

5.2.4 Sample preparation for ATR FTIR measurements

Samples were prepared by mixing PrP with the desired lipid in 5 mM sodium phosphate, pH 7.2 or 5 mM MES, pH 5.0 to final concentrations of 4 mM lipid and 24 µM protein. The presence of –COOH containing molecules (e.g., acetate, EDTA, TFA) must be avoided because they absorb in the same region as proteins and therefore would interfere with the protein signal. For this reason buffers containing acetate were substituted. PrP was stored in 20 mM sodium acetate buffer at pH 5.5 an aliquot was dialysed against 20 mM sodium phosphate, pH 5.7. This resulted in a final pH of the lipid-protein samples ~ 7.0 and ~ 5.3, respectively. The lipid-protein complexes were incubated for 2–3 minutes and an aliquot of 50 µL in total was applied to an 80 × 10 × 4 mm germanium (Ge) plate (Pike Technologies, Madison, Wisconsin, USA). Thin films were obtained by slow evaporation of the deposited sample under a stream of nitrogen. This procedure results in the formation of oriented lipid multilayers on the surface of the Ge plate (Fringeli & Günthard, 1981; Goormaghtigh et al., 1999). A schematic representation of the ATR set-up is shown in Figure 5.1. Protein films of PrP without lipid were also prepared in a similar manner from their buffer solutions. Typically, films contained 20 µg protein and ~ 154 µg lipid. Lipid-to-protein molar ratio was 167:1.

**Oriented Lipid-Protein
Film**

**Infrared
Light**

θ

Germanium Plate
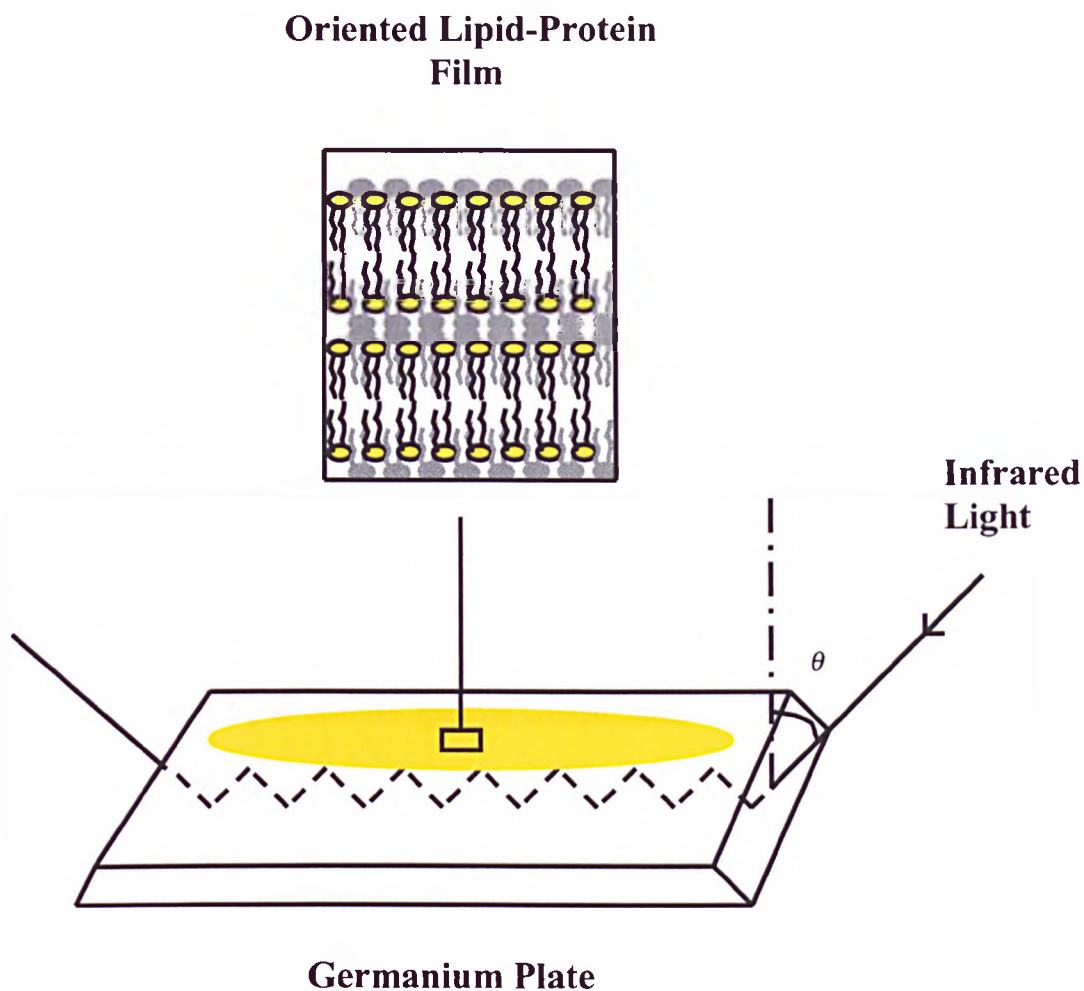
Figure 5.1: **Schematic representation of the ATR set-up.** The infrared beam is directed into a high refractive index medium, which is transparent for the IR radiation of interest. Germanium (Ge) was used as the internal reflection element for these experiments. The incident beam makes an angle θ with respect to the normal to the Ge surface. Above a critical angle, θ_c the light beam is completely reflected when it impinges on the surface of the Ge plate. Several internal total reflections occur within the Ge plate until the beam reaches the end. At each reflection, the beam penetrates the surface of the sample to a depth of a few µm. The intensity of the beam is attenuated according to the absorption characteristics of the sample, so enabling an absorption spectrum to be recorded (Fringeli & Günthard, 1981; Goormaghtigh *et al.*, 1999).

In between each sample the Ge plate was cleaned with detergent and then rinsed with tap water followed by de-ionised water. The Ge plate was placed in a shallow glass vessel containing methanol and then transferred to one containing chloroform, after which the Ge plate was wiped with soft tissue paper (Goormaghtigh *et al.*, 1999).

5.2.5 ATR FTIR measurements

ATR FTIR spectra were recorded on a Bruker Vector 22 infrared spectrophotometer equipped with a triglycine sulphate detector (TGS). Spectra were recorded with the Ge plate in a horizontal ATR configuration with an incidence angle of 45°, yielding 10 internal reflections. The spectrophotometer was continuously purged with N_2 to remove spectral contributions of atmospheric water vapour. Background spectra of the clean germanium plate were recorded prior to collecting sample spectra and the correction was done automatically after sample measurement was completed. Each spectrum was an average of 256 scans and all spectra were recorded with a nominal resolution of 2 cm^{-1}. Measurements were performed at room temperature. Spectra of the corresponding lipid backgrounds were also recorded. Atmospheric water spectrum was measured in the absence of a protein film on the Ge plate. The background was collected with the sample compartment purged with N_2 and the sample spectrum was acquired with a non-purged sample chamber, the resulting spectrum of atmospheric water was obtained.

5.2.6 Analysis of FTIR spectra

The infrared spectra of proteins and peptides exhibit nine characteristic amide bands, which represent different vibrations of the peptide group. Amide I

(1600–1700 cm^{-1}) and amide II (1500–1580 cm^{-1}) bands are the two predominant bands of the IR spectra of proteins and peptides. The amide I band is the most widely used in secondary structural studies of proteins. Amide I is composed mainly (80 %) of C=O stretching (ν) vibration of the peptide group coupled to the in-plane bending of the N–H bond and the stretching of the C–N bond (Goormaghtigh *et al.*, 1994).

Using synthetic polypeptides it was shown that this band was conformation sensitive, the α-helical structure having a maximum near 1655 cm^{-1} and the β-sheet structure having a maximum around 1630 cm^{-1} (Goormaghtigh *et al.*, 1994). However, the strong overlap of the different secondary structural components such as α-helices, β-sheets, turns, and non-ordered structures usually results in a broad featureless amide I band. The different structural elements can be separated by the use of resolution enhancement methods such as Fourier self-deconvolution (Goormaghtigh *et al.*, 1990).

Prior to analysis the FTIR spectra were corrected for the following:

- *Subtraction of water vapour from the traces:* Even though the sample chamber was continually purged with N$_2$, spectral contributions of atmospheric water were still present. The removal of traces of water vapour was carried out using OPUS software version 3 (Bruker) in an interactive mode. Water absorbance bands were subtracted from the protein spectra in the region between 1800–1400 cm^{-1}.

• *Baseline correction:* Straight baselines were passed through each spectra in the 1800–1400 cm^{-1} region using OPUS software version 3 (Bruker) in an interactive mode.

Two approaches were employed to analyse the FTIR data:

• *Difference spectroscopy:* This method has been used to report on the relative changes in the secondary structure of proteins, as conditions are changed (Gray & Tamm, 1997, 1998; Raussens *et al.*, 1999). In this case difference spectroscopy was used to determine the secondary structural changes in PrP upon binding to lipid membranes.

The spectra were rescaled to a constant amide I area computed between 1711 to 1584 cm^{-1}. Peak integration of the amide I region was performed with OPUS software version 3 (Bruker). The difference spectra of PrP associated to lipid membranes minus PrP in solution were calculated using Igor (Wavemetrics, Lake Oswego, Oregon).

• *Fourier self-deconvolution:* Fourier self-deconvolution was applied to increase the resolution of the spectra in the amide I region. The resolution enhancement that results from the deconvolution highlights the different structural components by decreasing the widths of the infrared bands, allowing for increased separation and thus better identification of the overlapping component bands. Fourier self-deconvolution was carried out using software written by Dr Erik Goormaghtigh at the Université Libre de Bruxelles, Belgium. The self-deconvolution was carried out using a Lorentzian line shape for the deconvolution and a Gaussian line shape for the apodization, as described by Kauppinen *et al.*

(1981). The input parameters for deconvolution and apodization were chosen according to work described by Goormaghtigh *et al.* (1990). It is essential that the parameters chosen do not lead to an under or over estimation of the secondary structural components. The parameters chosen were 30 cm^{-1} full-width at half-height Lorentzian line shape and a Gaussian line shape with a full-width at half-height of 15 cm^{-1} for apodization this resulted in a resolution enhancement factor (K) of 2. K is defined as the ratio of full-width at half-height of the deconvoluting Lorentzian to the full-width at half-height of the Gaussian used for apodization.

Table 5.1 shows the frequency limits for the commonly occurring structures in proteins. The frequency limits were used as guidelines for assigning the structural components of PrP. The amide I band positions are often good indicators of secondary structures in a large number of proteins, however there are some exceptions. For example α-helical structures normally absorb in the 1661–1648 cm^{-1} region, but some helical structures have been found to absorb in the 1630–1640 cm^{-1}, region which is normally assigned to β-sheet structure (Heimburg *et al.*, 1996).

Table 5.1: Assignment of the IR frequency regions for the different secondary structures in proteins[a]

Structure	Frequency Region (cm^{-1})
α-helix	1661–1648
β-sheet[b]	1689–1682
	1638–1628
Low-frequency β-sheet[c]	1628–1615
β-turns	1682–1661
Random	1645–1638

[a]Cabiaux *et al.*, 1989. [b]β-sheet structure is characterised by two absorption bands between 1689–1682 cm^{-1} and 1638–1628 cm^{-1}. [c]For this study the distinction between β-sheet and low-frequency β-sheet (LF β-sheet) structure is made since the latter has been found to be associated with the formation of intermolecular hydrogen bonding in monomer-monomer interaction and is usually observed with protein aggregation and gel formation (Jackson & Mantsch, 1991; Goormaghtigh *et al.*, 1994). This is of particular significance in the present study, since structural analysis of amyloid fibrils have revealed the importance of intermolecular hydrogen bonding between the polypeptide backbone (Sunde *et al.*, 1997; Liu *et al.*, 2000).

5.2.7 Electron microscopy

Protein and vesicles-protein samples, prepared as described for FTIR experiments were diluted to a concentration of 0.050 mg/mL, applied to electron microscope grids coated with carbon film and stained with 2 % uranyl acetate. The preparations were examined using a Philips CM120 electron microscope with an accelerated voltage of 100 kV. Electron micrographs were taken at a magnification of × 45 000 under low dose conditions. Electron microscopy was performed by Dr Catherine Vénien-Bryan at the University of Oxford.

5.3   Results

5.3.1   Circular dichroism spectroscopy

The far-UV CD spectrum of SHaPrP (90–231) in solution at pH 7 and 5 showed a double minimum at approximately 208 and 222 nm with molar ellipticity per residue values of −9324 and −8597 deg cm^2 dmol^{-1}, respectively, for PrP at pH 7 and −8486 and −8560 deg cm^2 dmol^{-1} for PrP at pH 5 (Figure 5.2 & 5.3). The
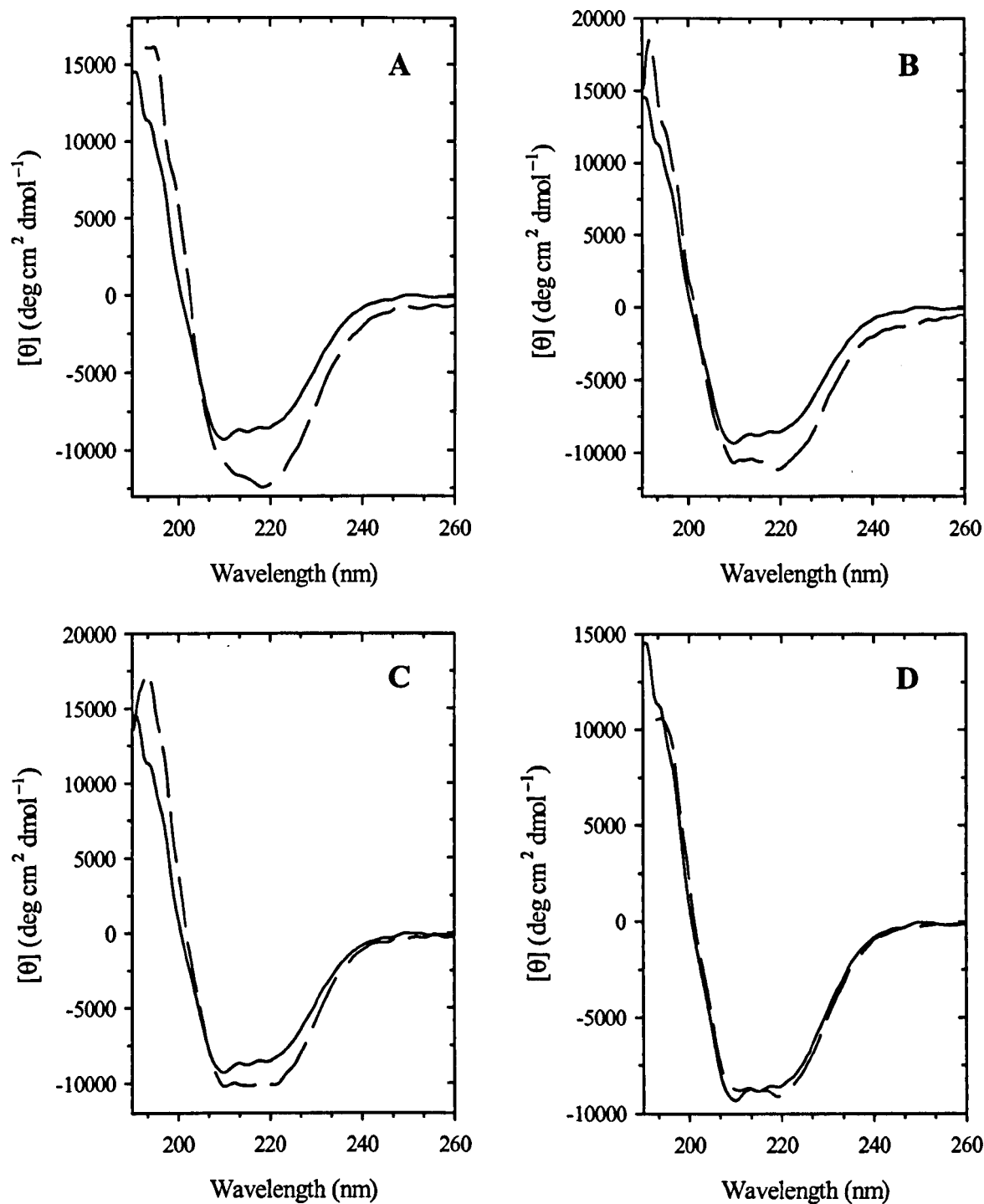
Figure 5.2: **Far-UV CD spectra of SHaPrP (90–231) in solution and with lipid membranes at pH 7.** Spectra of PrP in solution (solid line) and in the presence of lipid membranes (dashed line): (A) POPG, (B) DPPC/chol/SM (50:30:20 molar ratio), (C) DPPC and (D) POPC. Measurements were carried out at 20 °C on samples containing 7.5 µM protein and 1 mM lipid.
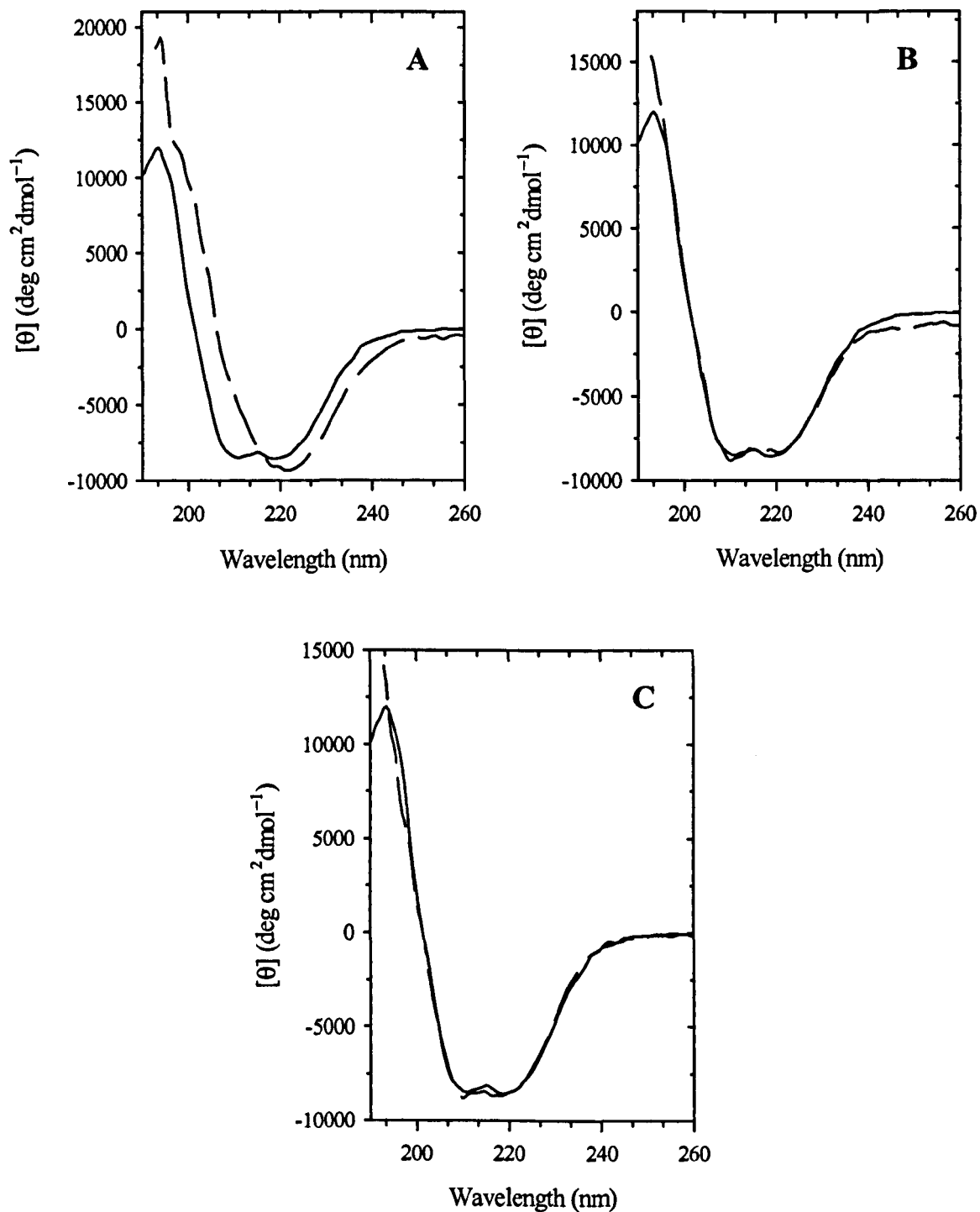
Figure 5.3: **Far-UV CD spectra of SHaPrP** **(90–231) in solution and with lipid**
membranes at pH 5. Spectra of PrP in solution (solid line) and in the presence of
lipid membranes (dashed line): (A) POPG, (B) DPPC/chol/SM (50:30:20 molar
ratio) and (C) POPC. Measurements were carried out at 20 °C on samples
containing 7.5 μM protein and 1 mM lipid.

141

results are indicative of a protein containing mainly α-helical structure. This is in good agreement with published CD spectra (Mehlhorn *et al.*, 1996; Zhang *et al.*, 1997) and the NMR structure of SHaPrP (90–231) (James *et al.*, 1997) which shows a mainly α-helical (44 %) protein with a small amount of β-sheet (4 %) structure.

Binding of PrP to negatively charged membranes of POPG at pH 5 and 7 induced a spectral change in the shape of the CD spectra. Less pronounced bands at 208 and 222 nm were observed and a single minimum at about 220 nm was detected (Figure 5.2A & 5.3A). The minimum was also more defined for PrP in POPG membranes at pH 5 compared to pH 7. The spectral changes suggest that binding of PrP to negatively charged membranes results in an increase in the β-sheet structure.

Incubation of PrP with liquid-crystalline zwitterionic membranes of POPC at pH 7 and 5 and raft-like membranes of DPPC/chol/SM at pH 5 showed no measurable change in the far-UV CD spectra of PrP (Figure 5.2D & 5.3B,C). These results are consistent with the absence of lipid-protein interactions as revealed by the Trp fluorescence binding data. In contrast, binding of PrP to gel-phase zwitterionic membranes of DPPC and its mixtures with cholesterol and sphingomyelin at pH 7 was accompanied by changes in the far-UV CD spectra (Figure 5.2B,C). An increase in the negative ellipticity at 208 and 222 nm was observed, which suggests an increase in the α-helical structure of PrP upon binding to DPPC and raft-like membranes at pH 7.

5.3.2 ATR FTIR spectroscopy

ATR FTIR has been successfully used to investigate the structure of soluble and membrane proteins. FTIR relies on the analysis of the vibration bands of

proteins and particularly on the amide I band (νC=O of the peptide bond) whose frequency of absorption is dependent upon the secondary structure.

The FTIR spectra of PrP in the absence and presence of different lipid membranes are presented in Figure 5.4. The amide I and amide II bands arising from the protein peptide group can be seen between 1700–1600 cm^{-1} and 1580–1510 cm^{-1}, respectively. The band at 1770–1705 cm^{-1} is due to the lipid carbonyl stretching vibration (νC=O).

The FTIR spectrum of PrP in solution at pH 5 exhibited an amide I band with maximum absorption at about 1657 cm^{-1}, which indicated the main component of the secondary structure to be α-helical. The spectra of PrP at pH 7 revealed a broader amide I band centred around 1654 cm^{-1} again suggesting the presence of α-helical structure. A shoulder at ~ 1631 cm^{-1} was also observed for protein at pH 5 and 7 and reflected the presence of some β-sheet structure (Figure 5.4).

The FTIR spectra for PrP associated to POPG membranes at pH 5 and 7 showed an amide I band with maximum absorption at ~ 1657 and 1654 cm^{-1}, respectively, which suggested the presence of significant amount α-helical structure. The band at 1631 cm^{-1} observed for PrP in solution is more defined upon association with POPG membranes at both pH 5 and 7, which indicates that the association of PrP with negatively charged membranes is accompanied by an increase in β-sheet structure (Figure 5.4A,B). In contrast, incubation with gel-phase zwitterionic membranes of DPPC and raft-like membranes composed of DPPC/chol/SM at pH 7 resulted in a more symmetrical and less broad amide I band with maximum absorption at ~ 1654 cm^{-1}, which suggests that α-helical structure is more prominent
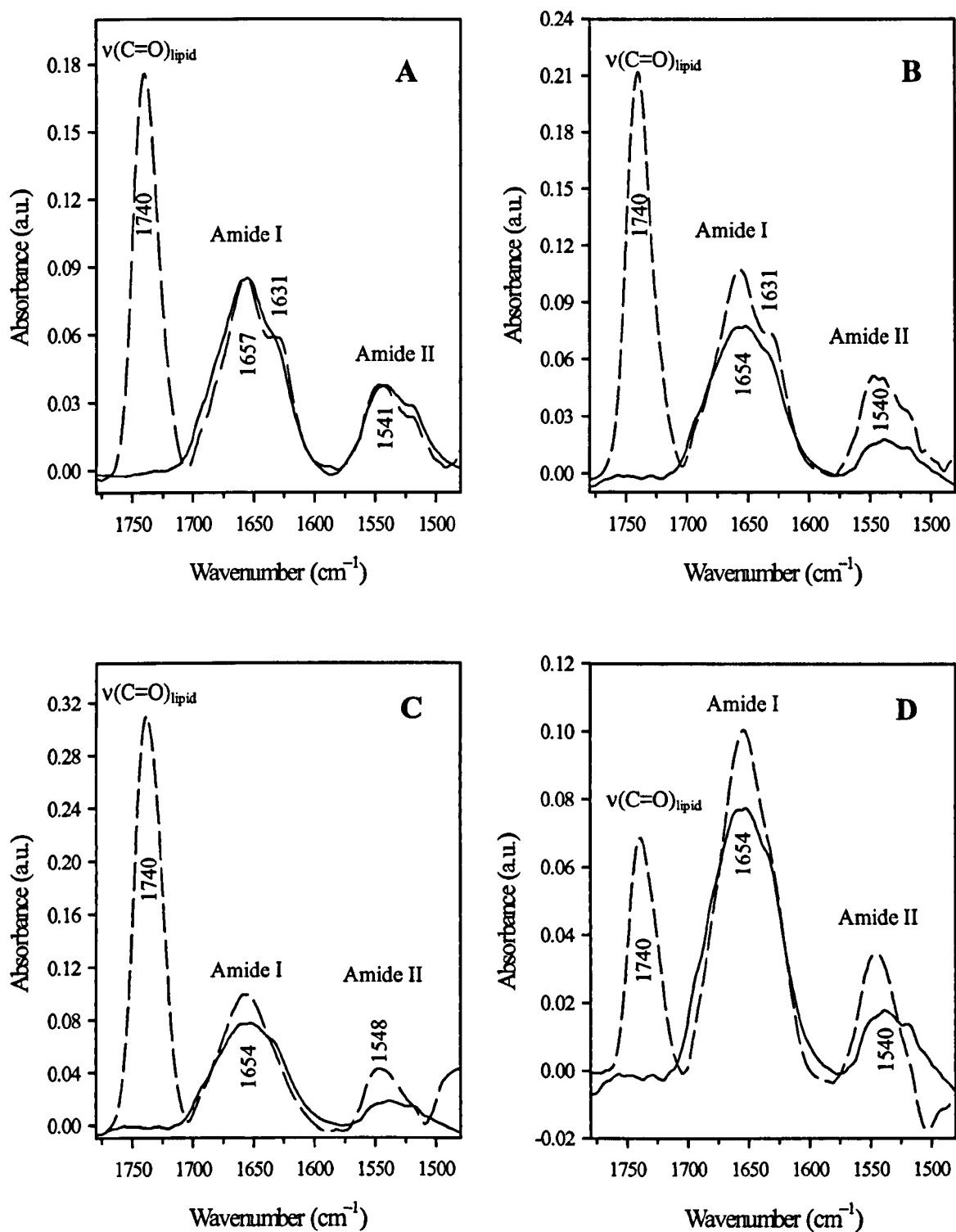
Figure 5.4: **FTIR spectra of SHaPrP (90–231) in absence and presence of lipid membranes.** PrP in the absence of lipid at (A) pH 5 and (B–D) pH 7 (solid line). PrP bound to lipid vesicles (dashed line): (A) POPG, pH 5, (B) POPG, pH 7, (C) DPPC, pH 7 and (D) DPPC/chol/SM (50:30:20 molar ratio), pH 7. The amide I, amide II and the lipid carbonyl stretching band are indicated. The amide I region has been normalized to a constant area. Spectra were recorded with a 2 cm^{-1} resolution and 256 scans were averaged for each spectrum.

in PrP with these membranes. Furthermore, the disappearance of the shoulder at 1631 cm^{-1} suggests a reduction in the β-sheet structure of the protein upon binding to DPPC and raft-like membranes at pH 7 (Figure 5.4C,D).

While the position of the amide I band initially revealed the dominant structures that were present in PrP further structural details were obscured by overlapping of the several spectral components associated with the different secondary structural elements. Fourier self-deconvolution was employed to resolve these overlapping spectral bands. The amide I region of the infrared spectrum of PrP and deconvoluted spectra of the corresponding traces are presented in Figures 5.5 & 5.6. Protein in the absence of lipid at pH 5 and 7 now clearly revealed three distinct components: the 1657 cm^{-1} main band assigned to α-helix and the 1628 cm^{-1} corresponding to low-frequency β-sheet structure, and the small component at 1692 cm^{-1}, tentatively assigned to the high frequency component of the β-sheet structure (Figure 5.5B,D & 5.6B,D). The positions of the β-sheet absorption bands matches well the absorption bands of known anti-parallel β-sheet polypeptides (Goormaghtigh et al., 1994) and indicate that the β-strands are in an anti-parallel configuration as seen in the NMR structure (James et al., 1997). The shoulder at 1677 cm^{-1} indicates the presence of β-turns.

PrP with negatively charged membranes composed of POPG at pH 5 and 7 exhibits an α-helical band at ∼ 1657 cm^{-1}, bands at ∼ 1627 and ∼ 1692 cm^{-1} assigned to low-frequency β-sheet structure and a β-turn band at ∼ 1677 cm^{-1} (Figure 5.5B,D). The band at ∼ 1627 cm^{-1} is more defined and intense than that observed in solution, which confirmed the earlier indication suggesting an increase in low-frequency β-sheet structure of PrP upon binding to POPG membranes.
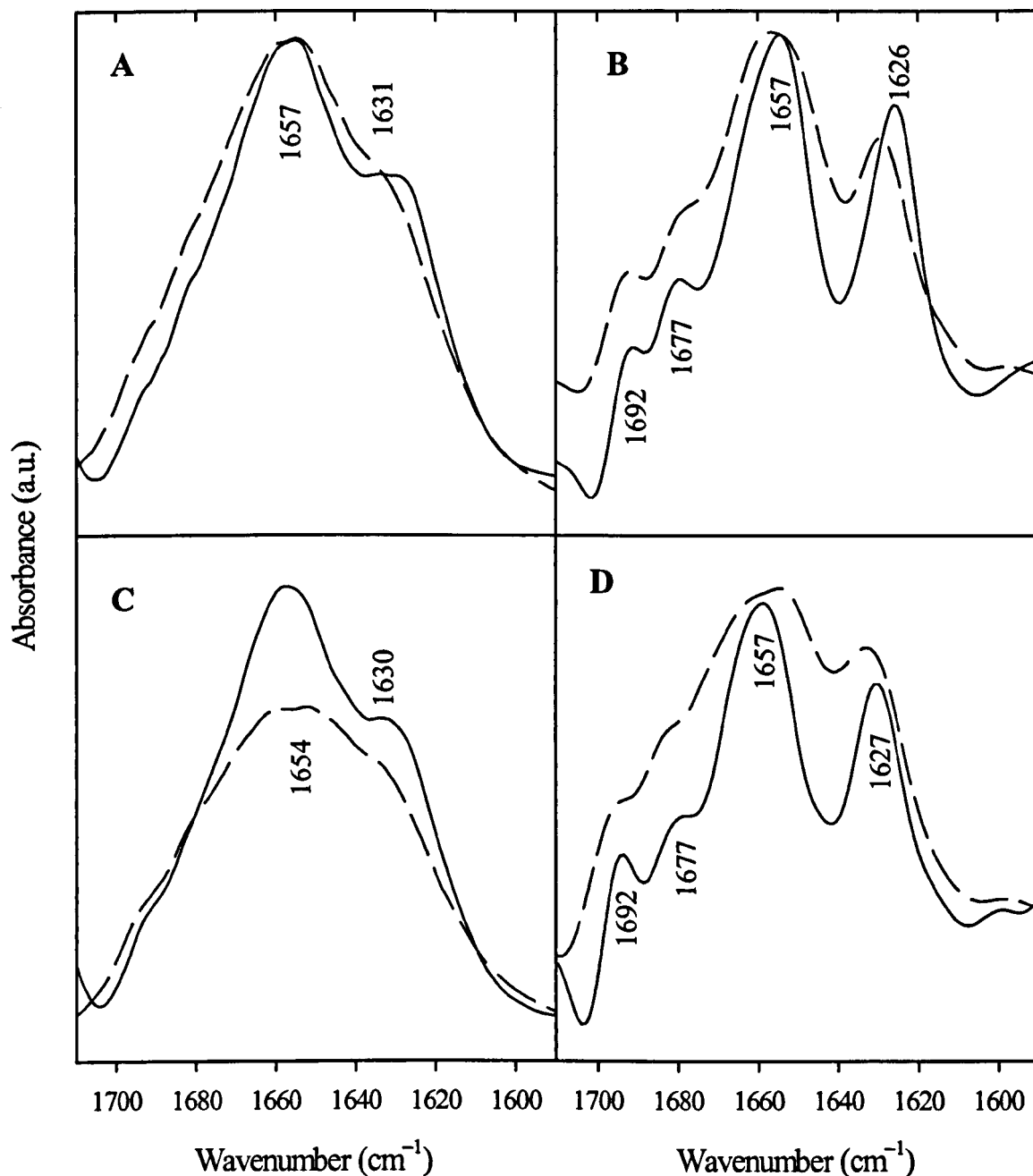
Figure 5.5: **Normalized amide I region of the FTIR spectra of SHaPrP (90–231) in the absence and presence of POPG membranes.** A and C are original spectra of PrP in the absence of lipid at (A) pH 5 and (C) pH 7 (dashed line) and bound to POPG membranes at pH 5 (A) and (C) pH 7 (solid line). (B) and (D) Same spectra as A and C after Fourier self-deconvolution. Spectra have been deconvoluted with a resolution enhancement factor, K=2 (see Materials and Methods section 5.2.6).

The deconvoluted amide I band of PrP in the presence of DPPC membranes and its mixtures with cholesterol and sphingomyelin at pH 7 revealed bands at ~ 1654, 1627, 1693 and 1677 cm^{-1} which were assigned to α-helix, low-frequency β-sheet and β-turns structures, respectively (Figure 5.6B,D). The band assigned to the low-frequency β-sheet structure was not as prominent as that in the presence of POPG vesicles and PrP in solution (Figure 5.5B,D and 5.6B,D) which suggested a decrease in β-sheet structure in PrP upon binding to DPPC and raft-like membranes at pH 7.

Valuable information on relative changes in the secondary structure of proteins as the environment changes may be obtained through difference spectroscopy. Difference spectra were calculated from the recorded FTIR spectra in the amide I region. Before subtraction the FTIR spectra were rescaled to a constant amide I area. Figure 5.7A shows the difference spectra of PrP in the presence of POPG membranes at pH 5 and 7 minus PrP in the absence of lipid at the corresponding pH. Positive deviations at ~ 1656 and ~ 1626 cm^{-1} were detected and imply that PrP exhibits greater intensity at these frequencies in the presence of POPG membranes at both pH 5 and 7. The results suggest that binding of PrP to negatively charged membranes induce α-helical and low-frequency β-sheet structures. The magnitude of the observed changes suggests that PrP bound to POPG membranes at pH 7 has a greater amount of α-helical structure compared to pH 5.

The difference spectra of PrP in the presence of DPPC and raft-like membranes of DPPC/chol/SM at pH 7 produced a spectra with positive deviations at
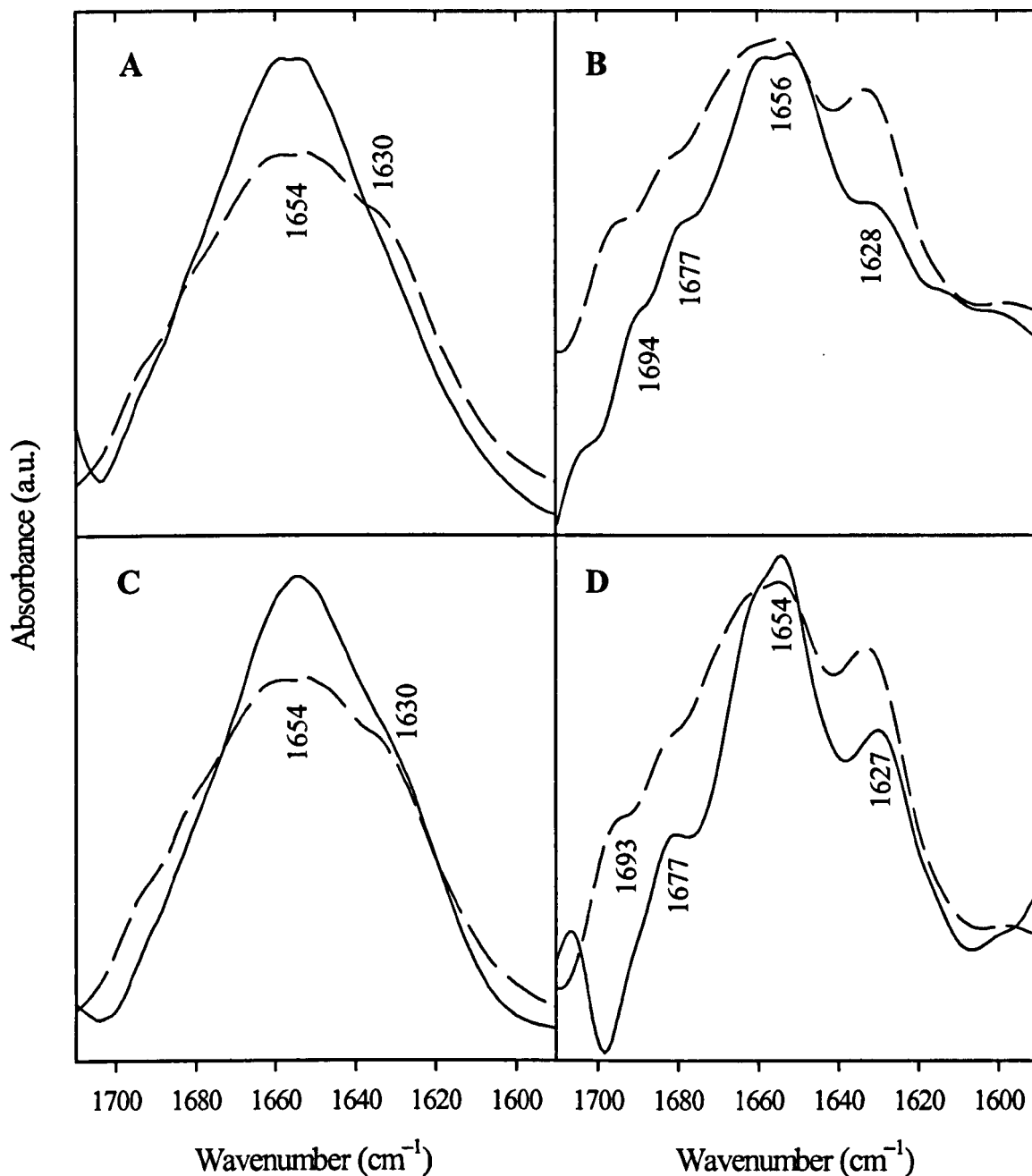
Figure 5.6: **Normalized amide I region of the FTIR spectra of SHaPrP (90–231) in the absence and presence of DPPC and raft-like membranes.** (A) and (C) are original spectra of PrP in the absence of lipid at pH 7 (dashed line) and bound to (A) DPPC membranes at pH 7 and (C) raft-like membranes of DPPC/chol/SM at pH 7 (solid line). (B) and (D) Same spectra as A and C after Fourier self-deconvolution. Spectra have been deconvoluted with a resolution enhancement factor, K=2 (see Materials and Methods section 5.2.6).
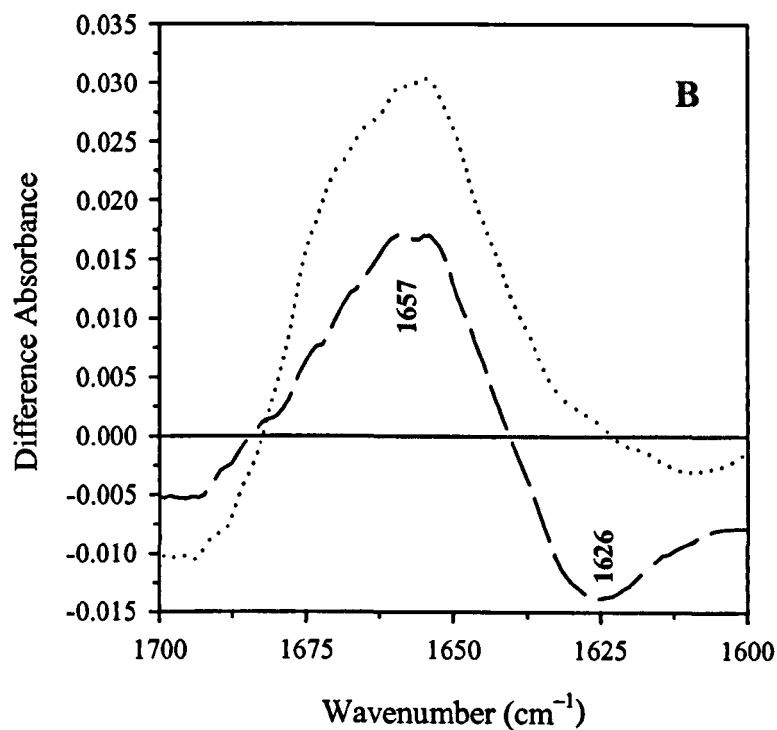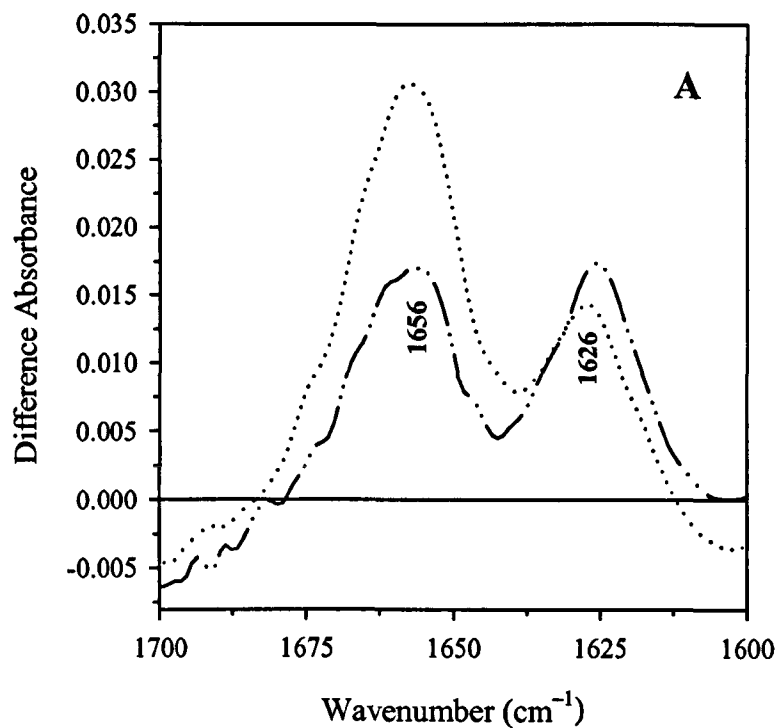
Figure 5.7: **FTIR difference spectra in the amide I region of SHaPrP (90–231).**
Difference spectra PrP bound to lipid membranes minus PrP in the absence of lipid
(A) PrP bound to POPG vesicles, pH 5 (dash-dot-dot line) and at pH 7 (dotted line).
(B) PrP bound to DPPC vesicles, pH 7 (dashed line) and DPPC/chol/SM (50:30:20
molar ratio), pH 7 (dotted line).

~ 1657 cm^{-1}(Figure 5.7B). An additional negative absorption band at ~ 1626 cm^{-1}, was also detected with DPPC membranes. The prominent positive band at 1657 cm^{-1} indicates that PrP contains a larger fraction of α-helical structure when associated to DPPC membranes and the raft-like membranes at pH 7 compared to protein in solution. The negative intensity at 1626 cm^{-1} observed with DPPC membranes suggests a decrease in low-frequency β-sheet structure.

5.3.3 Structural changes monitored over time

The FTIR samples were incubated at 20 °C for up to 18 days and monitored for further structural changes. The amide I region of the FTIR spectra of PrP incubated with lipid membranes are displayed in Figure 5.8. The shape of the amide I band remained virtually unaltered upon incubation with DPPC and raft-like membranes of DPPC/chol/SM at pH 7. The α-helical component at ~ 1657 cm^{-1} still dominated the amide I band, which suggests that gel-phase zwitterionic membranes of DPPC and raft-like membranes of DPPC/chol/SM at pH 7 induces a stable α-helical conformation of PrP. A slight increase in the intensity at ~ 1626 cm^{-1} with POPG membranes at pH 5 and 7 was observed and suggests a further increase in the low-frequency β-sheet structure in PrP upon incubation with negatively charged membranes.

5.3.4 Electron microscopy

The incubated lipid-PrP samples and protein in solution were also examined using negative-stain electron microscopy. The electron micrographs of PrP in
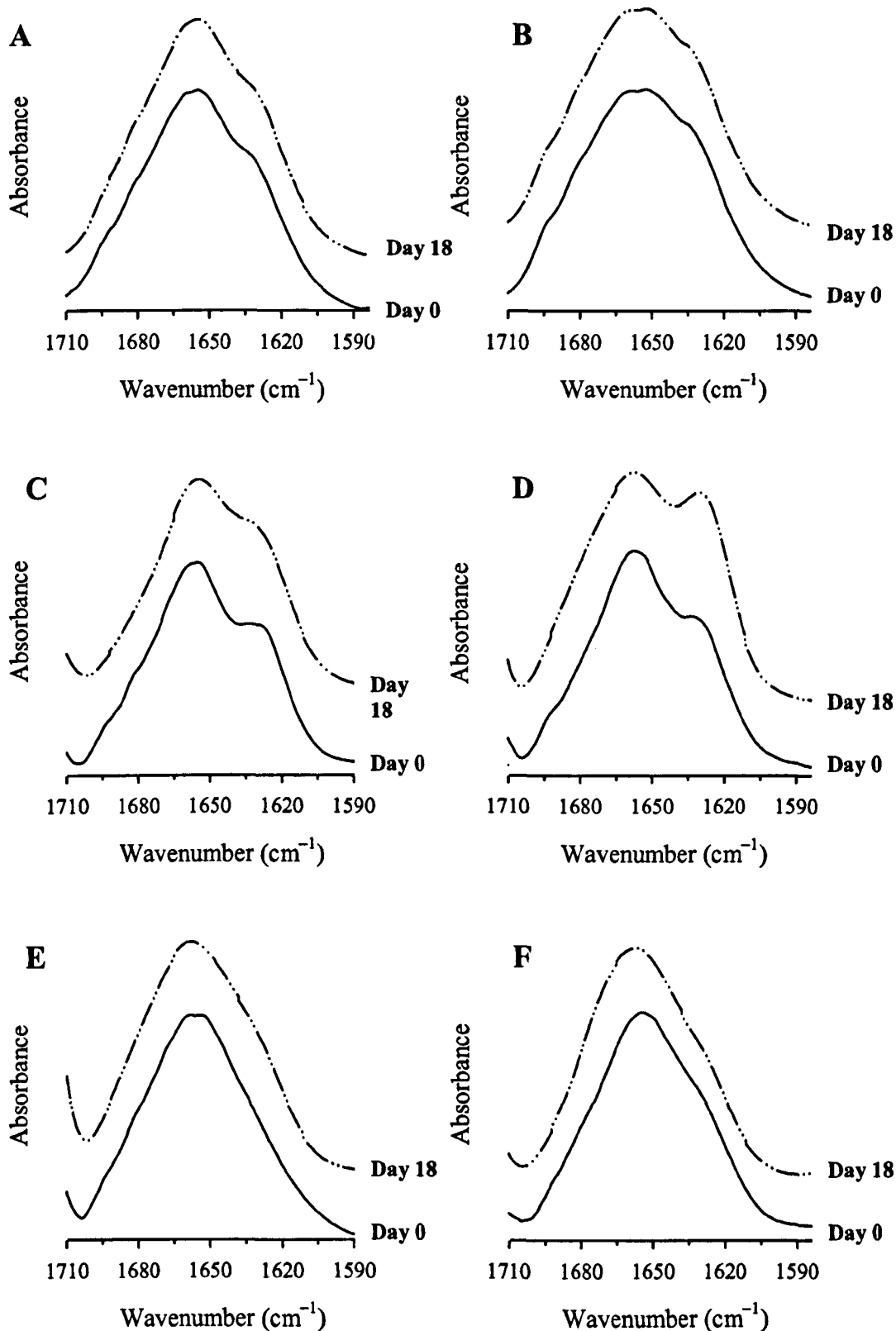
Figure 5.8: **Structural changes of SHaPrP (90–231) in the absence and presence of lipid membranes following incubation at 20 °C.** PrP in the absence of lipid at (A) pH 5 and (B) pH 7. PrP bound to (C) POPG membranes at pH 5, (D) POPG membranes at pH 7, (E) DPPC membranes at pH 7 and (F) DPPC/chol/SM mixed membranes at pH 7. The samples were incubated at 20 °C.

solution, both at pH 7 and 5 following incubation at 20 °C for 18-days, showed small uniform round aggregates, which were larger at pH 5 ~ 11.3 ± 1.8 nm (Figure 5.9A & B). The electron micrograph of PrP in the presence of POPC vesicles at pH 5 also revealed small round aggregates (Figure 5.9E) similar to those formed by PrP in solution at pH 5. In contrast, the electron micrograph of PrP with POPG vesicles at pH 5 (Figure 5.9C) revealed extensive aggregation of PrP around the lipid vesicles. The electron micrograph of PrP bound to the raft-like vesicles of DPPC/chol/SM at pH 7 (Figure 5.9D) shows no indication of protein aggregation around the lipid vesicles and unlike with POPC vesicles there also appeared to be less protein in solution. These observations are consistent with the fluorescence binding data (Chapter 4) where binding of PrP was observed to the raft-like membranes at pH 7, and no association was detected with POPC membranes. An electron micropgraph of the raft-like vesicles alone is also shown in Figure 5.9F, intact lipid vesicles were observed.

5.4 Discussion

Far-UV CD and ATR FTIR spectroscopy were employed to characterise the structural properties of SHaPrP (90–231) in solution and in negatively charged, zwitterionic and raft-like membranes at pH 5 and 7. Binding of PrP to negatively charged membranes of POPG, gel-phase zwitterionic membranes of DPPC and raft-like membranes of DPPC/chol/SM (50:30:20, molar ratio) results in significant structural changes in the protein.

The far-UV CD spectra of PrP in solution at pH 5 and 7 were very similar and displayed double minima at 208 and 222 nm (Figure 5.2 & 5.3) which indicated a relatively high content of α-helical structure. The FTIR results were also
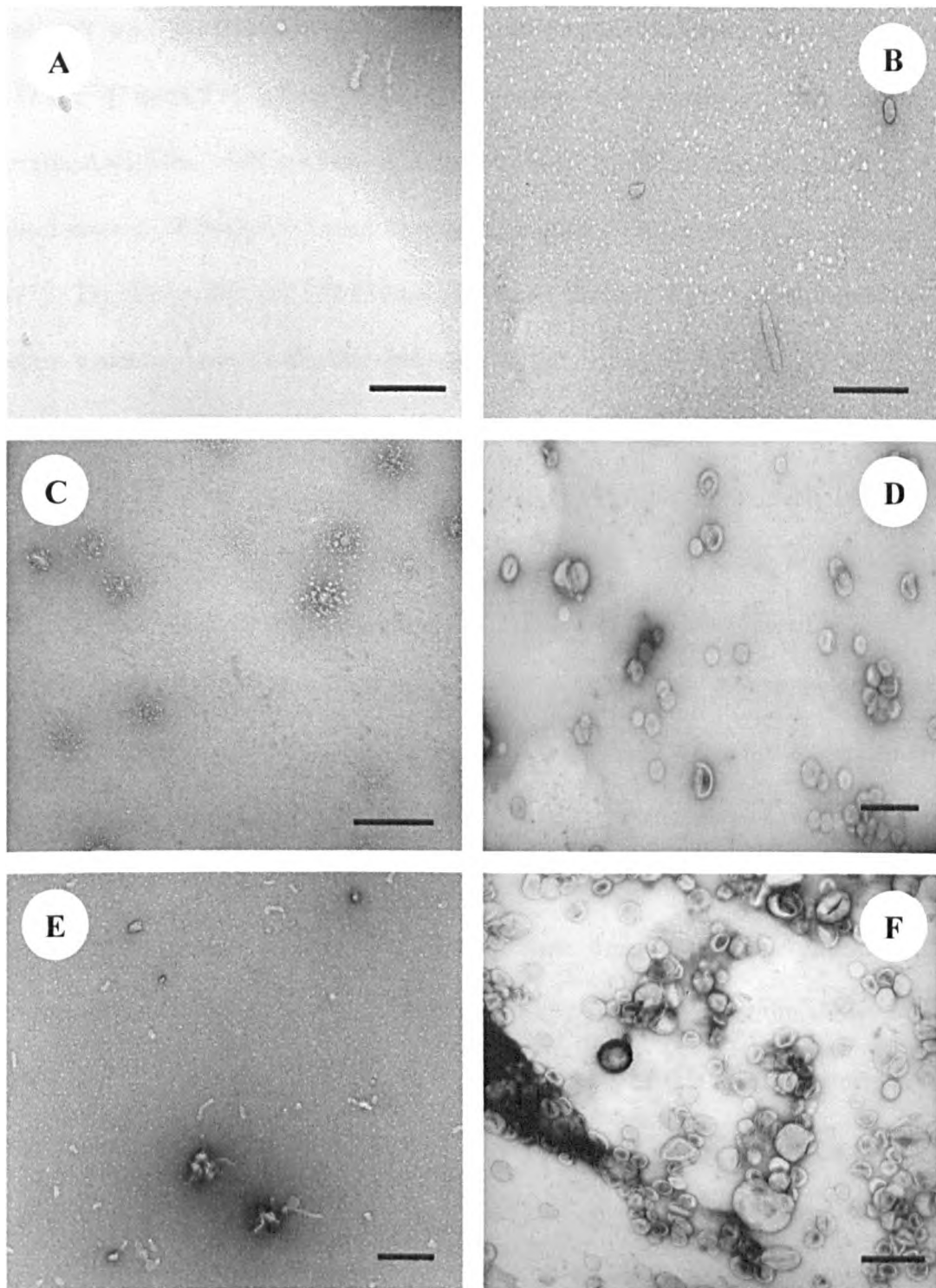
Figure 5.9: **Electron micrographs of SHaPrP (90–231) in solution and in the presence of lipid membranes.** (A) PrP in solution, pH 7, (B) PrP in solution, pH 5; PrP in the presence of (C) POPG vesicles, pH 5, (D) DPPC/chol/SM vesicles, pH 7 and (E) POPC vesicles, pH 5. (F) DPPC/chol/SM vesicles in the absence of PrP, pH 5. Samples were negatively stained using 2 % uranyl acetate. EM images were taken after incubation at 20 °C. Bar, 200 nm.

consistent with this interpretation, which revealed an amide I band centred around 1657 cm^{-1} (Figure 5.4), a frequency assigned to α-helical structure. This is in good agreement with the NMR structure of SHaPrP (90–231), which revealed a mainly α-helical protein (44 %) with a small amount of β-sheet (4 %) structure (James *et al.*, 1997). The deconvoluted FTIR spectra of PrP at pH 5 and 7 shows the presence of β-sheet structure, however the low frequency of the β-sheet component ~ 1626 cm^{-1} (Figure 5.5B,D) suggested that the β-strands were forming strong intermolecular hydrogen bonds. This component in the FTIR spectra has been previously observed in aggregated or oligomerized proteins (Cabiaux *et al.*, 1989; Wang *et al.*, 1996). Although ATR FTIR has been successfully used in the determination of secondary structure for soluble proteins (Goormaghtigh *et al.*, 1990), the slow evaporation of the aqueous protein sample during formation of the protein film on the germanium plate may cause aggregation of the some of the protein molecules. Low-frequency β-sheet component in the FTIR spectra has been observed for apocytochrome *c* and cytochrome *c*. In solution these proteins have been shown to be largely disordered and helical structures, respectively. However, the ATR FTIR spectrum showed the presence of aggregated β-sheet structure. It was concluded that this component was likely to result from the folding of unstructured domains of the proteins under the constraints of the FTIR films (Bryson *et al.*, 2000). This explanation may also apply to PrP. The NMR structure of SHaPrP (90–231) shows the amino-terminus to be unstructured (James *et al.*, 1997) and this region of the protein may form β-sheet structure during film formation, in which the β-strands form strong intermolecular hydrogen bonds. No visible signs of aggregation were detected prior to film formation. Furthermore, the presence of β-sheet structure was not evident from the solution CD spectra of PrP (Figure 5.2 & 5.3).

Binding of PrP to negatively charged membranes induces conformational changes in the protein. The far-UV CD spectra of PrP with negatively charged membranes of POPG at both pH 5 and 7 showed less defined α-helical bands at 208 and 222 nm and noticeable changes in the overall lineshape of the CD spectra were observed (Figure 5.2A & 5.3A). The spectra of PrP with POPG membranes at pH 5 and 7 appear to have a higher contribution from a single dichroic minimum at about 220 nm. The spectral changes in the CD spectra of PrP in POPG membranes at both pH 5 and 7 are indicative of a higher content of β-sheet structure. This interpretation is further supported by the ATR FTIR results, which after spectral deconvolution revealed an increase in the intensity of the β-sheet component at about 1626 cm^{-1} (Figure 5.5B,D). The low-frequency of the β-sheet structure in PrP indicated that the β-strands was forming strong intermolecular hydrogen bonds between oligomerised or aggregated protein at the surface or in lipid membranes.

Further information on structural changes in PrP upon binding to POPG membranes was obtained by difference spectroscopy. The difference spectra obtained from the subtraction of PrP in POPG membranes from PrP in solution at the corresponding pHs (Figure 5.7A) suggest that binding is accompanied by increased aggregated β-sheet structure, evidenced by the positive band at ~ 1626 cm^{-1}. In addition, the positive band at 1656 cm^{-1} suggests an increase in α-helical structure (Figure 5.7A). The incubation of PrP with POPG membranes at pH 5 and 7 induced a further increase in the low-frequency β-sheet structure (Figure 5.8C,D). The aggregation of PrP in the presence of POPG membranes is clearly evident from the electron micrographs (Figure 5.9B), which shows extensive aggregation around

POPG vesicles, confirming the FTIR and CD data, which revealed an increase in aggregated β-sheet structure.

The low-frequency β-sheet component observed in the FTIR spectra of PrP in POPG membranes has been previously seen in the FTIR spectra of purified infectious prion rods consisting of the N-terminally truncated domain (residues 90–231) from scrapie-infected hamster brains (Caughey *et al.*, 1991; Gasset *et al*, 1993; Pan *et al.*, 1993). These studies revealed that procedures that result in a decrease in the low-frequency β-sheet structure diminished scrapie infectivity. Thus supporting the hypothesis that the conversion of PrP^C to PrP^{Sc} and the acquisition of infectivity are consequences of a structural transition, which results in the conversion of soluble α-helical protein to an insoluble β-sheet state.

Binding of PrP to gel-phase zwitterionic membranes of DPPC and raft-like membranes of DPPC/chol/SM (50:30:20 molar ratio) at pH 7 induces conformational changes in the protein. The far-UV CD spectra of PrP with DPPC and raft-like membranes at pH 7 shows a marked increase in the intensity of the dichroic bands at 208 and 222 nm, indicative of a higher content of α-helical structure (Figure 5.2B,C). No changes in the far-UV CD spectra of PrP were observed with POPC membranes at both pH 7 (Figure 5.2D) and pH 5 (Figure 5.3C) and with raft-like membranes at pH 5 (Figure 5.3B) consistent with the absence of lipid-protein interactions as revealed by Trp fluorescence (Chapter 4).

The ATR FTIR results clearly shows an increase in the α-helical content of PrP upon binding to gel-phase zwitterionic membranes of DPPC and raft-like lipid membranes of DPPC/chol/SM at pH 7 (Figure 5.4C,D). Deconvolution of the amide

I band of the ATR FTIR spectra of PrP in the presence of these lipids revealed the α-helical band at ~1654 cm^{-1}. In addition, the intensity of the low-frequency β-sheet band at ~1627 cm^{-1} was less than that for PrP in the absence of lipid at pH 7 (Figure 5.6B,D) which suggests that the interaction was accompanied by a loss in aggregated β-sheet structure. This observation was also confirmed by difference spectroscopy, which revealed a positive band at ~ 1657 cm^{-1}, a frequency assigned to α-helical structure (Figure 5.7B). In addition, the difference spectra of PrP bound to DPPC membranes at pH 7 showed a negative band at 1626 cm^{-1}, confirming the earlier interpretation that interaction is accompanied by a loss in β-sheet structure and an increase in the α-helical content of PrP. No further spectral changes in the ATR FTIR spectra of PrP incubated with DPPC membranes and raft-like membranes at pH 7 for 18 days at 20 °C were evident, which suggests that the induced α-helical structure in PrP is stable.

No evidence for protein aggregation was detected from the electron micrographs of PrP and the raft-like membranes at pH 7 (Figure 5.8D). The results taken together suggest that PrP is most likely to adopt a stable α-helical structure within the raft domains in the plasma membrane.

In summary, the far-UV CD, FTIR and electron microscopy results suggests that: (a) binding of PrP to negatively charged membranes of POPG at pH 5 and 7 is accompanied by an increase in both α-helical and aggregated β-sheet structures with visible protein aggregation seen under the electron microscope; (b) interaction of PrP with zwitterionic gel-phase membranes of DPPC and raft-like lipid membranes of DPPC/chol/SM induces stable α-helical structure in PrP with a loss in the aggregated

β-sheet structure, and no signs of protein aggregation were detected from the EM images.

5.5 Conclusions

The present structural study of PrP revealed some important features of its interaction with lipid bilayers, which may be of relevance to the structural transitions that occur during the conversion of PrP^C to PrP^{Sc}. Both CD and FTIR data shows that the interaction of PrP with raft-like membranes induces stable α-helical structure. The interaction of PrP with negatively charged membranes at both pH 5 and 7 was accompanied by an increase in the low-frequency β-sheet structure, which suggests that the binding of PrP to negatively charged membranes induces protein aggregation or oligomerisation at the surface or in the lipid membranes. These findings were further supported by electron microscopy. Extensive protein aggregation was observed with POPG vesicles, aggregated structures were absent from the EM images of PrP with raft-like membranes.

Chapter 6: Membrane Binding/Insertion Kinetics of Syrian Hamster Prion Protein (SHaPrP) Residues 90–231 and PrP-Induced Membrane Destabilisation

6.1 Introduction

The precise mechanism of PrP-induced cell death remains unclear. *In vitro* studies have demonstrated that PrP is neurotoxic to cultured neurons (Forloni *et al.*, 1993; Brown *et al.*, 1996). Various hypotheses have been postulated to explain neuronal cell death. These include increased oxidative stress as a consequence of depleted levels of PrP^C (Brown *et al.*, 1997*b*). Others have proposed a mechanism for prion neurotoxicity through a direct perturbation of the plasma membrane of nerve cells as a consequence of PrP^{Sc} accumulation (Pillot *et al.*, 1997; Lin *et al.*, 1997). The results presented in this chapter provide a further insight into PrP-lipid interactions in particular to changes in the lipid bilayer integrity and/or permeability. The data discussed here was obtained from two fluorescence-based techniques. The first involved incorporating a lipid probe at the membrane surface, to monitor in real time the interaction of PrP with lipid membranes. The second approach involved following PrP-induced release of a fluorescent dye encapsulated in lipid vesicles.

6.1.1 Fluorescent probes at membrane surfaces

The localisation of the fluorescent probe fluorescein-phosphatidyl-ethanolamine (FPE) at the membrane surface has been used to measure in real time the interactions of peptides or proteins with membranes (Wall *et al.*, 1995; Golding *et al.*, 1996; Cladera *et al.*, 1999; Wolfe *et al.*, 1998). Figure 6.1 shows a schematic representation of the FPE method. The addition or removal of charged peptides or

A

Positively charged peptide

Binding to negatively charged membranes labelled with FPE

Insertion of peptide into the lipid bilayer

FPE

Glycerophospholipid

B

Fatty acid chains

$CH_3(CH_2)_{14}-\overset{O}{\overset{\|}{C}}-OCH_2$

$CH_3(CH_2)_{14}-\overset{}{\underset{O}{\overset{\|}{C}}}-OCH$

$CH_2\ O-\overset{O}{\overset{\|}{\underset{O^-}{P}}}-OCH_2CH_2NH-\overset{}{\underset{S}{\overset{\|}{C}}}-NH$

$(CH_3CH_2)_3\overset{+}{N}H$

FPE
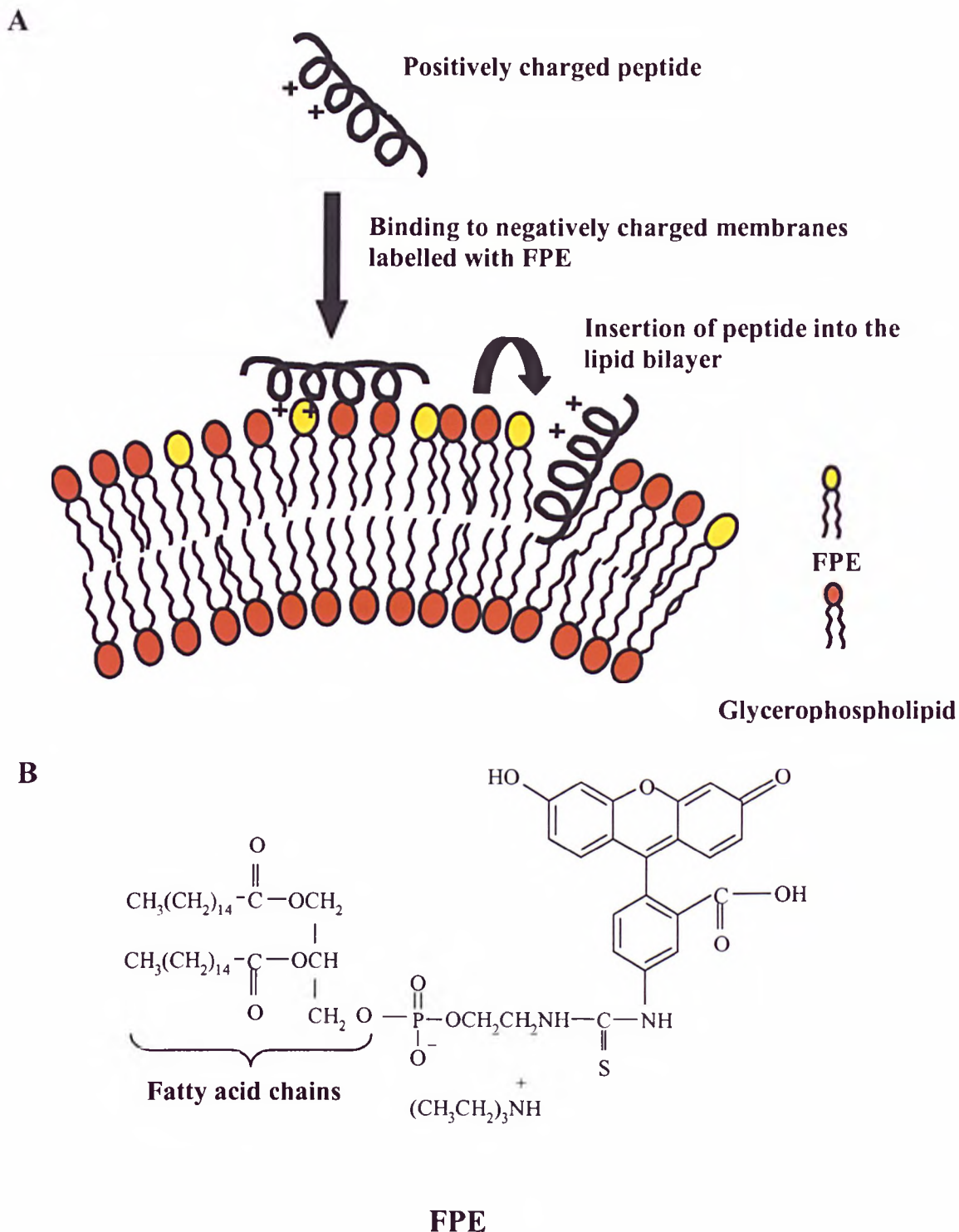
Figure 6.1: **Schematic representation of the FPE method.** (A) FPE is incorporated into the outer leaflet of preformed large unilamellar vesicles. Binding of positively charged peptide or protein causes increased electropositive potential at the surface of the membrane, which affects the protonation state of FPE and results in an enhancement of the fluorescence intensity of the probe. Insertion of the peptide would involve the loss of the charged species from the membrane surface and a decrease in the fluorescence signal. (B) Chemical structure of FPE. The protonation state of the acidic group of the xanthene ring system in FPE is affected during the binding and insertion of charged species (Wall *et al.*, 1995).

160

proteins causes changes to the electrostatic potential of the membrane surface and affects the protonation state of FPE, leading to changes of the fluorescence intensity of FPE. Figure 6.2 displays the excitation and emission spectra of FPE and a kinetic trace obtained from rapidly mixing melittin with FPE-labelled lipid vesicles (Wolfe *et al.*, 1998). The binding of positively charged melittin to PC labelled membranes led to an increase in the fluorescence intensity and the insertion of the protein into the bilayer was represented by a decrease in fluorescence. In the current study the outer-leaflet of preformed vesicles were labelled with FPE and the kinetics of the interaction of SHaPrP (90–231) with FPE-labelled lipid membranes were investigated by stopped-flow fluorescence.

6.1.2 Fluorescent dye release assay

Numerous studies have demonstrated that the interaction of peptides or proteins with lipid membranes alters the structure and changes the lipid bilayer permeability (Defrise-Quertain *et al.*, 1989; Wimley *et al.*, 1994; White & Wimley, 1998; Vogt & Bechinger, 1999). Membrane integrity maybe examined by dye release assays in which a fluorescent dye is encapsulated in lipid vesicles at concentrations at which its fluorescence is self-quenched. Addition of a membrane-destabilizing molecule would result in the release of the fluorescent dye to the external medium, leading to an increase in fluorescence caused by the dilution of the dye and the consequent relief of self-quenching. The integrity of lipid membranes upon binding of SHaPrP (90–231) was studied by following the release of the fluorescent dye calcein from lipid vesicles.
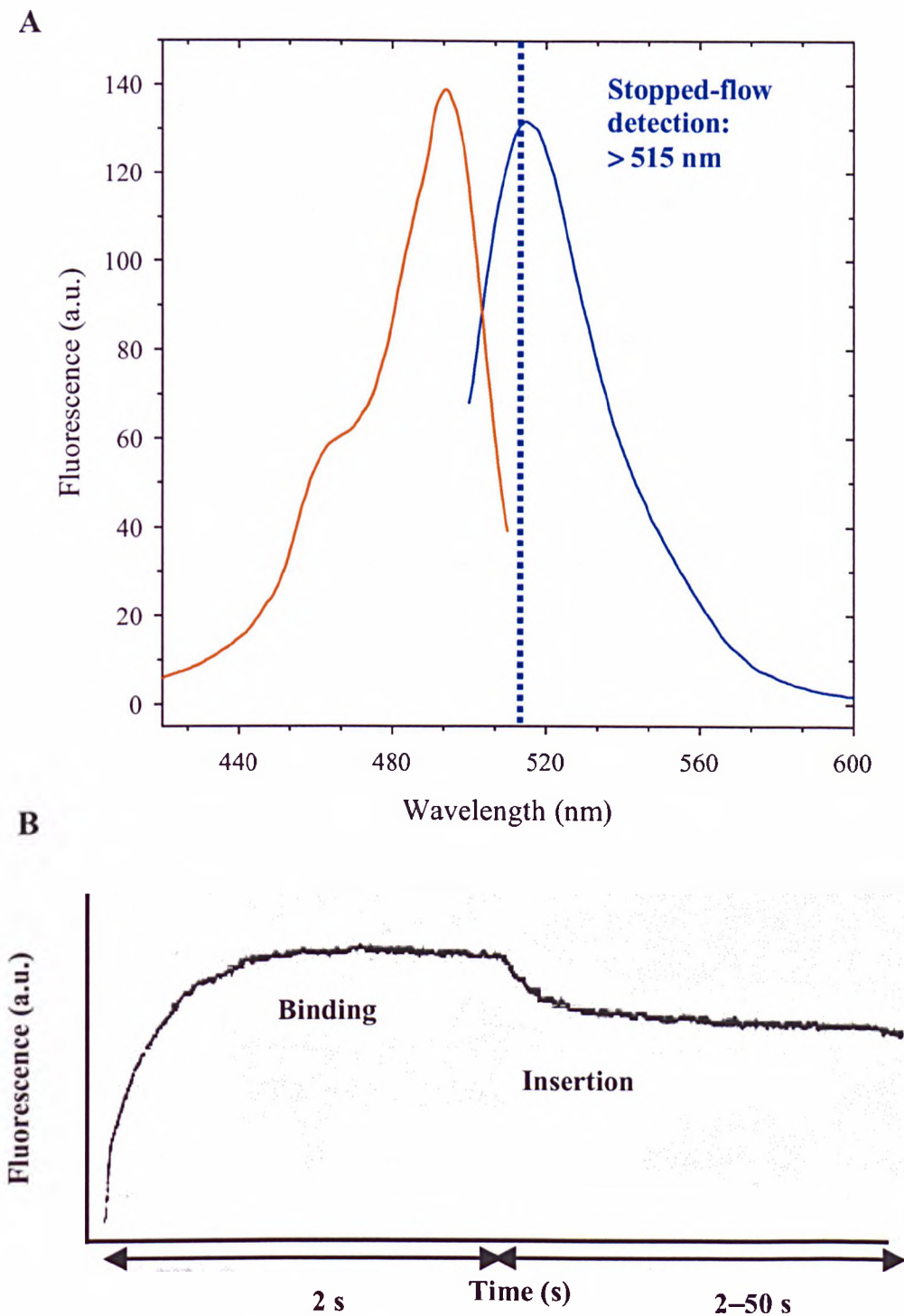
Figure 6.2: **Fluorescence properties of FPE.** (A) Excitation (red) and emission (blue) spectra of FPE. The spectra were recorded with 3 μM FPE in 20 mM sodium phosphate, pH 7.2. The excitation spectrum of FPE has maximum intensity (λ_{max}) at ∼ 490 nm and a fluorescence emission λ_{max} of ∼ 518 nm. The stopped-flow experiments described in this chapter involved monitoring the changes in fluorescence emission above 515 nm. (B) Representative kinetic trace obtained with melittin (reproduced from Wolfe *et al.*, 1998). The binding and insertion events are highlighted.

6.2 Material and Methods

6.2.1 Materials

POPG, POPC, sphingomyelin and cholesterol were purchased from Avanti Polar lipids (Birmingham, AL). DPPC was obtained from Sigma-Aldrich (Poole, UK). FPE and calcein were purchased from Molecular Probes, Oregon, USA. All other chemicals were obtained from Sigma-Aldrich (Poole, UK) unless otherwise stated.

6.2.2 FPE-labelling and stopped-flow measurements

6.2.2.1: FPE-labelling of lipid vesicles

The incorporation of FPE into the outer-leaflet of preformed vesicles was carried out according to Wall *et al.* (1995). Lipid films were prepared of the desired lipid or lipid mixtures as described in Chapter 4, Section 4.2.2. Large unilamellar vesicles were prepared by hydrating the lipid film with 20 mM sodium phosphate at pH 7.2, containing 280 mM sucrose. Lipid suspensions were subjected to 5 cycles of freeze-thawing and extruded ten times through 100 nm pore diameter polycarbonate filters (Nucleopore, CA, USA) using a Lipex extrusion apparatus (Lipex, Vancouver, Canada) at a pressure of 250 psi. An aliquot of the FPE probe was added from a stock ethanolic solution (5 mg/mL) to a level of 0.2 % w/w of the total lipid and incubated for 1 h at 20 °C in the dark. Typically, ~ 6 μL of the stock ethanolic FPE solution was added to about 1.5 mL of a 20 mM lipid solution. Non-incorporated FPE was removed from the FPE-labelled vesicles by gel filtration using Sephadex PD10 columns equilibrated with 25 mL of 20 mM sodium phosphate at pH 7.2, containing 280 mM sucrose. FPE-labelled vesicles were retained on the column

whilst free FPE was washed out in the flow through. The FPE-labelled vesicles were eluted with 3.5 mL of the phosphate buffer. The above procedure has been reported to incorporate 30–50 % of the externally added FPE into the outer leaflet of preformed vesicles (Wall *et al.*, 1995). Labelled vesicles were stored at 4 °C and used within one week.

6.2.2.2: *Check of the asymmetric labelling of lipid vesicles with FPE*

The following method was used to check that only the outside leaflet of vesicles was labelled. For a given preparation of FPE-labelled vesicles the fluorescence intensity at 518 nm was monitored following excitation at 490 nm (Figure 6.2A). The fluorescence intensity changes upon addition of 10 μL of 10 mM $CaCl_2$ to 200 μM lipid vesicles were monitored over time. Once the fluorescence emission intensity had stabilised, 6 μL of 3 μM solution of ionophore A23187 prepared in de-ionised H_2O was added and further changes in the fluorescence signal were noted. The addition of an ionophore would render the membrane permeable and facilitate the movement of the cations across the membrane. Further increase would be detected if the probe were also located on the internal leaflet. The fluorescence emission was recorded on a Photon Technology International spectrofluorimeter, using 4 mm pathlength quartz cells. Excitation and emission bandwidths were both set at 2 nm.

6.2.2.3: *Stopped-flow fluorescence spectroscopy*

FPE-labelled vesicles were rapidly mixed with an equal volume of PrP in a Micro Volume Stopped-Flow Reaction Analyser SX.18MV (Applied Photophysics Ltd., Leatherhead, UK), equipped with a modified T mixer and a 2 × 1 × 10 mm

flow-cell (Figure 6.3). A computer-triggered pneumatic ram was set up to drive a specified volume of the contents of two syringes into a T-mixer, where the solutions were rapidly mixed before entry into the optical cell. Electromagnetic radiation from a 150 W xenon arc lamp and a monochromator were used for excitation at 490 nm (4.2 nm bandwidth) along the 10 mm axis of the optical cell. A photomultiplier tube detected the fluorescence signal over time. In stopped-flow measurements a high-pass filter with a cut-off at 515 nm was placed between the optical cell and photomultiplier, this prevented excitation light getting into the detector and swamping the fluorescence signal. Figure 6.2A shows the excitation and emission spectra of FPE. The fluorescence emission λ_{max} of FPE occurred at 518 nm therefore, by including a 515 nm filter in the stopped-flow spectrofluorimeter a majority of the fluorescence emission is detected. Kinetics were measured by monitoring the emission from the 2-mm face of the cell over a time scale up to 10 s. The dead time for the stopped-flow instrument for 1:1 mixing of two solutions was ~ 3 ms.

Both lipid and protein were in 20 mM sodium phosphate buffer, pH 7.2 containing 280 mM sucrose. Final lipid concentration was 200 μM and protein concentration varied from 2 to 10 μM. Measurements were preformed at 20 °C.

One thousand data points were acquired in a logarithmic time. The advantage of using a logarithmic timebase is that data points are highly concentrated early on in the acquisition time *i.e.* where a fast kinetic phase may occur. The traces resulting from the 1:1 mixing of FPE-labelled vesicles and PrP were acquired and

Trigger/Stop

Optical Cell

115 μL ageing loop

T-Mixer

F

C

Drive Ram
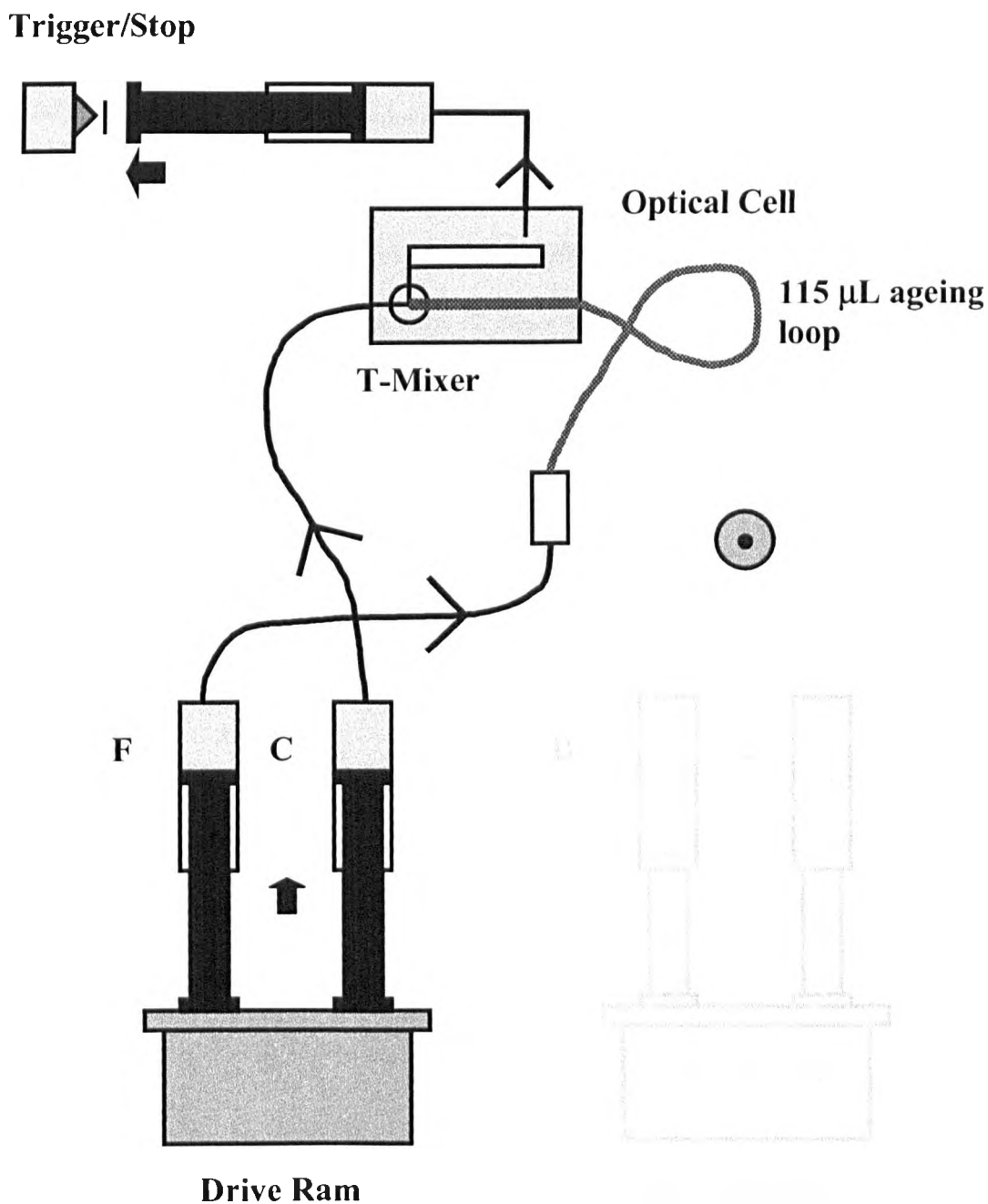
Figure 6.3: **Schematic representation of the single-mixing mode configuration of the stopped-flow spectrofluorimeter.** The solutions from drive syringes C and F are driven into the optical cell by a computer driven pneumatic ram. Light of a specified excitation wavelength enters the optical cell and a photomultiplier tube detects the fluorescence signal over time.

stored digitally using the accompanying Applied Photophysics software. For each set of experimental conditions four traces were averaged.

• *Data analysis:* The time courses for PrP-induced fluorescence changes of FPE were normalised to the initial fluorescence level of FPE-labelled vesicles without protein prior to data analysis. The kinetic parameters were obtained by fitting the fluorescence traces, to the sum of exponentials, using a non-linear least-squares algorithm to the equation:

$$\text{Observed signal} = \sum_{i=1}^{x} A_i e^{-k_i t} + \textit{offset} \qquad \text{(Eq. 6.1)}$$

where A_i and k_i are the amplitude and rate, respectively, of the fluorescent component i. The amplitude of the fluorescence trace comprised of the amplitudes of the various fluorescence components, $A_{total} = |A_1| + |A_2| + |A_3| \dots |A_n|$ and the fractional amplitude was expressed as a percentage of the total observed amplitude defined as

$$\frac{A_i}{A_{total}} \times 100$$

For each PrP concentration the kinetic traces were initially fitted to the lowest number of exponentials. If the residuals were obviously non-random then an improvement in the fit was sought by allowing additional components to fit the data.

6.2.3 Calcein release

6.2.3.1: Preparation of lipid vesicles loaded with calcein

Lipid vesicles containing 60 mM calcein in their aqueous core were prepared by hydrating the desired lipid film with the required buffer (50 mM MOPS buffer at pH 7.2, 10 mM EDTA or 50 mM sodium acetate buffer at pH 5.0, 10 mM EDTA) containing 60 mM calcein. At this concentration the calcein fluorescence is self-quenched. Lipid suspension was extruded as described earlier, using 100-nm pore membranes. Non-encapsulated calcein was removed by gel filtration using 2 mL columns packed with sephadex G-50. The columns were equilibrated with 1 mL × 3 of the required buffer (MOPS buffer, pH 7.2 or acetate buffer, pH 5.0) and centrifuged at 2000 rpm for 3-mins for each wash and a final spin at 3000 rpm for 45-secs. 100 μL of the lipid sample was applied to the columns. The columns were span again at 2000 rpm for 2-mins. The calcein-loaded vesicles were excluded from the column whereas the free calcein was retained.

The integrity of the lipid vesicles loaded with calcein in the absence of protein was determined by monitoring the spontaneous release of calcein and was found to be less than 1 % over 10-mins. The stability of the prepared vesicles was also monitored by comparing the fluorescence intensities of the calcein loaded vesicles in the absence of protein at the start and the end of the experiments and in all cases the fluorescence intensity did not differ by more than 5 %.

The release of calcein from lipid vesicles upon binding of PrP was monitored by calcein fluorescence emission at 512 nm over a time scale of 500 s after manually mixing 5 parts of lipid vesicles with 1 part of protein solution (5:1 v/v). The protein was in 20 mM sodium acetate pH 5.5 and lipid vesicles loaded with calcein were in 50 mM MOPS, pH 7.2 or 50 mM sodium acetate, pH 5.0, both buffers contained 10 mM EDTA. The final pH of the lipid-protein samples were 7.15 and 5.11, respectively. The deadtime of these measurements was 24 ± 4 s. The excitation wavelength was 490 nm and both the excitation and emission slits were set to 1 nm. Experiments were performed at 20 °C. Release of calcein to the external medium was detected by an increase in fluorescence. The final lipid concentration was 50 μM and protein concentrations varied from 10 to 500 nM. The fraction of calcein release (R_f) was calculated according to

$$R_f = (F - F_0)/(F_{tot} - F_0) \qquad \text{(Eq. 6.2)}$$

where F is the fluorescence intensity 500 s after adding the protein, F_0 is initial fluorescence intensity and F_{tot} is the total fluorescence intensity observed after release of all calcein by disrupting the vesicles with Triton X-100 to a final concentration of 0.5 % (v/v).

For the stopped-flow measurements the excitation wavelength was set at 490 nm and emission was detected using a high-pass filter with a cut-off at 515 nm and an electronic filter with a time constant of 100 μs. Kinetics were measured by monitoring the emission over a time scale up to 200 s. Manual-mixing and stopped-

flow experiments were performed at 20 °C. Data analysis was carried out using Applied Photophysics software and Igor (Wavemetrics, Lake Oswego, Oregon).

The kinetic parameters (rates and amplitudes) of calcein release, were obtained by non-linear least-squares analysis using a minimum number of exponential phases. The fluorescence changes, monitored over time, following manual mixing of vesicles and protein (deadtime 24 ± 4 s) and in stopped-flow measurements operating at a reduced drive pressure, which resulted in a deadtime of ~ 4.5 ms were fitted to equation 6.1.

6.3   Results

6.3.1   FPE-detected membrane binding and insertion kinetics

FPE-labelled membranes have been successfully used to obtain valuable information on binding and insertion events of charged peptides and protein into lipid bilayers (Wall *et al.*, 1995; Golding *et al.*, 1996; Wolfe *et al.*, 1998). In the current study PrP was rapidly mixed with FPE-labelled POPG membranes. The observed fluorescence changes are associated with changes in the electrostatic potential surrounding FPE upon binding and insertion of PrP.

The asymmetric labelling of lipid vesicles with FPE was determined prior to the stopped-flow experiments. The protocol followed was established by Wall *et al.* (1995), and relies on the addition of cations to the outer side of the membrane, which changes the membrane surface electrostatic potential and induce an enhancement of the fluorescence intensity of FPE. The vesicles were then rendered permeable by addition of an ionophore (A23187), which facilitated the equilibrium

of the cation concentration across the membrane. If the lipid vesicles were symmetrically labelled then a further increase of fluorescence would be detected on addition of the ionophore. Figure 6.4 shows the fluorescence changes of FPE-labelled POPG vesicles after the addition of calcium ions and ionophore A23187. An increase in the fluorescence intensity was detected upon addition of calcium ions. However, no further increase was detected following the introduction of the ionophore, indicating that only the outsides of the lipid vesicles were labelled with FPE. Furthermore, the labelled vesicles appeared to be stable over a time scale of a week, no transmembrane flipping of externally located FPE was observed over this period.

The FPE-detected kinetics of binding and insertion of PrP into POPG-labelled membranes were studied at a protein concentration range of 2–10 µM and lipid concentration of 200 µM. FPE-detected kinetics monitored in stopped-flow measurements for the interaction of PrP with POPG membranes at pH 7 are displayed in Figure 6.5A, where the changes in fluorescence are plotted on a logarithmic time scale. The kinetic traces were all fitted to three exponentials and a summary of rates and amplitudes at various protein concentrations is presented in Table 6.1. Stopped-flow control measurements in which POPG membranes without FPE were rapidly mixed with PrP at pH 7 are shown in Figure 6.5B. No change in the signal was detected in these experiments, which is consistent with the notion that the fluorescence changes observed with POPG-labelled vesicles are due to the fluorescence changes of FPE as a result of PrP interaction. Figure 6.6 shows the FPE-detected kinetic trace from stopped-flow measurements in which 200 µM FPE-labelled POPG membranes were rapidly mixed with 7 µM PrP and the residuals
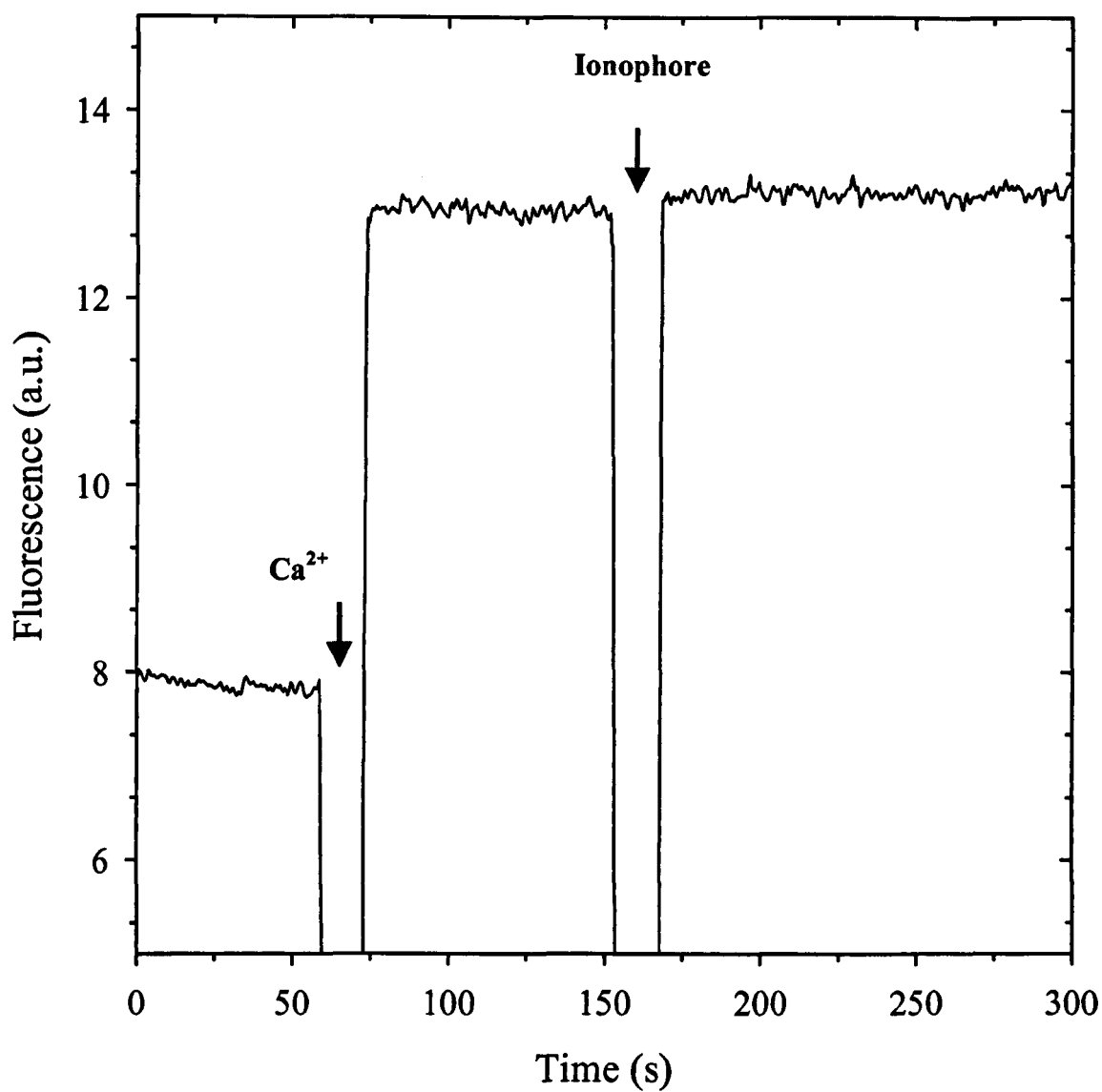
Figure 6.4: **Determination of the asymmetric incorporation of FPE into lipid vesicles.** Fluorescence intensity was recorded at 518 nm following excitation at 490 nm. At the arrow marked Ca^{2+}, 10 mM $CaCl_2$ was added and arrow labelled ionophore, 3 µM A23187 was added.
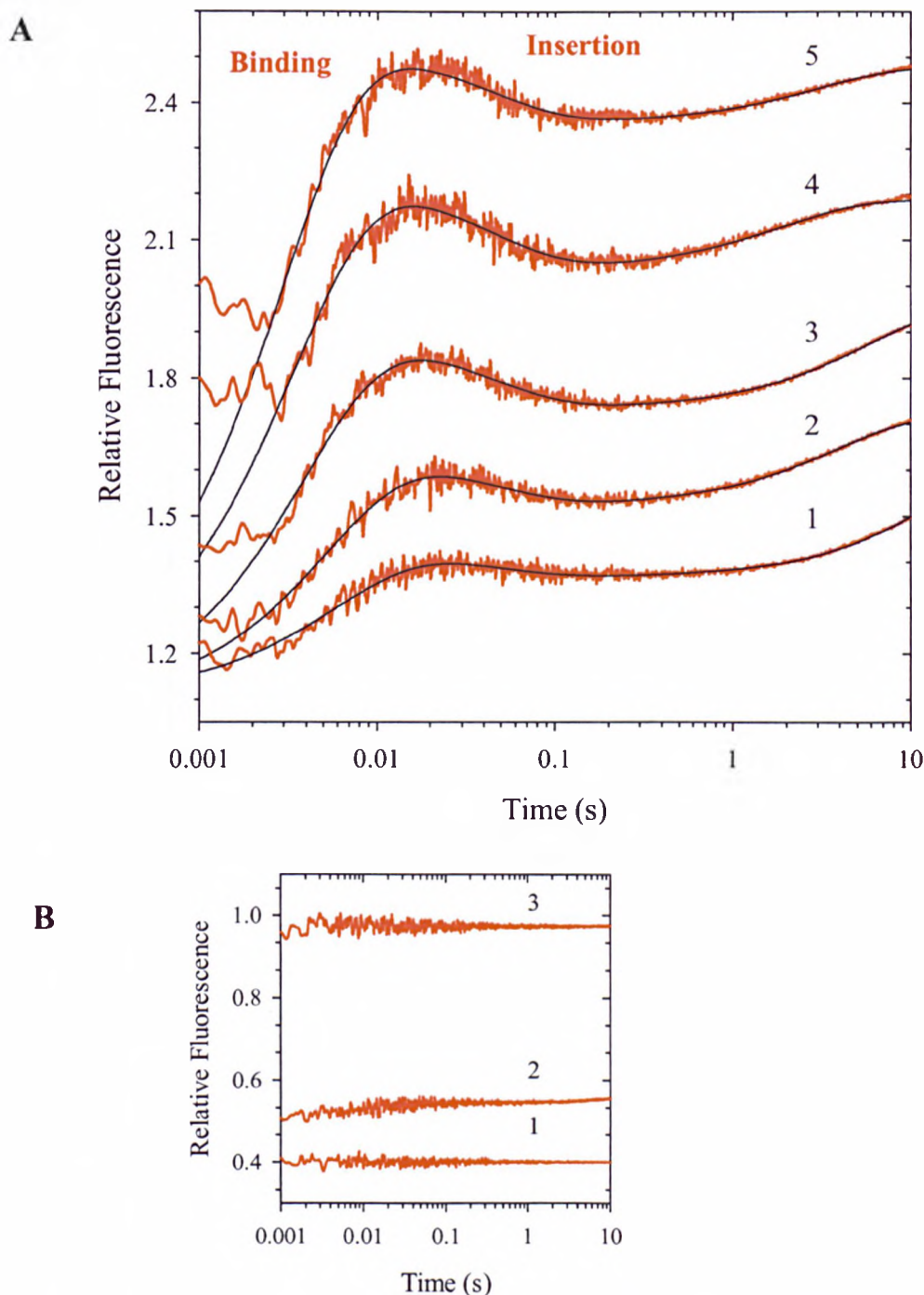
Fgure 6.5: **Representative kinetics for the interaction of SHaPrP (90–231) with FPE-labelled POPG membranes, pH 7.** (A) The fluorescence of FPE was monitored at 20 °C in stopped-flow measurements after rapidly mixing protein solution with FPE-labelled vesicles. Final lipid concentration was 200 µM and PrP concentrations were: (1) 2, (2) 3, (3) 5, (4) 7 and (5) 10 µM. Relative fluorescence was normalised to the initial fluorescence level of FPE-labelled POPG vesicles without protein. The experimental data is shown in red and fits are in black. The fluorescence changes associated with binding and insertion events are highlighted. (B) Controls: (1) POPG membranes no FPE, (2) PrP (10 µM) binding to POPG membranes, pH 7 (no FPE), (3) initial fluorescence level of FPE incorporated into POPG membranes, pH 7. The dead time of the instrument was ~3 ms and the data that is shown from 1–3 ms was acquired prior to the mixing of lipid and protein solutions. Data are displayed on a logarithmic timescale.

Table 6.1: Kinetic parameters for membrane binding and insertion of SHaPrP (90–231) with POPG membranes at pH 7[a]

[PrP] μM	k_1 (s^{-1})	A_1 (%)[b]	k_2 (s^{-1})	A_2 (%)[b]	k_3 (s^{-1})	A_3 (%)[b]	A_{tot}[c]
2	161 ± 6	47	24 ± 4	10	0.06 ± 0.01	43	1.99
3	183 ± 4	63	23 ± 2	14	0.25 ± 0.01	23	2.58
5	243 ± 4	67	23 ± 1	14	0.16 ± 0.01	19	3.60
7	295 ± 7	76	22 ± 1	14	0.50 ± 0.03	10	4.50
10	330 ± 6	82	22 ± 1	11	0.30 ± 0.02	7	5.08

[a]Rates (k_i) and amplitudes (A_i) were calculated from stopped-flow measurements at 20 °C using FPE-labelled membranes at a constant lipid concentration of 200 μM. [b]Fractional amplitude expressed as percentage of total observed amplitude (A_{tot}). [c]Total observed amplitude defined as $A_{tot} = |A_1| + |A_2| + |A_3|$.
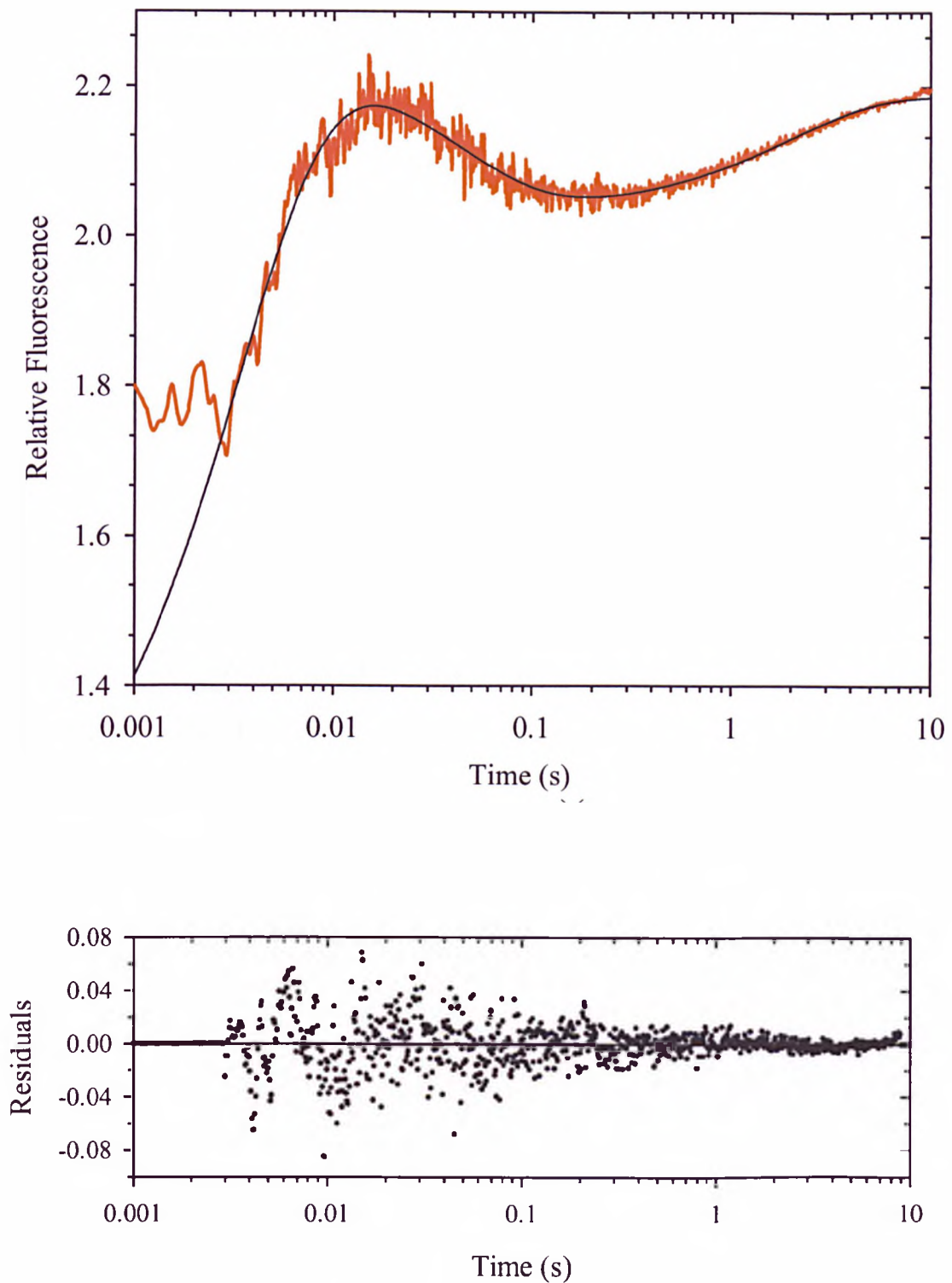
Figure 6.6: **Kinetics of FPE-detected binding and insertion of PrP into POPG membranes, pH 7**. The experimental data (red) and fit (black) are shown in the top panel. Residuals obtained from fitting the fluorescence trace to the sum of three expontentials are shown in the bottom panel and this shows the difference between the calculated and experimental data. Lipid and PrP concentration were 200 and 7 μM, respectively. Data are displayed on a logarithmic timescale.

obtained from fitting the kinetic data to the sum of three exponentials are also displayed.

The three kinetic phases detected in the stopped-flow experiments have the following properties:

- *Fast phase:* This phase is associated with an increase of fluorescence occurring over 3–6 ms. Both the rate constant (k_1) and amplitude (A_1) associated with this initial phase increase with protein concentration (Figure 6.7 and Table 6.1). The amplitude (A_1) of this fast phase accounts for the largest fraction of the total fluorescence change (47 % with 2 μM PrP and 82 % with 10 μM, Table 6.1). The rate constant increased more or less linearly up to about 8 μM PrP (Figure 6.7A). This phase is assigned to binding of positively charged PrP (+ 4) to the membrane surface.

- *Intermediate phase:* This component occurs within 50 ms and is associated with a decrease in the fluorescence intensity with rate constant (k_2) and amplitude (A_2) independent of protein concentration (Figure 6.7C,D & Table 6.1). This phase indicates a loss of the protein or positively charged regions of PrP from the membrane surface and represents the insertion of PrP into POPG membranes.

- *Slow phase:* An increase in the fluorescence intensity of FPE occurred during this phase and extends over several seconds (2–17 s). The amplitude (A_3) associated with this phase decreases with protein concentration and rate (k_3) increases with protein concentration (Figure 6.7E,F & Table 6.1). This slow phase following the binding and insertion of PrP into lipid membranes is probably associated with lipid rearrangement.

176
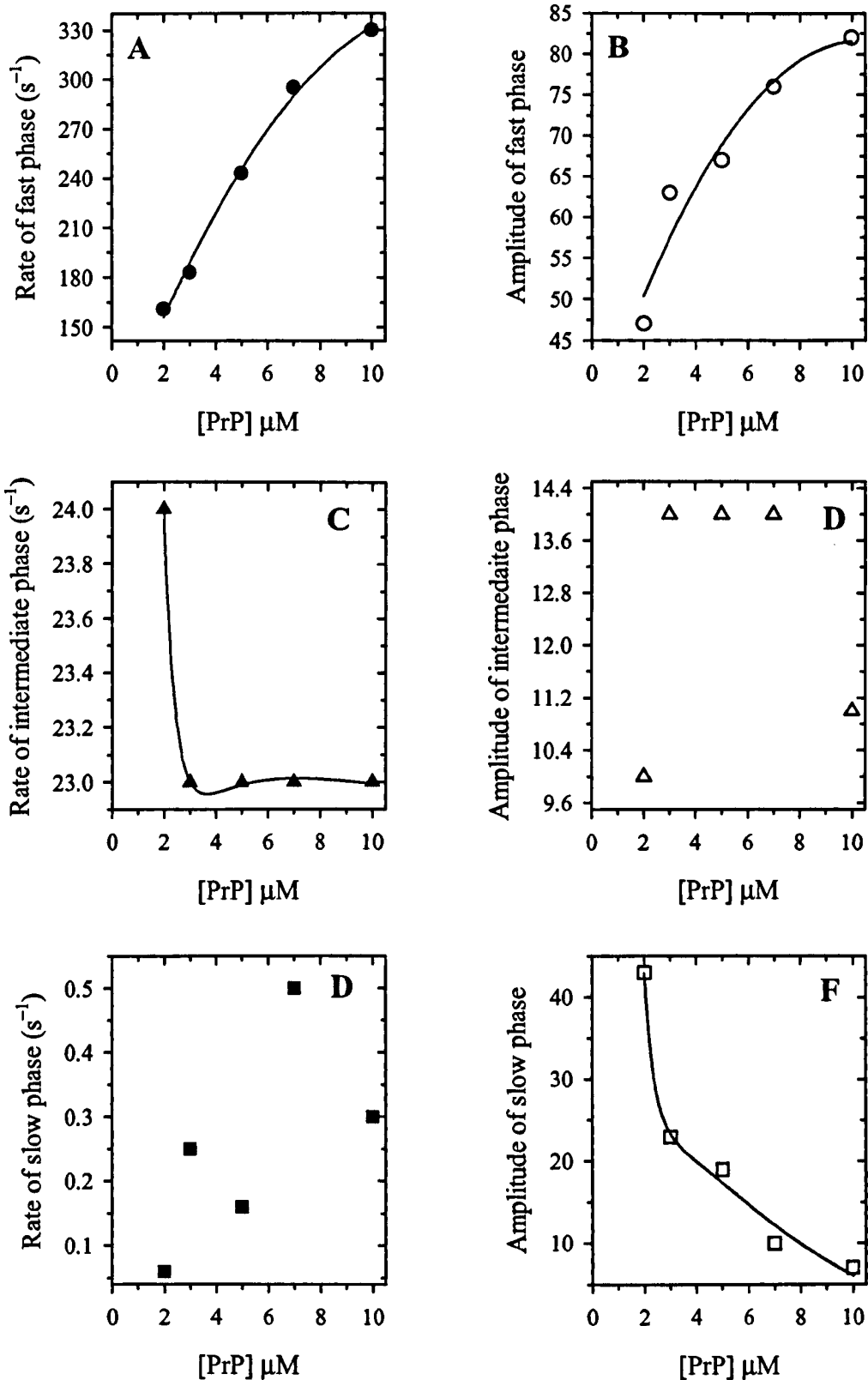
Figure 6.7: The dependence of FPE-detected kinetic parameters for the binding and insertion of PrP into POPG membranes on PrP concentration. Rates (k_i) (solid symbols) and amplitude (A_i) (open symbols), for the fast phase (circles), intermediate phase (triangles) and slow phase (squares) are plotted as a function of PrP concentration. Amplitudes are expressed as fractional amplitudes (percentage of total observed amplitude, see Materials and Methods). (A) k_1, (B) A_1, (C) k_2, (D) A_2, (E) k_3 and (F) A_3.

In order to access role of the membrane surface charge density on the binding and insertion of PrP, FPE-detected kinetic measurements were carried out with membranes of POPC containing only 30 % negative charge. The fluorescence binding results presented in Chapter 4 shows that PrP has a weak affinity for liquid-crystalline membranes composed of POPC. This means that the binding of the protein to membranes composed of POPC/POPG is mediated through electrostatic interactions between negatively charged lipid headgroups of POPG and positively charged amino acids in the protein. The changes in the fluorescence emission of FPE were monitored over a time range up to 10 s after rapid mixing with PrP. The FPE-detected kinetics were studied at a PrP concentration range of 2–10 μM and lipid concentration of 200 μM. The kinetic traces are shown in Figure 6.8, where the changes in fluorescence are plotted on a logarithmic time scale. Kinetic parameters were obtained by non-linear least-squares analysis using a minimum number of exponential phases and a summary of rates and amplitudes at various PrP concentrations is presented in Table 6.2. The results show that the interaction of PrP with mixed membranes of POPC and POPG at pH 7 (POPC/POPG, 70:30 molar ratio) monitored by FPE kinetics only revealed two phases of increasing fluorescence.

- *Fast phase:* An increase of fluorescence was detected during this phase (12–18 ms) and was assigned to the binding of PrP to POPC/POPG membranes. The rate (k_1) and amplitude (A_1) associated with this phase were found not to be strongly dependent on the protein concentration (Table 6.2).

- *Slow phase:* The slow phase also associated with an increase in the fluorescence intensity of FPE occurs over 1–3 s. The rate (k_2) increased with protein
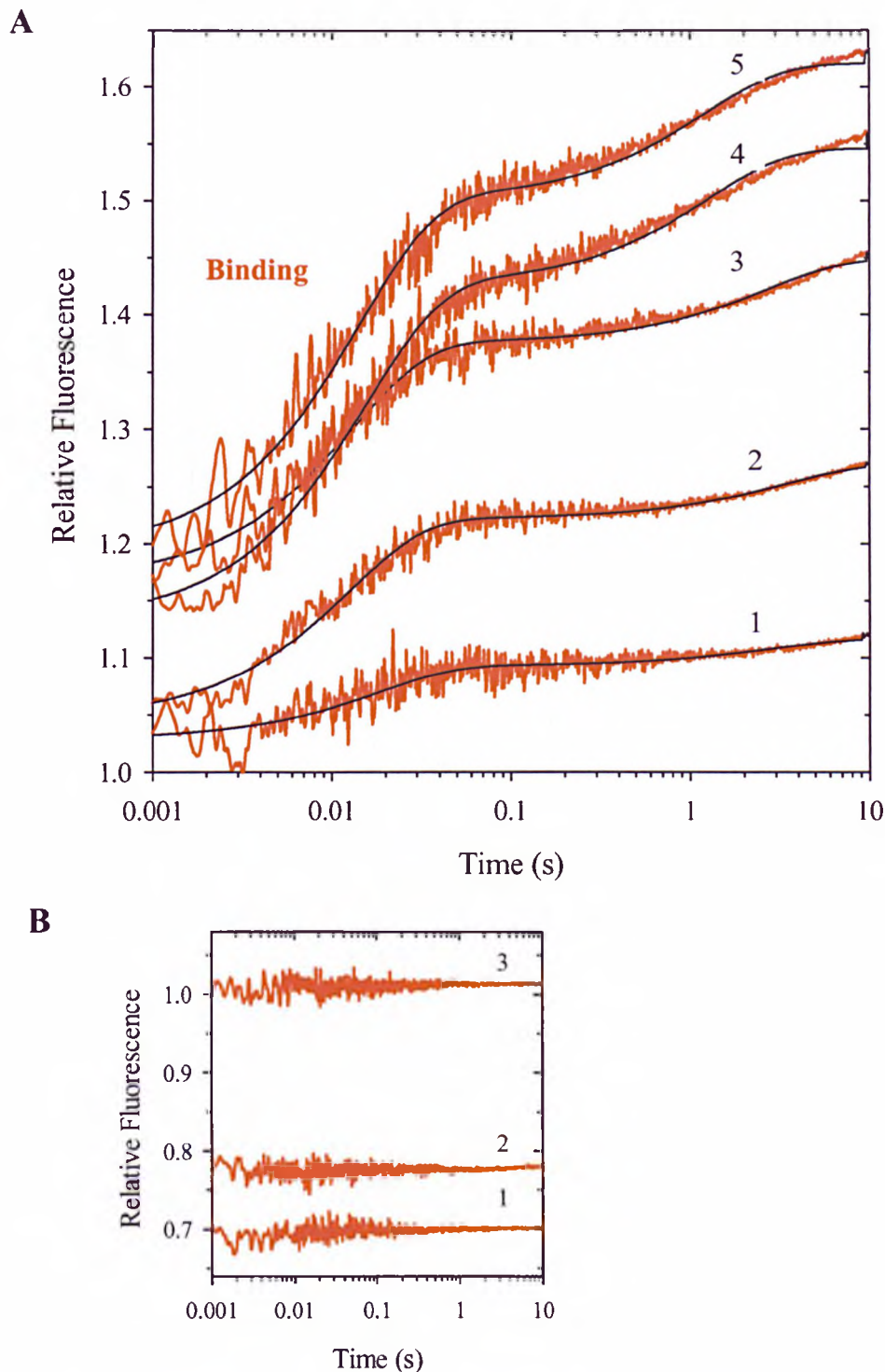
Figure 6.8: **Representative kinetics for the interaction of SHaPrP (90–231) with FPE-labelled POPC/POPG membranes (70:30 molar ratio), pH 7.** (A) The fluorescence of FPE was monitored at 20 °C in stopped-flow measurements after rapidly mixing protein solution with FPE-labelled vesicles. Final lipid concentration was 200 µM and PrP concentrations were: (1) 2, (2) 3, (3) 5, (4) 7 and (5) 10 µM. Relative fluorescence was normalised to the initial fluorescence level of FPE-labelled POPC/POPG vesicles without protein. The experimental data is shown in red and fits are in black. The fluorescence change associated with binding is highlighted. (B) Controls: (1) POPC/POPG membranes no FPE, (2) PrP (5 µM) binding to POPC/POPG membranes, pH 7 (no FPE), (3) initial fluorescence level of FPE incorporated into POPC/POPG membranes, pH 7. The dead time of the instrument was ~3 ms and the data that is shown from 1–3 ms was acquired prior to the mixing of the lipid and protein solutions. Data are displayed on a logarithmic timescale.

179

Table 6.2: Kinetic parameters for membrane binding of SHaPrP (90–231) with POPC/POPG membranes at pH 7 (70:30 molar ratio)[a]

[PrP] µM	k_1 (s^{-1})	A_1 (%)[b]	k_2 (s^{-1})	A_2 (%)[b]	A_{tot}[c]
2	56 ± 3	73	0.34 ± 0.08	27	0.30
3	81 ± 1	79	0.29 ± 0.03	21	0.75
5	78 ± 1	74	0.37 ± 0.02	26	0.95
7	65 ± 1	71	0.79 ± 0.03	29	1.40
10	71 ± 1	72	0.83 ± 0.03	28	1.44

[a]Rates (k_i) and amplitudes (A_i) were calculated from stopped-flow measurements at 20 °C using FPE-labelled membranes at a constant lipid concentration of 200 µM. [b]Fractional amplitude expressed as percentage of total observed amplitude (A_{tot}). [c]Total observed amplitude defined as $A_{tot} = |A_1| + |A_2|$.

concentration, however, no dependence was observed with the amplitude (A_2) (Table 6.2). This phase is probably associated with lipid rearrangement following the binding of PrP.

A reduction in the surface charge density of lipid membranes slowed the binding of PrP and in contrast with POPG membranes, no fluorescence decrease was detected following the initial increase, which would have suggested the insertion of PrP into lipid membranes. This result indicates that PrP remains at the membrane surface and that high negative surface charge density is required for the insertion event.

6.3.2 Calcein release

The ability of PrP to destabilise membranes was assessed using a dye release assay. The assay involves encapsulating calcein in lipid vesicles at a concentration where its fluorescence is self-quenched. A significant increase in the fluorescence intensity would occur upon the release of calcein into the surrounding medium. This approach has been widely used to characterise the membrane destabilisation induced by the binding of proteins and peptides (Defrise-Quertain *et al.*, 1989; Butko *et al.*, 1996; Vogt & Bechinger, 1999) and in the present study was used to investigate the membrane destabilising properties of SHaPrP (90–231).

The integrity of negatively charged membranes of POPG, zwitterionic membranes of POPC and raft-like membranes of DPPC/chol/SM (50:30:20, molar ratio) at pH 5 and 7 upon PrP binding was studied by following the release of calcein from these vesicles.

Binding of PrP to POPG membranes at pH 5 and 7 led to an increase in the fluorescence intensity, indicating that calcein was released from lipid vesicles. Figure 6.9 shows representative spectra of PrP binding to POPG loaded vesicles at pH 7. An increase in calcein fluorescence was detected with increasing concentrations of PrP. Figure 6.10 summarises the extent of calcein release from various lipid systems, as a fraction of total release upon detergent solubilisation of lipid vesicles. Binding of PrP to POPG membranes, at a lipid-protein ratio of 100:1 led to a total release of calcein from the lipid vesicles at pH 5 and 7. At equivalent lipid-protein ratios, only 25–30 % calcein was released from POPC membranes and no release was observed from the raft-like membranes of DPPC, cholesterol and sphingomyelin at pH 5 and 7. Furthermore, incubation of PrP with the raft-like membranes over a 12 h period did not lead to any release of calcein.

The kinetics of calcein release were monitored over a time scale up to 500 s after manually mixing loaded vesicles and PrP. Representative kinetic traces for POPG loaded vesicles at pH 5 and 7 are displayed in Figure 6.11 and kinetic parameters for all lipid systems studied are shown in Table 6.3. These measurements revealed that the release of calcein induced upon binding of PrP is very fast. With POPG membranes at pH 7, only a small fraction (< 20 %) of the total expected fluorescence change was observed (A_1, Table 6.3) and at pH 5 the release occurred within 24 ± 4 s *i.e.* during the deadtime of these measurement (A_0, Table 6.3). Release of calcein from POPC vesicles at pH 5 also occurred within the deadtime of these measurements, whilst 25 % of the expected fluorescence signal was observed after manually mixing POPC loaded vesicles at pH 7 with PrP.
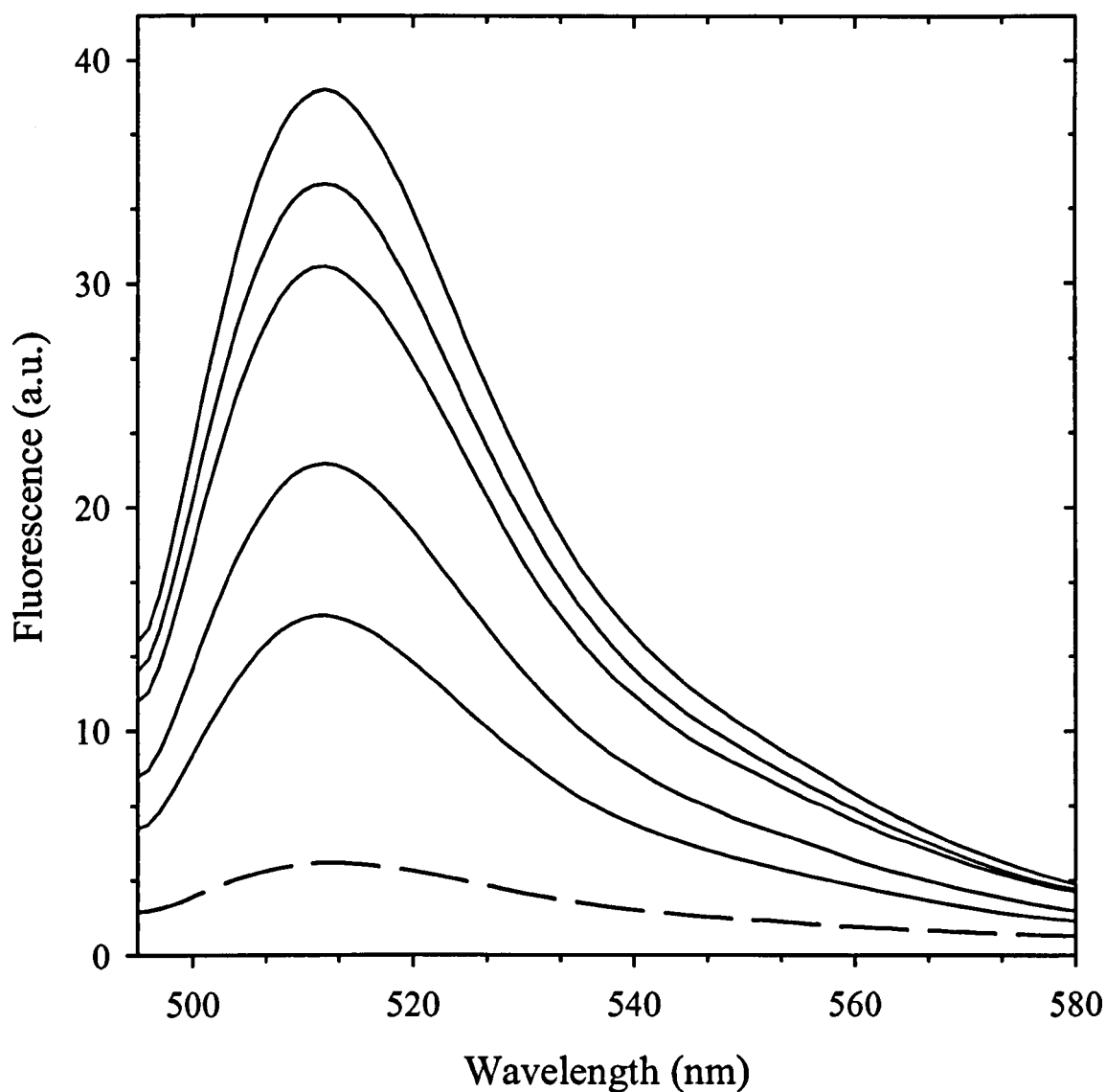
Figure 6.9: **Illustration of a series of fluorescence spectra of calcein release upon binding of SHaPrP (90–231).** Fluorescence spectrum of calcein loaded vesicles in the absence of PrP (dashed line) and with increasing concentration of PrP (solid line): 50, 100, 200, 250, 500 nM from bottom to top spectrum. The excitation wavelength was 490 nm and spectra were recorded at 20 °C.
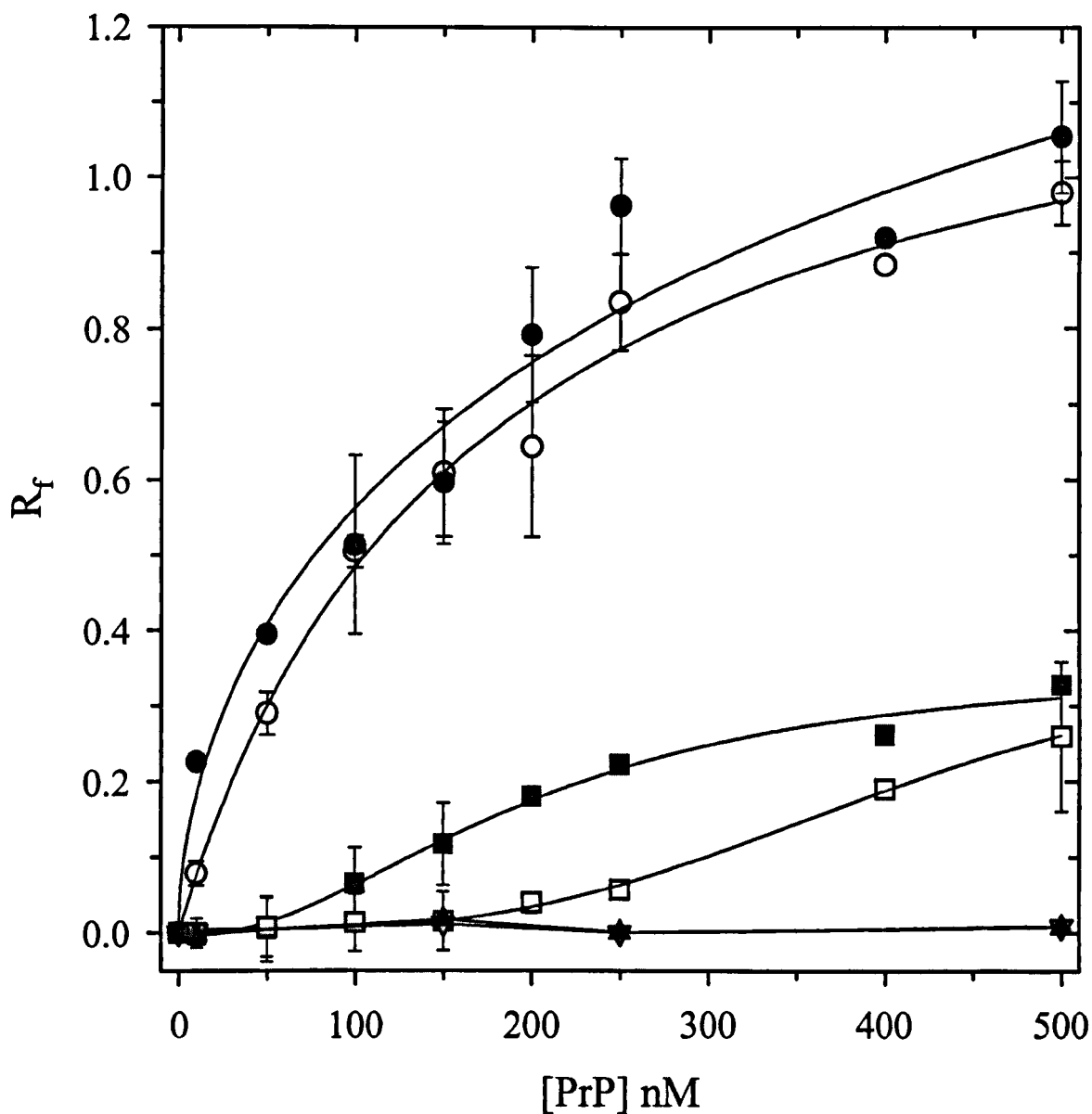
Figure 6.10: **Summary of the extent of PrP-induced release of calcein from various lipid membranes.** Calcein release is represented as a fraction of total release upon detergent solubilisation of vesicles for POPG (circles), POPC (squares) and raft-like membranes of DPPC/chol/SM (triangles) at pH 7 (open symbols) and pH 5 (solid symbols). Data points are the mean value of two measurements on separate samples and error bars show their standard deviations. Lines are for guidance only and have no theoretical significance.
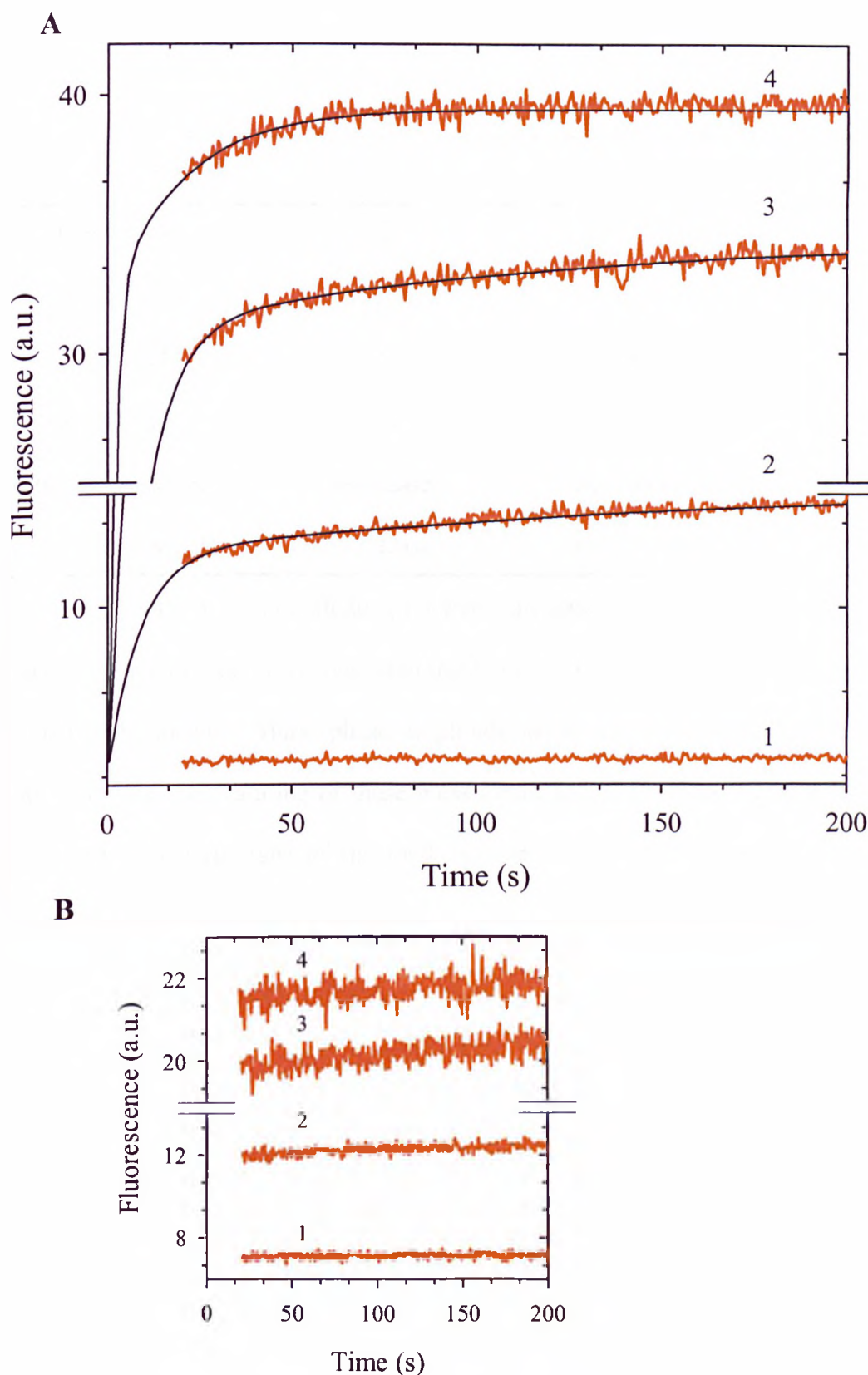
Figure 6.11: **Representative kinetic traces of PrP-induced release of calcein from POPG membranes.** (A) Release of calcein from POPG vesicles at pH 7 was measured by manually mixing protein in solution with POPG vesicles loaded with calcein (deadtime ~ 24 s). PrP concentrations were: (1) 0, (2) 50, (3) 250 and (4) 500 nM. (B) Equivalent measurements at pH 5. The experimental data is shown in red and the fits are in black.

Table 6.3: Kinetics of PrP-induced calcein release from lipid membranes[a]

Membrane System	$A_0 (\%)^b$	$t_1 (s)$	$A_1 (\%)$
POPG, pH 7	82	20–170	18
POPG, pH 5	100	___[c]	___[c]
POPC, pH 7	75	> 100	25
POPC, pH 5	100	___[c]	___[c]
DPPC/chol/SM, pH 7	no release	no release	no release
DPPC/chol/SM, pH 5	no release	no release	no release

[a]Time constant (t_1) and amplitudes (A_1) were calculated from the changes in calcein fluorescence emission with time after manually-mixing protein and lipid vesicles loaded with calcein. [b]Burst phase amplitude associated with an early release of calcein during the deadtime of these measurements, ~ 24 s, (see Figure 6.11) and expressed as a percentage of the total expected fluorescence signal. [c]Phase not observed.

In order to resolve the missing amplitudes of the manual mixing experiments stopped-flow fluorescence measurements were carried out. The drive pressure of the stopped-flow instrument was reduced to minimise any pressure-driven calcein release. Representative kinetics traces of calcein release from POPG membranes at pH 7, observed in stopped-flow measurements are shown in Figure 6.12. The traces were found to fit to the sum of 3 exponential phases and kinetic parameters are summarised in Table 6.4.

- *Fast phase:* This phase occurred at 335–700 ms with a rate (k_1) decreasing with protein concentration (3.0 s^{-1} at 150 nM PrP; 1.5 s^{-1} at 500 nM PrP, Table 6.4). The amplitude (A_1) associated with this phase increased with protein concentration (A_1 = 19 % for 150 nM PrP increasing to 36 % for 500 nM PrP, Table 6.4).

- *Intermediate phase:* This phase was observed over 2–4 s and 35 to 50 % of the total amplitude was associated with this phase. The rate (k_2) and amplitude (A_2) did not show a strong dependence on the protein concentration (Table 6.4).

- *Slow phase:* This phase occurred between 14–45 s and the rate and amplitude observed with this phase decreased with protein concentration (A_3 = 45 %, k_3 = 0.07 s^{-1} for 150 nM PrP decreasing to 27 % and 0.02 s^{-1}, respectively, at 500 nM PrP, Table 6.4).

The slow phase detected in the stopped-flow measurement corresponds to the phase observed in the manual-mixing experiments, more importantly the missing amplitude observed in the manual-mixing experiments was resolved and the fast release of calcein was found to be a biphasic process.
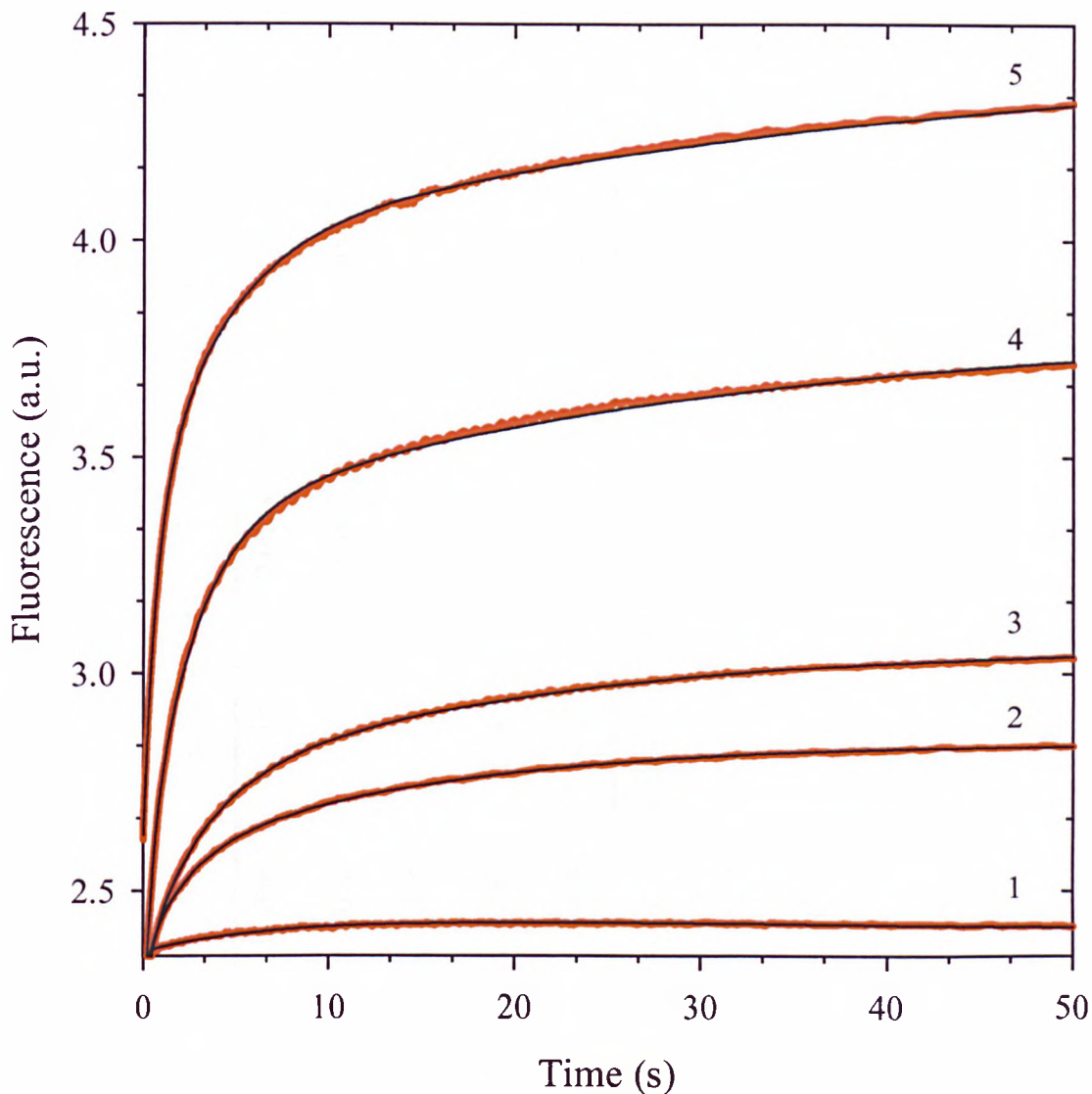
Figure 6.12: **Representative kinetic traces of PrP-induced release of calcein from POPG membranes at pH 7 monitored in stopped-flow measurements.** PrP concentrations were: (1) 50, (2) 150, (3) 200, (4) 250 and (5) 500 nM and lipid concentration was 50 μM. Fluorescence changes were detected above 515 nm and excitation wavelength of 490 nm (deadtime ~ 4.5 ms). Traces were fitted to the sum of three exponentials. The experimental data is shown in red and the fits are in black.

Table 6.4: Kinetic parameters for PrP-induced release of calcein from POPG membranes at pH 7[a]

[PrP] nm	k_1 (s^{-1})	A_1 (%)[b]	k_2 (s^{-1})	A_2 (%)[b]	K_3 (s^{-1})	A_2 (%)[b]	A_{tot}[c]
50	6.90 ± 0.02	14	0.155 ± 0.006	16	0.0013 ± 0.007	69	0.49
150	3.00 ± 0.01	19	0.437 ± 0.010	35	0.0685 ± 0.0007	45	0.62
200	2.90 ± 0.03	20	0.328 ± 0.004	41	0.0529 ± 0.0004	38	0.92
250	2.37 ± 0.04	24	0.381± 0.005	49	0.0334± 0.0004	27	1.71
500	1.46 ± 0.01	36	0.259 ± 0.004	39	0.0226± 0.0002	27	1.84

[a]Rates (k_i) and amplitudes (A_i) were calculated from stopped-flow measurements at 20 °C using POPG loaded vesicles at a constant lipid concentration of 50 μM. [b]Fractional amplitude expressed as percentage of total observed amplitude (A_{tot}). [c]Total observed amplitude defined as $A_{tot} = |A_1| + |A_2| + |A_3|$.

6.4 Discussion

Studies have demonstrated that peptide or protein binding to lipid membranes can alter the lipid bilayer integrity and/or permeability (White & Wimley, 1994). Lin *et al.* (1997) demonstrated that the binding of a synthetic peptide of PrP comprising residues 106–126 formed ion-permeable channels in lipid membranes and speculated that these channels may mediate cell death through changes in cellular ion homeostasis. In this chapter PrP binding and insertion kinetics into lipid bilayers is investigated by asymmetrically incorporating the fluorescent probe FPE onto the surface of lipid vesicles. The results were correlated with membrane destabilisation effects, measured by the release of a fluorescence dye from lipid vesicles.

Binding of changed peptides and proteins to lipid membranes causes changes of the electrostatic potential at the membrane surface. By locating a fluorescent probe such as FPE, which is sensitive to the membrane surface potential, it is possible to follow the binding and insertion of peptides and proteins into membranes in real time (Wall *et al.*, 1995).

Stopped-flow experiments in which PrP was rapidly mixed with negatively charged FPE-labelled membranes of POPG at pH 7, revealed three clearly resolved fluorescence kinetic phases. An enhancement of fluorescence was observed in the fast phase (3–6 ms, Figure 6.5A and Table 6.1) and the rates and amplitudes associated with this phase displayed a clear dependence on the protein concentration, consistent with an increased electropositive surface potential caused by the binding of positively charged PrP (Figure 6.7A,B and Table 6.1). The binding of PrP to negatively charged

membranes has been shown to be driven by electrostatic interactions between positively charged residues on the protein surface and negatively charged lipid headgroups on the membrane (Chapter 4). Most of the positive charged amino acids are clustered at the amino-terminus of PrP and this is the region that is most likely to bind to negatively charged membranes. The results from this study are consistent with this proposal, in which the positively charged amino-terminus binds to negatively charged membranes and brings the charged residues in close proximity to the membrane surface. This causes changes of the electrostatic potential at the membrane surface and leads to changes in the protonation state of FPE resulting in an increase in the fluorescence intensity of the probe.

The initial increase in fluorescence intensity was followed by a decrease, characterised by a time consistent of ~ 50 ms (Figure 6.5A and Table 6.1). The rate constants and amplitudes of this phase were found to be independent of protein concentration (Figure 6.7C, D and Table 6.1). This phase is assigned to the loss of a region of positive charged amino acids from the membrane surface, which in turn led to changes in the electrostatic potential at membrane surface and subsequently affected the protonation state of FPE resulting in a decrease in the fluorescence signal. This observation is consistent with the partial insertion of PrP into lipid membranes. This phase need not represent a transmembrane conformation of PrP and probably reports on the partial insertion of PrP into the lipid bilayer.

A slow phase associated with an increase in fluorescence was observed with a time constant of 2–17 s (Figure 6.5 and Table 6.1). The kinetic parameters associated with this phase displayed a dependence on PrP concentration. The amplitude decreases

with protein concentration and rate increases with PrP concentration (Figure 6.7 and Table 6.1). This phase might be associated with rearrangement of the lipid bilayer following the binding and insertion of PrP.

To examine the role of membrane surface charge density on the binding and insertion of PrP, the kinetics of PrP interaction with FPE-labelled membranes containing 30 % negative charged POPG lipids (POPC/POPG, 70:30 molar ratio), at pH 7 was investigated. FPE-detected kinetics shows two kinetic events: A fast phase of increasing FPE fluorescence associated with the binding of PrP to POPC/POPG membranes. The result shows that the binding of PrP to POPC/POPG membranes was slower compared to POPG membranes. For POPC/POPG membranes binding occurred over 12–18 ms compared to 3–6 ms for POPG bilayers (Table 6.1 & 6.2). Further both the rate (k_1) and amplitude (A_1) associated with this phase were independent of PrP concentration, which suggests that the negatively charged lipid binding sites on the membrane surface were saturated at the lowest protein concentration (2 µM) and increase in the PrP concentration resulted in no further binding. In contrast, with POPG membranes the insertion phase, which is associated with a decrease in the fluorescence signal of FPE following the initial increase, was not observed. A slow phase of further increase in the fluorescence intensity that occurs over 1–3 s was detected (Figure 6.8 and Table 6.2), and is probably due lipid rearrangement around PrP.

Changes in membrane integrity and/or permeability following the binding of PrP were investigated by monitoring the release of the fluorescent dye (calcein) from lipid vesicles. In this technique lipid vesicles were prepared containing calcein at a high

enough concentration at which its fluorescence was self-quenched (60 mM). Release of the dye resulted in an increase in the fluorescence signal of calcein caused by the dilution of the dye and a consequent relief of self-quenching. The results from the calcein release assay showed that binding of PrP to negatively charged membranes of POPG at pH 5 and 7 led to total release of calcein from loaded vesicles, indicating a strong destabilization of the lipid bilayer (Figure 6.10). Studies with peptides and proteins have demonstrated that binding to lipid membranes can alter the bilayer integrity by two mechanisms. The first involves the insertion of peptides and proteins into the bilayer and the formation of pores, which perturbs the lipid membrane and destabilises the lipid bilayer organisation (Matsuzaki *et al.*, 1994; Tejuca *et al.*, 1996). The second perturbs the membrane in a detergent-like manner (Butko *et al.*, 1996; Vogt & Bechinger, 1999). The precise mechanism of PrP-induced membrane destabilisation is not known, however the FPE kinetics, showed evidence for partial insertion of PrP into negatively charged lipid membranes.

Under the same experimental conditions PrP did not induce the release of calcein from raft-like mixed membranes composed of DPPC, cholesterol and sphingomyelin at pH 5 and 7 (Figure 6.10) and this observation remained unaltered over a 12 h period. This result indicates that the binding of PrP to raft-like membranes of DPPC/chol/SM does not destabilise the lipid bilayer. Surprisingly, PrP induced the release of 25–30 % of calcein from POPC membranes (Figure 6.10). The Trp fluorescence binding data presented in Chapter 4 suggests that PrP has a weak affinity for POPC membranes. The result from the destabilisation study with POPC membranes does not contradict this finding and may reflect the difference in the sensitivity of the two methods used, with

the calcein release assay being more sensitive in detecting PrP-POPC interactions than shifts in the λ_{max} of PrP (Chapter 4).

The kinetics of calcein release were investigated and stopped-flow measurements revealed that the kinetics were more complex than originally expected (Figure 6.12 & Table 6.4). The release of calcein from negatively charged POPG membranes showed three main kinetic phases associated with an increase of fluorescence (Table 6.4): (1) a fast phase occurring at 335–700 ms, (2) an intermediate phase with a time constant of 2–4 s and (3) a slow phase occurring over 14–45 s.

Combining the FPE kinetics and the results from the calcein release experiments, a proposed mechanism for the interaction of PrP with negatively charged membranes of POPG at pH 5 and 7 is illustrated in Figure 6.13A. In this scheme, subscript W represents protein in an aqueous environment, a subscript S indicates a membrane surface associated state and a state inserted in lipid membranes is labelled with a subscript M. PrP_W has the reported solution structure as determined by NMR (James *et al.*, 1997) and PrP_S is likely to have an altered conformation on association with lipid membranes. PrP_M inserts into the hydrophobic core of the lipid bilayer and results in membrane destabilisation. Binding of PrP to the surface of negatively charged membranes ($PrP_W \rightarrow PrP_S$) is most likely to be diffusion-controlled and driven largely by favourable electrostatic interactions between positive residues on the protein and the negative charged lipid headgroups.

A

$$\text{PrP}_W \xrightarrow{\text{POPG}} \rightleftharpoons \text{PrP}_S \rightleftharpoons \text{PrP}_M$$

B

$$\text{PrP}_W \xrightarrow{\text{DPPC/chol/SM}} \rightleftharpoons \text{PrP}_S$$
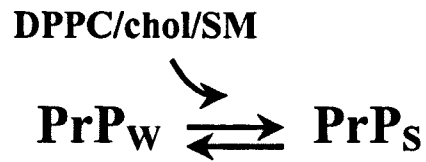
Figure 6.13: **Proposed kinetic model for the interaction of SHaPrP (90–231) with lipid membranes.** (A) Interaction of PrP with negatively charged membranes of POPG at pH 5 and 7 and (B) with raft-like membranes composed of DPPC, cholesterol and sphingomyelin at pH 7. PrP_W represents the protein in aqueous solution, PrP_S indicates a state associated with membrane surface and PrP_M denotes a membrane-inserted state.

After binding to the membrane surface the protein partially inserts into the lipid bilayer ($PrP_S \rightarrow PrP_M$). Insertion of PrP into lipid membrane is most likely to be responsible for the destabilision of the lipid bilayer, leading to the release of calcein from POPG vesicles.

A model for the interaction of PrP with the raft-like membranes composed of DPPC, cholesterol and sphingomyelin is also shown in Figure 6.13B. Although no FPE kinetic data is available for this membrane system due to difficulty in labelling the membranes, the calcein release, Trp fluorescence binding and Trp quenching data presented in Chapter 4, supports the interpretation that the protein is likely to remain at the membrane surface. This surface associated state does not lead to the destabilisation of the lipid bilayer.

6.5   Conclusions

The results presented in this chapter suggests that binding of PrP to negatively charged membranes causes perturbation of the lipid bilayer, which results in total release of the vesicle contents. The results do not elucidate on the molecular mechanism of PrP-induced destabilisation. However, the FPE kinetics shows evidence for partial insertion of PrP into POPG membranes. In contrast, PrP did not induce the release of calcein from raft-like mixed lipid membranes, which suggest that the binding of PrP does not alter the integrity of these membranes.

196

Chapter 7: General Discussion and Conclusions

7.1 Binding of PrP to Lipid Membranes Induces Protein Structural Changes and can Alter the Bilayer Integrity

PrP in living cells is GPI anchored to raft domains that are rich in cholesterol and sphingolipids on the exoplasmic side of the membrane (Vey *et al.*, 1996; Naslavsky *et al.*, 1997). Previous studies have shown that the lipid environment of PrP may play an important role in the degradation of PrP^C and also in the formation of PrP^{Sc} (Taraboulos *et al.*, 1995; Vey *et al.*, 1996; Naslavsky *et al.*, 1997). Evidence from scrapie-infected cells in culture indicated a direct interaction of PrP^{Sc} with the plasma membrane, other than *via* its GPI anchor (Stahl *et al.*, 1990; Safar *et al.*, 1991; Lehmann & Harris, 1995). In addition the plasma membrane has been proposed as a cellular site for the conversion of PrP^C to PrP^{Sc} (Taraboulos *et al.*, 1995; Naslavsky *et al.*, 1997). This has led to suggestions that membrane-PrP interactions could be involved in the conversion of the α-helical conformation of PrP to the aggregated β-sheet rich structure. However, very few studies have investigated the biophysical properties of membrane-associated PrP. In the current study the structural properties of membrane associated Syrian hamster prion protein (SHaPrP) comprising residues 90–231 is investigated.

Binding of PrP in an α-helical conformation resembling PrP^C, to various model membrane systems was studied at pH 7 to represent the pH surrounding the plasma membrane and pH 5 to model the acidic environment of endosomes. Evidence implicates endocytic organelles (Borchelt *et al.*, 1992; Arnold *et al.*, 1995) and the plasma membrane (Vey *et al.*, 1996; Naslavsky et al., 1997) as sites for PrP^{Sc} formation, but it is unclear which provides a more favourable environment for

conversion. The two tryptophan residues present at positions 99 and 145 in SHaPrP (90–231) were used as intrinsic fluorescence probes to monitor the binding of PrP to model lipid membranes. The Trp fluorescence results presented in Chapter 4 shows that PrP binds to gel-phase zwitterionic membranes of DPPC and raft-like membranes composed of DPPC, cholesterol and sphingomyelin at pH 7. The interaction of PrP with raft-like membranes was driven by predominantly hydrophobic lipid-protein interactions. Binding of PrP to raft-like membranes led to an intermediate protection to acrylamide quenching (Chapter 4). This result together with the shift in the fluorescence of PrP suggests that in these membranes PrP is likely to be surface associated.

The binding of PrP to raft-like membranes at pH 7 suggest that in addition to the carboxyl-terminal linked GPI anchor, direct interactions between the polypeptide chain of PrP and lipid membranes may be involved in membrane attachment of PrP to the cell surface. In contrast, no significant binding of PrP to raft-like membranes at pH 5 and liquid-crystalline zwitterionic membranes of DOPC or POPC, nor their mixtures with cholesterol and sphingomyelin at pH 7 and 5 was observed. These results suggest that PrP has a preference for gel-phase zwitterionic membranes and raft-like membranes at pH 7.

Far-UV CD and ATR FTIR spectroscopy revealed that an increase in the α-helical structure of PrP accompanied the interaction of PrP with raft-like membranes (Chapter 5). No visible signs of PrP aggregation were detected from the electron micrographs of PrP with the raft-like membranes (Chapter 6). These finding are consistent with the interpretation of the CD and FTIR results, which shows an increase in the α-helical structure of PrP and no evidence of aggregated β-sheet

structure. The calcein release data presented in Chapter 6 suggests that the binding of PrP to raft-like membranes did not destabilise the lipid bilayer, thus supporting a proposal where PrP is surface associated to raft-like membranes. These results taken together suggest that for the preferred localisation of PrP in raft domains within the plasma membrane hydrophobic lipid-protein interactions induce the formation of stable α-helical structure in PrP. This state rich in α-helical structure is likely to be surface associated and as a result does not affect the integrity of the lipid bilayer.

The Trp fluorescence binding and acrylamide quenching data (Chapter 4) shows that PrP binds to negatively charged lipid membranes of POPG at both pH 7 and 5. The interaction of PrP with lipid bilayers composed of negatively charged lipids was shown to be driven by electrostatic interactions between positively charged residues on the protein surface and negatively charged lipid headgroups. Inspection of the surface electrostatic potential of the structure of SHaPrP (90–231) revealed that most of the positive charges are clustered at the unstructured amino-terminus (Chapter 4). This region is therefore most likely to participate in the interaction with negatively charged membranes. The high degree of protection from acrylamide quenching, the large shifts in the fluorescence of PrP and the resistance of PrP to be released from negatively charged membranes by salt provided evidence for hydrophobic lipid-protein interactions following the initial charge driven association. Therefore, binding of PrP to the surface of negatively charged membranes appears to result in structural changes in the protein, which in turn lead to the exposure of hydrophobic residues that partially insert into the hydrophobic domain of the lipid bilayer. Further evidence for the partial insertion of PrP into POPG membranes was provided by FPE-detected kinetics (Chapter 6). In addition, the larger shift in the fluorescence of PrP and high degree of protection to

acrylamide quenching (Chapter 4) suggest that PrP in POPG membranes at pH 5 is more deeply inserted than at pH 7. Binding of PrP to POPG membranes at pH 5 and 7 led to total release of calcein from loaded vesicles, which indicates that the binding and the partial insertion of PrP into POPG membranes strongly destabilises the lipid bilayer structure.

Far-UV CD and ATR FTIR spectroscopy (Chapter 5) revealed that the interaction of PrP with negatively charged membranes was accompanied by an increase in both α-helical and β-sheet structure compared to the NMR structure of SHaPrP (90–231) in solution (James *et al.*, 1997). Furthermore the low-frequency of the β-sheet component detected during the FTIR experiments suggest that PrP was in an aggregated state when bound to negatively charged membranes. Electron microscopy revealed protein aggregation around the lipid vesicles. This observation is consistent with the interpretation of the CD and ATR FTIR data, which shows an increase in aggregated β-sheet structure of PrP. The results presented in this thesis suggest that the binding of PrP to negatively charged membranes driven by electrostatic lipid-protein interactions promotes the formation of aggregated β-sheet structure in PrP. This state in partially inserted into the hydrophobic domain of the lipid bilayer and leads to membrane destabilisation.

Equilibrium intermediates showing spectral characteristics of β-sheet proteins have been detected at acidic pH's during guanidine hydrochloride- and urea-induced unfolding transitions of various recombinant prion proteins (Swietnicki *et al.*, 1997; Zhang *et al.*, 1997; Hornemann & Glockshuber, 1998; Jackson *et al.*, 1999*a,b*). The results presented in this thesis also demonstrate the induction of β-sheet structure in PrP upon binding to negatively charged membranes. These

structural changes are likely to result from electrostatic interactions with the negatively charged lipid headgroups of POPG. In addition, the accumulation of protons near the negatively charged lipid headgroups has been shown to result in a lower local pH near the membrane surface compared to the bulk pH (Prats *et al.*, 1986). This could also contribute to the observed protein structural changes, as seen in the refolding/unfolding of PrP in solution at acidic pH.

The increase in β-sheet structure of PrP is also consistent with a previous study in which the binding of peptide spanning residues 106–126 of human PrP to negatively charged membranes was investigated. Binding of this peptide was shown to be accompanied by a structural transition from a random coil in solution to β-sheet structure when bound to negatively charged membranes (De Gioia *et al.*, 1994). The recent NMR structure of human PrP shows amino acids 106 to126 to lie within the unstructured amino-terminus of PrP (Zahn *et al.*, 2000) and the above finding suggests that this region is folded upon binding to membranes. This observation implies that the additional structure of SHaPrP (90–231) observed during the binding to lipid membranes is likely to arise from the folding of the unstructured amino-terminus.

7.2   *Biological Implications*

TSE diseases are a group of human and animal neurodegenerative disorders, in which the central pathogenic event, is the post-translational conversion of the normal cellular α-helical form of a host protein, prion protein (PrP^C) into an abnormal disease-causing β-sheet form, PrP^{Sc}. In the brains of most humans and animals that have died of TSE diseases, amyloid plaques containing PrP^{Sc} are

detected. The accumulation of an abnormal β-sheet protein is also associated with a number of other neurodegenerative disorders such as amyloid β-protein (Aβ) in Alzheimer's disease, islet-associated polypeptide (IAPP) in type II diabetes, α-synuclein in Parkinson's disease and huntingtin in Huntington's disease (review Rochet & Lansbury, 2000). Therefore information of the various events that lead to the formation of β-sheet aggregates from otherwise soluble proteins is essential not only in TSE diseases but may also help our understanding of processes that facilitate the development of other neurodegenerative disorders.

TSE diseases can be sporadic, inherited, or infectious disorders. The cause of sporadic forms of the disease is unknown; hypotheses include somatic mutation of the PrP gene and spontaneous conversion of wild type PrP^{C} to PrP^{Sc}. To date, 20 different mutations in the human PrP gene have been linked with inherited prion diseases (Prusiner, 1998). The molecular event that facilitates the spontaneous conversion of wild type and mutant PrP^{C} to the infectious isoform is not known. Thermodynamic studies of recombinant PrP containing disease related mutations indicated that inherited prion diseases cannot be rationalised by a lowered stability of PrP^{C} (Swietnicki *et al.*, 1998; Liemann & Glockshuber, 1999). An aberrant association of PrP^{C} containing specific point mutations, with cellular membranes has been proposed as an alternative hypothesis to explain spontaneous development of prions in inherited diseases.

The results presented here show that PrP binds to membranes, which resembles the lipid composition of rafts in the plasma membrane, where PrP is localised. The interaction appears to favour the folding of the unstructured amino-terminus of PrP, resulting in a protein with a higher content of α-helical structure

compared with the reported NMR structure in solution (James *et al.*, 1997). This α-helical rich state of PrP when bound to raft-like membranes did not alter the integrity of the lipid bilayer structure. No evidence of PrP aggregation when bound to the raft-like membranes at pH 7 was detected from the electron micrographs. The results suggest that the direct interaction of PrP with rafts domains would have the advantage of stabilizing an α-helical conformation of PrP without destabilising the plasma membrane.

Interestingly, no binding was detected for PrP with the raft-like membranes of DPPC/chol/SM membranes at pH 5. This observation may reflect the behaviour of PrP[C] following internalisation into the cell. Cell surface proteins and lipids first appear in early endosomes following re-entry into the cell (Gruenberg & Maxfield, 1995). The overall lipid composition of the early endosomes is similar to that of the plasma membrane (Van Meer, 1989). The low pH of the endosomes has been shown to cause the dissociation of protein ligands from their receptors. This may also be advantageous for the degradation of PrP in that it remains in solution and does not bind to the lipid rafts, which would facilitate the release of the protein from the membrane surface in readiness for proteolytic degradation.

At present, the molecular events that initiate PrP[Sc] aggregation are still unknown; however evidence suggests that the cellular membranes are involved in this process. The association of scrapie infectivity with membranes was emphasized early on in TSE research (reviewed in Prusiner, 1989). Studies of scrapie infected brains have demonstrated that the highest titers of infectious PrP[Sc] are associated with membrane fractions (Safar *et al.*, 1990). Furthermore aggregates of PrP 27–30, which are formed during the purification of scrapie prions were found to retain

infectivity when incorporated into detergent-lipid-protein complexes as well as liposomes and a significant increase in infectivity was also observed (Gabizon *et al.*, 1988*a,b*). Electron micrographs presented in this study revealed that negatively charged lipids at both pH 7 and 5 induced PrP aggregation, while no visual signs of protein aggregation was detected with the raft-like membranes at pH 7.

The plasma membrane of most cells typically contains an outer surface that is rich in cholesterol, sphingomyelin and zwitterionic PC glycerophospholipids. In contrast the inner surface contains negatively charged glycerophospholipids (van Meer, 1989). Under normal circumstances PrP is localised in lipid-rafts in the external leaflet of the plasma membrane and this environment appears to protect the protein from aggregation. The results presented in this thesis also show that binding of PrP to raft-like lipid membranes favours an α-helical conformation. However, during the internatisation of PrP^C either for degradation or recycling back to the plasma membrane, PrP^C may be exposed to negatively charged domains of cell membranes and this change in the lipid environment may trigger a conformational change in PrP^C, resulting in an increased β-sheet structure and protein aggregation. The results presented in this thesis show that the electrostatic interactions between PrP and negatively charged lipids promote the formation of aggregated β-sheet structures of PrP. Cellular membranes have also been proposed to play a role in the development of Parkinson's disease (Jo *et al.*, 2000) and Alzheimer's disease (McLaurin *et al.*, 1998). Lipid membranes have been shown to induce the formation of β-sheet structure in Aβ protein and the hydrophobic surface of membranes has been proposed to facilitate the polymerisation of Aβ in the development of Alzheimers disease.

The precise mechanism of PrP-induced cell death remains unclear. *In vitro* studies have demonstrated that PrP is neurotoxic to cultured neurons (Forloni *et al.*, 1993; Brown *et al.*, 1996). Various hypotheses have been postulated to explain neuronal cell death. These include increased oxidative stress as a result of depleted levels of PrP^C (Brown *et al.*, 1997*b*). Others have proposed a mechanism for prion neurotoxicity through a direct perturbation of the plasma membrane of nerve cells as a consequence of PrP^{Sc} accumulation (Pillot *et al.*, 1997; Lin *et al.*, 1997). Several studies have also proposed neurotoxicity in Alzheimer's and Parkinson's disease to be mediated by a direct interaction of Aβ (McLaurin *et al.*, 1996; Pillot *et al.*, 1996; Koppaka & Axelsen, 2000) and α-synuclein (Jo *et al.*, 2000) respectively with lipid membrane.

The binding of a synthetic peptide of PrP comprising residues 106–126 has been demonstrated to form ion permeable channels in the lipid bilayer and these channels have been speculated to mediate cell death through changes in cellular ion homeostasis (Lin *et al.*, 1997). The results presented here show that PrP in lipid rafts acquires a higher α-helical content and this membrane-associated state does not induce membrane destabilisation. However, the interaction of PrP with negatively charged membranes led to an increase in β-sheet structure, compared to the NMR structure in solution (James *et al.*, 1997). This membrane state of PrP was found to destabilise the bilayer structure of membranes, therefore the segregation of PrP to negatively charged membrane domains could potentially lead to leakage of cell contents and would eventually cause cell death. The findings presented here support previous studies that propose a mechanism for neurotoxicity through a direct interaction of PrP^{Sc} and/or PrP intermediates with neuronal membranes.

The PrP-lipid interactions and the formation of β-sheet structure may partially explain some of the pathological finding reported for prion diseases. The simplest implication would be that PrP surface binding to negatively charged lipids may explain the association of PrP^{Sc} plaques with neuronal and microglial membranes that are sometimes detected in the brains of humans and animals.

7.3 In Summary

The results presented in this thesis show that interaction of PrP with lipid membranes falls into two categories:

(1) Binding of PrP to raft-like membranes of DPPC/chol/SM at pH 7 is driven by hydrophobic lipid-protein interactions, which promotes the formation of stable α-helical structure in PrP. No signs of PrP aggregation were detected from the electron micrographs of PrP with the raft-like membranes. The intermediate protection from acrylamide quenching and the shift in PrP fluorescence suggest that this state richer in α-helical structure is likely to be surface associated and as a result does not lead to membrane destabilisation, as monitored by calcein release.

(2) Binding of PrP to negatively charged membranes is driven by electrostatic lipid-protein interactions, which induces the formation of aggregated β-sheet structure in PrP. Extensive aggregation of PrP was evident from the electron micrographs of PrP with negatively charged membranes. Additional hydrophobic lipid-protein interactions take place after the initial charge driven binding. The high degree of protection to acrylamide quenching, large shifts in the fluorescence of PrP and the insertion phase detected in FPE kinetics point to the partial insertion of PrP into the hydrophobic core of the lipid bilayer. Calcein release data suggests that this membrane-inserted state induce a strong destabilisation of the lipid bilayer structure.

References

Agranoff, B. W. and Hajra, A. K. (1994). Lipids. In *Basic neurochemistry*, 5th edn, pp. 97–116. Edited by Siegel, G. J. Agranoff, B. W., Albers, R. W. and Molinoff, P. B. New York, Raven press Ltd.

Arbuzova, A., Murray, D. and McLaughlin, S. (1998). MARCKS, membranes, and calmodulin: kinetics of their interaction. *Biochimica et Biophysica Acta* **1376**, 369–379.

Arnold, J. E., Tipler, C., Laszlo, L., Hope, J., London, M. and Mayer, R. J. (1995). Abnormal isoform of the prion protein accumulates in late endosome-like organelles in scrapie-infected mouse brain. *J. Pathol.* **176**, 403–411.

Baldwin, M. A., Cohen, F. E. and Prusiner, S. B. (1995). Prion protein isoforms, a convergence of biological and structural investigations. *J. Biol. Chem.* **270**, 19197-19200.

Bandekar, J. (1992). Amide modes and protein conformation. *Biochimica et Biophysica Acta* **1120**, 121–143.

Basler, K., Oesch, B., Scott, M., Westaway, D., Wälchli, M., Groth, D. F., McKinley, M. P., Prusiner, S. B. and Weissman, C. (1986). Scrapie and cellular PrP isoforms are encoded by the same chromosomal gene. *Cell* **46**, 417-428.

Bessen, R. A. and Marsh, R. F. (1994). Distinct PrP properties suggest the molecular basis of strain variation in transmissible mink encephalopathy. *J. Virol.* **68**, 7859–7868.

Bessen, R. A., Kocisko, D. A., Raymond, G. J., Nandan, S, Lansbury, P. T. and Caughey, B. (1995). Non-genetic propagation of strain-specific properties of scrapie prion protein. *Nature* **375**, 698–700.

Borchelt, D. R., Scott, M., Taraboulos, A., Stahl, N. and Pruisner, S. B. (1990). Scrapie and cellular prion proteins differ in their kinetics of synthesis and topology in cultured cells. *J. Cell Biol.* **110**, 743–752.

Borchelt, D. R., Taraboulos, A. and Prusiner, S. B. (1992). Evidence for synthesis of scrapie prion proteins in the endocytic pathway. *J. Biol. Chem.* **267**, 16188–16199.

Brown, D. A. and London, E. (1998). Functions of lipid rafts in biological membranes. *Annu. Rev. Cell Dev. Biol.* **14**, 111–136.

Brown, D. R., Qin, K., Herms, J. W., Madlung, A., Manson, J., Strome, R., Fraser, P. E., Kruck, T., von Bohlen, A., Schulz-Schaeffer, W., Giese, A., Westaway, D. and Kretzschmar, H. (1997*a*). The cellular prion protein binds copper *in vivo*. *Nature* **390**, 684–687.

Brown, D. A. and Rose, J. K. (1992). Sorting of GPI-anchored proteins to glycolipid-enriched membrane subdomains during transport to the apical cell surface. *Cell* **68**, 533–544.

Brown, D. R., Schmidt, B. and Kretzschmar, H. A. (1996). Role of microglia and host prion protein in neurotoxicity of a prion protein fragment. *Nature* **380**, 345–347.

Brown, D. R., Schulz-Schaeffer, W, J., Schmidt, B. and Kretzschmar, H. A. (1997*b*). Prion protein-deficient cells show altered response to oxidative stress due to decreased SOD-1 activity. *Exp. Neurol.* **146**, 104–112.

Bruce, M. E., Will, R. G., Ironside, J. W., McConnell, I., Drummond, D., Suttie, A., McCardle, L., Chree, A., Hope, J., Birkett, C., Cousens, S., Fraser, H. and Bostock, C. J. (1997). Transmissions to mice indicate that 'new variant' CJD is caused by the BSE agent. *Natue* **389**, 498–501.

Bryson, E. A., Rankin, S. E., Goormaghtigh, E., Ruysschaert, J.-M., Watts, A. and Pinheiro, T. J. T. (2000). Structure and dynamics of lipid-associated states of apocytochrome *c. Eur. J. Biochem.* **267**, 1390–1396.

Büeler, H., Fischer, M., Lang, Y., Bluethmann, H., Lipp, H.-P., DeArmond, S. J., Prusiner, S. B., Aguet, M. and Weissmann, C. (1992). Normal development and behaviour of mice lacking the neuronal cell-surface PrP protein. *Nature* **356**, 557–582.

Büeler, H., Aguzzi, A., Sailer, A., Greiner, R.-A., Autenried, P., Aguet, M. and Weissmann, C. (1993). Mice devoid of PrP are resistant to scrapie. *Cell* **73**, 1339–1347.

Butko, P., Huang, F., Pusztai-Carey, M. and Surewicz, W. K. (1996). Membrane permeabilization induced by cytolytic δ-endotoxin cytA from *Bacillus thuringiensis* var. *israelensis*. *Biochemistry* **35**, 11355–11360.

Cabiaux, V., Brasseur, R., Wattiez, R., Falmagne, P., Ruysschaert, J.-M. and Goormaghtigh, E. (1989). Secondary structure of diphtheria toxin and its fragments interacting with acidic liposomes studied by polarised infrared spectroscopy. *J. Biol. Chem.* **264**, 4928–4938.

Carlson, G. A., Ebeling, C., Yang, S.-L., Telling, G., Torchia, M., Groth, D., Westaway, D., DeArmond, S. J. and Prusiner, S. B. (1994). Prion isolated specified allotypic interactions between the cellular and scrapie prion proteins in congenic and transgenic mice. *Proc. Natl. Acad. Sci. USA* **91**, 5690–5694.

Caughey, B., Race, R. E., Ernst, D., Buchmeier, M. J. and Chesebro, B. (1989). Prion protein (PrP) biosynthesis in scrapie-infected and uninfected neuroblastoma cells. *J. Virol.* **63**, 175–181.

Caughey, B. (1991). Cellular metabolism of normal and scrapie-associated forms of PrP. *Sem. Virology* **2**, 189–196.

Caughey, B., Dong, A., Bhat, K. S., Ernst, D., Hayes, S. F. and Caughey, W. S. (1991). Secondary structure analysis of the scrapie-associated protein PrP 27–30 in water by infrared spectroscopy. *Biochemistry* **30**, 7672–7680.

Caughey, B. and Raymond, G. J. (1991). The scrapie-associated form of PrP is made from a cell surface precursor that is both protease- and phospholipase-sensitive. *J. Biol. Chem.* **266**, 18217–18223.

Chang, C. N., Rey, M., Bochner, B., Heyneker, H. and Gray, G. (1987). High-level secretion of human growth hormone by Escherichia coli. *Gene* **55**, 189-196.

Chesebro, B., Race, R., Wehrly, K., Nishio, J., Bloom, M., Lechner, D., Bergstrom, S., Robbins, K., Mayer, L., Keith, J. M., Garon, C. and Haase, A. (1985). Identification of scrapie prion protein-specific mRNA in scrapie-infected and uninfected brain. *Nature* **315**, 331–333.

Cladera, J., Martin, I., Ruysschaert, J.-M. and O'Shea, P. (1999). Characterisation of the sequence of interactions of the fusion domain of simian immunodeficiency virus with membranes. *J. Biol. Chem.* **274**, 29951–29959.

Collinge, J., Whittington, M. A., Sidle, K. C. L., Smith, C. J., Palmer, M. S., Clarke, A. R. and Jefferys, J. G. R. (1994). Prion protein is necessary for normal synaptic function. *Nature* **370**, 295–297.

DeArmond, S. J., Mobley, W. C., DeMott, D. L., Barry, R. A., Beckstead, J. H. and Prusiner, S. B. (1987). Changes in the localisation of brain prion proteins during scrapie infection. *Neurology* **37**, 1271–1280.

DeArmond, S. J. and Prusiner, S. B. (1995). Etiology and pathogenesis of prion diseases. *Am. J. Pathol.* **146**, 785–811.

Deber, C. M. and Goto, N. K. (1996). Folding proteins into membranes. *Nat. Struct. Biol.* **3**, 815–818.

Defrise-Quertain, F., Cabiuax, V., Vandenbranden, M., Wattiez, R., Falmagne, P. and Ruysschaert, J.-M. (1989). pH-dependent bilayer destabilization and fusion of phospholipidic large unilamellar vesicles induced by diphtheria toxin and its fragments A and B. *Biochemistry* **28**, 3406–3413.

De Gioia, L., Selvaggini, C., Ghibaudi, E., Diomede, L., Bugiani, O., Forloni, G., Tagliavini, F. and Salmona, M. (1994). Conformational polymorphism of the amyloidogenic and neurotoxic peptide homologous to residues 106–126 of the prion protein. *J. Biol. Chem.* **269**, 7859–7862.

Donne, D. G., Viles, J. H., Groth, D., Mehlhorn, I., James, T. L., Cohen, F. E., Prusiner, S. B., Wright, P. E. and Dyson, H. J. (1997). Structure of the

recombinant full-length hamster prion protein PrP (29–231): The N terminus is highly flexible. *Proc. Natl. Acad. Sci. USA* **94**, 13452–13457.

Endo, T., Groth, D., Prusiner, S. B. and Kobata, A. (1989). Diversity of oligosaccharide structures linked to asparagines of the scrapie prion protein. *Biochemistry* **28**, 8380–8388.

Epand, R. (1998). Lipid polymorphism and protein-lipid interaction. *Biochimica et Biophysica Acta* **1376**, 353–368.

Ferguson, M. A. J. and Williams, A. F. (1988). Cell-surface anchoring of proteins via glycosylphosphatidylinositol structures. *Ann. Rev. Biochem.* **57**, 285–320.

Forloni, G., Angeretti, N., Chiesa, R., Monzani, E., Salmona, M., Bugiani, O. and Tagliavini, F. (1993). Neurotoxicity of a prion protein fragment. *Nature* **362**, 543-546.

Friedrichson, T. and Kurzchalia, T. V. (1998). Microdomains of GPI-anchored proteins in living cells revealed by crosslinking. *Nature* **394**, 802–805.

Fringeli, U. P. and Günthard, H. H. (1981). Infrared membrane spectroscopy. *Mol. Biol. Biochem. Biophys.* **31**, 270–332.

Gabizon, R., McKinley, M. P., Groth, D. F., Kenaga, L. and Prusiner, S. B. (1988a). Properties of scrapie prion protein liposomes. *J. Biol. Chem.* **263**, 4950–4955.

Gabizon, R., McKinley, M. P., Groth, D. F. and Prusiner, S. B. (1988b). Immunoaffinity purification and neutralisation of scrapie prion infectivity. *Proc. Natl. Acad. Sci. USA* **85**, 6617–6621.

García, F. L., Zahn, R., Riek, R. and Wuthrich, K. (2000). NMR structure of the bovine prion protein. *Proc. Natl. Acad. Sci. USA* **97**, 8334-8339.

Gasset, M., Baldwin, M. A., Fletterick, R. J. and Prusiner, S. B. (1993). Perturbation of the secondary structure of the scrapie prion protein under conditions that alter infectivity. *Proc. Natl. Acad. Sci. USA* **90**, 1–5.

Gill, S. C. and von Hippel, P. H. (1989). Calculation of protein extinction coefficients from amino acid sequence data. *Anal. Biochem.* **182**, 319-326.

Glover, J. R., Kowal, A. S., Schirmer, E. C., Patino, M. M., Liu, J.-J. and Lindquist, S. (1997). Self-seeded fibers formed by Sup35, the protein determinant of [*PSI*⁺], a heritable prion-like factor of S.cerevisiae. *Cell* **89**, 811–819.

Golding, C., Senior, S., Wilson M. T. and O'Shea, P. (1996). Time resolution of binding and membrane insertion of a mitochondrial signal peptide: correlation with structural changes and evidence for cooperativity. *Biochemistry* **35**, 10931–10937.

Goormaghtigh, E., Cabiaux, V. and Ruysschaert, J.-M. (1990). Secondary structure and dosage of soluble and membrane proteins by attenuated total reflection Fourier-transform infrared spectroscopy on hydrated films. *J. Biochem.* **193**, 409–420.

Goormaghtigh, E., Cabiaux, V. and Ruysschaert, J.-M. (1994). Determination of soluble and membrane protein structure by Fourier transform infrared spectroscopy. In *subcellular biochemistry, vol. 23: physicochemical methods in the study of biomembranes,* pp 320–363. Edited by Hilderson, H. J. and Ralston, G. B. Plenum press, New York.

Goormaghtigh, E., Raussens, V. and Ruysschaert, J.-M. (1999). Attenuated total reflection infrared spectroscopy of proteins and lipids in biological membranes. *Biochimica et Biophysica Acta* **1422**, 105–185.

Gray, C. and Tamm, L. K. (1997). Structural studies on membrane-embedded influenza hemagglutinin and its fragments. *Prot. Sci.* **6**, 1993–2006.

Gray, C. and Tamm, L. K. (1998). PH-induced conformational changes of membrane-bound influenza hemagglutinin and its effect on target lipid bilayers. *Prot. Sci.* **7**, 2359–2373.

Gruenberg, J. and Maxfield, F. R. (1995). Membrane transport in the endocytic pathway. *Curr. Opi. Cell Biol.* **7**, 552-563.

Harder, T. and Simons, K. (1997). Caveolae, DIGS, and the dynamics of sphingolipid-cholesterol microdomains. *Curr. Opin. Cell Biol.* **9**, 534–542.

Hegde, R. S. and Lingappa, V. R. (1997). Membrane protein biogenesis: regulated complexity at the endoplasmic reticulum. *Cell* **91**, 575–582.

Hegde, R. S., Mastrianni, J. A., Scott, M. R., DeFea, K. A., Tremblay, P., Torchia, M., DeArmond, S. J., Prusiner, S. B. and Lingappa, V. R. (1998*a*). A transmembrane form of the prion protein in neurodegenerative disease. *Science* **279**, 827–834.

Hegde, R. S., Voigt, S. and Lingappa, V. R. (1998*b*). Regulation of protein topology by trans-acting factors at the endoplasmic reticulum. *Mol. Cell* **2**, 85–91.

Hegde, R., Tremblay, P., Groth, D., DeArmond, S. J., Prusiner, S. B. and Lingappa, V. R. (1999). Transmissible and genetic prion diseases share a common pathway of neurodegeneration. *Nature* **402**, 822–826.

Heimburg, T., Schuenemann, J., Weber, K. and Geisler, N. (1996). Specific recognition of coiled coils by infrared spectroscopy: analysis of the three structural domains of type III intermediate filament proteins. *Biochemistry* **35**, 1375–1382.

Hill, A. F., Desbruslais, M., Joiner, S., Sidle, K. C. L., Gowland, I. And Collinge, J. (1997). The same prion strain causes vCJD and BSE. *Nature* **389**, 448–450.

Hill, A. F., Antoniou, M. and Collinge, J. (1999). Protease-resistant prion protein produced *in vitro* lacks detectable infectivity. *J. Gen. Virol.* **80**, 11–14.

Homans, S. W., Ferguson, M. A. J., Dwek, R. A, Rademacher, T. W. Anand, R. and Williams, A. F. (1998). Complete structure of the glycosylphosphatidylinositol membrane anchor of rat brain THY-1 glycoprotein. *Nature* **333**, 269–272.

Hope, J., Morton, L. J. D., Farquhar, C. F., Multhaup, G., Beyreuther, K. and Kimberlin, R. H. (1986). The major polypeptide of scrapie-associated fibrils (SAF) has the same size, charge distribution and N-terminal protein sequence as predicted for the normal brain protein (PrP). *EMBO J.* **5**, 2591–2597.

Horiuchi, M., Priola, S. A., Chabry, J. and Caughey, B. (2000). Interactions between heterologous forms of prion protein: binding, inhibition of conversion and species barriers. *Proc. Natl. Acad. Sci. USA* **97**, 5836–5841.

Hornemann, S. and Glockshuber, R. (1996). Autonomous and reversible folding of a soluble amino-terminally truncated segment of the mouse prion protein. *J. Mol. Biol.* **262**, 614-619.

Hornemann, S., Korth, C., Oesch, B., Riek, R., Wider, G., Wuthrich, K. and Glockshuber, R. (1997). Recombinant full-length murine prion protein, *m*PrP (23–231): purification and spectroscopic characterisation. *FEBS* **413**, 277-281.

Hornemann, S. and Glockshuber, R. (1998). A scrapie-like unfolding intermediate of the prion protein domain PrP (121–231) induced by acidic pH. *Proc. Natl. Acad. Sci. USA* **95**, 6010–6014.

Horwich, A. L. and Weissman, J. S. (1997). Deadly conformations-protein misfolding in prion disease. *Cell* **89**, 499–510.

Hsiao, K. K., Groth, D., Scott, M., Yang, S. –L., Serban, H., Rapp, D., Foster, D., Torchia, M., DeArmond, S. J. and Prusiner, S. B. (1994). Serial transmission in rodents of neurodegeneration from transgeneic mice expressing mutant prion protein. *Proc. Natl. Acad. Sci. USA* **91**, 9126-9130.

Huang, Z., Prusiner, S. B. and Cohen, F. E. (1995). Scrapie prions: a three-dimensional model of an infectious fragment. *Folding & Design* **1**, 13–19.

Jackson, G. S., Hill, A. F., Joseph, C., Hosszu, L., Power, A., Waltho, J, P., Clarke, A. R. and Collinge, J. (1999*a*). Multiple folding pathways for heterologously expressed human prion protein. *Biochimica et Biophysica Acta* **1431**, 1-13.

Jackson, G. S., Hosszu, L. L. P., Power, A., Hill, A. F., Kenney, J., Saibil, H., Craven, C. J., Waltho, J. P., Clarke, A. R. and Collinge, J. (1999*b*). Reversible conversion of monomeric human prion protein between native and fibrilogenic conformations. *Science* **283**, 1935-1937.

Jackson, M. and Mantsch, H. H. (1991). Beware of proteins in DMSO. *Biochimica et Biophysica. Acta* **1078**, 231–235.

Jacobson, K., Sheets, E. D. and Simson, R. (1995). Revisiting the fluid mosaic model of membranes. *Science* **268**, 1441–1442.

James, T. L., Liu, H., Ulyanov, N. B., Farr-Jones, S., Zhang, H., Donne, D. G., Kaneko, K., Groth, D., Mehlhorn, I., Prusiner, S. B. and Cohen, F. E. (1997). Solution structure of a 142-residue recombinant prion protein corresponding to the infectious fragment of the scrapie isoform. *Proc. Natl. Acad. Sci. USA* **94**, 10086–10091.

Jarrett, J. T. and Lansbury, P. T. (1993). Seeding "one-dimensional crystallisation" of amyloid: a pathogenic mechanism in Alzheimer's disease and Scrapie. *Cell* **73**, 1055–1058.

Jo, E., McLaurin, J, Yip. C. M., George-Hyslop, P. S. and Fraser, P. E. (2000). α-Synuclein membrane interactions and lipid specificity. *J. Biol. Chem.* **275**, 34328–34334.

Kaneko, K., Zulianello, L., Scott, M., Cooper, C. M., Wallace, A. C., James, T. L. Cohen, F. E. and Prusiner, S. B. (1997). Evidence for protein X binding to a discontinuous epitope on the cellular prion protein during scrapie prion propagation. *Proc. Natl. Acad. Sci USA* **94**, 10069–10074.

Kaneko, K., Ball, H. L., Wille, H., Zhang, H., Groth, D., Torchia, M., Tremblay, P., Safar, J., Prusiner, S. B., DeArmond, S. J., Baldwin, M. A. and Cohen, F. E. (2000). A synthetic peptide initiates Gerstmann-Sträussler-Scheinker (GSS) disease in transgenic mice. *J. Mol. Biol.* **295**, 997–1007.

Kauppinen, J. K., Moffatt, D. J., Cameron, D. G. and Mantsch, H. H. (1981). Noise in Fourier self-deconvolution. *Appl. Optics* **20**, 1866–1879.

Kellings, K., Meyer, N., Mirenda, C., Prusiner, S. B. and Riesner, D. (1992). Further analysis of nucleic acids in purified scrapie prion preparations by improved return refocusing gel electrophoresis. *J. Gen. Virol.* **73**, 1025–1029.

Kobayashi, T., Gu, F. and Gruenberg, J. (1998). Lipids, lipid domains and lipid-protein interactions in endocytic membrane traffic. *Seminars in Cell Dev. Biol.* **9**, 517–526.

Kocisko, D. A., Come, J. H., Priola, S. A., Chesebro, B. Raymond, G. J., Lansbury, P. T. and Caughey, B. (1994). Cell-free formation of protease-resistant prion protein. *Nature* **370**, 471–474.

Kocisko, D. A., Priola, S. A., Raymond, G. J., Chesebro, B. Lansbury, P. T. and Caughey, B. (1995). Species specificity in the cell-free conversion of prion protein to protease-resistant forms: A model for the scrapie species barrier. *Proc. Natl. Acad. Sci. USA* **92**, 3923–3927.

Koppaka, V. and Axelsen, P. H. (2000). Accelerated accumulation of amyloid β proteins on oxidatively damaged lipid membranes. *Biochemistry* **39**, 10011–10016.

Kraulis, P. J. (1991). MOLSCRIPT: a program to produce both detailed and schematic plots of protein structures. *J. Appl. Cryst.* **24**, 946–950.

Kretzschmar, H. A., Stowring, L. E., Westaway, D., Stubblebine, W. H., Prusiner, S. B. and DeArmond, S. J. (1986). Molecular cloning of a human prion protein cDNA. *DNA* **5**, 315–324.

Krimm, S. and Bandekar, J. (1986). Vibrational spectroscopy and conformation of peptides, polypeptides and proteins. *Adv. Prot. Chem.* **38**, 181–269.

Kurzban, G. P., Gitlin, G., Bayer, E. A., Wilchek, M. and Horowitz, P. M. (1989). Shielding of tryptophan residues of Avidin by the binding of Biotin. *Biochemistry* **28**, 8537–8542.

Laemmli, U. K. (1970). Cleavage of structural proteins during the assembly of the head of bacteriophage T4. *Nature* **227**, 680–685.

Lakowicz, J. R. (1983). Principles of fluorescence spectroscopy. Plenum Press, New York and London.

Lehmann, S. and Harris, D. A. (1997). Blockade of glycosylation promotes acquisition of scrapie-like properties by prion protein in cultured cells. *J. Biol. Chem.* **272**, 21479–21487.

Liemann, S. and Glockshuber, R. (1999). Influence of amino acid substitutions related to inherited human prion diseases on the thermodynamic stability of the cellular prion protein. *Biochemistry* **38**, 3258–3267.

Lindquist, S. (1997). Mad cows meet Psi-chotic yeast: the expansion of the prion hypothesis. *Cell* **89**, 495–498.

Lin, M-C., Mirzabekov, T. and Kagan, B. L. (1997). Channel formation by a neurotoxic prion protein fragment. *J. Biol. Chem.* **272**, 44–47.

Liu, K., Cho, H. S., Lashuel, H. A., Kelly, J. W. and Wemmer, D. E. (2000). A glimpse of a possible amyloidogenic intermediate of transthyretin. *Nat. Struct. Biol.* **7**, 754–757.

Lopez, C. D., Yost, C. S., Prusiner, S. B., Myers, R. M. and Lingappa, V. R. (1990). Unusual topogenic sequence directs prion protein biogenesis. *Science* **248**, 226–229.

Ma, J. and Lindquist, S. (1999). De novo generation of a PrP^{Sc}-like conformation in living cells. *Nat. Cell Biol.* **1**, 358–361.

Manson, J. C., Clarke, A. R., Hooper, M. L., Aitchison, L., McConnell, I. and Hope, J. (1994). 129/Ola mice carrying a null mutation in PrP that abolishes mRNA production are developmentally normal. *Mol. Neurobiol.* **8**, 121–127.

Makrides, S. C. (1996). Strategies for achieving high-level expression of genes in *Escherichia coli. Microbiological Reviews* **60**, 512–538.

Marcotte, E. M. and Eisenberg, D. (1999). Chicken prion tandem repeats form a stable, protease-resistant domain. *Biochemistry* **38**, 667–676.

Matsuzaki, K., Murase, O., Tokuda, H., Funakoshi, S., Fujii, N. and Miyajima, K. (1994). Orientational and aggregational states of magainin 2 in phospholipid bilayers. *Biochemistry* **33**, 3342–3349.

McKinley, M. P., Bolton, D. C. and Prusiner, S. B. (1983). A protease-resistant protein is a structural component of the scrapie prion. *Cell* **35**, 57–62.

McKinley, M. P., Meyer, R. K., Kenaga, L., Rahbar, F., Cotter, R., Serban, A. and Prusiner, S. B. (1991). Scrapie prion rod formation in vitro requires both detergent extraction and limited proteolysis. *J. Virol.* **65**, 1340–1351.

McLaughlin, S. and Aderem, A. (1995). The myristoyl-electrostatic switch: a modulator of reversible protein-membrane interactions. *TIBS* **20**, 272–276.

McLaurin , J. and Chakrabartty, A. (1996). Membrane disruption by Alzheimer β-amyloid peptides mediated through specific binding to either phospholipids or gangliosides. *J. Biol. Chem.* **271**, 26482–26489.

McLaurin, J., Franklin, T., Chakrabartty, A. and Fraser, P. E. (1998). Phosphatidylinositol and inositol involvement in Alzheimer amyloid-β fibril growth and arrest. *J. Mol. Biol.* **278**, 183–194.

Mehlhorn, I., Groth, D., Stockel, J., Moffat, B., Reilly, D., Yansura, D., Willett, W. S., Baldwin, M., Fletterick, R., Cohen, F. E., Vandlen, R., Henner, D. and Prusiner, S. B. (1996). High-level expression and characterisation of a purified 142-residue polypeptide of the prion protein. *Biochemistry* **35**, 5528–5537.

Merritt, E. A. and Bacon, D. J. (1997). RASTER3D: photorealististic molecular graphics. *Method Enzymol.* **277**, 505–524.

Meyer, R. K., McKinley, M. P., Bowman, K. A., Braunfeld, M. B., Barry, R. A. and Prusiner, S. B. (1986). Separation and properties of cellular and scrapie prion proteins. *Proc. Natl. Acad. Sci. USA* **83**, 2310–2314.

Meyer, N., Rosenbaum, V., Schmidt, B., Gilles, K., Mirenda, C., Groth, D. Prusiner, S. B. and Riesner, D. (1991). Search for a putative scrapie genome in purified prion fractions reveals a paucity of nucleic acid. *J. Gen. Virol.* **72**, 37–49.

215

Milhavet, O., McMahon, H. E. M., Rachidi, W., Nishida, N., Katamine, S., Mangé, A., Arlotto, M., Casanova, D., Riondel, J., Favier, A. and Lehmann, S. (2000). Prion infection impairs the cellular response to oxidative stress. *Proc. Natl. Acad. Sci. USA* **97**, 13937–13942.

Miura, T., Hori-I, A., Mototani, H. and Takeuchi, H. (1999). Raman spectroscopic study on the copper (II) binding mode of prion octapeptide and its pH dependence. *Biochemistry* **38**, 11560–11569.

Moore, R. C., Lee, I. Y., Silverman, G. L., Harrison, P. M., Strome, R., Heinrich, C., Karunaratne, A., Pasternak, S. H., Chishti, M. A., Liang, Y., Mastrangelo, P., Wang, K., Smit, A. F. A., Katamine, S., Carlson, G. A., Cohen, F. E., Prusiner, S. B., Melton, D. W., Tremblay, P., Hood, L. E. and Westaway, D. (1999). Ataxia in prion protein (PrP)-deficient mice is associated with upregulation of the novel PrP-like protein doppel. *J. Mol. Biol.* **292**, 797–817.

Morillas, M., Swietnicki, W., Gambetti, P. and Surewicz, W. K. (1999). Membrane environment alters the conformational structure of the recombinant human prion protein. *J. Biol. Chem.* **274**, 36859–36865.

Muramoto, T., Scott, M., Cohen, F. E. and Prusiner, S. B. (1996). Recombinant scrapie-like prion protein of 106 amino acids is soluble. *Proc. Natl. Acad. Sci. USA* **93**, 15457–15462.

Naslavsky, N., Stein, R., Yanai, A., Friedlander, G. and Taraboulos, A. (1997). Characterisation of detergent-insoluble complexes containing cellular prion protein and its scrapie isoform. *J. Biol. Chem.* **272**, 6324–6331.

Negro, A., De Filippis, V., Skaper, S. D., James, P. and Sorgato, M. C. (1997). The complete mature bovine prion protein highly expressed in *Escherichia coli*: biochemical and structural studies. *FEBS* **412**, 359–364.

Nguyen, J., Baldwin, M. A., Cohen, F. E. and Prusiner, S. B. (1995). Prion protein peptides induce α-helix to β-sheet conformational transitions. *Biochemistry* **34**, 4186–4192.

Nicholls, A., Sharp, K. and Honig, B. (1991). Protein folding and association: insights from the interfacial and thermodynamic properties of hydrocarbons. *Proteins: Struct. Funct. Genet.* **11**, 281–296.

Oesch, B., Westaway, D., Wälchli, M., Mckinley, M. P., Kent, S. B. H., Aebersold, R., Barry, R. A., Tempst, P., Teplow, D, B., Hood, L. E. Prusiner, S. B. and Weissmann, C. (1985). A cellular gene encodes scrapie PrP 27–30 protein. *Cell* **40**, 735–746.

Pan, K-M., Baldwin, M., Nguyen, J., Gasset, M., Serban, A., Groth, D., Mehlhorn, I., Huang, Z., Fletterick, R. J., Cohen, F. E. and Prusiner, S. B. (1993). Conversion of α-helices into β-sheets features in the formation of the scrapie prion proteins. *Proc. Natl. Acad. Sci. USA* **90**, 10962–10966.

Peitzsch, R. M. and Mclaughlin, S. (1993). Binding of acylated peptides and fatty acids to phospholipid vesicles: pertinence of myristoylated proteins. *Biochemistry* **32**, 10436–10443.

Peretz, D., Williamson, R. A., Matsunaga, Y., Serban, H., Pinilla, C., Bastidas, R. B. Rozenshteyn, R., James, T. L., Houghten, R. A., Cohen, F. E., Prusiner, S. B. and Burton, D. R. (1997). A conformational transition at the N terminus of the prion protein features in formation of the scrapie isoform. *J. Mol. Biol.* **273**, 614–622.

Pergami, P., Jaffe, H. and Safar, J. (1996). Semipreparative chromatographic method to purify the normal cellular isoform of the prion protein in non-denatured form. *Anal. Biochem.* **236**, 63–73.

Pillot, T., Goethals, M., Vanloo, B., Talussot, C., Brasseur, R., Vandekerckhove, J., Rosseneu, M. and Lins, L. (1996). Fusogenic properties of the C-terminal domain of the Alzheimer β-amyloid peptide. *J. Biol. Chem.* **271**, 28757–28765.

Pillot, T., Lins, L., Goethals, M., Vanloo, B., Baert, J., Vandekerckhove, J., Rosseneu, M. and Brasseur, R. (1997). The 118–135 peptide of the human prion protein forms amyloid fibrils and induces liposome fusion. *J. Mol. Biol.* **274**, 381–393.

Pohl, T. (1990). Concentration of proteins and removal of solutes. In *Methods in Enzymology, Guide to protein purification*, vol. 182, pp. 68–83. Edited by Deutscher, M. P. Academic Press.

Prats, M., Teissié, J. and Tocanne, J.-F. (1986). Lateral proton conduction at lipid-water interfaces and its implications for chemiosmotic-coupling hypothesis. *Nature* **322**, 756–758.

Prusiner, S. B. (1982). Novel proteinaceous infectious particles cause scrapie. *Science* **216**, 136–144.

Prusiner, S. B., Bolton, D. C., Groth, D. G., Bowman, K. A., Cochran, S. P. and McKinley, M. P. (1982). Further purification and characterisation of scrapie prion. *Biochemistry* **21**, 6942–6950.

Prusiner, S. B. (1989). Scrapie prions. *Annu. Rev. Microbiol.* **43**, 345–374.

Prusiner, S. B., Scott, M., Foster, D., Pan, K.-M., Groth, D., Mirenda, C., Torchia, M., Yang, S.-L., Serban, D., Carlson, G. A., Hoppe, P. C., Westaway, D. and DeArmond, S. J. (1990). Transgenetic studies implicate interactions between homologous PrP isoforms in scrapie prion replication. *Cell* **63**, 673–686.

Prusiner, S. B. (1992). Chemistry and biology of prions. *Biochemistry* **31**, 12277–12288.

Prusiner, S. B. (1997). Prion diseases and the BSE crisis. *Science* **278**, 245–250.

Prusiner, S. B. and Scott, M. R. (1997). Genetics of prions. *Annu. Rev. Genet.* **31**, 139–175.

Prusiner, S. B. (1998). Prions. *Proc. Natl. Acad. Sci. USA* **95**, 13363–13383.

Prusiner, S. B., Scott, M. R., DeArmond, S. J. and Cohen, F. E. (1998). Prion protein biology. *Cell* **93**, 337–348.

Rankin, S. E., Watts, A. and Pinheiro, T. J. T. (1998). Electrostatic and hydrophobic contributions to the folding of apocytochrome *c* driven by the interaction with lipid. *Biochemistry* **37**, 12588–12595.

Rapoport, T. A., Jungnickel, B. and Kutay, U. (1996). Protein transport across the eukaryotic endoplasmic reticulum and bacterial inner membranes. *Annu. Rev. Biochem* **65**, 271–303.

Raussens, V., Pézolet, M., Ruysschaert, J.-M. and Goormaghtigh, E. (1999). Structural differences in the H^+, K^+-ATPase between the E1 and E2 conformations. *Eur. J. Biochem.* **262**, 176–183.

Riek, R., Hornemann, S., Wider, G., Billeter, M., Glockshuber, R. and Wüthrich, K. (1996). NMR structure of the mouse prion protein domain PrP (121–231). *Nature* **382**, 180–182.

Riek, R., Hornemann, S., Wider, G., Glockshuber, R. and Wüthrich, K. (1997). NMR characterisation of the full-length recombinant murine prion protein, mPrP (23–231). *FEBS* **413**, 282–288.

Rochet, J.-C. and Lansbury, P. T. (2000). Amyloid fibrillogenesis: themes and variations. *Curr. Opi. Struct. Biol.* **10**, 60–68.

Rodger, A. and Norden, B. (1997). Circular dichroism and linear dichroism, vol 1. Oxford university press, oxford.

Rogers, M., Yehiely, F., Scott, M. and Prusiner, S. B. (1993). Conversion of truncated and elongated prion proteins into the scrapie isoforms in cultured cells. *Proc. Natl. Acad. Sci. USA* **90**, 3182–3186.

Rudd, P. M., Wormald, M. R., Wing, D. R., Prusiner, S. B. and Dwek, R. A. (2001). Prion glycoprotein: structure, dynamics, and roles for the sugars. *Biochemistry* **40**, 3759–3766.

Safar, J., Ceroni, M., Piccardo, P., Liberski, P. P., Miyazaki, M., Gajdusek, D. C. and Gibbs, C. J. (1990). Subcellular distribution and physicochemical properties of scrapie associated precursor protein and relationship with scrapie agent. *Neurology* **40**, 503–508.

Safar, J., Ceroni, M., Gajdusek, D. C. and Gibbs, C. J. (1991). Differences in the membrane interaction of scrapie amyloid precursor proteins in normal and scrapie-or Creutzfeldt-Jakob disease-infected brains. *J. Inf. Diseases* **163**, 488–494.

Sakaguchi, S., Katamine, S., Nishida, N., Moriuchi, R., Shigematsu, K., Sugimoto, T., Nakatani, A., Kataoka, Y., Houtani, T., Shirabe, S., Okada, H., Hasegawa, S., Miyamoto, T. and Noda, T. (1996). Loss of cerebellar Purkinje cells in aged mice homozygous for a disrupted PrP gene. *Nature* **380**, 528–531.

Sambrook, J., Fritsch, E. F. and Maniatis, T. (1989). *Molecular cloning a laboratory manual, 2rd edition.* Cold spring Harbor press.

Schätzl, H. M., Da Costa, M., Taylor, L., Cohen, F. E. and Prusiner, S. B. (1995). Prion protein gene variation among primates. *J. Mol. Biol.* **245**, 362-374.

Schroeder, R., London, E. and Brown, D. (1994). Interactions between saturated acyl chains confer detergent resistance on lipids and glycosylphosphatidylinositol (GPI) anchored proteins: GPI-anchored proteins in liposomes and cells show similar behaviour. *Proc. Natl. Acad. Sci. USA* **91**, 12130-12134.

Schroeder, R., Ahmed, S. N., Zhu, Y., London, E. and Brown, D. (1998). Cholesterol and sphingolipid enhance the triton X-100 insolubility of glycosylphosphatidylinositol-anchored proteins by promoting the formation of detergent-insoluble ordered membrane domains. *J. Biol. Chem.* **273**, 1150–1157.

Scott, M., Groth, D., Foster, D., Torchia, M., Yang, S.-L., DeArmond, S. J. and Prusiner, S. B. (1993). Propagation of prions with artificial properties in transgenic mice expressing chimeric PrP genes. *Cell* **73**, 979–988.

Sigal, C. T., Zhou, W., Buser, C. A., Mclaughlin, S. and Resh, M. D. (1994). Amino-terminal basic residues of Src mediate membrane binding through electrostatic interaction with acidic phospholipids. *Proc. Natl. Acad. Sci. USA* **91**, 12253-12257.

Simons, K. and Ikonen, E. (1997). Functional rafts in cell membranes. *Nature* **387**, 569–572.

Skoog, D. A., West, D. M. and Holler F. J. (1996). An introduction to spectrochemical methods. In *Fundamentals of analytical chemistry*, 7th edn, pp 497–526. Saunders college publishing.

Sparkes, R. S., Simon, M., Cohn, C. H., Fournier, R. E. K., Lem, J, Klisak, I., Heinzmann, C., Blatt, C., Lucero, M., Mohandas, T., DeArmond, S. J., Westaway, D., Prusiner, S. B. and Weiner, L. P. (1986). Assignment of the human and mouse prion protein genes to homologous chromosomes. *Proc. Natl. Acad. Sci. USA* **83**, 7358-7362.

Sparrer, H. E., Santose, A., Szoka, F. C. and Weissman, J. S. (2000). Evidence for the prion hypothesis: induction of the yeast [*PSI⁺*] factor by in vitro-converted Sup35 protein. *Science* **289**, 595–599.

Stahl, N., Borchelt, D. R., Hsiao, K. and Prusiner, S. B. (1987). Scrapie prion protein contains a phosphatidylinositol glycolipid. *Cell* **51**, 229 –240.

Stahl, N., Borchelt, D. R. and Prusiner, S. B. (1990). Differential release of cellular and scrapie prion proteins from cellular membranes by phosphatidylinositol-specific phospholipase C. *Biochemistry* **29**, 5405–5412.

Stahl, N., Baldwin, M. A., Teplow, D. B., Hood, L., Gibson, B. W., Burlingame, A. L. and Prusiner, S. B. (1993). Structural studies of the scrapie prion protein using mass spectrometry and amino acid sequencing. *Biochemistry* **32**, 1991–2002.

Stewart, R. S. and Harris, D. A. (2001). Most pathogenic mutations do not alter the membrane topology of the prion protein. *J. Biol. Chem* **276**, 2212–2220.

Stöckel, J., Safar, J., Wallace, A. C., Cohen, F. E. and Prusiner, S. B. (1998). Prion protein selectively binds copper (II) ions. *Biochemistry* **37**, 7185–7193.

Sunde, M., Serpell, L. C., Bartlam, M., Fraser, P. E., Pepys, M. B. and Blake, C. C. F. (1997). Common core structure of amyloid fibrils by synchrotron X-ray diffraction. *J. Mol. Biol.* **273**, 729–739.

Swietnicki, W., Petersen, R., Gambetti, P. and Surewicz, W. K. (1997). pH-dependent stability and conformation of the recombinant human prion protein PrP (90–231). *J. Biol. Chem.* **272**, 27517-27520.

Swietnicki, W., Petersen, R. B., Gambetti, P. and Surewicz, W. K. (1998). Familial mutations and the thermodynamic stability of the recombinant human prion protein. *J. Biol. Chem.* **273**, 31048–31052.

Taraboulos, A., Rogers, M., Borchelt, D. R., Mckinley, M. P., Scott, M., Serban, D. and Prusiner, S. B. (1990*a*). Acquisition of Protease resistance by prion proteins in scrapie-infected cells does not require asparagine-linked glycosylation. *Proc. Natl. Acad. Sci. USA* **87**, 8262–8266.

Taraboulos, A., Serban, D. and Prusiner, S. B. (1990*b*). Scrapie prion proteins accumulates in the cytoplasm of persistently infected cultured cells. *J. cell Biol.* **110**, 2117–2132.

Taraboulos, A., Jendroska, K., Serban, D., Yang, S.-L., DeArmond, S. J. and Prusiner, S. B. (1992). Regional mapping of prion proteins in brains. *Proc. Natl. Acad. Sci. USA* **89**, 7620 –7624.

Taraboulos, A., Scott, M., Semenov, A., Avraham, D., Laszlo, L. and Prusiner, S. B. (1995). Cholesterol depletion and modification of COOH-terminal targeting sequence of the prion inhibit formation of scrapie isoform. *J. Cell Biol.* **129**, 121–132.

Tejuca, M., Serra, M. D., Ferreras, M., Lanio, M. E. and Menestrina, G. (1996). Mechanism of membrane permeabilization by sticholysin I, a cytolysin isolated from

the venom of the sea anemone *Stichodactyla helianthus*. *Biochemistry* **35**, 14947–14957.

Telling, G. C., Scott, M., Mastrianni, J., Gabizon, R., Torchia, M., Cohen, F. E., DeArmond, S. J. and Prusiner, S. B. (1995). Prion propagation in mice expressing human and chimeric PrP transgenes implicates the interaction of cellular PrP with another protein. *Cell* **83**, 79–90.

Telling, G. C., Parchi, P., DeArmond, S. J., Cortelli, P., Montagna, P., Gabizon, R., Mastrianni, J., Lugaresi, E., Gambetti, P. and Prusiner, S. B. (1996). Evidence for the conformation of the pathologic isoform of the prion protein enciphering and propagating prion diversity. *Science* **274**, 2079–2082.

Tobler, I., Gaus, S. E., Deboer, T., Achermann, P., Fischer, M., Rülicki, T., Moser, M., Oesch, B., McBride, P. A. and Manson, J. C. (1996). Altered circadian activity rhythms and sleep in mice devoid of prion protein. *Nature* **380**, 639–642.

Tompa, P., Tusnady, G. E., Cserzo, M. and Simon, I. (2001). Prion protein: evolution caught en route. *Proc. Natl. Acad. Sci USA* **98**, 4431–4436.

Turk, E., Teplow, D. B., Hood, L. E. and Prusiner, S. B. (1988). Purification and properties of the cellular and scrapie hamster prion protein. *Eur. J. Biochem.* **176**, 21 –29.

Van Meer, G. (1989). Lipid traffic in animal cells. *Annu. Rev. Cell. Biol* **5**, 247–275.

Vey, M., Pilkuhn, S., Wille, H., Nixon, R., DeArmond, S. J., Smart, E. J., Anderson, R. G. W., Taraboulos, A. and Prusiner, S. B. (1996). Subcellular colocalisation of the cellular and scrapie prion proteins in caveolae-like membranous domains. *Proc. Natl. Acad. Sci. USA* **93**, 14945–14949.

Viles, J. H., Cohen, F. E., Prusiner, S. B., Goodin, D. B., Wright, P. E. and Dyson, H. J. (1999). Copper binding to the prion protein: structural implications of four identical co-operative binding sites. *Proc. Natl. Acad. Sci. USA* **96**, 2042–2047.

Vogt, T. C. B. and Bechinger, B. (1999). The interactions of histidine-containing amphipathic helical peptide antibiotics with lipid bilayers. *J. Biol. Chem.* **274**, 29115–29121.

Wall, J., Golding, C. A., Van Veen, M. and O'Shea, P. O. (1995). The use of fluoresceinphosphatidylethanolamine (FPE) as a real-time probe for peptide-membrane interactions. *Mol. Membr. Biol.* **12**, 183–192.

Wang, X.-M, Mock, M., Ruysschaert, J.-M. and Cabiaux, V. (1996). Secondary structure of anthrax lethal toxin proteins and their interaction with large unilamellar vesicles: a Fourier-transform infrared spectroscopy approach. *Biochemistry* **35**, 14939–14946.

Warwicker, J. (1997). A hypothesis describing a potential link between molecular structure and TSE strains. *Biochem. Biophys. Res. Commun.* **238**, 185–190.

Warwicker, J. (1999). Modelling charge interactions in the prion protein: predictions for pathogenesis. *FEBS* **450**, 144–148.

Weissmann, C. (1999). Molecular genetics of transmissible spongiform encephalopathies. *J. Biol. Chem.* **274**, 3–6.

White, S. H. and Wimley, W. C. (1994). Peptides in lipid bilayers: structural and thermodynamic basis for partitioning and folding. *Curr. Opi. Struct. Biol* **4**, 79–86.

White, S. H. and Wimley, W. C. (1998). Hydrophobic interactions of peptides with membrane interfaces. *Biochimica et Biophysica Acta* **1376**, 339–352.

Wildegger, G., Liemann, S. and Glockshuber, R. (1999). Extremely rapid folding of the C-terminal domain of the prion protein without kinetic intermediates. *Nature Struc. Biol.* **6**, 550–553.

Wimley, W. C., Selsted, M. E. and White, S. H. (1994). Interactions between human defensins and lipid bilayers: evidence for formation of multimeric pores. *Prot. Sci.* **3**, 1362–1373.

Wimley, W. C. and White, S. H. (1996). Experimentally determined hydrophobicity scale for proteins at membrane interfaces. *Nat. Struct. Biol.* **3**, 842–848.

Wolfe, C., Cladera, J. and O'Shea, P. (1998). Amino acid sequences which promote and prevent the binding and membrane insertion of surface-active peptides: comparison of melittin and promelittin. *Mol. Membr. Biol.* **15**, 221–227..

Wood, R. W. (1996). Theory of CD. In *Circular Dichroism and the conformational analysis of biomolecules*, pp. 25–67. Edited by Fasman, G. D. Plenum press, New York & London.

Wopfner, F., Weidenhöfer, G., Schneider, R., von Brunn, A., Gilch, S., Schwarz, T. F., Werner, T. and Schätzl, H. M. (1998). Analysis of 27 mammalian and 9 avian PrPs reveals high conservation of flexible regions of the prion protein. *J. Mol. Biol.* **289**, 1163–1178.

Yost, C. S., Lopez, C. D., Prusiner, S. B., Myers, R. M. and Lingappa, V. R. (1990). Non-hydrophobic extracytoplasmic determinant of stop transfer in the prion protein. *Nature* **343**, 669–672.

Zahn, R., von Schroetter, C. and Wuthrich, K. (1997). Human prion proteins expressed in *Escherichia coli* and purified by high-affinity column refolding. *FEBS* **417**, 400–404.

Zahn, R., Liu, A., Luhrs, T., Riek, R., Von Schroetter, C., Garcia, F. L., Billeter, M., Calzolai, L., Wider, G. and Wuthrich, K. (2000). NMR solution structure of the human prion protein. *Proc. Natl. Acad. Sci. USA* **97,** 145–150.

Zhang, H., Stockel, J., Mehlhorn, I., Groth, D., Baldwin, M. A., Prusiner, S. B., James, T. L. and Cohen, F. E. (1997). Physical studies of conformational plasticity in a recombinant prion protein. *Biochemistry* **36,** 3543–3553.

Zhou, W., Parent, L. J., Willis, J. W. and Resh, M. D. (1994). Identification of a membrane binding domain within the amino-terminal region of the human immunodeficiency virus type-1 GAG protein which interacts with acidic phospholipids. *J. Virol.* **68,** 2556–2569.